

# Existence and Stability of Spatially Localized Planar Patterns

by

Elizabeth Makrides

B.S., The University of North Carolina, Chapel Hill, NC, 2005

M.S., Tufts University, Medford, MA, 2010

M.S., Brown University, Providence, RI, 2011

A dissertation submitted in partial fulfillment of the  
requirements for the degree of Doctor of Philosophy  
in The Division of Applied Mathematics at Brown University

PROVIDENCE, RHODE ISLAND

May 2016

© Copyright 2016 by Elizabeth Makrides

Abstract of “ Existence and Stability of Spatially Localized Planar Patterns ” by Elizabeth Makrides, Ph.D., Brown University, May 2016

Spatially localized structures, in which a spatially oscillatory pattern on a finite spatial range connects to a trivial homogeneous solution outside this range, have been observed in numerous physical contexts, including cellular buckling, plane Couette flow, vegetation patterns, optical cavity solitons, crime hotspots, and many others. Despite the widely disparate contexts in which they arise, the bifurcation diagrams of such patterns often exhibit similar snaking behavior, in which branches of symmetric solutions, connected by bifurcating branches of asymmetric solutions, wind back and forth between two limits of an appropriate parameter. In this thesis we address the existence and stability of stationary localized solutions of parabolic partial differential equations (PDEs) on the line and the plane. One particular model system supporting localized structures is the Swift–Hohenberg system, and we use this system for numerical illustration of our existence and stability results.

Our main results are as follows: we give a new proof of the existence asymmetric localized structures, utilizing information about the underlying front structure and providing a unified approach to the existence of all localized structures. This enables a rigorous proof of the stability properties of symmetric and asymmetric structures. We show that the temporal eigenvalues of localized structures in the right half plane are exponentially close to those of the front and back added with multiplicity, and furthermore that the eigenvalue at the origin remains simple. We then address numerical results showing unexpected behavior of eigenvalues within the essential (or absolute) spectrum, and propose an analytical explanation of these results. We conclude by predicting the results of perturbative terms in PDE systems supporting localized snaking solutions, and make qualitative and quantitative predictions for topological changes to the associated bifurcation diagrams, as well as drift speeds of particular solutions.

This dissertation by Elizabeth Makrides is accepted in its present form  
by The Division of Applied Mathematics as satisfying the  
dissertation requirement for the degree of Doctor of Philosophy.

Date \_\_\_\_\_

Björn Sandstede, Ph.D., Advisor

Recommended to the Graduate Council

Date \_\_\_\_\_

Margaret Beck, Ph.D., Reader

Date \_\_\_\_\_

Govind Menon, Ph.D., Reader

Approved by the Graduate Council

Date \_\_\_\_\_

Peter Weber, Dean of the Graduate School

# Vitae

## Education

- Brown University, Providence, RI, 2010-2015  
Ph.D. in Applied Mathematics, expected Dec. 2015  
M.S. in Applied Mathematics, 2011
- Tufts University, Medford, MA, 2008-2010  
M.S. in Biology
- University of North Carolina at Chapel Hill, 2001-2005  
B.S. in Biology / B.A. in Economics, Phi Beta Kappa, Highest Honors

## Honors and Awards

- Deans Faculty Fellowship for excellence in research and teaching, 2015-2016
- Various travel awards through BIRS, IMA, MBI, NSF and SIAM, 2011-2014
- NSF IGERT Fellowship, 2011-2013
- Phi Beta Kappa, Vice-President, 2004-2005
- Senior Marshal, 2004-2005

- Order of the Old Well, recognizing exemplary service to the University, 2004

## Employment and Appointments

- Visiting Assistant Professor, Brown University Providence RI, 2016 (via Deans Faculty Fellowship)
- Manager, Business Development, Bascom-Turner Instruments Norwood MA, 2007-2010
- Associate, The Boston Consulting Group Bethesda MD, 2005-2007
- Summer Intern, Merck & Co. Whitehouse Station NJ, 2004

## Teaching Experience

- Visiting Assistant Professor, APMA 1070 Quantitative Models of Biological Systems  
Brown University, Spring 2016
- Instructor and team leader, Brown-ICERM-Kobe Simulation Summer School on high performance computing and visualization, Brown and Kobe Universities, August 2015
- Instructor, Basic College Mathematics Womens Correctional Facility (via CCRI), Warwick RI, 2013-2014
- Teaching Assistant, APMA 1720 Monte Carlo Simulation with Applications in Finance, Brown University, Spring 2013

- Classroom volunteer, Transitional Math  
Hope High School, Providence RI, Spring 2013
- Teaching Assistant, APMA 1650 Statistical Inference I  
Brown University, Fall 2012
- Grader, APMA 1690 Computational Probability and Statistics  
Brown University, Fall 2011
- Teacher for diverse student groups, campus and community, 2001-2005
  - HYPE: Provided after-school help and support for middle and high-school students in Chapel Hill public housing
  - ESL: Constructed lesson plans and taught adults in Chapel Hill and surrounding community
  - GED: Tutored maintenance and cleaning personnel at UNC
- Instructor, introductory and mixed-level vinyasa yoga classes; classes taught at three locations: Eyes of the World Yoga, Church of St. Mary on Broadway, and Roger Williams National Memorial. 200-hour Yoga Alliance certification through Eyes of the World Yoga, 2013-2014.

## Service and Professional Activities

- Graduate Student Liaison, Sheridan Center for Teaching and Learning, 2011-2014
  - Certificate in Reflective Teaching (yearlong teaching seminar)
- Rose Whelan Society for Women in Mathematics at Brown, 2011-present

- Carolina For the Kids, benefitting NC Childrens Hospital, 2001-2005
  - Outreach Chair, 2004-2005: Led team of 18 to expand awareness and support in wider community
  - Performance Coordinator, 2003-2004: Scheduled 50 groups and activities for 24-hours of entertainment at main fundraiser
  - Committee member, 2002-2003; Fundraiser & dancer, 2001-2002
- Cellar Door literary magazine staff editor for fiction, 2002-2005

## Publications

- E. Makrides and B. Sandstede. Stability of Localized Snaking Patterns, in preparation 2015.
- C. J. Graves\*, E. Makrides\*, V. Schmidt\*, A. E. Giblin, Z. G. Cardon, D. M. Rand, Functional responses of salt marsh microbial communities to long-term nutrient enrichment, submitted 2015. (Joint first author)
- A. N. Ford Versypt\*, E. Makrides\*, J. C. Arciero, L. Ellwein, and A. T. Layton, Bifurcation Study of Blood Flow Control in the Kidney, *Mathematical Biosciences*, 263, 169-179, 2015. (Joint first author and corresponding author)
- J. C. Arciero, L. Ellwein, A. N. Ford Versypt, E. Makrides, and A. T. Layton, Modeling Blood Flow Control in the Kidney, T. Jackson, A. Radunskaya (eds.), *Applications of Dynamical Systems in Biology and Medicine*, The IMA Volumes in Mathematics and its Applications 158, Springer, New York, 55-74, 2015.

- E. Makrides and B. Sandstede. Predicting the Bifurcation Structure of Localized Snaking Patterns, *Physica D* 268, 59-78, 2014.

## Presentations

- “Understanding the Structure and Stability of Localized Patterns.” Minisymposium talk, SIAM Conference on Analysis of Partial Differential Equations, Scottsdale, AZ. December 7-10, 2015.
- “Understanding the Structure and Stability of Localized Patterns. Math department colloquium, Tufts University, Medford, MA. October 2, 2015.
- “Modeling autoregulation in the kidney.” Joint seminar / weekly meeting talk, Duke University, Durham, NC. January 8, 2014.
- “From knee deep in \*\*\*\* to neck deep in data: the journey of team powersoil.” Joint talk with C. Graves and V. Schmidt, EEB Brown Bag Seminar, Brown University, Providence, RI. December 6, 2013.
- “Predicting the Bifurcation Diagrams of Localized Structures.” Talk at RTG in Stochastics and Dynamics Recruitment Day, Brown University, Providence, RI. November 22, 2013.
- “Detecting the influence of long-term sewage exposure and natural salinity gradients on functional gene abundances in salt marsh sediment microbial communities.” Poster Presentation with C. Graves and V. Schmidt, Brown-MBL Retreat, Marine Biological Laboratory, Woods Hole, MA. November 8-9, 2013
- “Predicting the Bifurcation Diagrams of Localized Structures.” Seminar Talk, Graduate Student Seminar, Brown University, Providence, RI. October 18,

2013.

- “Modeling Autoregulation in the Kidney.” Joint talk, Workshop on Dynamical Systems with Applications to Biology and Medicine, Institute for Mathematics and its Applications (IMA), Minneapolis, MN. Sept 9-13, 2013.
- “Predicting the Bifurcation Structure of Localized Snaking Patterns.” Poster presentation, Joint US-Japan Workshop for Young Researchers on Interactions among Localized Patterns in Dissipative Systems, Institute for Mathematics and its Applications (IMA), Minneapolis, MN. June 3-7, 2013.
- “Asymmetric Coherent Structures in One and Two Space Dimensions.” Poster presentation, SIAM Conference on Dynamical Systems, Snowbird, UT. May 19-23, 2013.
- “Understanding microbial community structure via metagenomic analysis.” Poster presentation, Workshop for Women in Probability, Duke University, Durham, NC. October 14-16, 2012.
- “On patterns and microbes.” Graduate student talk, Program on Computational Challenges in Probability, Institute for Computational and Experimental Research in Mathematics (ICERM), Providence, RI September 7, 2012.
- “One man’s trash is another’s treasure: Understanding microbial diversity and community structure via metagenomic analysis in sediments near a sewage outfall.” Poster presentation, IGERT Annual PI Meeting, Washington, DC. May 30-June 1, 2012.
- “Uniform Distributions on Integer Matrices.” Joint presentation with J. Loper to graduate students and faculty, Brown University, Providence, RI. May 13, 2011.

## Professional Associations

- American Mathematical Society (AMS)
- Association for Women in Mathematics (AWM)
- Mathematical Association of America (MAA)
- Society for Industrial and Applied Mathematics (SIAM)

## Acknowledgements

First and foremost, thank you to my advisor, Björn Sandstede, for his (uncountably) infinite patience. From fielding both my excitement and frustration at each new line of reasoning or series of calculations, to carefully reviewing everything from conference abstracts to job application materials, to patiently revisiting proofs as many times as necessary, Björn has been an amazing advisor, mentor, and friend.

I would also like to thank Professors Margaret Beck and Govind Menon for agreeing to serve on my committee, and for generously donating their time in this capacity.

To the faculty, staff, and students—past and present—in both mathematics and applied mathematics: I have enjoyed and benefitted from so many interactions, structured and casual, and I have been truly lucky to find myself in such a wonderful environment.

To friends and family near and far, I doubt you will ever read this, but in case you happen to flip through the pages (or pictures), thank you for your encouragement and support, and for occasionally listening to me prattle on about patterns.

Finally thank you to my amazing boys. Jack, thank you for believing in your mama, or at the very least allowing me a liberal interpretation of “mama, mama ... go, go, go.” And to my one and only MAGS, thank you for being you.

# Contents

<b>Vitae</b>	<b>iv</b>
<b>Acknowledgments</b>	<b>xi</b>
<b>1 Introduction</b>	<b>1</b>
1.1 Spatially localized structures in the natural world . . . . .	2
1.2 Snaking bifurcation diagrams . . . . .	5
1.3 A brief history of mathematical approaches . . . . .	10
1.4 Outline and overview of results . . . . .	13
<b>2 Background</b>	<b>16</b>
2.1 A motivating example . . . . .	17
2.2 A formal framework . . . . .	20
2.2.1 System structure . . . . .	20
2.2.2 Wave trains, fronts and backs . . . . .	21
2.2.3 Symmetric localized solutions: construction via “gluing” . . . . .	22
2.2.4 Solution lengths and parameter dependence . . . . .	24
2.2.5 Bifurcation structure of localized solutions . . . . .	27
2.2.6 Bifurcation structure of localized solutions with $\mathbb{Z}_2$ symmetry . . . . .	29
2.2.7 Breaking $\mathbb{Z}_2$ symmetry or variational structure . . . . .	31
<b>3 Existence of Localized Patterns</b>	<b>33</b>
3.1 Introduction . . . . .	34
3.2 The gluing construction in $\mathbb{R}^4$ . . . . .	36
3.2.1 Additional details for the construction . . . . .	46
3.3 The gluing construction in $\mathbb{R}^{2n}$ . . . . .	52
3.4 Numerical illustrations . . . . .	61
<b>4 Stability of Localized Patterns</b>	<b>65</b>
4.1 Introduction . . . . .	66
4.2 Exponential dichotomies and general approach . . . . .	68

4.3	Eigenvalues in the right half plane . . . . .	70
4.4	The translation eigenvalue at $\lambda = 0$ . . . . .	92
4.5	Special case: simple eigenvalue of the front . . . . .	94
4.6	Numerical results . . . . .	95
4.6.1	Symmetric localized solutions . . . . .	97
4.6.2	Asymmetric localized solutions . . . . .	100
<b>5</b>	<b>Embedded Eigenvalues and the Spectrum of Fronts</b>	<b>105</b>
5.1	Introduction . . . . .	106
5.2	Preliminaries . . . . .	108
5.2.1	Analyticity of Floquet representation . . . . .	110
5.2.2	Gap and conjugation lemmas with periodic coefficients . . . . .	114
5.3	Hypotheses and motivations . . . . .	119
5.3.1	A PDE system . . . . .	124
5.4	The extended Evans function . . . . .	129
5.5	The eigenvalue at $\lambda = 0$ . . . . .	133
5.5.1	Special case: symmetric localized solutions . . . . .	135
5.5.2	General localized solutions . . . . .	141
5.6	The behavior of the saddle node eigenvalue . . . . .	148
<b>6</b>	<b>Predicting the Effects of Perturbations</b>	<b>156</b>
6.1	Introduction . . . . .	157
6.2	Predicting results of breaking $\mathbb{Z}_2$ symmetry . . . . .	160
6.2.1	Dynamical reformulation of the problem . . . . .	160
6.2.2	Implications for particular forms of $z$ . . . . .	168
6.3	Full <i>a priori</i> characterization of perturbed bifurcation diagrams . . . . .	175
6.3.1	Breaking variational structure . . . . .	176
6.3.2	Breaking $\mathbb{Z}_2$ symmetry . . . . .	180
6.3.3	Breaking reversibility . . . . .	183
6.4	Numerical confirmation of predictions . . . . .	185
6.4.1	1D Swift–Hohenberg . . . . .	185
6.4.2	Planar Swift–Hohenberg . . . . .	191
<b>7</b>	<b>Conclusion</b>	<b>199</b>
<b>A</b>	<b>Foundational Theorems, Definitions and Formulae</b>	<b>202</b>
A.1	Exponential dichotomies . . . . .	203
A.2	Variation of constants with exponential dichotomies . . . . .	205
<b>B</b>	<b>Elements of Spectral Stability Analysis</b>	<b>207</b>
B.1	Setting the stage: PDE and ODE formulations . . . . .	208
B.2	The operator family $\mathcal{T}(\lambda)$ , Fredholm properties and exponential dichotomies . . . . .	210
B.3	Locating the essential spectrum . . . . .	212
B.4	Locating the point spectrum: the Evans function . . . . .	214

<b>C Further Analysis: Simple Eigenvalue of a Front</b>	<b>216</b>
C.1 Problem and system set-up . . . . .	217
C.2 Solving the fixed point equation for $\tilde{w}$ . . . . .	225
C.3 Solving for $(a, \tilde{w})$ . . . . .	228
C.4 Solving for $(a, b, \tilde{w})$ . . . . .	232
C.5 Satisfying the jump condition . . . . .	239
<b>Bibliography</b>	<b>242</b>

# List of Tables

- 6.1 Observed and calculated offsets over 8 saddle nodes, i.e., a full  $2\pi$  period of the function  $z$ , for the planar stripe and spot pattern of (4.4), with additional perturbative term  $\varepsilon G(u)$  as indicated. . . . . 193

# List of Figures

1.1	The evolution of residential burglaries over two three-month periods beginning in June 2001 in Long Beach, CA. . . . .	2
1.2	Stable multipeaked cavity soliton clusters in a driven optical cavity containing a saturable absorber. . . . .	3
1.3	A localized solution for plane Couette flow at Reynolds number 400. . . . .	4
1.4	Deflection and stress functions for localized solutions of the buckling problem described by the Kármán–Donell equations. . . . .	4
1.5	Examples of localized and domain filling patterns of vegetative growth in Israel (A), Niger (B,C) and Namibia (D). . . . .	4
1.6	Schematic of a snaking bifurcation diagram for a reversible system, including illustrative solution profiles. . . . .	5
1.7	A schematic snaking bifurcation diagram for a reversible system with additional $\mathbb{Z}_2$ symmetry, including illustrative solution profiles. . . . .	7
1.8	Examples of bifurcation diagrams corresponding to widely disparate physical systems with similar underlying mathematical structure. . . . .	8
1.9	Examples of localized patterns on the plane. The “stripes and spots” pattern (left) is localized in one spatial dimension and periodic in the other, while the hexagon patch (right) is fully localized. . . . .	9
1.10	The degenerate Hamiltonian–Hopf bifurcation, also called a reversible 1-1 resonance. . . . .	11
2.1	Illustration of a front and a back, related by $x \mapsto -x$ . . . . .	22
2.2	Possible phases $\varphi = 0, \pi$ for a localized solution invariant under $x \mapsto -x$ . . . . .	23
2.3	Solutions invariant under $u(x) \mapsto -u(-x)$ , with phases $\varphi = \frac{\pi}{2}, \frac{3\pi}{2}$ . . . . .	23
2.4	The length of a localized structure . . . . .	24
2.5	The characteristic length of a front . . . . .	25
2.6	Typical bifurcation and existence diagrams for fronts on $(\mu_1, \mu_2) \times S^1$ , where $l$ is the characteristic length of fronts and $\mu$ is a system parameter. . . . .	26
2.7	An asymmetric localized structure of length $2\bar{L}$ , which can be viewed as the result of combining a front of characteristic length $\bar{L} - \varphi$ with a back of characteristic length $\bar{L} + \varphi$ , where $\varphi$ is the phase at the midpoint of the localized structure. . . . .	28
2.8	Illustration that the function $z$ will be $\pi$ -periodic whenever the periodic orbit $v(x)$ respects both $x \mapsto -x$ and $u \mapsto -u$ symmetries. . . . .	30

2.9	A high-level summary of the effects of breaking $\mathbb{Z}_2$ symmetry, variational structure, or both. Perturbations breaking reversibility can also be overlaid on each of these, and are discussed in Section 6.3.3.	31
3.1	A schematic view of the analytic gluing construction.	35
3.2	A three-dimensional schematic view of the analytic gluing construction, including the manifolds and sections of interest.	41
3.3	Bifurcation diagram and selected planar stripes and spots solutions in the cubic-quintic planar Swift–Hohenberg equation, illustrating the gluing construction for asymmetric solutions along a cross-connecting branch.	62
3.4	Bifurcation diagram and selected planar stripes and spots solutions in the cubic-quintic planar Swift–Hohenberg equation, illustrating the gluing construction for asymmetric solutions along a self-connecting branch.	63
4.1	Schematic diagrams of spectra for the front and pulse solutions. $\Sigma_{ess}^0$ refers to the essential spectrum of the trivial state, and $\Sigma_{ess}^\gamma$ and $\Sigma_{abs}^\gamma$ to the essential and absolute spectra of the patterned state. The crosses indicate individual eigenvalues.	67
4.2	Selected branches in the bifurcation diagram for stripe and spot patterns, showing the three branches of solutions whose spectra will be analyzed in the following.	96
4.3	Eigenvalues for symmetric localized solutions along one period of the $\mathcal{R}$ -symmetric snaking branch, with $\text{Re } \lambda$ plotted as a function of the cumulative change in $\mu$ .	98
4.4	Eigenvalues for symmetric localized solutions, with eigenvalues for corresponding fronts overlaid along one period of a snaking branch.	98
4.5	Detail of the top left quadrant of Figure 4.4, focusing on the leading eigenvalues for the first unstable portion of the symmetric branch.	99
4.6	Eigenvalues for asymmetric localized solutions along a cross-connecting branch, with $\text{Re } \lambda$ plotted as a function of the cumulative change in $\mu$ .	101
4.7	Eigenvalues for asymmetric localized solutions along a cross-connecting branch, with eigenvalues for corresponding fronts and backs overlaid.	101
4.8	Detail of Figure 4.7, focusing on the leading eigenvalues.	102
4.9	Eigenvalues for asymmetric localized solutions along a self-connecting branch, with $\text{Re } \lambda$ plotted as a function of the cumulative change in $\mu$ .	102
4.10	Eigenvalues for asymmetric localized solutions along self-connecting branch, with eigenvalues for corresponding fronts and backs overlaid.	103
4.11	Detail of Figure 4.10, focusing on the leading eigenvalues.	104
5.1	Spatial (Floquet) eigenvalues for the ODE corresponding to the PDE eigenvalue problem for the periodic solution.	106
5.2	Spatial eigenvalues closest to the origin, labeled as functions of $\lambda$ and of $\gamma$ .	107
5.3	Schematic depiction of the regions the complex $\gamma$ and $\lambda$ planes where we have a simple root in $\lambda$ near zero.	136
5.4	Numerical illustration of the scaling $\mu \propto \lambda^2$ of the saddle node eigenvalue along a branch of asymmetric stripes and spots solutions in the planar cubic-quintic Swift–Hohenberg equation.	152

6.1	<i>Left:</i> Schematic of the bifurcation diagram for the unperturbed system (1.2) with $\varepsilon = 0$ . <i>Right:</i> Schematic of the bifurcation diagram for a perturbed system as in (1.2) with $\varepsilon \neq 0$ . . . . .	158
6.2	Different renderings of the bifurcation diagram for a system characterized by $z$ possessing exactly one maximum and one minimum per period. . . . .	161
6.3	Bifurcation diagram for a system as in Figure 6.2a after $\kappa$ symmetry breaking. On the left is the interpretation of the branches as zero energy solutions of a Hamiltonian system, as in Figure 6.2b; in the center is the same diagram without the vector field interpretation; and on the right the branches are shown in the $(\mu = z(L + \varphi), L)$ plane. . . . .	169
6.4	Bifurcation structure of a system characterized by $\pi$ -periodic $z$ possessing two distinct maxima per period. . . . .	171
6.5	Bifurcation structure of the system illustrated in Figure 6.4, after the addition of a $\kappa$ symmetry breaking perturbative term causing the sign of $Z$ to be the same at adjacent local extrema. . . . .	172
6.6	Symmetry breaking with the opposite relative movement of adjacent local extrema from that displayed in Figure 6.5. . . . .	174
6.7	Four successive saddle nodes, i.e., one full $2\pi$ -period along the snaking $\mathcal{R}$ -symmetric branch, for the one-dimensional Swift–Hohenberg equation without perturbation. . . . .	186
6.8	The same four successive saddle nodes as in Figure 6.7, but now showing the pointwise product of the eigenfunction $v(x)$ with $u(x)$ , $u^2(x)$ , and $u^4(x)$ . . . . .	187
6.9	<i>Left:</i> Bifurcation diagram for the one-dimensional cubic–quintic Swift–Hohenberg equation, with $\varepsilon = 0$ . <i>Right:</i> $\frac{dc}{d\varepsilon}$ for the perturbation $G(u) = u_x^2$ , computed along the unperturbed branches shown at left . . . . .	188
6.10	<i>Left:</i> Bifurcation diagram for (4.1) with $G(u) = u_x^2$ , and $\varepsilon = 0.01$ . <i>Right:</i> Numerically observed and computed drift speeds. . . . .	188
6.11	Value of $\tau$ at which transition from snaking to isolas occurs as a function of $\nu$ , as predicted from the unperturbed bifurcation diagram, along with partial bifurcation diagrams for (4.3) with $\varepsilon = 0.01$ at particular values of $\nu$ and $\tau$ , confirming predictions. . . . .	192
6.12	Comparison of numerically computed bifurcation diagrams for (4.5) and (4.6) with predicted bifurcation diagrams according to the analysis in Section 6.2. Vertical lines indicate the correspondence between the extrema (saddle nodes) of the $\mathcal{R}$ -symmetric branch and the saddle nodes of the asymmetric branches, including the isola. . . . .	194
6.13	Several views of the isola for (4.5) with $\varepsilon = -0.01$ along with the original ( $\varepsilon = 0$ ) $\kappa\mathcal{R}$ -symmetric branch and the original ( $\varepsilon = 0$ ) self-connecting asymmetric branch, illustrating its construction via combination of $\kappa\mathcal{R}$ -symmetric and asymmetric branches. . . . .	196
6.14	Comparison of predicted and observed speeds for stripe and spot solutions to (4.7). The left panel corresponds to a self-connecting asymmetric branch, while the right panel corresponds to a cross-connecting asymmetric branch. . . . .	196
6.15	Computed speed via numerical continuation along a newly formed isola, and predicted speeds from the appropriate original asymmetric branch and relevant portion of the $\kappa\mathcal{R}$ -symmetric branch, for the system (4.8) with $\varepsilon = 0.01$ . . . . .	197

# CHAPTER ONE

---

## Introduction



**Figure 1.1:** The evolution of residential burglaries over two three-month periods beginning in June 2001 in Long Beach, CA. These localized structures are referred to as crime hotspots [61].

## 1.1 Spatially localized structures in the natural world

Spatially localized structures—roughly, those in which one type of pattern with a finite spatial range is embedded within a second background state—appear in a wide variety of physical contexts, including crime hotspots [40, 61], plane Couette flow [60], optical cavity solitons [44], cellular buckling [27], and vegetation patterns [45]. We will be particularly interested in localized structures consisting of an oscillatory pattern with finite spatial range, appearing within a homogeneous background state, as may be seen in all of these systems.

In Figure 1.1 we show the evolution of a crime "hotspot," using actual data on residential burglaries in Long Beach, CA [61]. Figure 1.2 shows examples of stable multi-peaked cavity solitons, as found in [44]. A localized solution found numerically for plane Couette flow, as described by the incompressible Navier–Stokes equations,

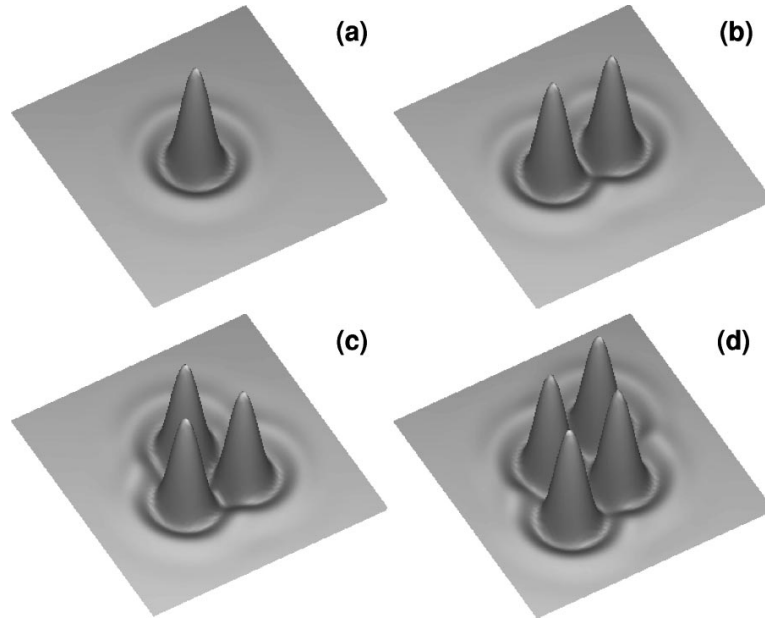


**Figure 1.2:** Stable multip peaked cavity soliton clusters in a driven optical cavity containing a saturable absorber [44].

is shown in Figure 1.3 [60]. Localized buckling structures are shown in Figure 1.4, reproduced from [27]. Finally, in Figure 1.5 we show various patterns of vegetation growth, as depicted in [45].

In fact, these systems comprise only a small subset of those in which localized structures have been observed. We refer to [2, 5, 6, 13, 52] for additional physical settings supporting localized structures, including liquid crystals, magnetoconvection, current filaments in a driven semiconductor-gas discharge system, and so on. The review articles [15, 35, 36] contain an even larger selection of examples and references.

In the following, we will be particularly interested in spatially localized structures that are stationary in time, though in Chapter 6 we also consider spatially localized structures that move with constant speed.

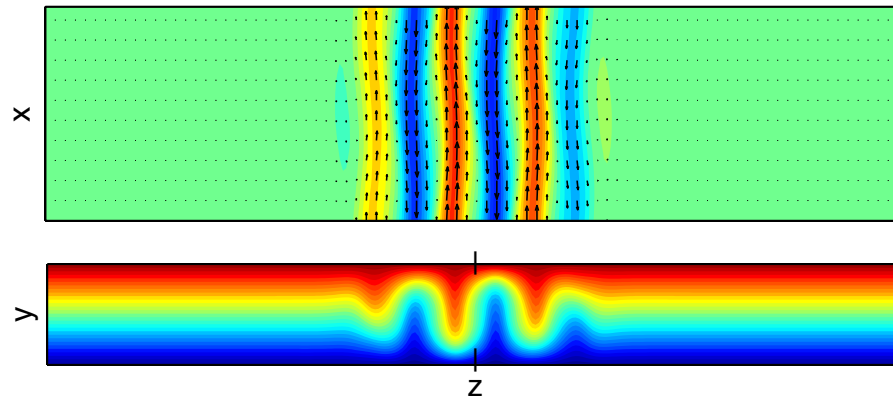


**Figure 1.3:** A localized solution for plane Couette flow at Reynolds number 400. The top figure shows the velocity field in the  $y = 0$  midplane, with arrows indicating in-plane velocity and the color scale streamwise velocity. The bottom figure shows the  $x$ -averaged streamwise velocity [60].

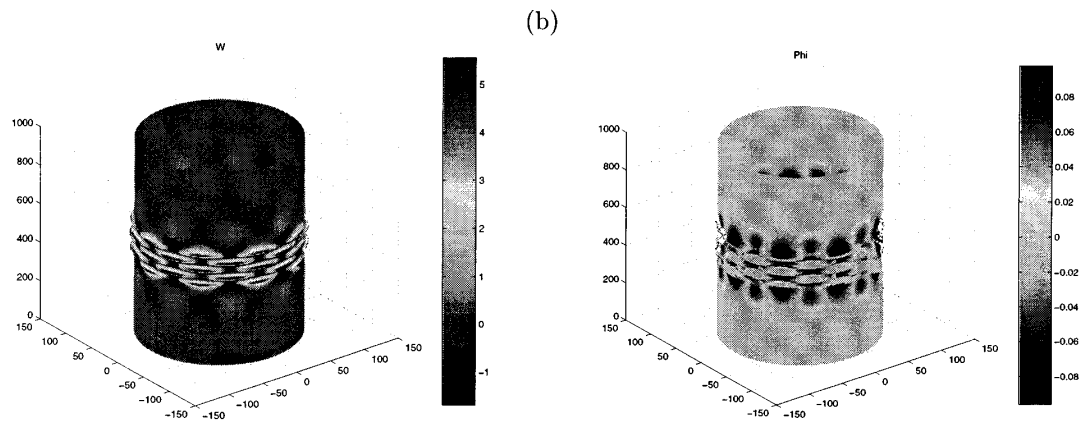


**Figure 1.4:** Deflection (left) and stress functions (right) for localized solutions of the buckling problem described by the Kármán–Donell equations [27].

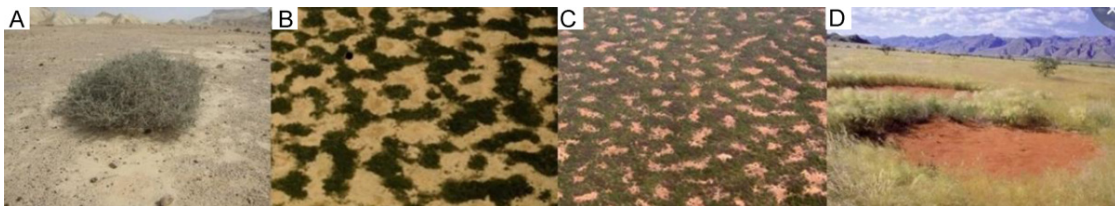


**Figure 1.5:** Examples of localized and domain filling patterns of vegetative growth in Israel (A), Niger (B,C) and Namibia (D) [45].

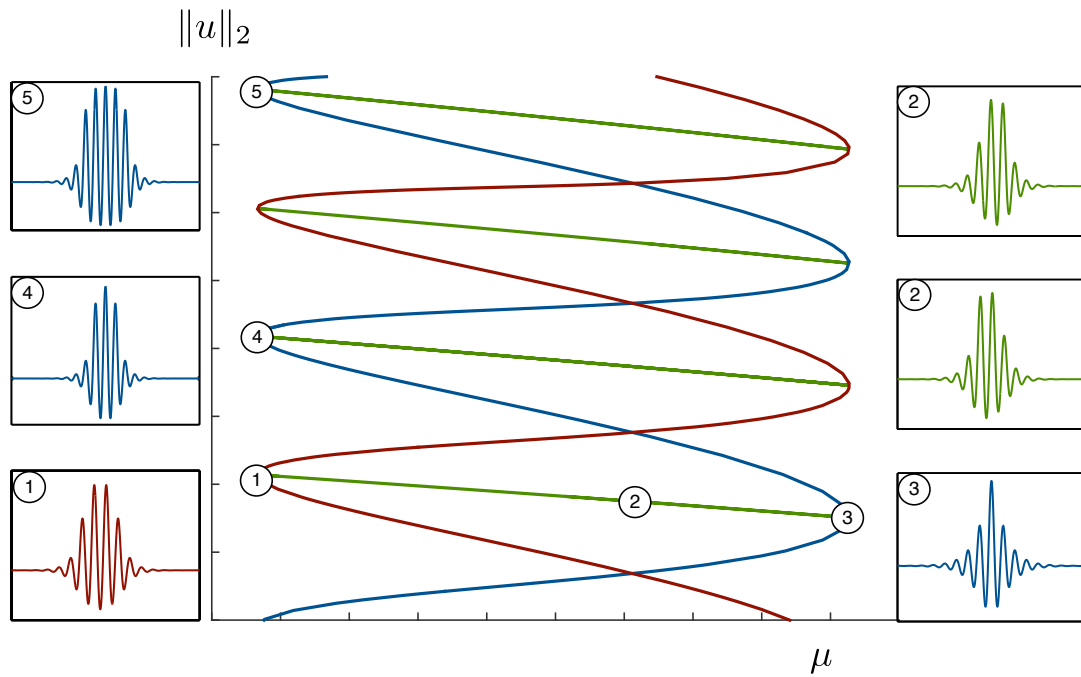


**Figure 1.6:** A schematic snaking bifurcation diagram for a reversible system, including illustrative solution profiles. The blue branch corresponds symmetric solutions with a maximum in the center, while the red branch corresponds to symmetric solutions with a minimum in the center, and each green branch corresponds to a pair of asymmetric solutions related by the reverser  $\mathcal{R}$ .

## 1.2 Snaking bifurcation diagrams

The bifurcation diagrams for localized structures in disparate systems have proven to be remarkably similar, often exhibiting “snaking” behavior, in which a branch of symmetric solutions winds back and forth between two limits of an appropriate parameter, allowing for patterns of arbitrary spatial extent. Figure 1.6 provides a schematic illustration of a snaking bifurcation diagram for a reversible system with reverser  $\mathcal{R}$ . Here we review some of the main features of such diagrams.

In general, snaking diagrams consist of two intertwined branches of symmetric solutions, along with branches of asymmetric solutions which run between the two. At the limits of the snaking region, homoclinic solutions appear and disappear in fold

bifurcations, while asymmetric solutions bifurcate at pitchforks exponentially close to the saddle nodes. Asymmetric solution branches connecting symmetric snaking branches were discovered numerically in [8], using the Swift–Hohenberg model system in one dimension. Moving up along a symmetric snaking branch, localized structures grow by increasing the extent of the spatially periodic region between the trivial homogeneous state. Similarly, along each successive ladder branch moving up the bifurcation diagram, we find patterned regions of larger extent. We note that there are two asymmetric solutions at each point along ladder branch, which are related by the reverser  $\mathcal{R}$ .

In Figure 1.7 we show a schematic bifurcation diagram for a system possessing an additional  $\mathbb{Z}_2$  symmetry  $\kappa : u \mapsto -u$ . In this case, the snaking branch in blue consists of two  $\mathcal{R}$ -symmetric solution branches lying on top of each other in the  $(\mu, \|u\|_2)$  plane, one consisting of symmetric solutions with a central maximum and the other one of symmetric solutions with a central minimum. In other words these two solution profiles are transformed into each other by the symmetry  $\kappa$ . We note that without an additional  $\mathbb{Z}_2$  symmetry, these two solution types had formed the two intertwined snaking branches. Similarly, the red snaking branch is actually two branches of  $\kappa\mathcal{R}$ -symmetric solutions. Finally, each asymmetric ladder branch corresponds to four separate solutions, which we may write as  $u, \mathcal{R}u, \kappa u, \kappa\mathcal{R}u$ .

To illustrate the widespread nature of the snaking phenomenon, in Figure 1.8 we reproduce bifurcation diagrams from previously published work on systems describing some of the physical phenomena mentioned in Section 1.1. References are given in the caption.

We note that the bifurcation diagrams of fully localized planar patterns (as in Figure 1.9, right) can be far more complicated than those of structures which are

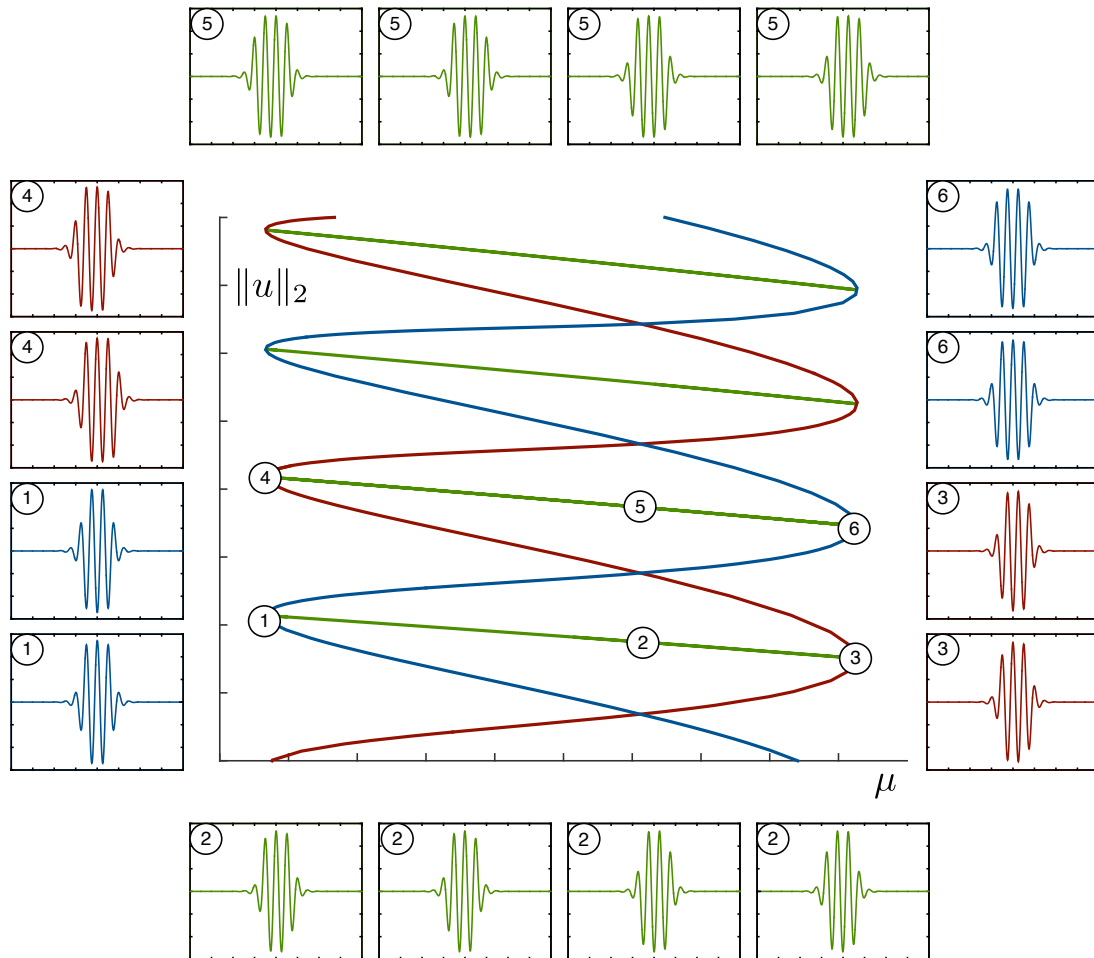


**Figure 1.7:** A snaking bifurcation diagram for a reversible system with additional  $\mathbb{Z}_2$  symmetry, including illustrative solution profiles. The blue branch corresponds to two sets of even parity solutions, with particular solutions shown at points 1 and 6. The red branch corresponds to two sets of odd parity solutions, with solutions shown at points 3 and 4. Finally, each green branch corresponds to four sets of asymmetric solutions, as shown at points 2 and 5.

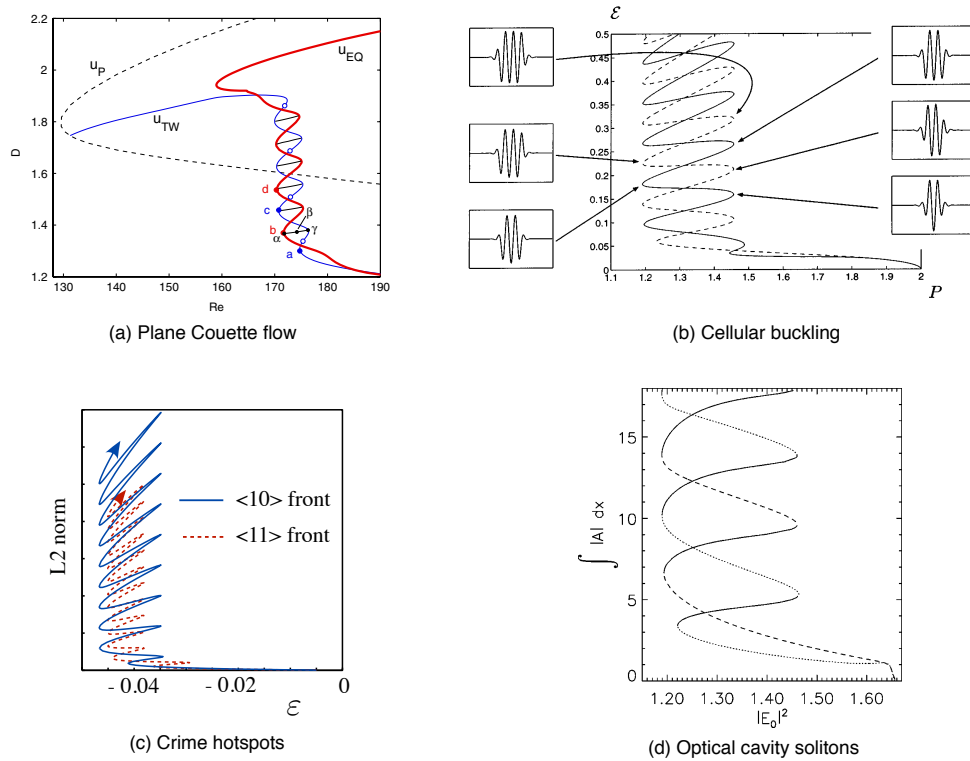


**Figure 1.8:** Examples of bifurcation diagrams corresponding to widely disparate physical systems with similar underlying mathematical structure. Figures are reproduced from published works as follows: (a) plane Couette flow [60]; (b) cellular buckling [27]; (c) crime hotspots [40]; (d) optical cavity solitons [44].

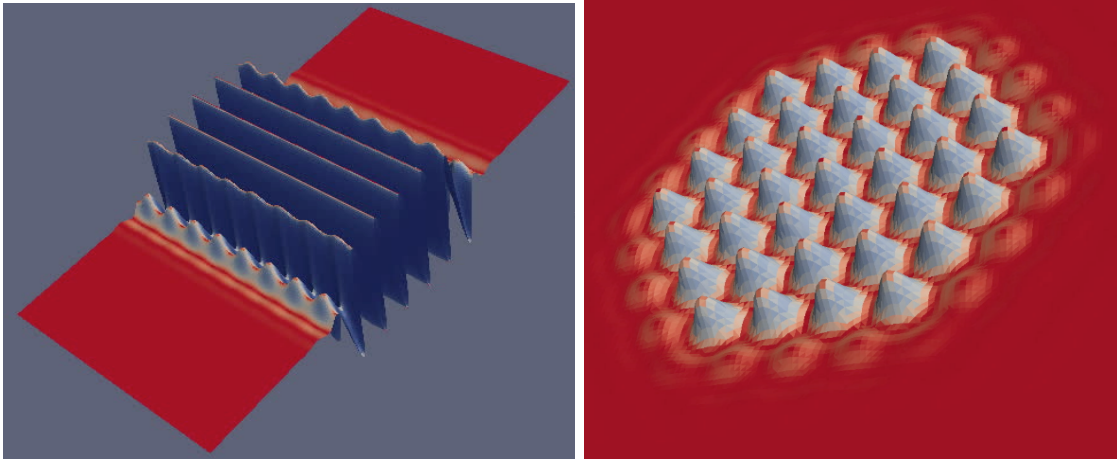


**Figure 1.9:** Examples of localized patterns on the plane. The “stripes and spots” pattern (left) is localized in one spatial dimension and periodic in the other, while the hexagon patch (right) is fully localized.

localized in one spatial direction (compare Figure 1.9, left). Extensive numerical studies of fully localized structures have been carried out in [3, 41]. In general, progress on fully localized structures in two or more dimensions is challenging, and at present there are few analytical tools available to study such structures (excluding radially symmetric solutions; in this case see, for example, [43]). We do not solve this problem here, though we comment on some work in this direction in the conclusion.

In the following, we employ a spatial dynamics approach to study the existence, uniqueness and stability of localized structures that arise as solutions to partial differential equations (PDEs). We address patterns on the line and those on the plane that are localized in one direction and periodic in the other. Rather than studying particular PDEs, we examine classes of systems which support snaking behavior, and in this context, we study existence and stability as well as the effects of various hypotheses about the underlying system in perturbative and non-perturbative regimes. Before describing our main results, we review some of the mathematical approaches previously employed in studying localized structures.

### 1.3 A brief history of mathematical approaches

Having remarked briefly on the wide range of physical systems in which localized solutions have been studied, and in a general way on the particular parameter-dependent behavior of localized solutions in which we will be interested, we now give a short (and necessarily selective!) overview of mathematical approaches to localized structures. Such structures and particular features of snaking bifurcation diagrams have attracted interest from a variety of communities for nearly 30 years.

In [53, Section 3], Pomeau first gave a heuristic argument for the existence of a finite region in which stationary fronts between two phases should exist; whereas a front between two spatially homogeneous states might be expected to move except at a particular parameter value, Pomeau argued that a stationary front between a spatially homogeneous state and a patterned region should exist for a nontrivial range of parameters, which he termed the “pinning” region. Arguing by analogy with crystal growth, Pomeau wrote “Accordingly a finite amount of disequilibrium [*sic*] between the two phases is needed to make the interface moving. . . . Thus there is a finite range of values of the control parameter around which the velocity of the interface should stay equal to zero.”

A detailed numerical study of the generalized Swift–Hohenberg equation (see Section 2.1) in one and two dimensions was undertaken in [25]. Here the authors showed the coexistence of a wide variety of patterned states in appropriate parameter regions and, using numerical integration, identified pinning regions supporting localized structures biasymptotic to a homogenous steady state. Again using a Swift–Hohenberg-type equation, [54] numerically established the existence of stable localized patterns on the plane, noting that these patterns exhibited strong hystere-

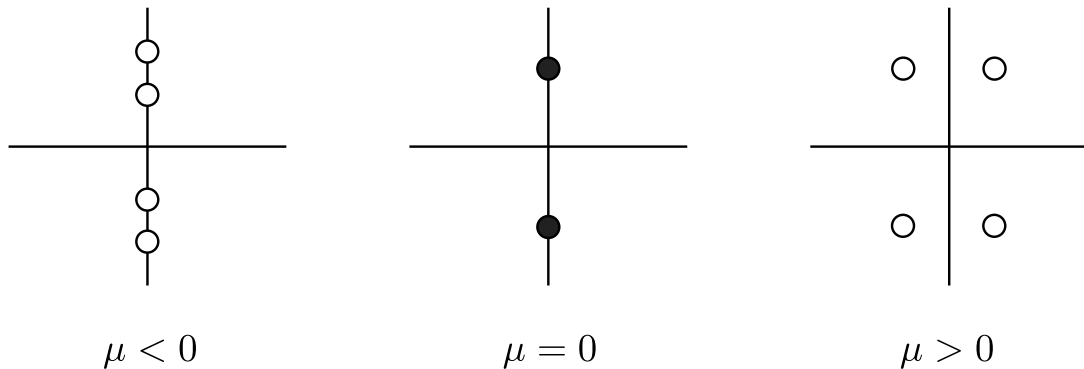


**Figure 1.10:** The degenerate Hamiltonian–Hopf bifurcation, also called a reversible 1-1 resonance. Note that the signs of the parameter  $\mu$  correspond to our parameterization of the Swift–Hohenberg equation, see (1.1) in Section 2.1, but some authors use the opposite sign convention for  $\mu$ .

sis. Moreover, the authors found many such localized patterns of varying spatial extent existing in the same parameter region, and remarked: “[w]e underscore that such a stable coexistence of stationary states with a number of different sizes is novel and has not been obtained for the other cases for which stable, spatially localized states have been reported.”

In [63], where the term “snaking” was first introduced, the unfolding of a degenerate Hamiltonian–Hopf bifurcation (also referred to as a reversible 1-1 resonance, see Figure 1.10) was studied for a fourth-order reversible ODE. This system had previously been studied [17, 28] in the context of capillary-gravity interfacial waves, in which case the sign of one of the normal form coefficients was fixed. The authors in [63] completed the analysis, and observed that resolving the one-parameter family of heteroclinic connections at a particular  $\mu = \mu_D$  suggested by the normal form analysis would require the inclusion of remainder terms breaking the phase invariance (as had, in fact, been noted by Pomeau in his original heuristic argument: “As often noted the sort of adiabatic expansion leading to (4) makes appears a spurious

phase invariance. . . . [T]his leads to the fact that those nonadiabatic phenomena are of a transcendently small order in the small parameter. That should be true for the width of the locking region in the parameter space for instance” [53]). Woods and Champneys suggested a possible unfolding in which the degenerate family of heteroclinic orbits breaks up into two heteroclinic tangencies for nearby values of  $\mu$ , which they illustrated using formal Poincaré sections, and further supported with numerical experiments. The “sister” paper [27] to this one further noted the subtly different bifurcation diagram obtained upon inclusion of an additional  $\mathbb{Z}_2$  symmetry, as described in the previous section.

At about the same time, [12] gave an early explanation of the appearance of stationary localized structures in variational and non-variational reversible PDEs. The authors employed a geometric spatial dynamics approach, noting the existence of a one-parameter family of periodic orbits,  $P_\lambda$ , as a consequence of reversibility, and employing Poincaré maps to explain the appearance of homoclinic orbits to a fixed point,  $A$ , assuming the existence of transverse intersections of the unstable manifold  $W^u(A)$  and the stable manifold  $W^s(P)$ . A global PDE bifurcation diagram was deduced, plotting the wave speed  $c$  of the localized solutions as a function of the parameter  $\lambda$ , and indicating the nontrivial region in which the wave speed  $c$  is identically 0.

The issue of the  $S^1$  symmetry in the normal form studied in [63] and later in [8] was finally resolved by an asymptotics beyond all orders analysis [9, 38], which identified the the  $\varphi = 0$  and  $\varphi = \pi$  phases near the codimension-two point  $(\mu, \nu) = (0, \sqrt{27/38})$  of the Swift–Hohenberg equation (see Section 2.1; note that the Hamiltonian–Hopf bifurcation occurs at  $\mu = 0$  for all  $\nu$ , and switches from supercritical to subcritical at  $\nu = \sqrt{27/38}$ ). The second of these papers [9] further identified the asymmetric solutions appearing at pitchfork bifurcations exponentially close to

the saddle node bifurcations.

A rigorous spatial dynamics approach was developed in [4] to explain the origin of the symmetric and asymmetric solution branches in snaking bifurcation diagrams, assuming the existence of fronts satisfying certain nondegeneracy conditions, as captured by assumptions on the intersections of appropriate manifolds. This analysis did not require closeness to a Hamiltonian–Hopf bifurcation, and in fact allowed for more complicated front structures. It is this approach that we will extend in the following.

## 1.4 Outline and overview of results

We begin in Chapter 2 by introducing the Swift–Hohenberg equation, which provides motivation for our analytical results, and which we will use throughout for numerical computations illustrating our results. We also provide intuitive arguments as to how the existence and stability of localized snaking patterns can be understood from the perspective of combining fronts and backs. This is intended to motivate our later results rather than rigorously describe a particular system, but we believe it indicates the broad applicability of our rigorous formulation. It also provides an easy point of entry for results on localized patterns in non-conservative, non-reversible, and non-symmetric perturbative settings, which are covered in Chapter 6.

Following the background and framework developed in Chapter 2, in Chapter 3 we prove an analytic gluing result that encompasses both asymmetric and symmetric solutions. This unified approach to the existence and uniqueness of symmetric and asymmetric localized solutions extends the results in [4]. Importantly, we prove the

exponential closeness of localized solutions to fronts and backs, which we can then use to rigorously address the stability of localized solutions.

In Chapter 4, we study the stability of localized solutions. Using the exponential closeness of the localized solutions to the fronts and backs as shown in the existence results, our results here show that temporal eigenvalues of localized solutions lying in the right half plane (outside the essential spectrum of the homogeneous solution and of the rolls) are exponentially close to eigenvalues of the associated front and back solutions, added with multiplicity. This result makes use of the roughness theorem for exponential dichotomies, and covers both symmetric and asymmetric localized solutions. We support our results with numerical computations on planar systems.

In Chapter 5, we continue our exploration of the stability of localized structures, extending our analysis into the essential spectrum of the periodic solutions via an extended Evans function [1, 31]. This involves first proving periodic versions of the gap lemma [21, 30] and conjugation lemma [46]. Here we show that for both symmetric and asymmetric localized solutions, the eigenvalue at  $\lambda = 0$  remains simple, so that taken together with our results in Chapter 4, we have a complete result on the eigenvalues of localized solutions in the close right half plane. We then make further use of the extended Evans function to analyze the behavior of the saddle node eigenvalue as it moves inside the essential spectrum of the periodic orbits.

Finally, results on perturbations are covered in Chapter 6. We show that perturbative terms breaking symmetry or variational structure affect solution profiles and overall bifurcation structure in ways which are fully predictable analytically; generally speaking, breaking reversibility or  $\mathbb{Z}_2$  symmetry leads to a rearrangement of bifurcation branches, while breaking variational structure leads to patterns that drift

with nonzero speed. We introduce expressions involving only solutions of the unperturbed system and perturbative terms evaluated at unperturbed solutions which can be used to predict *a priori* which of many topologically distinct bifurcation diagrams will emerge upon introduction of perturbative terms, as well as the drift speeds of asymmetric solutions where appropriate. We also show isolas may arise, and provide an easy way to locate them numerically. Our results are illustrated and confirmed with numerous numerical examples.

# CHAPTER TWO

---

## Background

## 2.1 A motivating example

One particular, and in some sense canonical, example of a PDE exhibiting localized snaking patterns is the Swift–Hohenberg equation:

$$U_t = -(1 + \Delta)^2 U - \mu U + \nu U^2 - U^3, \quad (1.1)$$

with  $U = U(x, t)$  or  $U(x, y, t)$  and  $x \in \mathbb{R}$  or  $(x, y) \in \mathbb{R}^2$ . The above equation is referred to as the quadratic-cubic form, due to the powers in the nonlinearity, while

$$U_t = -(1 + \Delta)^2 U - \mu U + \nu U^3 - U^5, \quad (1.2)$$

is referred to as the cubic-quintic form.

Solutions of the Swift–Hohenberg equation have been studied extensively in the pattern formation literature, in the context of both domain-filling and localized patterns. We note that both (1.1) and (1.2) are reversible under  $x \mapsto -x$ , while only (1.2) is equivariant under the  $\mathbb{Z}_2$  symmetry  $U \mapsto -U$ . Moreover, both systems admit a variational structure.

A schematic bifurcation diagram corresponding to (1.1) was given in Figure 1.6, along with sample solution profiles, while Figure 1.7 shows the bifurcation diagram and solution profiles for a system of the form (1.2).

As was first suggested by Kirchgässner [34] and is now routine, we follow a spatial dynamics approach, analyzing evolution in the spatial variable  $x$ . Since we

are looking for stationary localized solutions, we consider

$$0 = -(1 + \Delta)^2 U - \mu U + \nu U^2 - U^3. \quad (1.3)$$

When considering patterns on the line, this may then be recast as the 4-dimensional ODE

$$\begin{pmatrix} u_1 \\ u_2 \\ u_3 \\ u_4 \end{pmatrix}_x = \begin{pmatrix} 0 & 1 & 0 & 0 \\ 0 & 0 & 1 & 0 \\ 0 & 0 & 0 & 1 \\ -1 - \mu & 0 & -2 & 0 \end{pmatrix} \begin{pmatrix} u_1 \\ u_2 \\ u_3 \\ u_4 \end{pmatrix} + \begin{pmatrix} 0 \\ 0 \\ 0 \\ \nu u_1^2 - u_1^3 \end{pmatrix} \quad (1.4)$$

with  $u = (u_1, u_2, u_3, u_4)^T = (U, U_x, U_{xx}, U_{xxx})^T \in \mathbb{R}^4$ . When considering patterns on the plane which are localized in one direction ( $x$ ) and periodic in the second ( $y$ ), we take  $x \in \mathbb{R}$  and  $y \in S^1$ , and arrive at the infinite dimensional ODE

$$\begin{pmatrix} u_1 \\ u_2 \\ u_3 \\ u_4 \end{pmatrix}_x = \begin{pmatrix} 0 & 1 & 0 & 0 \\ 0 & 0 & 1 & 0 \\ 0 & 0 & 0 & 1 \\ -(1 + \partial_y^2)^2 - \mu & 0 & -2(1 + \partial_y^2) & 0 \end{pmatrix} \begin{pmatrix} u_1 \\ u_2 \\ u_3 \\ u_4 \end{pmatrix} + \begin{pmatrix} 0 \\ 0 \\ 0 \\ \nu u_1^2 - u_1^3 \end{pmatrix} \quad (1.5)$$

with  $u = (u_1, u_2, u_3, u_4)^T = (U, U_x, U_{xx}, U_{xxx})^T \in H^3(S^1) \times H^2(S^1) \times H^1(S^1) \times L^2(S^1)$ .

In Chapter 3 we show how locally, i.e., away from bifurcation points, all the results formulated in [4] may be understood via a single matching procedure, so that we get existence of both symmetric and asymmetric solutions from the same result.

Having found a particular localized solution  $U_\ell(x)$  or  $U_\ell(x, y)$  of (1.1), we are then interested in its stability. This may be addressed by considering the eigenvalue problem

$$\lambda U = -(1 + \Delta)^2 U - \mu U + (2\nu U_\ell - 3U_\ell^2)U. \quad (1.6)$$

Again this may be reformulated as the ordinary differential equation

$$\begin{aligned} \begin{pmatrix} u_1 \\ u_2 \\ u_3 \\ u_4 \end{pmatrix}_x &= \begin{pmatrix} 0 & 1 & 0 & 0 \\ 0 & 0 & 1 & 0 \\ 0 & 0 & 0 & 1 \\ -1 - \mu + 2\nu U_\ell(x) - 3U_\ell(x)^2 & 0 & -2 & 0 \end{pmatrix} \begin{pmatrix} u_1 \\ u_2 \\ u_3 \\ u_4 \end{pmatrix} \\ &+ \lambda \begin{pmatrix} 0 & 0 & 0 & 0 \\ 0 & 0 & 0 & 0 \\ 0 & 0 & 0 & 0 \\ -1 & 0 & 0 & 0 \end{pmatrix} \begin{pmatrix} u_1 \\ u_2 \\ u_3 \\ u_4 \end{pmatrix} \end{aligned} \quad (1.7)$$

Writing (1.4) as  $u_x = f(u, \mu, \nu)$ , we note that (1.7) can be written as

$$u_x = f_u(u_\ell, \mu, \nu)u + \lambda B u. \quad (1.8)$$

Similarly the planar case may be formulated as

$$\begin{aligned} \begin{pmatrix} u_1 \\ u_2 \\ u_3 \\ u_4 \end{pmatrix}_x &= \begin{pmatrix} 0 & 1 & 0 & 0 \\ 0 & 0 & 1 & 0 \\ 0 & 0 & 0 & 1 \\ -(1 + \partial_y^2)^2 - \mu + 2\nu U_\ell(x, y) - 3U_\ell(x, y)^2 & 0 & -2(1 + \partial_y^2) & 0 \end{pmatrix} \begin{pmatrix} u_1 \\ u_2 \\ u_3 \\ u_4 \end{pmatrix} \\ &+ \lambda \begin{pmatrix} 0 & 0 & 0 & 0 \\ 0 & 0 & 0 & 0 \\ 0 & 0 & 0 & 0 \\ -1 & 0 & 0 & 0 \end{pmatrix} \begin{pmatrix} u_1 \\ u_2 \\ u_3 \\ u_4 \end{pmatrix}, \end{aligned} \quad (1.9)$$

which again is of the form (1.8). This is our starting point for Chapter 4.

## 2.2 A formal framework

*We note that this material, along with the results in Chapter 6, has been published in [42]. We further note that when we use  $u(x)$  in the following, we have in mind a solution of a PDE system. Elsewhere we will typically use lower case variables for ODE systems.*

Our aim in this section is to link the rigorous spatial dynamics analysis, as developed in [4] and extended in this thesis, to a formal approach that views the emergence of localized roll patterns via gluing together appropriate building blocks consisting of fronts and backs. This section is intended to provide intuition and motivate the particular hypotheses employed in the following, rather than to present precise results for a particular system.

### 2.2.1 System structure

We will begin by assuming three properties of our system: first, that it is reversible, i.e., possesses  $x \mapsto -x$  symmetry, with  $x \in \mathbb{R}$ , so that if  $u(x) \in \mathbb{R}^n$  is a solution, so is  $u(-x)$ . Second, we assume it possesses a  $\mathbb{Z}_2$  symmetry  $\kappa$ , which for simplicity we take to be  $\kappa : u \mapsto -u$ , so that if  $u(x)$  is a solution, so is  $-u(x)$ . Third, we assume that the system is variational and can be written as

$$u_t = -\nabla \mathcal{E}(u) \tag{2.1}$$

with

$$\mathcal{E}(u) = \int_{\mathbb{R}} \mathcal{L}(u(x), u_x(x), u_{xx}(x)) dx$$

(or, more generally,  $\mathcal{L} = \mathcal{L}(u, u_x, \dots, \partial_x^n u)$  for some  $n$ ). The existence of a variational structure implies that if  $u(x - ct)$  is a localized solution to (2.1), then necessarily  $c = 0$  (see Section 6.3.1 below). The variational structure also implies the existence of a spatial Hamiltonian  $H$  that is conserved pointwise along any solution  $u(x)$  of the steady state equation  $-\nabla\mathcal{E}(u) = 0$ ; see, for example, [41].

### 2.2.2 Wave trains, fronts and backs

We next assume that our system possesses wave trains, that is, spatially oscillatory solutions with nonzero minimal period. Spatial reversibility implies that wave trains should come in a one-parameter family, which we take to be parameterized by the variable  $e$ , with spatial periods  $p(e)$ . We refer to this family as  $v(x, e)$ , and assume that each member of the family is invariant under  $x \mapsto -x$ . Whenever the symmetry  $\kappa : u \mapsto -u$  is present in our system, we will assume that  $v(x, e)$  is compatible with this symmetry for each  $e$  so that  $v(-x, e) = -v(x, e)$ . Finally, for variational systems, the wave trains will generically be parameterized by  $e = H$ , the value of the spatial Hamiltonian evaluated along the wave train.

We make the further assumption that the system admits fronts, i.e., solutions evolving from a constant state to a spatially oscillatory one. More precisely, we assume that there exist steady states  $u_f(x)$  such that  $u_f(x) \rightarrow u_0$  as  $x \rightarrow -\infty$  and  $u_f(x) \rightarrow v(x)$  as  $x \rightarrow +\infty$ , where  $v(x)$  is a member of the family  $v(x, e)$ . Assuming that  $H(u_0) = 0$ , the selected periodic solution  $v(x)$  will satisfy  $e = H = 0$ . We note that we can rescale  $x$  so that  $p(0) = 2\pi$ .

In fact, we can more generally consider systems admitting solutions  $u_f(x, y)$ , where  $y \in \Omega \Subset \mathbb{R}^{d-1}$ , which satisfy  $u_f(x, y) \rightarrow w(y)$  as  $x \rightarrow -\infty$ , where  $w(y)$  is any

function independent of  $x$ , as well as  $u_f(x, y) \rightarrow v(x, y)$  as  $x \rightarrow +\infty$ , where  $v(x, y)$  is periodic in  $x$ . In essence we require only that the evolution in space occur along one dimension, perhaps after an appropriate coordinate transformation. For simplicity in this section we write solutions as  $u(x)$ , but in subsequent sections we will use the more general formulation both analytically and numerically.

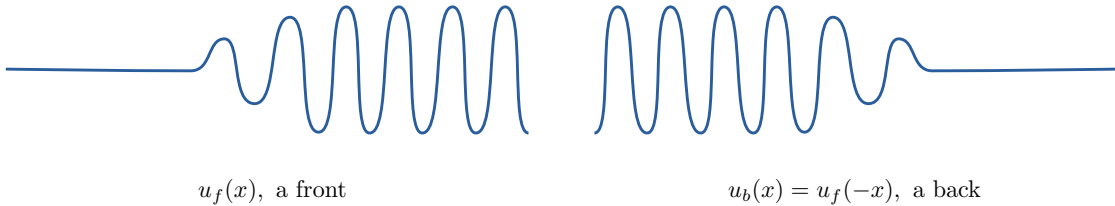


**Figure 2.1:** Illustration of a front and a back, related by  $x \mapsto -x$ .

In the case that  $u_f(x)$  is a front,  $u_b(x) := u_f(-x)$  exists by reversibility, and is termed a back; see Figure 2.1. Since we have assumed that the limiting oscillatory solution  $v(x)$  is compatible with the  $\kappa$  symmetry, given a front solution  $u_f(x)$  we will also have the front solution  $u_{f2}(x) := -u_f(x)$ , as well as the back solutions  $u_{b1}(x) := u_f(-x)$  and  $u_{b2}(x) := -u_f(-x)$ .

### 2.2.3 Symmetric localized solutions: construction via “gluing”

We now wish to “glue” together front and back solutions to form a localized stationary solution  $u_{loc}(x)$  which is invariant under  $u(x) \mapsto u(-x)$ . Clearly this is only possible if we have a maximum or minimum at the center of the localized oscillatory structure. Defining the phase  $\varphi$  at the center of the localized solution to be the distance traveled past a maximum, and rescaling  $x$  if necessary so that the spatially oscillatory limiting solution  $v(x)$  mentioned above has period  $2\pi$ , this is equivalent

to requiring that the phase at the center of the structure satisfies  $\varphi = 0$  or  $\varphi = \pi$ ; see Figure 2.2.

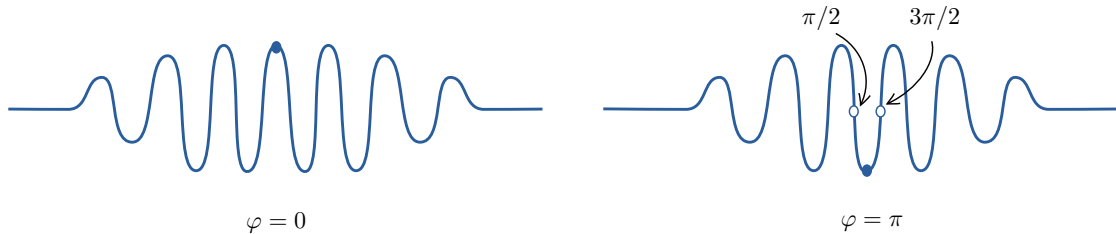


**Figure 2.2:** Possible phases  $\varphi = 0, \pi$  for a localized solution invariant under  $x \mapsto -x$ . The closed circles indicate the midpoint of the pattern, while the labels  $\frac{\pi}{2}$  and  $\frac{3\pi}{2}$  indicate the value of  $\varphi$  at the open circles.

In the case that we have the additional symmetry  $\kappa : u \mapsto -u$ , compatibility of the  $2\pi$ -periodic solution  $v_x$  with  $\kappa$  implies that  $-v(x) = v(x + \pi)$ , and we recall that the existence of a front solution  $u_f(x)$  implies the existence of the front solution  $u_{f2}(x) := -u_f(x)$  and the back solutions  $u_{b1}(x) := u_f(-x)$  and  $u_{b2}(x) := -u_f(-x)$ . Thus we can form solutions invariant under  $u(x) \mapsto -u(-x)$  by gluing a front  $u_f(x)$  to a back  $u_{b2} = -u_f(-x)$  with phase  $\varphi = \frac{\pi}{2}$  or  $\varphi = \frac{3\pi}{2}$ ; see Figure 2.3.

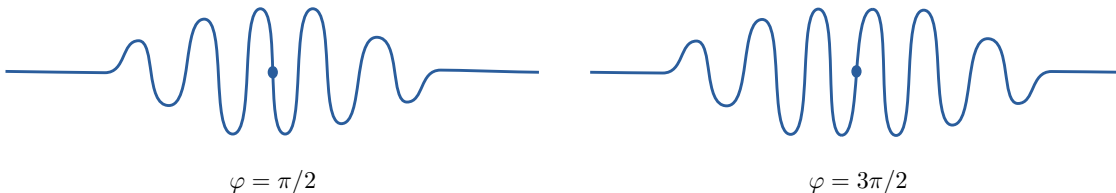


**Figure 2.3:** Solutions invariant under  $u(x) \mapsto -u(-x)$ , with phases  $\varphi = \frac{\pi}{2}, \frac{3\pi}{2}$ .

Moving forward, we will refer to solutions invariant under  $u(x) \mapsto u(-x)$  as symmetric, or  $\mathcal{R}$ -symmetric. In the case that the system possesses the additional  $\kappa : u \mapsto -u$  symmetry, we will also refer to solutions invariant under  $u(x) \mapsto -u(-x)$  as symmetric, or  $\kappa\mathcal{R}$ -symmetric. Any localized solution which is not invariant under either of these operations will be called asymmetric.

## 2.2.4 Solution lengths and parameter dependence

To this point, we have not considered the role of parameters in our system. If we only had one “type” of front present, which is to say all front solutions could be mapped to each other via a translation in  $x$ , then we would only be able to get symmetric localized states in lengths of multiples of  $2\pi$  (or, if  $u \mapsto -u$  symmetry is present, in multiples of  $\pi$ ); see Figure 2.4. If, however, we can define a characteristic length of fronts such that the length of the fronts present in our system varies continuously with a parameter, then our system will typically admit localized symmetric solutions of arbitrary length via parameter variation.

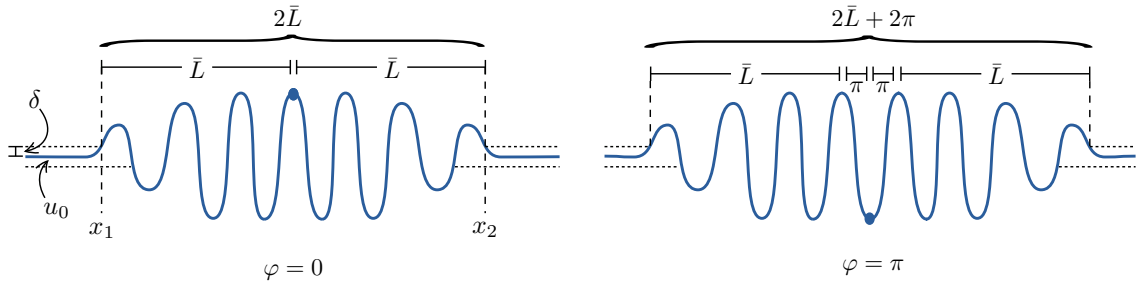


**Figure 2.4:** The length of a localized structure, measured as the distance between the largest  $x$ , labeled  $x_1$ , such that  $|u(x) - u_0| < \delta$  for all  $x < x_1$ , and the smallest  $x$ , labeled  $x_2$  such that  $|u(x) - u_0| < \delta$  for all  $x > x_2$ , for some fixed tolerance  $\delta$ .

We pause here to consider the notion of length. Although there is a natural and rigorous way to measure these lengths in a dynamical systems setting, using Poincaré sections near the oscillatory solution, we will not aim at fully rigorous definitions and instead suggest an approximate measurement using only the solution profiles. Specifically, we will make use of two distinct lengths: first, the *length of a localized structure* is the extent of the region where our localized solution lies near the oscillatory solution. We will generally denote this by  $2\bar{L}$ , since we are usually interested in half this length. To measure the length of a localized oscillatory solution, we can look at the difference between the largest  $x$ , called  $x_1$  in Figure 2.4,

such that  $u_{loc}(x)$  is within some tolerance of the constant solution, and the smallest  $x$ , called  $x_2$  in Figure 2.4, such that it is again within this tolerance. Alternatively, assuming  $u_0 = 0$ , we can use the  $L^2$  norm of the whole localized solution. The former measurement is more natural for theoretical development, while the latter is more convenient for numerically computed bifurcation diagrams, but fundamentally both capture the same information.

Second, the *characteristic length of a front*, which we denote by  $l$  and define modulo  $2\pi$ , corresponds to the length of the interface region between the constant and oscillatory solution measured to a peak, modulo  $2\pi^1$ . That is, we look at the difference between the largest  $x$  such that  $u_{loc}(x)$  is within some tolerance of the constant solution to the smallest  $x$  corresponding to a peak (i.e.,  $u'(x) = 0$ ,  $u''(x) < 0$ ) within some tolerance of the amplitude of the limiting oscillatory solution  $v(x)$ ; see Figure 2.5. Again, assuming  $u_0 = 0$ , we can also measure this via the  $L^2$  norm of the portion of a front lying to the left of an oscillatory peak within some tolerance of the maximum amplitude.

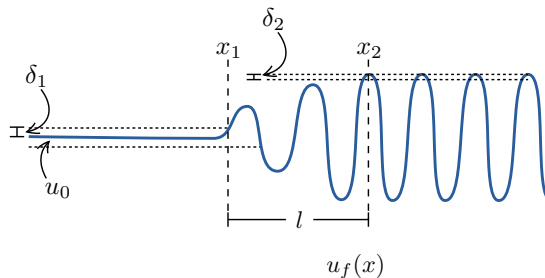


**Figure 2.5:** The characteristic length of a front for some fixed tolerances  $\delta_1$  and  $\delta_2$ , measured as the distance between the largest  $x$ , labeled  $x_1$ , such that  $|u(x) - u_0| < \delta_1$  for all  $x < x_1$ , and the smallest  $x$ , labeled  $x_2$ , such that  $u'(x_2) = 0$ ,  $u''(x_2) < 0$ , and  $|u(x_2) - v(x_*)| < \delta_2$ , where  $v(\cdot)$  is the limiting oscillatory solution, and  $v(x_*)$  has phase  $\varphi = 0$ .

Having established these two types of length, and approximately how to measure

<sup>1</sup>Note that we are assuming all fronts connect to oscillatory solutions with the same period, which we normalize without loss of generality to  $2\pi$ . In the case that the underlying periods of the oscillatory are distinct, we can rescale  $x$  in a  $\mu$ -dependent fashion to ensure that each has period  $2\pi$ .

them, we finally wish to include dependence on a system parameter  $\mu$ . In general, fronts will come locally in branches (smooth solution curves) as the only steady-state bifurcations they typically undergo in 1-parameter systems are saddle node bifurcations (possibly after ignoring bifurcations caused by symmetry breaking in the transverse  $y$ -direction.) If we assume that fronts exist only for  $\mu \in (\mu_1, \mu_2)$ , then plotting  $(\mu, l)$  along the branch of fronts, we obtain typical bifurcation or existence diagrams as shown in Figure 2.6. On the cylinder  $(\mu_1, \mu_2) \times S^1$  (recall the characteristic length  $l$  of fronts is taken modulo  $2\pi$ ), the connected branch containing our front solution can have any one of these forms, as well as others not shown in Figure 2.6.

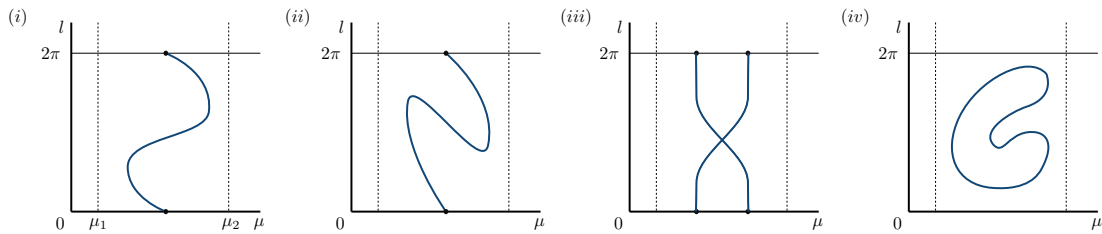


**Figure 2.6:** Typical bifurcation and existence diagrams for fronts on  $(\mu_1, \mu_2) \times S^1$ , where  $l$  is the characteristic length of fronts and  $\mu$  is a system parameter.

Though the approach outlined below applies to all of these, we will assume for the sake of clarity that each  $l$  corresponds to a unique  $\mu$ , so that the branch on  $(\mu_1, \mu_2) \times S^1$  can be written as  $\mu = z(l)$  with  $l \in [0, 2\pi]/\sim$  for some function  $z$ , as illustrated in Figure 2.6(i). We can extend the function  $z$  to all of  $\mathbb{R}$  by considering the argument modulo  $2\pi$ . We will generally write  $z(L)$  to indicate the extended version.

### 2.2.5 Bifurcation structure of localized solutions

Now suppose we have a symmetric localized structure of length  $2\bar{L}$  with maximum in the center, i.e., with phase  $\varphi = 0$ . Such a structure may be formed from a front of characteristic length  $l = \bar{L} \bmod 2\pi$  and a back of the same characteristic length, so that such a solution exists for  $\mu = z(\bar{L})$ . On the other hand, a symmetric localized structure of length  $2\bar{L}$  with minimum in the center (phase  $\varphi = \pi$ ) is formed from a front of characteristic length  $(\bar{L} - \pi) \bmod 2\pi$  and a back of characteristic length  $(\bar{L} + \pi) \bmod 2\pi$ , so that such a solution exists for  $\mu = z(\bar{L} + \pi)$ ; recall here that  $z$  is  $2\pi$ -periodic so that  $z(\bar{L} + \pi) = z(\bar{L} - \pi)$ . Consequently, in a bifurcation diagram displaying the length ( $L^2$  norm) of a localized solution versus parameter  $\mu$ , the curve  $\mu = z(\bar{L})$  will be the branch of symmetric localized solutions with maxima in the center, while the branch of solutions with minima in the center will be given by  $\mu = z(\bar{L} + \pi)$ . The resulting bifurcation diagram of symmetric branches for  $z$  as given in Figure 2.6(i) therefore consists of snaking branches which are intertwined in the sense of Figure 1.6.

Turning to asymmetric solutions, suppose we have a localized structure of length  $2\bar{L}$ , and again define the phase  $\varphi$  at the midpoint to be the distance past the nearest maximum on the left. Such a structure is formed from a front of characteristic length  $(\bar{L} - \varphi) \bmod 2\pi$  and a back of characteristic length  $(\bar{L} + \varphi) \bmod 2\pi$ ; see Figure 2.7.

Thus we can have a localized structure of length  $2\bar{L}$  and phase  $\varphi$  if and only if  $\mu = z(\bar{L} + \varphi)$  and  $\mu = z(\bar{L} - \varphi)$ , requiring in particular that  $z(\bar{L} + \varphi) = z(\bar{L} - \varphi)$ . In other words, a localized structure of length  $2\bar{L}$  can exist at a particular  $\mu$  if and only if there exists a  $\varphi$  such that  $\mu = z(\bar{L} + \varphi) = z(\bar{L} - \varphi)$ . Of course, if we have a localized structure  $u(x)$  of length  $2\bar{L}$  for some  $\mu$ , we will also have a localized structure  $u(-x)$  with length  $2\bar{L}$  at this  $\mu$ , so that in a bifurcation diagram plotting solution length or

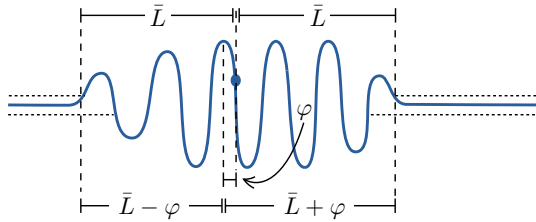


**Figure 2.7:** An asymmetric localized structure of length  $2\bar{L}$ , which can be viewed as the result of combining a front of characteristic length  $\bar{L} - \varphi$  with a back of characteristic length  $\bar{L} + \varphi$ , where  $\varphi$  is the phase at the midpoint of the localized structure.

norm vs.  $\mu$ , every point along a branch of asymmetric solutions will correspond to two separate asymmetric solutions related by  $x \mapsto -x$ . This can also be understood by noting that if  $u(x)$  has phase  $\varphi$ ,  $u(-x)$  will have phase  $\tilde{\varphi} = 2\pi - \varphi$ , so that by virtue of the  $2\pi$ -periodicity of  $z$ ,  $\mu = z(\bar{L} + \tilde{\varphi}) = z(\bar{L} - \tilde{\varphi})$  will be satisfied.

In summary, all solution branches can be found by determining the values of  $L$  and  $\varphi$  such that

$$Z(L, \varphi) := z(L + \varphi) - z(L - \varphi) = 0. \quad (2.2)$$

The corresponding values of  $\mu$  for which these solutions exist are determined by the relation  $\mu = z(L + \varphi)$ , which is of course equivalent to  $\mu = z(L - \varphi)$  for all  $(L, \varphi)$  such that  $Z(L, \varphi) = 0$ . In particular, since  $z$  is  $2\pi$ -periodic, we will have symmetric localized solutions for any  $L$  with  $\varphi = 0$  or  $\varphi = \pi$ , whereas asymmetric solutions will exist for particular values of  $L$  and  $\varphi \notin \{0, \pi\}$  satisfying  $Z(L, \varphi) = 0$ . The resulting bifurcation diagram of symmetric and asymmetric branches, for  $z$  as given in Figure 2.6(i), is therefore as shown in Figure 6.1: to understand the shape of the bifurcation branches, we needed only the existence of fronts,  $x \mapsto -x$  symmetry, and a relationship between the length of the interface region of fronts and a system parameter.

We now connect the function  $z$  and the bifurcation equation (2.2), obtained

here via formal gluing arguments, to the rigorous approach developed in [4] and extended here. In that paper, it was shown that symmetric and asymmetric branches correspond to solutions of a system of the form

$$Z(L, \varphi) + O(e^{-\eta L}) = 0 \tag{2.3}$$

for some constant  $\eta > 0$ : for  $L$  large enough, regular zeros of (2.2) correspond to regular zeros of (2.3), and vice versa. In particular,  $\mathcal{R}$ -symmetric solutions that spend time  $2L$  near the periodic orbit exist for points  $(\mu, L)$  with  $\mu = \mu_*(L, \varphi_0) = z(L + \varphi_0) + O(e^{-\eta L})$  for some  $\eta > 0$  with  $\varphi_0 \in \{0, \pi\}$ . Furthermore, all other single-pulse solutions that spend time  $2L$  near the periodic orbit are exponentially close in  $L$  to the set of points  $(\mu, L)$  such that  $\mu = z(L + \varphi) = z(L - \varphi)$ . Finally, it was shown in [4] that the function  $z$  appearing in (2.3) has a natural interpretation in terms of the intersection of invariant manifolds, and we will use this again in Chapter 3, where we will show that the gluing procedure outlined above is not merely a formal construction, but can be rigorously realized.

### 2.2.6 Bifurcation structure of localized solutions with $\mathbb{Z}_2$ symmetry

In the presence of a  $\mathbb{Z}_2$  symmetry  $\kappa$ , the main distinction from Section 2.2.5 above is that the function  $z$  is now automatically  $\pi$ -periodic: supposing our symmetry to be  $u \mapsto -u$ , if a front  $u(x)$  of length  $l$  exists at some parameter value  $\mu$ , then a front  $-u(x)$  with characteristic length  $(l + \pi) \bmod 2\pi$  must also exist at this  $\mu$ ; see Figure 2.8.

Thus  $z(l) = z(l + \pi)$  for all  $l$ , i.e.,  $z$  is  $\pi$ -periodic. As a consequence, the bifurcation

branch of symmetric solutions with maxima in the center will lie on top of those with minima in the center [ $z(L) = z(L + \pi)$ .] Moreover, the branches of  $\kappa\mathcal{R}$ -symmetric solutions with  $\varphi = \frac{\pi}{2}$  or  $\varphi = \frac{3\pi}{2}$  described previously will lie on top of each other for the same reason. Of course, the branches of the  $\mathcal{R}$ - and  $\kappa\mathcal{R}$ -symmetric solutions will be offset from each other by half a period, so that they have the appearance of being intertwined.

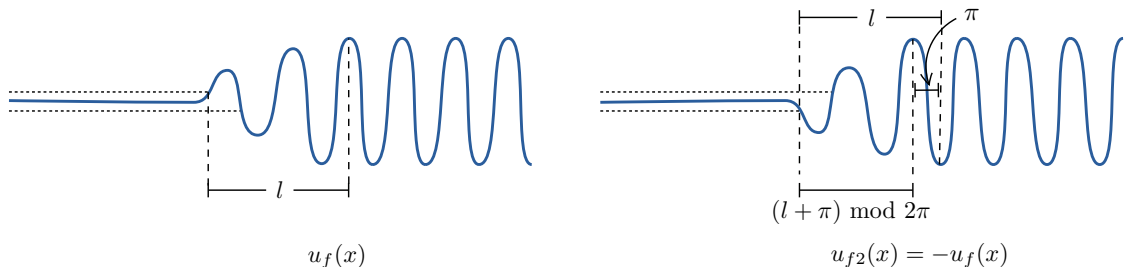


**Figure 2.8:** Illustration that the function  $z$  will be  $\pi$ -periodic whenever the periodic orbit  $v(x)$  respects both  $x \mapsto -x$  and  $u \mapsto -u$  symmetries. *Left:* A front  $u_f(x)$  with characteristic length  $l$ , which we assume exists at some  $\mu_0$ . *Right:* The front  $u_{f2}(x) := -u_f(x)$  will also exist for this  $\mu_0$ , and will have characteristic length  $l + \pi$ .

Asymmetric solutions of length  $2\bar{L}$  will again exist whenever we can satisfy  $\mu = z(\bar{L} + \varphi) = z(\bar{L} - \varphi)$ , keeping in mind that  $z$  is now  $\pi$ -periodic. Note that each point on a bifurcation branch of asymmetric solutions will now correspond to four such solutions: the “original”  $u(x)$  plus  $u(-x)$ ,  $-u(x)$  and  $-u(-x)$ . We note in passing that all of these will satisfy  $\mu = z(\bar{L} + \varphi) = z(\bar{L} - \varphi)$  for their particular  $\varphi$ , and that we will have exactly one solution with phase  $\varphi$  in each of the regions  $(0, \frac{\pi}{2}), (\frac{\pi}{2}, \pi), (\pi, \frac{3\pi}{2}), (\frac{3\pi}{2}, 2\pi)$ .

Thus, as in the case where we had only  $x \mapsto -x$  symmetry, we again see that the zero-level set of the function  $Z(L, \varphi) := z(L + \varphi) - z(L - \varphi)$  describes all bifurcation branches of localized oscillatory structures. The  $\mathcal{R}$ -symmetric solution branches are those with  $\varphi = 0$  and  $\varphi = \pi$ , while the  $\kappa\mathcal{R}$  branches correspond to  $\varphi = \frac{\pi}{2}$  and  $\varphi = \frac{3\pi}{2}$ . Both these solution types exist for all values of  $L$ . Finally, asymmetric solutions exist

only for those values of  $L$  and  $\varphi \notin \{0, \frac{\pi}{2}, \pi, \frac{3\pi}{2}\}$  such that  $Z(L, \varphi) = 0$ . See Figure 1.7 for the bifurcation diagram when  $z$  has the shape outlined in Figure 2.6(i).

Similar to the case without symmetry, these results have been derived rigorously in [4]: if a  $\mathbb{Z}_2$  symmetry  $\kappa$  is present, the function  $z$  will be  $\pi$  rather than  $2\pi$ -periodic, and two additional snaking branches with  $\kappa\mathcal{R}$  symmetry will exist for  $\mu = \mu_*(L, \varphi_0) = z(L + \varphi_0) + O(e^{-\eta L})$  for some  $\eta > 0$  with  $\varphi_0 \in \{\frac{\pi}{2}, \frac{3\pi}{2}\}$ .

## 2.2.7 Breaking $\mathbb{Z}_2$ symmetry or variational structure

We now preview the effects of adding a general reversible perturbation, which we will expand upon in Chapter 6. Figure 2.9 provides an overview of these effects at the highest level.

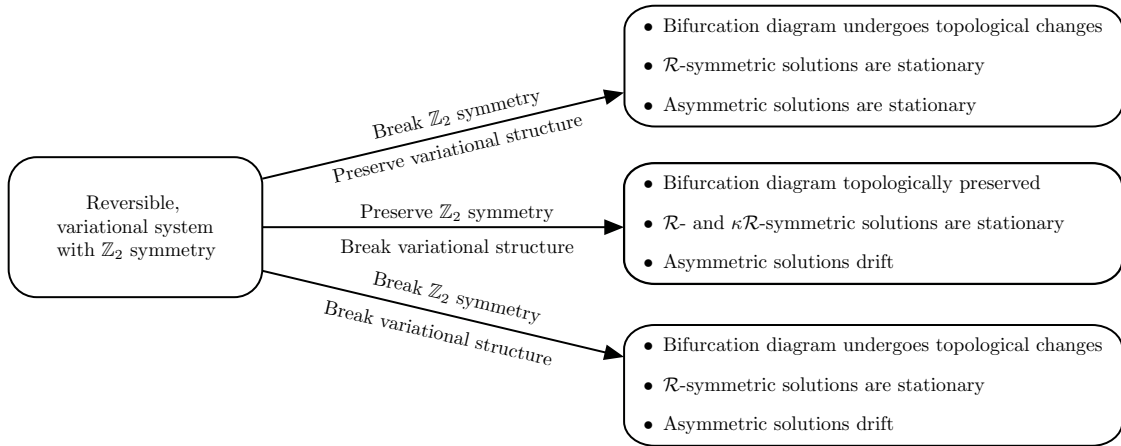


**Figure 2.9:** A high-level summary of the effects of breaking  $\mathbb{Z}_2$  symmetry, variational structure, or both. Perturbations breaking reversibility can also be overlaid on each of these, and are discussed in Section 6.3.3.

First, those parts of the perturbation that break the  $\mathbb{Z}_2$  symmetry will generically cause qualitative (topological) changes to the bifurcation diagram and underlying solution profiles, as they will induce changes in the function  $z$  and, in particular,

break its  $\pi$ -periodicity. The new form of the bifurcation diagram can be determined by solving

$$Z(L, \varphi, \varepsilon) = z(L + \varphi, \varepsilon) - z(L - \varphi, \varepsilon) = 0, \quad (2.4)$$

where  $z(\varphi, \varepsilon)$  is the  $\varepsilon$ -dependent  $z$  function. We discuss this further in Section 6.2.

Second, the nonvariational parts of the perturbation may cause localized patterns to drift: the existence of perturbed profiles and shape of the bifurcation branches is determined by (2.4); however, unless the perturbation also breaks the reversibility or  $\mathbb{Z}_2$  symmetry, we do not expect qualitative differences in the solution profiles or branch shapes. On the other hand, these perturbed solutions may travel with nonzero speed, and Lemma 6.3.1 below predicts their speed to be

$$c = -\frac{1}{\|u_x\|_{L^2}^2} \langle u_x, G(u) \rangle_{L^2}$$

along a perturbed profile  $u$ .

# CHAPTER THREE

---

## Existence of Localized Patterns

### 3.1 Introduction

In the following we provide a unified approach to the existence of both symmetric and asymmetric localized snaking solutions. Previously, in [4], an analytic gluing argument was used to show the existence of symmetric solutions; asymmetric solutions were then shown to appear at pitchfork bifurcations, and a condition was given for the continuation of these branches. A formal argument based on collective coordinates was then used to predict the stability of asymmetric solutions. Here we show how these arguments may be unified with a single, analytically rigorous approach. We begin by formulating our results for the simplest case—a dynamical system in  $\mathbb{R}^4$ . This may be motivated by considering, for example, localized solutions of the Swift–Hohenberg equation on the real line, as discussed in Chapter 2. We then extend these results to the more general case of a system in  $\mathbb{R}^{2n}$ , from which point the generalization to an infinite dimensional dynamical system, necessary for addressing patterns in the plane, is clear. We will use the existence results contained in this chapter to obtain rigorous stability results in Chapter 4.

Essentially, we show that heteroclinic connections (fronts and backs) from a fixed point at the origin to a family of periodic orbits give rise to localized solutions (homoclinic to the origin), which are symmetric if the front and back have the same phase, and asymmetric if they do not. The phase refers to the particular strong stable and unstable fibers of the periodic orbit that intersect the unstable and stable manifolds to the origin at fixed incoming and outgoing sections. Figure 3.1 gives a schematic view of our construction, in which a localized solution is constructed from a front with phase  $\varphi_1$  and a back with phase  $\varphi_2$ . The precise results are given in Theorem 3.1 on page 40 and Theorem 3.2 on page 55.

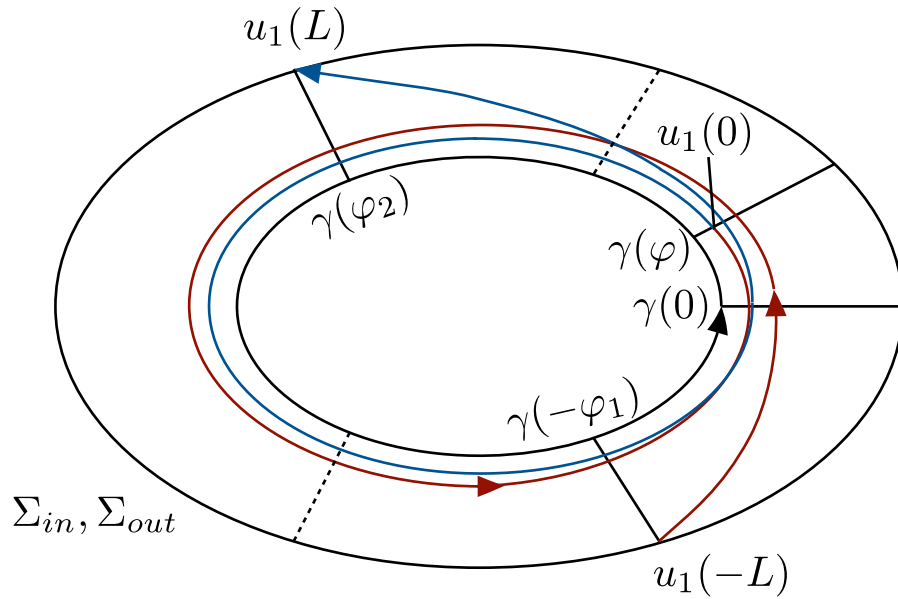


**Figure 3.1:** A schematic view of the analytic gluing construction, with the localized solution  $u_1(x)$  shown in red for  $x \leq 0$  and in blue for  $x \geq 0$ , indicating the time periods over which it remains exponentially close to the front and back, respectively. At  $x = -L$ , the localized solution  $u_1(x)$  passes through the section  $\Sigma_{in}$  exponentially close (in  $L$ ) to the point where the unstable manifold of the origin,  $W^u(0, \mu)$ , intersects the (center) stable manifold  $W^s(\gamma(x, \mu), \mu)$  of the periodic orbit in the section  $\Sigma_{in}$ ; this point is in the strong stable fiber  $W^{ss}(\gamma(-\varphi_1, \mu), \mu)$ . Meanwhile, at  $x = L$ , the localized solution  $u_1(x)$  passes through the section  $\Sigma_{out}$  exponentially close (in  $L$ ) to the point where the stable manifold of the origin,  $W^s(0, \mu)$ , intersects the (center) unstable manifold  $W^u(\gamma(x, \mu), \mu)$  of the periodic orbit in the section  $\Sigma_{out}$ ; this point is in the strong unstable fiber  $W^{uu}(\gamma(\varphi_2, \mu), \mu)$ . At  $x = 0$ , the localized solution has center coordinate  $\varphi \approx \frac{\varphi_2 - \varphi_1}{2}$ . The sections  $\Sigma_{in, out}$  are depicted in the same plane for schematic clarity. The dotted lines indicate the strong stable and unstable fibers  $W^{ss}(\gamma(-\varphi_2, \mu), \mu)$  and  $W^{uu}(\gamma(\varphi_1, \mu), \mu)$ , which, by reversibility, intersect  $W^u(0, \mu)$  and  $W^s(0, \mu)$  in the sections  $\Sigma_{in}$  and  $\Sigma_{out}$ , and give rise to the family of localized solutions  $u_2(x; k)$ . Symmetric localized solutions are formed from a front and back with the same phase ( $\varphi_1 = \varphi_2 \pmod{2\pi}$ ), while asymmetric localized solutions are formed by combining a front and back with different phases ( $\varphi_1 \neq \varphi_2 \pmod{2\pi}$ ). In this illustration,  $k = 1$  and  $m = 0$ .

## 3.2 The gluing construction in $\mathbb{R}^4$

Consider the system

$$u_x = f(u, \mu), \tag{2.1}$$

with  $u \in \mathbb{R}^4$ ,  $\mu \in \mathbb{R}$ , and we assume  $f$  is smooth (at least  $C^2$  in  $u$  and  $C^1$  in  $\mu$ ). We suppose that this is a reversible, conservative system such that the origin is hyperbolic and there exists a family of symmetric periodic orbits depending smoothly on  $\mu$ . More precisely:

**Hypothesis 3.2.1.** *There exists a linear map  $\mathcal{R} : \mathbb{R}^4 \rightarrow \mathbb{R}^4$  with  $\mathcal{R}^2 = I$  and  $\dim \text{Fix } \mathcal{R} = 2$  so that  $f(\mathcal{R}u, \mu) = -\mathcal{R}f(u, \mu)$  for all  $(u, \mu)$ .*

A solution  $u(x)$  is called **symmetric** if  $u(x) = \mathcal{R}u(-x)$  for all  $x$  or, equivalently,  $u(0) \in \text{Fix } \mathcal{R}$ .

**Hypothesis 3.2.2.** *There exists a smooth function  $\mathcal{H} : \mathbb{R}^4 \times \mathbb{R} \rightarrow \mathbb{R}$  with  $\mathcal{H}(\mathcal{R}u, \mu) = \mathcal{H}(u, \mu)$  and  $\langle \nabla_u \mathcal{H}(u, \mu), f(u, \mu) \rangle = 0$  for all  $(u, \mu)$ .*

**Hypothesis 3.2.3.** *For all  $\mu$ ,  $f(0, \mu) = 0$  and  $\text{Re } \sigma f_u(0, \mu) \subset (-\infty, \alpha^s) \cup (\alpha^u, \infty)$  for  $\alpha^s < 0 < \alpha^u$ .*

We normalize the function  $\mathcal{H}$  from Hypothesis 3.2.2 such that  $\mathcal{H}(0, \mu) = 0$  for all  $\mu$ . Moreover, due to Hypothesis 3.2.1, the spectrum of  $f_u(u, \mu)$  is invariant under multiplication by  $-1$ , so we may take  $\alpha^s = -\alpha^u$  in Hypothesis 3.2.3.

**Hypothesis 3.2.4.** *There is a closed interval  $J \subset \mathbb{R}$  with nonempty interior such that (2.1) has, for each  $\mu \in J$ , a periodic orbit  $\gamma(x, \mu)$  with minimal period  $l(\mu)$  such that:*

- (i) *The family  $\gamma(x, \mu)$  depends smoothly on  $\mu \in J$ .*

- (ii)  $\gamma(x, \mu)$  is symmetric with  $\gamma(0, \mu) \in \text{Fix } \mathcal{R}$  for all  $\mu \in J$ .
- (iii) For each  $\mu \in J$ ,  $\mathcal{H}(\gamma(x, \mu), \mu) = 0$  and  $\mathcal{H}_u(\gamma(x, \mu), \mu) \neq 0$  for one and hence all  $x$ .
- (iv)  $\gamma(x, \mu)$  has two positive, nontrivial Floquet multipliers,  $e^{\pm 2\pi\alpha(\mu)}$  with  $\alpha(\mu) > 0$  for all  $\mu \in J$ .

We assume without loss of generality that the minimal period  $l(\mu) = 2\pi$  for all  $\mu$ .

**Lemma 3.2.5.** ([4]) *Assume that Hypotheses 3.2.1—3.2.4 are met. Then there exist  $\delta > 0$ , a smooth reversible change of coordinates near  $\gamma(\cdot, \mu)$  and smooth real-valued functions  $h^c$ ,  $h_j^s$ , and  $h_j^u$ ,  $j = 1, 2$ , so that (2.1) restricted to the zero energy level set is for all  $\mu \in J$  of the form*

$$\begin{aligned}
v_x^c &= 1 + h^c(v, \mu)v^s v^u, \\
v_x^s &= -[\alpha(\mu) + h_1^s(v, \mu)v^s + h_2^s(v, \mu)v^u]v^s, \\
v_x^u &= [\alpha(\mu) + h_1^u(v, \mu)v^s + h_2^u(v, \mu)v^u]v^u,
\end{aligned} \tag{2.2}$$

where  $v = (v^c, v^s, v^u) \in \mathcal{V} := S^1 \times I \times I$  and  $I = [-\delta, \delta]$ .  $\mathcal{R}$  acts on  $v$  via

$$\mathcal{R}(v^c, v^s, v^u) = (-v^c, v^s, v^u). \tag{2.3}$$

In this coordinate system, we define the sections

$$\Sigma_{in} := S^1 \times \{v^s = \delta\} \times I, \quad \Sigma_{out} := S^1 \times I \times \{v^u = \delta\}. \tag{2.4}$$

We also define the set

$$\Gamma := \{(\varphi, \mu) \in S^1 \times J : W^s(0, \mu) \cap W^{uu}(\gamma(\varphi, \mu), \mu) \cap \Sigma_{out} \neq \emptyset\}. \quad (2.5)$$

We now assume  $\Gamma$  is the graph of a smooth function, and that locally near each heteroclitic orbit, the intersection of the stable manifold  $W^s(0, \mu)$  with the section  $\Sigma_{out}$  is also described by a smooth function.

**Hypothesis 3.2.6.** *The set  $\Gamma$  is the graph of a smooth function  $z : S^1 \rightarrow \mathring{J}$ . Furthermore, there exist an open neighborhood  $U_\Gamma$  of  $\Gamma$  in  $S^1 \times J$ , positive constants  $\epsilon, b > 0$ , and a smooth function  $g : U_\Gamma \rightarrow I$  so that*

$$\{(\varphi, v^s, \delta) \in W^s(0, \mu) \cap \Sigma_{out} : |v^s| < \epsilon, (\varphi, \mu) \in U_\Gamma\} = \{(\varphi, v^s, \delta) = (\varphi, g(\varphi, \mu), \delta) : (\varphi, \mu) \in U_\Gamma\} \quad (2.6)$$

and  $|g_\mu(\varphi, \mu)| \geq b > 0$  for all  $(\varphi, \mu) \in U_\Gamma$ .

**Lemma 3.2.7.** *([4]) There exist positive constants  $L_0$  and  $\eta$  so that the following is true for all  $L > L_0$  and  $\varphi \in S^1$ : there is a unique solution  $v(x)$  of (2.2), defined for  $x \in [-L, L]$  such that*

$$v(-L) \in \Sigma_{in}, \quad v(L) \in \Sigma_{out}, \quad v^c(0) = \varphi, \quad v(x) \in \mathcal{V} \quad \forall x \in [-L, L].$$

Furthermore, we have

$$\begin{aligned} v(-L) &= (\varphi - L + O(e^{-\eta L}), \delta, \delta e^{-2\alpha(\mu)L} (1 + O(e^{-\eta L}))) \\ v(0) &= (\varphi, \delta e^{-\alpha(\mu)L} (1 + O(e^{-\eta L})), \delta e^{-\alpha(\mu)L} (1 + O(e^{-\eta L}))) \\ v(L) &= (\varphi + L + O(e^{-\eta L}), \delta e^{-2\alpha(\mu)L} (1 + O(e^{-\eta L})), \delta). \end{aligned} \quad (2.7)$$

The solution  $v(x)$  is smooth in  $(L, \varphi, \mu)$  and the error estimates in (2.7) can be

*differentiated.*

We now show that fronts and backs, i.e., solutions that approach the homogeneous rest state in backward (respectively forward) time and the periodic orbit  $\gamma$  in forward (respectively backward) time, can be “glued” together to form both symmetric and asymmetric localized solutions. Moreover, these solutions depend continuously on the phases  $\varphi_1$  and  $\varphi_2$  of the associated fronts and backs. We start by introducing and parameterizing the front and back solutions in a convenient fashion.

For each  $\varphi \in S^1$ , we define  $u_f(x; \varphi)$  to be the solution such that

$$u_f(0; \varphi) \in \Sigma_{in} \cap W^u(0, z(\varphi)) \cap W^{ss}(\gamma(-\varphi, z(\varphi)), z(\varphi)). \quad (2.8)$$

Further defining  $u_b(x; \varphi) := \mathcal{R}u_f(-x; \varphi)$ , we have

$$u_b(0; \varphi) \in \Sigma_{out} \cap W^s(0, z(\varphi)) \cap W^{uu}(\gamma(\varphi, z(\varphi)), z(\varphi)). \quad (2.9)$$

We note that these definitions imply

$$|u_f(x; \varphi) - \gamma(x - \varphi)| \leq Ce^{-\eta x}, \quad x \geq 0 \quad (2.10)$$

$$|u_b(x; \varphi) - \gamma(x + \varphi)| \leq Ce^{\eta x}, \quad x \leq 0 \quad (2.11)$$

with positive constants  $C, \eta > 0$  that do not depend on  $\varphi$ .

In the coordinate system introduced in Lemma 3.2.5 near the periodic orbit  $\gamma$ , we record that

$$u_f(0; \varphi) = (-\varphi, \delta, 0), \quad (2.12)$$

$$u_b(0; \varphi) = (\varphi, 0, \delta). \quad (2.13)$$

In Figure 3.2 we show a schematic illustration of the localized solution whose existence and uniqueness we prove in the following:

**Theorem 3.1.** (*Gluing fronts and backs to produce localized solutions*) Fix  $\epsilon > 0$ , then there exist  $\eta, K, C > 0$  such that for each  $\varphi_1^*, \varphi_2^* \in S^1$  with  $\mu = z(\varphi_1^*) = z(\varphi_2^*)$  and  $|z'(\varphi_1^*)|, |z'(\varphi_2^*)| \geq \epsilon$ , and for each  $k \in \mathbb{N}, k \geq K$ , and  $m \in \{0, 1\}$ , we can define  $\varphi_1 = \varphi_1^*, \varphi_2 = \varphi_2^* + 2m\pi$ , and

$$L = L(\varphi_1, \varphi_2, k) := \frac{\varphi_1 + \varphi_2}{2} + 2k\pi + O(e^{-\eta 2k\pi}), \quad (2.14)$$

$$\varphi = \varphi(\varphi_1, \varphi_2, k) := \frac{\varphi_2 - \varphi_1}{2} + O(e^{-\eta 2k\pi}) \quad (2.15)$$

such that there exists a unique solution  $u_1(x) = u_1(x; \varphi_1, \varphi_2, k)$  of (2.1), depending smoothly on  $(\varphi_1, \varphi_2)$  for each  $k$ , with  $\lim_{|x| \rightarrow \infty} |u_1(x)| = 0$ ,  $u_1(x) \in \mathcal{V}$  for  $x \in [-L, L]$ , and in the coordinate system introduced in Lemma 3.2.5 near the periodic orbit  $\gamma$  we have

$$\begin{aligned} u_1(-L) &= (\varphi - L + O(e^{-\eta L}), \delta, \delta e^{-2\alpha(\mu)L} (1 + O(e^{-\eta L}))) \\ u_1(0) &= (\varphi, \delta e^{-\alpha(\mu)L} (1 + O(e^{-\eta L})), \delta e^{-\alpha(\mu)L} (1 + O(e^{-\eta L}))) \\ u_1(L) &= (\varphi + L + O(e^{-\eta L}), \delta e^{-2\alpha(\mu)L} (1 + O(e^{-\eta L})), \delta), \end{aligned} \quad (2.16)$$

where the first coordinate is understood to be taken modulo  $2\pi$ . Moreover,

$$|u_1(x) - u_f(x + L; \varphi_1)| \leq C e^{\eta x}, \quad x \leq -L \quad (2.17)$$

$$|u_1(x) - u_f(x + L; \varphi_1)| \leq C e^{-\eta L}, \quad x \in [-L, 0] \quad (2.18)$$

$$|u_1(x) - u_b(x - L; \varphi_2)| \leq C e^{-\eta L}, \quad x \in [0, L] \quad (2.19)$$

$$|u_1(x) - u_b(x - L; \varphi_2)| \leq C e^{-\eta x}, \quad x \geq L \quad (2.20)$$

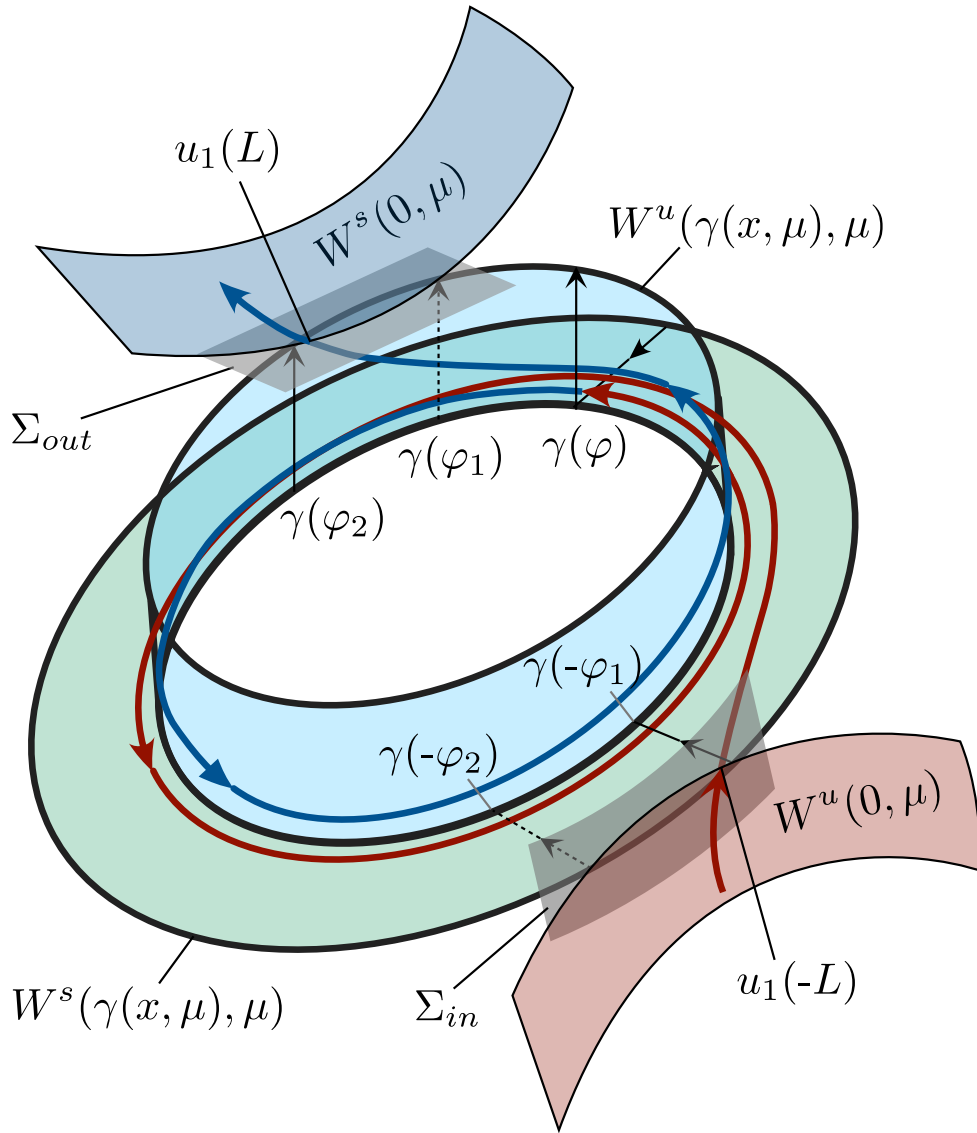


**Figure 3.2:** A three-dimensional schematic view of the analytic gluing construction, including the manifolds and sections of interest. Of course, this schematic is only valid locally as the three dimensional manifold is immersed in four dimensional space. The localized solution  $u_1(x)$  is shown in red for  $x \leq 0$  and in blue for  $x \geq 0$ , indicating the time periods over which it remains exponentially close to the front and back, respectively.  $u_1(-L)$  passes through the section  $\Sigma_{in}$  exponentially close (in  $L$ ) to the point where the unstable manifold of the origin,  $W^u(0, \mu)$ , intersects the (center) stable manifold  $W^s(\gamma(x, \mu), \mu)$  of the periodic orbit in the section  $\Sigma_{in}$ ; this point is in the strong stable fiber  $W^{ss}(\gamma(-\varphi_1, \mu), \mu)$ . Meanwhile,  $u_1(L)$  passes through the section  $\Sigma_{out}$  exponentially close (in  $L$ ) to the point where the stable manifold of the origin,  $W^s(0, \mu)$ , intersects the (center) unstable manifold  $W^u(\gamma(x, \mu), \mu)$  of the periodic orbit in the section  $\Sigma_{out}$ ; this point is in the strong unstable fiber  $W^{uu}(\gamma(\varphi_2, \mu), \mu)$ . At  $x = 0$  (indicated by the change from red to blue coloring),  $u_1(0)$  has center coordinate  $\varphi \approx \frac{\varphi_2 - \varphi_1}{2}$  (see (2.15)). Dotted lines indicate the strong stable and unstable fibers  $W^{ss}(\gamma(-\varphi_2, \mu), \mu)$  and  $W^{uu}(\gamma(\varphi_1, \mu), \mu)$ , which, by reversibility, intersect  $W^u(0, \mu)$  and  $W^s(0, \mu)$  in the sections  $\Sigma_{in}$  and  $\Sigma_{out}$ , as seen in the figure, and give rise to the family of localized solutions  $u_2(x; k)$ . Symmetric localized solutions are formed from a front and back with the same phase ( $\varphi_1 = \varphi_2 \pmod{2\pi}$ ), while asymmetric localized solutions are formed by combining a front and back with different phases ( $\varphi_1 \neq \varphi_2 \pmod{2\pi}$ ). In this illustration,  $k = 1$  and  $m = 0$ .

Similarly, there exists a unique solution  $u_2(x) = u_2(x; \varphi_1, \varphi_2, k)$  of (2.1), depending smoothly on  $(\varphi_1, \varphi_2)$  for each  $k$ , and with  $L$  and  $\varphi$  as in (2.14) and (2.15), such that  $\lim_{|x| \rightarrow \infty} |u_2(x)| = 0$ ,  $u_2(x) \in \mathcal{V}$  for  $x \in [-L, L]$ , and

$$\begin{aligned} u_2(-L) &= \left(-\varphi - L + O(e^{-\eta L}), \delta, \delta e^{-2\alpha(\mu)L} (1 + O(e^{-\eta L}))\right) \\ u_2(0) &= \left(-\varphi, \delta e^{-\alpha(\mu)L} (1 + O(e^{-\eta L})), \delta e^{-\alpha(\mu)L} (1 + O(e^{-\eta L}))\right) \\ u_2(L) &= \left(-\varphi + L + O(e^{-\eta L}), \delta e^{-2\alpha(\mu)L} (1 + O(e^{-\eta L})), \delta\right), \end{aligned} \quad (2.21)$$

where again the first coordinate is understood to be taken modulo  $2\pi$ . Moreover,

$$|u_2(x) - u_f(x + L; \varphi_2)| \leq C e^{\eta x}, \quad x \leq -L \quad (2.22)$$

$$|u_2(x) - u_f(x + L; \varphi_2)| \leq C e^{-\eta L}, \quad x \in [-L, 0] \quad (2.23)$$

$$|u_2(x) - u_b(x - L; \varphi_1)| \leq C e^{-\eta L}, \quad x \in [0, L] \quad (2.24)$$

$$|u_2(x) - u_b(x - L; \varphi_1)| \leq C e^{-\eta x}, \quad x \geq L \quad (2.25)$$

**Remark 3.2.8.** By setting  $\varphi_1^* = \varphi_2^*$  and  $m = 0$ , we recover the branch of symmetric solutions with center coordinate  $\varphi = 0$  at  $x = 0$ . By setting  $\varphi_1^* = \varphi_2^*$  and  $m = 1$ , we recover the second branch of symmetric solutions with center coordinate  $\varphi = \pi$  at  $x = 0$ . In each case the families of solutions  $u_1(x)$  and  $u_2(x)$  are the same.

**Remark 3.2.9.** It is evident from the proof of Theorem 3.1 that we have a unique gluing solution for any  $\varphi_1^*, \varphi_2^*$  with  $z(\varphi_1^*) = z(\varphi_2^*)$  and  $z'(\varphi_1^*), z'(\varphi_2^*) \neq 0$ . We fix  $\epsilon > 0$  only in order to have uniform constants  $\eta, K, C$ . Thus we have the following corollary:

**Corollary 3.2.10.** For any  $\varphi_1^*, \varphi_2^*$  with  $\mu = z(\varphi_1^*) = z(\varphi_2^*)$  and  $|z'(\varphi_1^*)|, |z'(\varphi_2^*)| \neq 0$  there exist  $\eta, K, C > 0$  such that for each  $k \geq K$  and  $m \in \{0, 1\}$ , there exists a unique solution  $u_1(x)$  satisfying the conditions in Theorem 3.1. The solution  $u_2(x)$  is distinct from  $u_1(x)$  provided that  $\varphi_1^* \neq \varphi_2^*$ .

**Proof.** (Theorem 3.1) We first prove all statements for  $u_1(x)$ . In order for a solution  $u_1(x)$  to satisfy  $\lim_{|x| \rightarrow \infty} |u_1(x)| = 0$  and  $u_1(\pm L) \in \mathcal{V}$ , we must have

$$u_1(-L) \in \Sigma_{in} \cap W^u(0, z(\varphi_1)), \quad u_1(L) \in \Sigma_{out} \cap W^s(0, z(\varphi_2)). \quad (2.26)$$

[Recall  $z(\varphi_1) = z(\varphi_2)$ .] From Hypothesis 3.2.6 we have that  $(\varphi, v^s, \delta) \in W^s(0, \mu) \cap \Sigma_{out}$  if and only if  $v^s = g(\varphi, \mu)$ . Then using (2.3),  $(\varphi, \delta, v^u) \in W^u(0, \mu) \cap \Sigma_{in}$  if and only if  $\mathcal{R}(\varphi, \delta, v^u) = (-\varphi, v^u, \delta) \in W^s(0, \mu) \cap \Sigma_{out}$  if and only if  $v^u = g(-\varphi, \mu)$ .

Thus (2.26) is equivalent to

$$u_1^u(-L) = g(-u_1^c(-L), z(\varphi_1)) \quad (2.27)$$

$$u_1^s(L) = g(u_1^c(L), z(\varphi_2)). \quad (2.28)$$

We now let

$$L = L(\varphi_1, \varphi_2, k, \varepsilon_1) := \frac{\varphi_1 + \varphi_2}{2} + 2k\pi + \varepsilon_1, \quad (2.29)$$

$$\varphi = \varphi(\varphi_1, \varphi_2, k, \varepsilon_2) := \frac{\varphi_2 - \varphi_1}{2} + \varepsilon_2. \quad (2.30)$$

We will show that  $\varepsilon_1$  and  $\varepsilon_2$  can be chosen such that (2.26) holds and both are  $O(e^{-\eta 2k\pi})$ . We note that  $L + \varphi = \varphi_2 + \varepsilon_1 + \varepsilon_2 \pmod{2k\pi}$  and  $L - \varphi = \varphi_1 + \varepsilon_1 - \varepsilon_2 \pmod{2k\pi}$ . So by Lemma 3.2.7, the unique solution associated to  $(L, \varphi)$  as defined in (2.29)–(2.30) has

$$u_1(-L) = (-\varphi_1 - \varepsilon_1 + \varepsilon_2 + O(e^{-\eta L}), \delta, \delta e^{-2\alpha(\mu)L} (1 + O(e^{-\eta L}))) \quad (2.31)$$

$$u_1(0) = (\varphi, \delta e^{-\alpha(\mu)L} (1 + O(e^{-\eta L})), \delta e^{-\alpha(\mu)L} (1 + O(e^{-\eta L}))) \quad (2.32)$$

$$u_1(L) = (\varphi_2 + \varepsilon_1 + \varepsilon_2 + O(e^{-\eta L}), \delta e^{-2\alpha(\mu)L} (1 + O(e^{-\eta L})), \delta). \quad (2.33)$$

Thus  $u_1^c(-L) - u_f^c(0; \varphi_1) = -\varepsilon_1 + \varepsilon_2 + O(e^{-\eta L})$ . To solve (2.27), we substitute from (2.31) and expand  $g(-u_1^c(-L), z(\varphi_1))$  about  $(-u_f^c(0; \varphi_1), z(\varphi_1))$ , arriving at

$$\begin{aligned} \delta e^{-2\alpha(\mu)L} (1 + O(e^{-\eta L})) &= g(-u_f^c(0; \varphi_1), z(\varphi_1)) + g_\varphi(-u_f^c(0; \varphi_1), z(\varphi_1))(-\varepsilon_1 + \varepsilon_2 + O(e^{-\eta L})) \\ &\quad + O((- \varepsilon_1 + \varepsilon_2 + O(e^{-\eta L}))^2). \end{aligned} \quad (2.34)$$

By Hypothesis 3.2.6,

$$g(\varphi, z(\varphi)) \equiv 0 \quad (2.35)$$

so  $g(-u_f^c(0; \varphi_1), z(\varphi_1)) = g(\varphi_1, z(\varphi_1)) = 0$ . Thus

$$\varepsilon_1 = -\frac{\delta e^{-2\alpha(\mu)L} (1 + O(e^{-\eta L})) + O((- \varepsilon_1 + \varepsilon_2 + O(e^{-\eta L}))^2)}{g_\varphi(\varphi_1, z(\varphi_1))} + \varepsilon_2 + O(e^{-\eta L}). \quad (2.36)$$

Now returning to (2.28), we substitute from (2.33), note that  $u_1^c(L) - u_b^c(0; \varphi_2) = \varepsilon_1 + \varepsilon_2 + O(e^{-\eta L})$  and expand  $g(u_1^c(L), z(\varphi_2))$  about  $(u_b^c(0; \varphi_2), z(\varphi_2))$  to get

$$\begin{aligned} \delta e^{-2\alpha(\mu)L} (1 + O(e^{-\eta L})) &= g(u_f^c(0; \varphi_2), z(\varphi_2)) + g_\varphi(u_f^c(0; \varphi_2), z(\varphi_2))(-\varepsilon_1 - \varepsilon_2 + O(e^{-\eta L})) \\ &\quad + O((\varepsilon_1 + \varepsilon_2 + O(e^{-\eta L}))^2). \end{aligned} \quad (2.37)$$

Then using  $g(u_f^c(0; \varphi_2), z(\varphi_2)) = 0$  as before,

$$\varepsilon_1 + \varepsilon_2 = \frac{\delta e^{-2\alpha(\mu)L} (1 + O(e^{-\eta L})) + O((\varepsilon_1 + \varepsilon_2 + O(e^{-\eta L}))^2)}{g_\varphi(\varphi_2, z(\varphi_2))} + O(e^{-\eta L}) \quad (2.38)$$

so that combining this with (2.36), we have

$$\begin{aligned} \varepsilon_2 &= \frac{1}{2} \left[ \frac{\delta e^{-2\alpha(\mu)L} (1 + O(e^{-\eta L})) + O((\varepsilon_1 + \varepsilon_2 + O(e^{-\eta L}))^2)}{g_\varphi(\varphi_2, z(\varphi_2))} \right. \\ &\quad \left. + \frac{\delta e^{-2\alpha(\mu)L} (1 + O(e^{-\eta L})) + O((- \varepsilon_1 + \varepsilon_2 + O(e^{-\eta L}))^2)}{g_\varphi(\varphi_1, z(\varphi_1))} \right] + O(e^{-\eta L}). \end{aligned} \quad (2.39)$$

Now by (2.35),  $g_\varphi(\varphi_1, z(\varphi_1)) = -g_\mu(\varphi_1, z(\varphi_1))z'(\varphi_1)$  and similarly for  $\varphi_2$ , so that by our original assumption combined with Hypothesis 3.2.6,  $|g_\varphi(\varphi_1, z(\varphi_1))|, |g_\varphi(\varphi_2, z(\varphi_2))| > b\epsilon$ . Thus we have  $\varepsilon_1, \varepsilon_2$  in (2.29)–(2.30) so that (2.26) holds, and both  $\varepsilon_1, \varepsilon_2$  are  $O(e^{-\eta L})$ .

Now since we have a solution  $u_1(x)$  such that  $u_1(-L) = (\varphi_1 + O(e^{-\eta L}), \delta, \delta e^{-2\alpha(\mu)L}(1 + O(e^{-\eta L})))$ , it follows that  $|u_1(-L) - u_f(0; \varphi_1)| = O(e^{-\eta L})$ . Similarly,  $|u_1(L) - u_b(0; \varphi_2)| = O(e^{-\eta L})$ . Now since both  $u_1(-L) \in W^u(0, \mu)$  and  $u_f(-\varphi) \in W^u(0, \mu)$ , the exponential approach in backward time expressed in (2.17) follows from the stable manifold theorem. Similarly,  $u_1(L) \in W^s(0, \mu)$  and  $u_b(\varphi_2) \in W^s(0, \mu)$  implies (2.20). On the other hand, from the expression (2.2) we have that  $|u_1(x) - u_f(x + L; \varphi_1)| = O(e^{-\eta L})$  on  $-L \leq x \leq 0$ , so that for  $K$  sufficiently large, there exists a constant  $C$  such that for all  $L(k)$  with  $k \geq K$ , (2.18) is satisfied. The relation (2.19) is shown analogously.

The claims for  $u_2(x)$  follow upon setting  $u_2(x) = \mathcal{R}u_1(-x)$ . In particular, the expressions in (2.21) follow from those in (2.16) by using, for example,  $u_2(-L) = \mathcal{R}u_1(L)$  along with the relation  $\mathcal{R}(v^c, v^s, v^u) = (-v^c, v^u, v^s)$ . Furthermore,

$$|u_1(x) - u_f(x + L; \varphi_1)| \leq C e^{\eta x}, \quad x \leq -L$$

implies

$$\begin{aligned} |u_1(-y) - u_f(-y + L; \varphi_1)| &\leq C e^{-\eta y}, \quad y \geq L \\ |\mathcal{R}u_1(-y) - \mathcal{R}u_f(-y + L; \varphi_1)| &\leq C e^{-\eta y}, \quad y \geq L \\ |u_2(y) - u_b(y - L; \varphi_1)| &\leq C e^{-\eta y}, \quad y \geq L \end{aligned}$$

upon employing the coordinate transform  $y = -x$  and applying  $\mathcal{R}$ , so that (2.17)

implies (2.25) and the other relations follow similarly. ■

### 3.2.1 Additional details for the construction

While the proof of Theorem 3.1 is complete as presented, in the following we explicitly construct solutions near the periodic orbits for  $[-L, L]$  rather than invoking Lemma 3.2.7. In other words, we prove the first part of Lemma 3.2.7: there exist positive constants  $L_0$  and  $\eta$  so that for all  $L > L_0$  and  $\varphi \in S^1$ , there is a unique solution  $u(x)$  of (2.1) defined for  $x \in [-L, L]$  and lying in the zero-energy level set such that

$$u(-L) \in \Sigma_{in}, \quad u(L) \in \Sigma_{out}, \quad u^c(0) = \varphi,$$

and  $u(x)$  stays near the periodic orbits for all  $x \in [-L, L]$ . We closely follow the proof of Lemma 6.2 in [4], an analogue of Lemma 3.2.7 for the Swift–Hohenberg equation posed as an ODE on  $H_e^3(S^1) \times H_e^2(S^1) \times H_e^1(S^1) \times L_e^2(S^1)$  (the “e” stands for even periodic functions, but this is not essential). We believe these arguments bear repeating in order to clarify both the result and the pieces needed for extension to  $\mathbb{R}^{2n}$  and appropriate Banach spaces. Moreover, the construction introduces techniques closely related to those which we will employ in analyzing the stability of localized solutions.

The basic idea in the following is to construct two solutions, one of which starts in  $\Sigma_{in}$  and is the sum of a strong stable fiber to the periodic orbits plus an offset that is complementary in  $\Sigma_{in}$ , and a second of which ends in  $\Sigma_{out}$  and is the sum of a strong unstable fiber and an offset that is complementary in  $\Sigma_{out}$ . We then match these solutions in the middle. For convenience we write the two solutions as  $u^+(x)$  for  $x \in [0, L]$  and  $u^-(x)$  for  $x \in [-L, 0]$ , so that  $u(x) = u^+(x+L)$  for  $x \in [-L, 0]$  and

$u(-x) = u^-(x - L)$  for  $x \in [0, L]$ . The key ingredients necessary for the construction are smooth foliations and the existence of exponential dichotomies for the system when linearized about the strong (un)stable fibers.

Instead of using Fenichel coordinates in the three dimensional zero energy subspace, we proceed in the full four dimensional space. We have a two-parameter family of periodic orbits  $\gamma(\cdot, \mu, e)$  which are smooth in  $\mu, e$ , where  $e := \mathcal{H}(\gamma(0, \mu, e), \mu)$  for  $e$  near zero, and we normalize the periodic orbits such that  $\gamma(0, \mu, e) \in \text{Fix } \mathcal{R}$  for each  $(\mu, e)$ . We assumed in Hypothesis 3.2.4 that  $\alpha(\mu) > 0$  for all  $\mu \in J$ , where  $\pm 2\pi\alpha(\mu)$  are the two Floquet exponents associated with the zero-energy periodic orbit. Thus there exists a neighborhood,  $E$ , of zero so that for all  $(\mu, e) \in J \times E$ , there exists an  $\eta > 0$  such that the two Floquet exponents away from zero have magnitude greater than  $\eta$ , and the other two are fixed at zero.

Now for fixed  $(\varphi, \mu, e)$ , the strong stable fiber of  $\gamma(x + \varphi, \mu, e)$ , denoted by  $q^+(x, \varphi, \mu, e)$ , will be unique up to shifts, i.e., we need only fix its location at a single value of  $x$  to define it uniquely. We then use  $b^+$  to parameterize  $q^+$ , so that  $q^+(x, \varphi, \mu, e, b^+)$  is smooth in all arguments and there is a unique  $b^+(\varphi, \mu, e)$  such that  $q^+(0, \varphi, \mu, e, b^+(\varphi, \mu, e)) \in \Sigma_{in}$  and we can use  $b^+$  to parameterize this condition.<sup>1</sup> We then have

$$|\gamma(x + \varphi, \mu, e) - q^+(x, \varphi, \mu, e, b^+)| \leq Ce^{-\eta x}, \quad x \geq 0, \quad (2.40)$$

for some  $C > 0$ . In the following  $C$  will denote any bounded uniform constant, without keeping track of these constants separately.

---

<sup>1</sup>In higher dimensional settings, in addition to capturing the  $x$  dependence,  $b^+$  will parameterize the space corresponding to all but the weakest Floquet multiplier (see Hypothesis 3.3.1) and so will have dimension equal to the dimension of this space plus 1. We then have further smooth dependence of the solutions on these additional coordinates. See Section 3.3 for precise statements.

The strong unstable fiber  $q^-(x, \varphi, \mu, e, b^-)$  of  $\gamma(x + \varphi, \mu, e)$  is defined analogously and we have

$$|\gamma(x + \varphi, \mu, e) - q^-(x, \varphi, \mu, e, b^-)| \leq Ce^{\eta x}, \quad x \leq 0. \quad (2.41)$$

Now linearizing  $u_x = f(u, \mu)$  about a particular fiber  $q^+(x, \varphi^+, \mu, e^+, b^+)$  for  $x \geq 0$  yields

$$u_x = f_u(q^+, \mu)u \quad (2.42)$$

and since the Floquet spectrum of the periodic orbits  $\gamma(\cdot)$  has a gap between the two Floquet exponents fixed at 0 is bounded away from zero in absolute value by  $\eta > 0$ , with the exception of , (2.42) has exponential dichotomies (see Appendix A.1)  $\Phi_+^{cs}(x, y)$  and  $\Phi_+^u(x, y)$  on  $\mathbb{R}^+$  that are smooth in  $(\varphi^+, \mu, e^+, b^+)$ : fixing  $\epsilon > 0$  such that  $\eta > \epsilon > 0$ , there exists a  $C > 0$  such that

$$|\Phi_+^{cs}(x, y)| \leq Ce^{\epsilon(x-y)}, \quad x \geq y \geq 0, \quad (2.43)$$

$$|\Phi_+^u(x, y)| \leq Ce^{-\eta(y-x)}, \quad y \geq x \geq 0. \quad (2.44)$$

We denote by  $P_+^{cs}(x)$  and  $P_+^u(x)$  the projections associated with these exponential dichotomies, so that  $P_+^{cs}(x) = \Phi_+^{cs}(x, x)$  and  $P_+^u(x) = \Phi_+^u(x, x)$ .

Similarly,

$$u_x = f_u(q^-, \mu)u \quad (2.45)$$

has exponential dichotomies  $\Phi_-^s(x, y)$  and  $\Phi_-^{cu}(x, y)$  on  $\mathbb{R}^-$  that are smooth in  $(\varphi^-, \mu, e^-, b^-)$ , and we again denote by  $P_-^s(x)$  and  $P_-^{cu}(x)$  the projections associated with these dichotomies.

We wish to find solutions  $u^\pm(x)$  to (2.1) that satisfy

$$\begin{aligned} u^+(x) &= q^+(x, \varphi^+, \mu, e^+, b^+) + w^+(x), \quad x \in [0, L] \\ u^+(0) &\in \Sigma_{in} \\ u^-(x) &= q^-(x, \varphi^-, \mu, e^-, b^-) + w^-(x), \quad x \in [-L, 0] \\ u^-(0) &\in \Sigma_{out} \\ u^+(L) &= u^-(-L). \end{aligned}$$

Since  $q^+(x)$  solves (2.1), in order for  $u^+(x)$  to satisfy (2.1) for  $x \in [0, L]$  we must have

$$q_x^+ + w_x^+ = f(q^+ + w^+, \mu) = q_x^+ - f(q^+, \mu) + f(q^+ + w^+, \mu)$$

so that  $w^+(x)$  satisfies

$$\begin{aligned} w_x^+ &= f(q^+ + w^+, \mu) - f(q^+, \mu) \\ &= f_u(q^+, \mu)w^+ + N^+(q^+, w^+, \mu) \end{aligned} \tag{2.46}$$

for  $x \in [0, L]$  and where we have defined  $N^+(q^+, w^+, \mu) := f(q^+ + w^+, \mu) - f(q^+, \mu) - f_u(q^+, \mu)w^+$ . We observe that  $N^+(q^+, w^+, \mu) = O(|w^+|^2)$ , and also note that if  $f \in C^k$  then  $N^+ \in C^{k-1}$  so that since  $q^+$  is smooth in  $(\varphi, \mu, e, b)$ ,  $N^+$  is also smooth in each of these.

We have already noted the exponential dichotomies  $\Phi_+^{cs}(x, y), \Phi_+^u(x, y)$  for the linear part of (2.46), so using the variation of constants formula along with these dichotomies (see Appendix A.2) and letting  $a^+ \in \text{Rg } P_+^u(L)$  an arbitrary element, we

have

$$\begin{aligned}
w^+(x) &= \Phi_+^u(x, L)a^+ + \int_L^x \Phi_+^u(x, y)N^+(q^+(y), w^+(y), \mu)dy \\
&\quad + \int_0^x \Phi_+^{cs}(x, y)N^+(q^+(y), w^+(y), \mu)dy \\
&=: [\mathcal{F}(\mu, \varphi^+, e^+, b^+, a^+, w^+)](x)
\end{aligned} \tag{2.47}$$

so that solutions of (2.46) correspond to solutions of (2.47) on  $[0, L]$ . Since  $\Phi_+^{cs}$  and  $\Phi_+^u$  are smooth in  $(\mu, \varphi^+, e^+, b^+)$ , as is  $N^+$ , it is clear that  $\mathcal{F}$  is smooth in  $(\mu, \varphi^+, e^+, b^+, a^+)$ . Now for each fixed  $(\mu, \varphi^+, e^+, b^+, a^+)$ , we show that  $\mathcal{F}$  maps  $C^0([0, L], \mathbb{R}^4)$  with weighted norm  $\|w^+\| := \sup_{0 \leq x \leq L} e^{\eta(L-x)}|w^+(x)|$  into itself. Using the inequalities from (2.43) and (2.44) along with  $N^+(q^+, w^+, \mu) = O(|w^+|^2)$ , we have:

$$\begin{aligned}
&\|\mathcal{F}(\mu, \varphi^+, e^+, b^+, a^+, w^+)\| \\
&\leq C|a^+| + \sup_{0 \leq x \leq L} C e^{\eta(L-x)} \int_L^x e^{-\eta(y-x)} e^{-2\eta(L-y)} \|w^+\|^2 dy \\
&\quad + \sup_{0 \leq x \leq L} K e^{\eta(L-x)} \int_0^x e^{\epsilon(x-y)} e^{-2\eta(L-y)} \|w^+\|^2 dy \\
&= C|a^+| + \sup_{0 \leq x \leq L} C e^{-\eta L} \int_L^x e^{\eta y} \|w^+\|^2 dy + \sup_{0 \leq x \leq L} C e^{-\eta(L+x)} e^{\epsilon x} \int_0^x e^{(2\eta-\epsilon)y} \|w^+\|^2 dy \\
&= C|a^+| + \sup_{0 \leq x \leq L} C e^{-\eta L} (e^{\eta x} - e^{\eta L}) \|w^+\|^2 + \sup_{0 \leq x \leq L} K e^{-\eta(L+x)} e^{\epsilon x} (e^{(2\eta-\epsilon)x} - 1) \|w^+\|^2 \\
&= C|a^+| + \sup_{0 \leq x \leq L} C (e^{\eta(x-L)} - 1) \|w^+\|^2 + \sup_{0 \leq x \leq L} C e^{-\eta L} (e^{\eta x} - e^{(-\eta+\epsilon)x}) \|w^+\|^2 \\
&\leq C|a^+| + C\|w^+\|^2,
\end{aligned}$$

where we have used the convention noted above of subsuming constants, independent of parameters and variables, into  $C$ . Then for any  $a^+$  sufficiently small, (2.47) has a unique solution  $w^+$  satisfying  $|w^+(x)| \leq C|a^+|e^{-\eta(L-x)}$  for  $x \in [0, L]$  so that in

particular  $|w^+(0)| \leq C|a^+|e^{-\eta L}$ . Moreover, we have

$$w^+(L) - a^+ = \int_0^L \Phi_+^{cs}(L, y) N^+(q^+(y), w^+(y), \mu) dy$$

so that  $|w^+(L) - a^+| \leq C|a^+|^2$ .

Similarly,  $w^-(x)$  satisfies

$$\begin{aligned} w^-(x) &= \Phi_+^s(x, -L)a^- + \int_{-L}^x \Phi_-^s(x, y) N^-(q^-(y), w^-(y), \mu) dy \\ &\quad + \int_0^x \Phi_-^{cu}(x, y) N^-(q^-(y), w^-(y), \mu) dy \end{aligned} \quad (2.48)$$

for  $x \in [-L, 0]$ , with  $a^- \in \text{Rg } P_-^s(-L)$ . Again for any  $a^-$  sufficiently small, (2.48) has a unique solution  $w^-(x)$  satisfying  $|w^-(x)| \leq C|a^-|e^{-\eta(L-x)}$  for  $x \in [0, L]$ , and as before,  $|w^-(-L) - a^-| \leq C|a^-|^2$ .

Then to satisfy the matching condition  $u^+(L) = u^-(L)$ , by definition we require  $q^+(L, \varphi^+, \mu, e^+, b^+) + w^+(L) - q^-(-L, \varphi^-, \mu, e^-, b^-) - w^-(-L) = 0$ , or, using (2.40) and (2.41),

$$\gamma(L + \varphi^+, \mu, e^+) - \gamma(-L + \varphi^-, \mu, e^-) + a^+ - a^- = O(|a^+|^2 + |a^-|^2 + e^{-\eta L}). \quad (2.49)$$

We now fix  $(\varphi, e)$ , and set

$$\begin{aligned} e^+ &= e + \hat{e}, & \varphi^+ &= \varphi + \hat{\varphi} - L \\ e^- &= e - \hat{e}, & \varphi^- &= \varphi - \hat{\varphi} + L \end{aligned}$$

for  $(\hat{\varphi}, \hat{e})$  small. Then since for  $(\hat{\varphi}, \hat{e}, a^+, a^-) = 0$  the left hand side of (2.49) vanishes, and its derivative with respect to these variables is invertible, we have a locally

unique solution  $(\hat{\varphi}_0, \hat{e}_0, a_0^+, a_0^-)$  of (2.49) that is smooth in  $(\mu, e, \varphi, L)$ , and we have  $(\hat{\varphi}_0, \hat{e}_0, a_0^+, a_0^-) = O(e^{-\eta L})$ . We then set  $b^+, b^-$  such that  $q^+(0, \varphi + \hat{\varphi}_0 - L, \mu, e + \hat{e}_0, b^+) \in \Sigma_{in}$  and  $q^-(0, \varphi + \hat{\varphi}_0 - L, \mu, e + \hat{e}_0, b^+) \in \Sigma_{in}$ . Then since  $w^+(0) \in \text{Rg } P_+^u(0)$  and  $|w^+(0)| = O(e^{-2\eta L})$ , we have  $u^+(0) \in \Sigma_{in}$ . Similarly,  $w^-(0) \in \text{Rg } P_-^s(0)$  and  $|w^-(0)| = O(e^{-2\eta L})$ , so that  $u^-(0) \in \Sigma_{out}$ .

We finish by establishing that for an appropriate choice of  $e$ , the solutions  $u^\pm$  will lie in the zero-energy level set. We first show that  $\mathcal{H}(u^+(0)) = \mathcal{H}(\gamma(0, \mu, e)) + O(e^{-\eta L})$  so that  $\frac{d}{de} \mathcal{H}(u^+(0)) \neq 0$  for  $e$  near 0 by assumption:

$$\begin{aligned} \mathcal{H}(u^+(0)) &= \mathcal{H}(u^+(L)) = \mathcal{H}(q^+(L, \mu, e, \varphi - L, b^+) + O(e^{-\eta L})) \\ &= \mathcal{H}(\gamma(\varphi, \mu, e) + O(e^{-\eta L})) = \mathcal{H}(\gamma(0, \mu, e)) + O(e^{-\eta L}). \end{aligned}$$

Thus for  $e$  near 0, we can determine the unique  $e = e(\mu, \varphi, L)$  so that  $\mathcal{H}(u^+) = 0$ .

### 3.3 The gluing construction in $\mathbb{R}^{2n}$

We now consider the system

$$u_x = f(u, \mu), \tag{3.1}$$

with  $u \in \mathbb{R}^{2n}$  and  $\mu \in \mathbb{R}$ , and again we assume  $f$  is a smooth function. The first three hypotheses are completely analogous to those for the system in  $\mathbb{R}^4$ , and we do not repeat them here. The fourth hypothesis is modified as follows:

**Hypothesis 3.3.1.** *There is a closed interval  $J \subset \mathbb{R}$  with nonempty interior such that (2.1) has, for each  $\mu \in J$ , a periodic orbit  $\gamma(x, \mu)$  with minimal period  $l(\mu)$  such that:*

- (i) The family  $\gamma(x, \mu)$  depends smoothly on  $\mu \in J$ .
- (ii)  $\gamma(x, \mu)$  is symmetric with  $\gamma(0, \mu) \in \text{Fix } \mathcal{R}$  for all  $\mu \in J$ .
- (iii) For each  $\mu \in J$ ,  $\mathcal{H}(\gamma(x, \mu), \mu) = 0$  and  $\mathcal{H}_u(\gamma(x, \mu), \mu) \neq 0$  for one and hence all  $x$ .
- (iv)  $\gamma(x, \mu)$  has two simple Floquet multipliers,  $e^{\pm 2\pi\alpha(\mu)}$ , with  $\alpha(\mu) > 0$  for all  $\mu \in J$ , and there is an  $\eta > 0$  such that the remaining Floquet multipliers have modulus less than  $e^{-2\pi(\alpha(\mu)+\eta)}$  or greater than  $e^{2\pi(\alpha(\mu)+\eta)}$  uniformly in  $\mu \in J$ .

We again assume without loss of generality that the minimal period  $l(\mu) = 2\pi$  for all  $\mu$ . In this case, for  $\delta > 0$  sufficiently small we can write the space  $\mathcal{V}$  in the zero energy level set near  $\gamma(x, \mu)$  as

$$\mathcal{V} := S^1 \times I \times B \times I \times B, \quad I = [-\delta, \delta], \quad B = B_\delta(0) \in \mathbb{R}^{n-2} \quad (3.2)$$

with the corresponding coordinate system

$$v = (v^c, v^s, v^{ss}, v^u, v^{uu}), \quad (3.3)$$

so that within  $\mathcal{V}$ ,  $W^{ss}(\gamma(\varphi, \mu), \mu) = (\varphi, v^s, v^{ss}, 0, 0)$  and  $W^{uu}(\gamma(\varphi, \mu), \mu) = (\varphi, 0, 0, v^u, v^{uu})$ .

We then define the sections

$$\Sigma_{in} := S^1 \times \{v^s = \delta\} \times B \times I \times B, \quad \Sigma_{out} := S^1 \times I \times B \times \{v^u = \delta\} \times B. \quad (3.4)$$

As before we define the set

$$\Gamma := \{(\varphi, \mu) \in S^1 \times J : W^s(0, \mu) \cap W^{uu}(\gamma(\varphi, \mu), \mu) \cap \Sigma_{out} \neq \emptyset\}. \quad (3.5)$$

Our final hypothesis is then similar to that for  $\mathbb{R}^4$ , and additionally enforces that the stable manifold  $W^s(0, \mu)$  approaches the unstable manifold  $W^u(\gamma(x, \mu), \mu)$  in backward time along the most weakly unstable direction of the flow near the periodic orbit.

**Hypothesis 3.3.2.** *The set  $\Gamma$  is the graph of a smooth function  $z : S^1 \rightarrow J$ . Furthermore, there exist an open neighborhood  $U_\Gamma$  of  $\Gamma$  in  $S^1 \times J$ , positive constants  $\epsilon, b > 0$ , and smooth functions  $g : U_\Gamma \times B \rightarrow I$  and  $h : U_\Gamma \times B \rightarrow B$  so that*

$$\begin{aligned} & \{(\varphi, v^s, v^{ss}, \delta, v^{uu}) \in W^s(0, \mu) \cap \Sigma_{out} : |v^s| < \epsilon, (\varphi, \mu) \in U_\Gamma, v^{ss} \in B\} \\ & = \{(\varphi, v^s, v^{ss}, \delta, v^{uu}) = (\varphi, g(\varphi, \mu, v^{ss}), v^{ss}, \delta, h(\varphi, \mu, v^{ss})) : (\varphi, \mu) \in U_\Gamma, v^{ss} \in B\} \end{aligned} \quad (3.6)$$

and  $|g_\mu(\varphi, \mu, v^{ss})| \geq b > 0$  for all  $(\varphi, \mu, v^{ss}) \in U_\Gamma \times B$ .

Under these conditions, we have the following analogue of Lemma 3.2.7:

**Lemma 3.3.3.** *(See Section 3.2.1 and Lemma 6.2 in [4]) There exist positive constants  $L_0$  and  $\eta$  so that the following is true for all  $L > L_0$  and  $\varphi \in S^1$ : for each  $v^{ss}, v^{uu} \in B$  there is a unique solution  $v(x)$  of (3.1), defined for  $x \in [-L, L]$  such that*

$$v(-L) \in \Sigma_{in}, \quad v(L) \in \Sigma_{out}, \quad v^c(0) = \varphi, \quad v(x) \in \mathcal{V} \quad \forall x \in [-L, L].$$

Furthermore, we have

$$\begin{aligned} v(-L) &= (\varphi - L + O(e^{-\eta L}), \delta, O(e^{-\eta L}), v^{ss} + O(e^{-\eta L}), O(e^{-\eta L})) \\ v(0) &= (\varphi, O(e^{-\eta L}), O(e^{-\eta L}), O(e^{-\eta L}), O(e^{-\eta L})) \\ v(L) &= (\varphi + L + O(e^{-\eta L}), O(e^{-\eta L}), O(e^{-\eta L}), \delta, v^{uu} + O(e^{-\eta L})). \end{aligned} \quad (3.7)$$

The solution  $v(x)$  is smooth in  $(L, \varphi, \mu, v^{ss}, v^{uu})$  and the error estimates in (3.7) can be differentiated.

We now introduce the front and back solutions. As before, we define  $u_f(x; \varphi)$  so that

$$u_f(0; \varphi) \in \Sigma_{in} \cap W^u(0, z(\varphi)) \cap W^{ss}(\gamma(-\varphi, z(\varphi)), z(\varphi)), \quad (3.8)$$

and with  $u_b(x; \varphi) := \mathcal{R}u_f(-x; \varphi)$ , we have

$$u_b(0; \varphi) \in \Sigma_{out} \cap W^s(0, z(\varphi)) \cap W^{uu}(\gamma(\varphi, z(\varphi)), z(\varphi)). \quad (3.9)$$

By Hypothesis 3.3.2 we then have

$$u_f(0; \varphi) = (-\varphi, \delta, h(\varphi, z(\varphi), 0), 0, 0) \quad (3.10)$$

$$u_b(0; \varphi) = (\varphi, 0, 0, \delta, h(\varphi, z(\varphi), 0)). \quad (3.11)$$

Under these conditions we have the following analogue of Theorem 3.1:

**Theorem 3.2.** *Fix  $\epsilon > 0$ , then there exist  $\eta, K, C > 0$  such that for each  $\varphi_1^*, \varphi_2^* \in S^1$  with  $\mu = z(\varphi_1^*) = z(\varphi_2^*)$  and  $|z'(\varphi_1^*)|, |z'(\varphi_2^*)| \geq \epsilon$ , and for each  $k \in \mathbb{N}, k \geq K$ , and  $m \in \{0, 1\}$ , we can define  $\varphi_1 = \varphi_1^*, \varphi_2 = \varphi_2^* + 2m\pi$ , and*

$$L = L(\varphi_1, \varphi_2, k) := \frac{\varphi_1 + \varphi_2}{2} + 2k\pi + O(e^{-\eta 2k\pi}), \quad (3.12)$$

$$\varphi = \varphi(\varphi_1, \varphi_2, k) := \frac{\varphi_2 - \varphi_1}{2} + O(e^{-\eta 2k\pi}) \quad (3.13)$$

*such that there exists a unique solution  $u_1(x) = u_1(x; \varphi_1, \varphi_2, k)$  of (3.1), depending smoothly on  $(\varphi_1, \varphi_2)$  for each  $k$ , with  $\lim_{|x| \rightarrow \infty} |u_1(x)| = 0$ ,  $u_1(x) \in \mathcal{V}$  for  $x \in [-L, L]$ ,*

and in the coordinate system introduced in (3.3) near the periodic orbit  $\gamma$  we have

$$\begin{aligned}
u_1(-L) &= (\varphi - L + O(e^{-\eta L}), \delta, h(\varphi_1, 0, z(\varphi_1)) + O(e^{-\eta L}), O(e^{-\eta L}), O(e^{-\eta L})) \\
u_1(0) &= (\varphi, O(e^{-\eta L}), O(e^{-\eta L}), O(e^{-\eta L}), O(e^{-\eta L})) \\
u_1(L) &= (\varphi + L + O(e^{-\eta L}), O(e^{-\eta L}), O(e^{-\eta L}), \delta, h(\varphi_2, 0, z(\varphi_2)) + O(e^{-\eta L})),
\end{aligned} \tag{3.14}$$

where the first coordinate is understood to be taken modulo  $2\pi$ . Moreover,

$$|u_1(x) - u_f(x + L; \varphi_1)| \leq C e^{\eta x}, \quad x \leq -L \tag{3.15}$$

$$|u_1(x) - u_f(x + L; \varphi_1)| \leq C e^{-\eta L}, \quad -L \leq x \leq 0 \tag{3.16}$$

$$|u_1(x) - u_b(x - L; \varphi_2)| \leq C e^{-\eta L}, \quad 0 \leq x \leq L \tag{3.17}$$

$$|u_1(x) - u_b(x - L; \varphi_2)| \leq C e^{-\eta x}, \quad x \geq L \tag{3.18}$$

Similarly, there exists a unique solution  $u_2(x) = u_2(x; \varphi_1, \varphi_2, k)$  of (2.1), depending smoothly on  $(\varphi_1, \varphi_2)$  for each  $k$ , and with  $L$  and  $\varphi$  as in (3.12) and (3.13), such that  $\lim_{|x| \rightarrow \infty} |u_2(x)| = 0$ ,  $u_2(x) \in \mathcal{V}$  for  $x \in [-L, L]$ , and

$$\begin{aligned}
u_2(-L) &= (-\varphi - L + O(e^{-\eta L}), \delta, h(\varphi_2, 0, z(\varphi_2)) + O(e^{-\eta L}), O(e^{-\eta L}), O(e^{-\eta L})) \\
u_2(0) &= (-\varphi, O(e^{-\eta L}), O(e^{-\eta L}), O(e^{-\eta L}), O(e^{-\eta L})) \\
u_2(L) &= (-\varphi + L + O(e^{-\eta L}), O(e^{-\eta L}), O(e^{-\eta L}), \delta, h(\varphi_1, 0, z(\varphi_1)) + O(e^{-\eta L})),
\end{aligned} \tag{3.19}$$

where again the first coordinate is understood to be taken modulo  $2\pi$ . Moreover,

$$|u_2(x) - u_f(x + L; \varphi_2)| \leq Ce^{\eta x}, \quad x \leq -L \quad (3.20)$$

$$|u_2(x) - u_f(x + L; \varphi_2)| \leq Ce^{-\eta L}, \quad -L \leq x \leq 0 \quad (3.21)$$

$$|u_2(x) - u_b(x - L; \varphi_1)| \leq Ce^{-\eta L}, \quad 0 \leq x \leq L \quad (3.22)$$

$$|u_2(x) - u_b(x - L; \varphi_1)| \leq Ce^{-\eta x}, \quad x \geq L \quad (3.23)$$

**Proof.** As before, we wish to show that for  $L$  and  $\varphi$  as in (3.12)–(3.13) we can satisfy

$$u_1(-L) \in \Sigma_{in} \cap W^u(0, z(\varphi_1)), \quad u_1(L) \in \Sigma_{out} \cap W^s(0, z(\varphi_2)). \quad (3.24)$$

We note that  $(\varphi, \delta, v^{ss}, v^u, v^{uu}) \in \Sigma_{in} \cap W^u(0, \mu)$  if and only if  $\mathcal{R}(\varphi, \delta, v^{ss}, v^u, v^{uu}) = (-\varphi, v^u, v^{uu}, v^s, v^{ss}) \in \Sigma_{out} \cap W^s(0, \mu)$ . So by Hypothesis 3.3.2, the conditions in (3.24) are equivalent to the  $2n - 2$  conditions

$$u_1^u(-L) = g(-u_1^c(-L), z(\varphi_1), u_1^{uu}(-L)) \quad (3.25)$$

$$u_1^{ss}(-L) = h(-u_1^c(-L), z(\varphi_1), u_1^{uu}(-L)) \quad (3.26)$$

$$u_1^s(L) = g(u_1^c(L), z(\varphi_2), u_1^{ss}(L)) \quad (3.27)$$

$$u_1^{uu}(L) = h(u_1^c(L), z(\varphi_2), u_1^{ss}(L)) \quad (3.28)$$

Define

$$L = L(\varphi_1, \varphi_2, k, \varepsilon_1) := \frac{\varphi_1 + \varphi_2}{2} + 2k\pi + \varepsilon_1 \quad (3.29)$$

$$\varphi = \varphi(\varphi_1, \varphi_2, \varepsilon_2) := \frac{\varphi_2 - \varphi_1}{2} + \varepsilon_2 \quad (3.30)$$

$$w^{ss} = w^{ss}(\varphi_1, \varepsilon_3) := h(\varphi_1, z(\varphi_1), 0) + \varepsilon_3 \quad (3.31)$$

$$w^{uu} = w^{uu}(\varphi_2, \varepsilon_4) := h(\varphi_2, z(\varphi_2), 0) + \varepsilon_4 \quad (3.32)$$

with  $\varepsilon_1, \varepsilon_2 \in \mathbb{R}$  and  $\varepsilon_3, \varepsilon_4 \in \mathbb{R}^{n-2}$ . Let  $u_1(x) = u_1(x; L, \varphi, w^{ss}, w^{uu})$  be the unique solution such that  $u_1(x) \in \mathcal{V}$  for  $x \in [-L, L]$  and

$$\begin{aligned} u_1(-L) &= (\varphi - L + O(e^{-\eta L}), \delta, w^{ss} + O(e^{-\eta L}), O(e^{-\eta L}), O(e^{-\eta L})) \\ u_1(0) &= (\varphi, O(e^{-\eta L}), O(e^{-\eta L}), O(e^{-\eta L}), O(e^{-\eta L})) \\ u_1(L) &= (\varphi + L + O(e^{-\eta L}), O(e^{-\eta L}), O(e^{-\eta L}), \delta, w^{uu} + O(e^{-\eta L})). \end{aligned} \quad (3.33)$$

Then substituting from (3.33) into (3.25), Taylor expanding about

$$(-u_f^c(0; \varphi_1, z(\varphi_1), u_f^{uu}(0; \varphi_1)) = (\varphi_1, z(\varphi_1), 0),$$

and using (3.29)–(3.30), we have

$$\begin{aligned} O(e^{-\eta L}) &= g(\varphi_1, z(\varphi_1), 0) + g_{v^c}(\varphi_1, z(\varphi_1), 0)(\varepsilon_2 - \varepsilon_1 + O(e^{-\eta L})) \\ &\quad + g_{v^{ss}}(\varphi_1, z(\varphi_1), 0)O(e^{-\eta L}) + O((\varepsilon_2 - \varepsilon_1 + O(e^{-\eta L}))^2) + O(e^{-2\eta L}). \end{aligned} \quad (3.34)$$

By Hypothesis 3.3.2,  $g(\varphi_1, z(\varphi_1), 0) = 0$ , so

$$\varepsilon_1 = \frac{O(e^{-\eta L})(1 + g_{v^{ss}}(\varphi_1, z(\varphi_1), 0)) + O((\varepsilon_2 - \varepsilon_1 + O(e^{-\eta L}))^2)}{g_{v^c}(\varphi_1, z(\varphi_1), 0)} + \varepsilon_2 + O(e^{-\eta L}). \quad (3.35)$$

Similarly, substituting from (3.33) into (3.27), Taylor expanding about

$$(u_b^c(0; \varphi_2), z(\varphi_2), u_b^{ss}(0; \varphi_2)) = (\varphi_2, z(\varphi_2), 0),$$

and using (3.29)–(3.30), we have

$$\begin{aligned} O(e^{-\eta L}) &= g(\varphi_2, z(\varphi_2), 0) + g_{vc}(\varphi_2, z(\varphi_2), 0)(\varepsilon_1 + \varepsilon_2 + O(e^{-\eta L})) \\ &\quad + g_{vss}(\varphi_2, z(\varphi_2), 0)O(e^{-\eta L}) + O((\varepsilon_1 + \varepsilon_2 + O(e^{-\eta L}))^2) + O(e^{-2\eta L}) \end{aligned} \quad (3.36)$$

so that

$$\begin{aligned} \varepsilon_2 &= \frac{O(e^{-\eta L})(1 - g_{vss}(\varphi_2, z(\varphi_2), 0)) + O((\varepsilon_1 + \varepsilon_2 + O(e^{-\eta L}))^2)}{g_{vc}(\varphi_2, z(\varphi_2), 0)} \\ &\quad - \frac{O(e^{-\eta L})(1 + g_{vss}(\varphi_1, z(\varphi_1), 0)) + O((\varepsilon_2 - \varepsilon_1 + O(e^{-\eta L}))^2)}{g_{vc}(\varphi_1, z(\varphi_1), 0)} + O(e^{-\eta L}). \end{aligned} \quad (3.37)$$

Then since  $g(\varphi, z(\varphi), 0) \equiv 0$  for all  $\varphi$  and  $|g_\mu(\varphi, z(\varphi), 0)| > 0$  by Hypothesis 3.3.2, and  $|z'(\varphi_i)| > 0$  for  $i = 1, 2$  by assumption, both  $\varepsilon_1$  and  $\varepsilon_2$  are  $O(e^{-\eta L})$ .

Turning now to  $\varepsilon_3$  and  $\varepsilon_4$ , substituting from (3.33) into (3.26), Taylor expanding about  $h(-u_f^c(0; \varphi_1), z(\varphi_1), u_f^{uu}(0; \varphi_1)) = h(\varphi_1, z(\varphi_1), 0)$ , and using (3.31), we have

$$\begin{aligned} h(\varphi_1, z(\varphi_1), 0) + \varepsilon_3 + O(e^{-\eta L}) &= h(\varphi_1, z(\varphi_1), 0) + h_{vc}(\varphi_1, z(\varphi_1), 0)((\varepsilon_2 - \varepsilon_1 + O(e^{-\eta L})) \\ &\quad + h_{vss}(\varphi_1, z(\varphi_1), 0)(O(e^{-\eta L})) + O((\varepsilon_2 - \varepsilon_1 + O(e^{-\eta L}))^2) + O(e^{-2\eta L}) \end{aligned} \quad (3.38)$$

so that  $\varepsilon_3 = O(e^{-\eta L})$ . By an analogous argument,  $\varepsilon_4 = O(e^{-\eta L})$ . Thus  $u_1(x)$  with  $L, \varphi, w^{ss}, w^{uu}$  as in (3.29)–(3.32) satisfies (3.24), and since  $\varepsilon_i = O(e^{-\eta L})$ ,  $i = 1, 2, 3, 4$ , the expressions in (3.14) also hold.

Now (3.14) combined with (3.10)–(3.11) shows  $|u_1(-L) - u_f(0; \varphi_1)| = O(e^{-\eta L})$  and  $|u_1(L) - u_b(0; \varphi_2)| = O(e^{-\eta L})$ . Then the expressions (3.15) and (3.18) follow from the stable manifold theorem, while (3.16) and (3.17) follow from the proof of

Lemma 3.3.3 (see [4], Lemma 6.2 and Section 3.2.1 above). The claims for  $u_2(x) = \mathcal{R}u_1(-x)$  follow as before. ■

**Remark 3.3.4.** *These results can be extended to an appropriate infinite dimensional Banach space, as is necessary to address patterns on the plane which are localized in one direction and periodic in the second. Our results immediately carry over to the infinite dimensional case provided the system is such that we can apply the results developed in [51, 58] on exponential dichotomies and the existence of stable and unstable manifolds of the periodic orbits  $\gamma(x, \mu)$ , foliated by smooth strong stable and strong unstable fibers. We refer to the treatment of the Swift–Hohenberg equation on the plane in Section 6.3 of [4] for further details.*

While we have not explicitly addressed the presence of an additional  $\mathbb{Z}_2$  symmetry here, we remark the results carry over from [4] in a straightforward way. As shown there, the presence of an additional  $\mathbb{Z}_2$  symmetry  $\kappa$  implies that  $z(\varphi)$  will be  $\pi$ -periodic (recall that we have taken the minimal period  $l(u)$  of the periodic orbits to be  $2\pi$ .) To see that this implies the existence of four asymmetric solutions with the same  $L$  and  $\varphi$  for a given  $\mu$ , we take without loss of generality  $\varphi_1^*, \varphi_2^* \in [0, \pi)$  and note that  $\mu = z(\varphi_1^*) = z(\varphi_2^*)$  implies  $\mu = z(\varphi_1^* + \pi) = z(\varphi_2^* + \pi)$  and the solutions corresponding to  $\varphi_1^*, \varphi_2^*, m = 0, k = k_0$  will have the same  $L$  and  $\varphi$ , up to exponentially small corrections, as  $\varphi_1^* + \pi, \varphi_2^* + \pi, m = 1, k = k_0 - 1$ . That the four solutions actually have the same  $L$  and  $\varphi$  follows by applying  $\kappa$  and invoking uniqueness. We note that the solutions can thus be written  $u_1(x)$ ,  $\mathcal{R}u_1(-x)$ ,  $\kappa u_1(x)$ , and  $\kappa \mathcal{R}u_1(-x)$ .

### 3.4 Numerical illustrations

We now demonstrate that the appearance of asymmetric patterns is as expected based on the above arguments, using the planar stripe and spot pattern of the planar cubic–quintic Swift–Hohenberg equation:

$$U_t = -(1 + \partial_x^2 + \partial_y^2)^2 U - \mu U + \nu U^3 - U^5, \quad (x, y) \in \mathbb{R} \times S^1 \quad (4.1)$$

where  $S^1 = \mathbb{R}/2L_y\mathbb{Z}$  for some  $L_y > 0$ . We note that the bifurcation diagram for these patterns was first computed in [3]. We recall that steady-state solutions of (4.4) can be considered as solutions to a spatial dynamical system in  $u = (u, u_x, u_{xx}, u_{xxx}) \in Y := H^3(S^1) \times H^2(S^1) \times H^1(S^1) \times L^2(S^1)$ .

Numerical simulations were completed in MATLAB, using a modified version of EPCONT, a predecessor of COCO [14], as in [3]. The modifications made to EPCONT include employing the Newton trust-region solver FSOLVE, and projecting out the approximate translation directions in each predictor step. We use spectral differentiation matrices in the periodic  $y$ -direction, and centered finite differences in the  $x$ -direction. In particular, we used  $n_y = 8$  Fourier modes and  $n_x = 800$  equidistant points on the domain  $[-50, 50] \times [0, \pi]$  with Neumann boundary conditions. These computations appeared in [42].

Figure 3.3 shows the bifurcation diagram for the stripe and spot pattern of (4.1), along with selected solution profiles along an  $\mathcal{R}$ -symmetric snaking branch and a cross-connecting branch of asymmetric solutions. The term “cross-connecting” refers to the fact that the solution branch originates in a pitchfork bifurcation from the  $\mathcal{R}$ -symmetric branch, and terminates at a pitchfork bifurcation at the  $\kappa\mathcal{R}$ -symmetric branch, where  $\kappa : u(y) \mapsto -u(L_y - y)$ . The solution profiles are shown with the

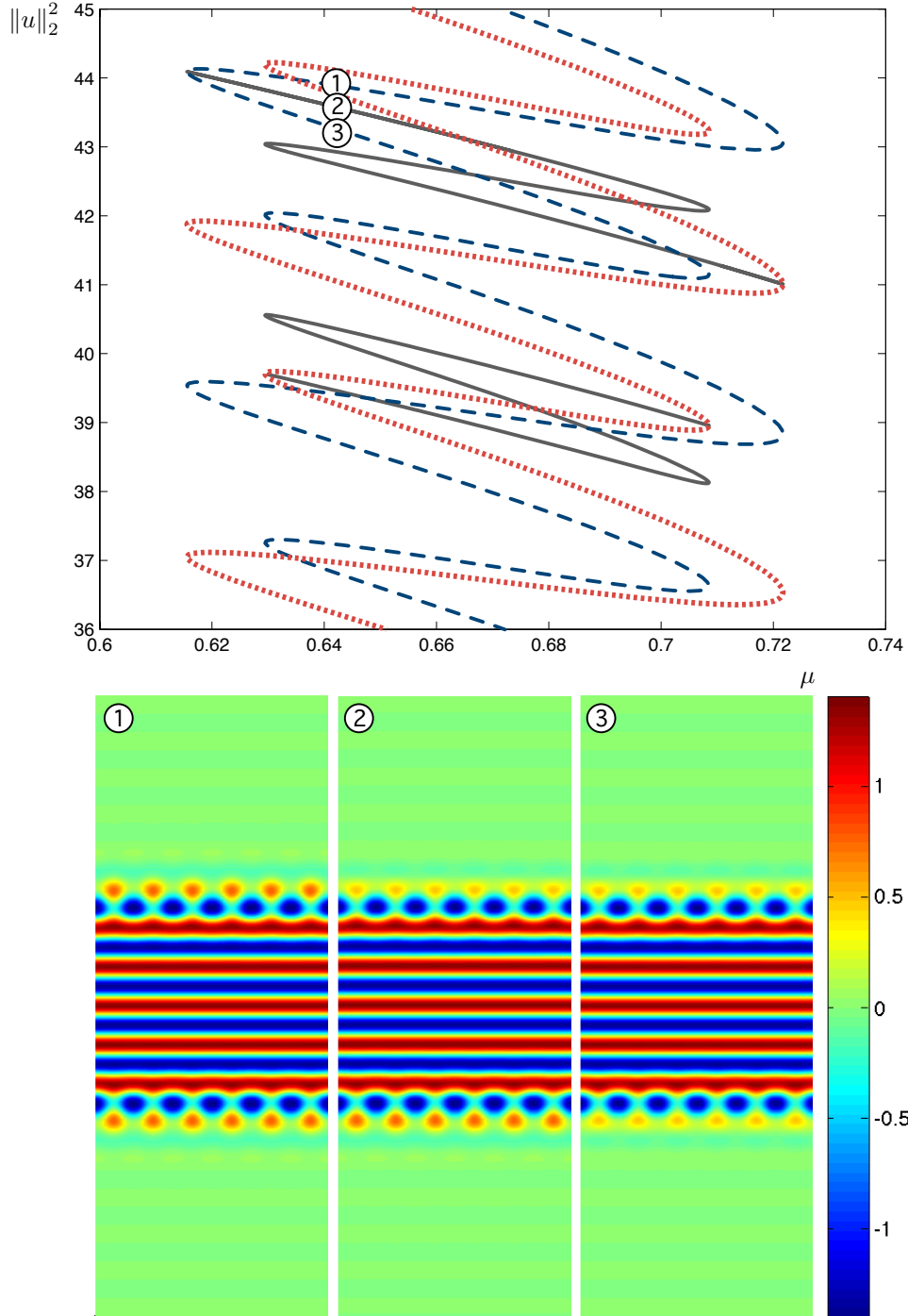


**Figure 3.3:** Bifurcation diagram and particular planar stripes and spots solutions to (4.1), with numbers indicating the correspondence between the bifurcation diagram and solution profiles. In the bifurcation diagram,  $\mathcal{R}$ -symmetric branches are shown in dashed blue,  $\kappa\mathcal{R}$ -symmetric branches are in dotted orange, and representative asymmetric branches are in solid gray. Solution profiles are oriented with the  $x$ -axis pointing up, and the color indicating the height of the solution, as indicated in the color bar. Recalling that solutions are periodic in the  $y$ -direction, we show 6 periods for each solution. Solutions 1 and 3 are  $\mathcal{R}$ -symmetric solutions, while solution 2 is an asymmetric solution at the same parameter value. We observe that solution 2 matches solution 1 for  $x \leq 0$ , i.e., the bottom half of the profiles, while solution 2 matches solution 3 for  $x \geq 0$ , i.e., the top half of the profiles. The bifurcation diagram for these patterns was first computed in [3].

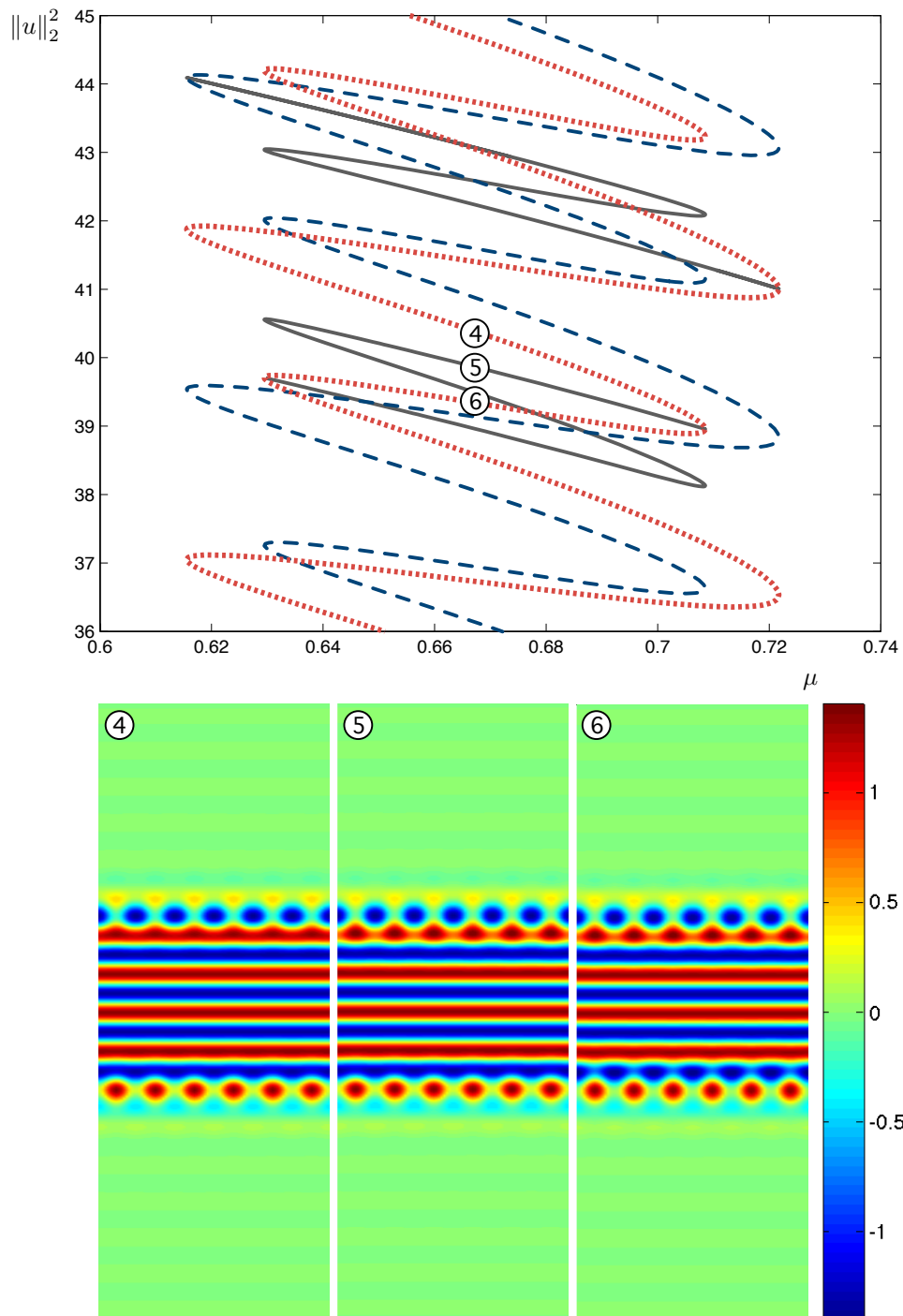


**Figure 3.4:** Bifurcation diagram as in Figure 3.3 and additional planar stripes and spots solutions, again with numbers indicating the correspondence between the bifurcation diagram and solution profiles. Here solutions 4 and 6 are  $\kappa\mathcal{R}$ -symmetric solutions, while solution 5 is an asymmetric solution at the same parameter value. We observe that solution 5 matches solution 4 for  $x \leq 0$ , i.e., the bottom half of the profiles, while solution 5 matches solution 6 for  $x \geq 0$ , i.e., the top half of the profiles.

periodic  $y$ -axis in the horizontal direction, and the  $x$ -axis, along which localization occurs, in the vertical direction. Solutions 1 and 3 are  $\mathcal{R}$ -symmetric solutions, while solution 2 is an asymmetric solution, all existing for the same value of  $\mu$ . We observe that solution 2 matches solution 1 for  $x \leq 0$  (the top half of the profiles), while it matches solution 3 for  $x \geq 0$  (the bottom half of the profiles).

In Figure 3.4 we provide an additional illustration of our results. We again show the bifurcation diagram for the stripe and spot pattern of (4.1), along with additional solution profiles, in this case along a  $\kappa\mathcal{R}$ -symmetric branch and a self-connecting asymmetric branch. A “self-connecting” branch is one that begins and ends at pitchfork bifurcations from the same symmetric branch, in this case a  $\kappa\mathcal{R}$ -symmetric branch. Here solutions 4 and 6 are  $\kappa\mathcal{R}$ -symmetric solutions, while solution 5 is an asymmetric solution. Again we observe that solution 5 matches solution 4 for  $x \leq 0$  and solution 6 for  $x \geq 0$ .

# CHAPTER FOUR

---

## Stability of Localized Patterns

## 4.1 Introduction

We now turn to the question of stability for localized patterns. Stability is, of course, an important consideration if we hope to be able to say something about which solutions are experimentally relevant or physically observable in the wide range of natural systems mentioned at the outset. In the following two chapters, we will consider several questions related to the spectra of localized solutions and fronts. In Figure 4.1, we have plotted the expected spectra of the PDE operators linearized about a front and localized solution, respectively. We emphasize that the bottom diagram depicts our expectation, but remains to be rigorously established under suitable hypotheses in the following.

We first make some remarks on the spectral plots in Figure 4.1. The fact that the essential spectrum of a localized solution biasymptotic to the trivial state will correspond to  $\Sigma_{ess}^0$ , the essential spectrum of the trivial state, is well known and we refer to the review article [56], as well as Appendix B. The appearance of the spectrum for localized solutions in the left half plane, in which the essential spectrum of the periodic state,  $\Sigma_{ess}^\gamma$ , breaks up into  $O(L)$  eigenvalues has been explained in [57]. As to the eigenvalues with  $\text{Re } \lambda \geq 0$ , a frequently used result establishing the nonlinear stability of traveling wave solutions is that, loosely stated, spectral stability implies nonlinear asymptotic stability provided that the spectrum is bounded away from 0 in the left half plane, with the exception of a simple eigenvalue at  $\lambda = 0$  [24]. The application of the result in this case is somewhat delicate due to the accumulation of spectrum up to the imaginary axis as  $L \rightarrow \infty$ , but in any event, the absence of spectrum in the right half plane is a necessary condition for stability.

There are essentially three questions we wish to address. First, is it true that

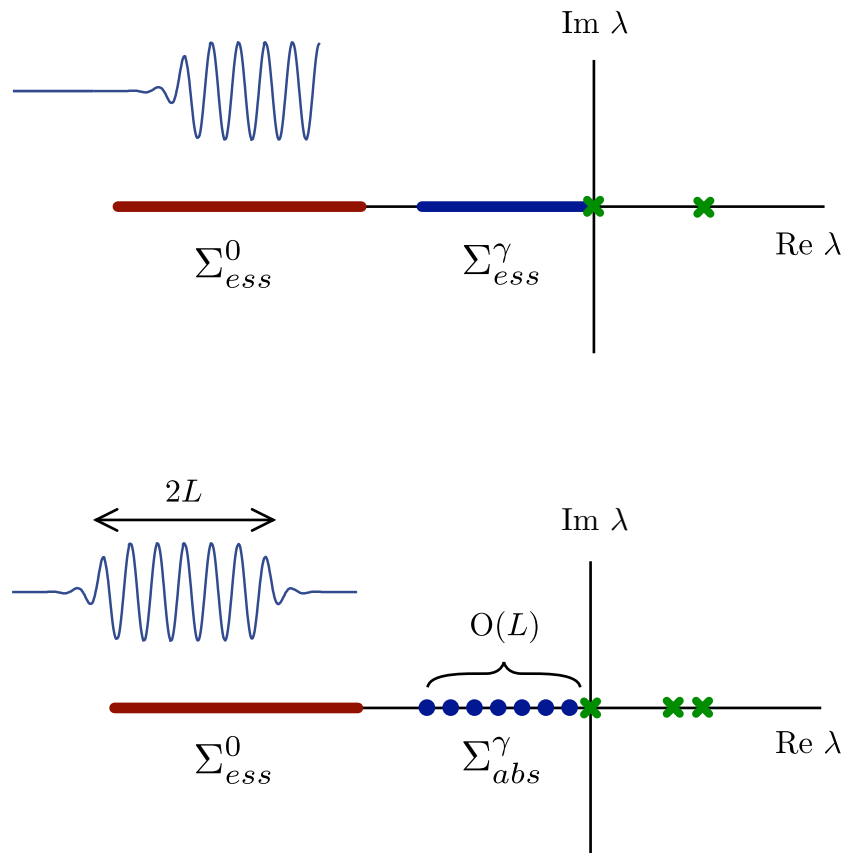


**Figure 4.1:** Schematic diagrams of spectra for the front and pulse solutions.  $\Sigma_{ess}^0$  refers to the essential spectrum of the trivial state, and  $\Sigma_{ess}^\gamma$  and  $\Sigma_{abs}^\gamma$  to the essential and absolute spectra of the patterned state. The crosses indicate individual eigenvalues.

eigenvalues of a localized solution in the right half plane correspond to those of the front and back from which the solution is formed, added with multiplicity? Second, is the eigenvalue of the localized solution at  $\lambda = 0$  simple, provided that the eigenvalue of the front at  $\lambda = 0$  is simple in an appropriate sense, or is it too added with multiplicity? And finally, as eigenvalues corresponding to saddle node and pitchfork bifurcations move in and out of the right half plane upon varying a parameter, what happens as they enter the left half plane? We will address the first question in this chapter, answering in the affirmative. The analysis of the second and third questions, the latter of which we will define more precisely, requires an analytic extension of the Evans function of the fronts (and backs) into the left half plane; we construct this extension in Chapter 5. We then show that the eigenvalue at  $\lambda = 0$  is in fact simple for a localized solution, but we also observe that there is a sense in which this corresponds to adding with multiplicity. We will approach all stability problems from an ODE perspective, as was briefly motivated in Section 2.1, and is discussed more fully in Appendix B.

## 4.2 Exponential dichotomies and general approach

For the results in this chapter we do not require the full set of hypotheses used for the existence results given in the previous chapter. We do, however, wish to use the results on the exponential closeness of the localized solutions  $u_1(x)$  to the fronts and backs  $u_f(x)$  and  $u_b(x)$  and in turn to the periodic solution  $\gamma(x)$ , as captured in Theorems 3.1 and 3.2. In order to clearly identify the hypotheses that are necessary for our results, and to avoid introducing additional assumptions or machinery, we reformulate the results of Theorem 3.2 and introduce them as Hypothesis 4.3.1. We further show how Hypotheses 4.3.1 and 4.3.2 are satisfied in the context of Section

3.3 (see Lemma 4.3.4).

In the following, we will consider a localized solution along with the front and back to which it is exponentially close, and show that its temporal eigenvalues in the right half plane are exponentially close to those of the front and back, added with multiplicity.

We again consider

$$u_x = f(u, \mu) \tag{2.1}$$

with  $u \in \mathbb{R}^{2n}$  and  $\mu \in \mathbb{R}$ .

As described for the particular example of the Swift–Hohenberg equation in Section 2.1 and discussed in Appendix B, we will be interested in systems of the form

$$\dot{v} = [f_u(u_*(x), \mu) + \lambda B(u_*(x), \mu)]v \tag{2.2}$$

with  $v \in \mathbb{C}^{2n}$ ,  $\lambda \in \mathbb{C}$  and  $B : \mathbb{R}^{2n} \times \mathbb{R} \rightarrow \mathbb{R}^{2n \times 2n}$ , and where  $u_*(x)$  is a particular solution of (2.1). We assume that  $f$  and  $B$  are smooth (at least  $C^2$  and  $C^1$ , respectively).

We will make use of exponential dichotomies possessed by several systems of the form (2.2) and refer to Appendix A.1 for the relevant definition, as well as the statement of the so-called roughness theorem for exponential dichotomies. We further refer to Appendix B for results on the relationship between the spectrum of a PDE operator, exponential dichotomies of the corresponding ODE, and the Fredholm properties of the family of operators  $\mathcal{T}(\lambda)$ .

The general idea will be to use information about (2.2) with  $u_*(x) = u_f(x), u_b(x), \gamma(x)$

and the trivial 0 solution at  $\lambda = \lambda_*$  to establish the presence or absence of nontrivial, bounded solutions of (2.2) with  $u_*(x) = u_\ell(x)$ , with  $u_\ell(x)$  a localized solution, for  $\lambda$  near  $\lambda_*$ . There are (at least) two possible ways in which to proceed:

- (i) Write the solution to the eigenvalue problem (2.2) with  $u_*(x) = u_\ell(x)$  for  $\lambda$  near  $\lambda_*$  in terms of the exponential dichotomies for  $u_f$  and  $u_b$  at  $\lambda = \lambda_*$ , using the variation of constants formula. We take this approach in Section 4.5 and Appendix C, assuming a simple eigenvalue of the front at  $\lambda_*$ ; as compared to our second approach, it yields more precise information about the eigenvalue location and eigenfunction form as a perturbation of the eigenfunction of the front, but at least in the context of determining when a localized solution is stable, this level of detail is not necessary.
- (ii) Write the solution to the eigenvalue problem (2.2) with  $u_*(x) = u_\ell(x)$  for  $\lambda$  near  $\lambda_*$  directly in terms of exponential dichotomies for this system depending smoothly on  $\lambda$  sufficiently near  $\lambda_*$ , which exist due to the roughness theorem for exponential dichotomies. This is the approach we take in Section 4.3 to study eigenvalues of arbitrary multiplicity in the right half plane. Since we care primarily about the presence or absence of eigenvalues in the right half plane, rather than precise locations or characterization of the corresponding eigenfunctions, this approach provides shorter and cleaner results.

### 4.3 Eigenvalues in the right half plane

We note that in the following we refer to various constants and rates by  $C, \eta > 0$  without keeping track of them individually. All such constants may be chosen independently of  $L$  for  $L > L_*$  sufficiently large and other relevant variables. In

particular, we do not distinguish the constants appearing in our hypotheses regarding (1) the exponential closeness of the localized solutions to fronts and backs, (2) the exponential closeness and decay of the fronts and backs to the periodic solution and the trivial state, and (3) the existence of particular exponential dichotomies. A localized solution will be unstable if it has an eigenvalue in the right half plane, and we wish only to establish the presence or absence of such eigenvalues. Thus, more careful bookkeeping is not relevant in this context.

We let  $\Omega = \{\lambda \in \mathbb{C} : \operatorname{Re}\lambda > 0\}$ . We fix  $\mu$  so that the following hypotheses are satisfied, and suppress all  $\mu$  dependence for the remainder of this section.

As described in Lemma 4.3.4 below, our first hypothesis allows us to introduce a reformulated version of the results given in Theorem 3.2 without requiring additional hypotheses that are extraneous to our present purposes.

**Hypothesis 4.3.1.** *There exists a family of solutions  $u_{\ell,L}(x)$  to (2.1), parameterized by  $L = L(k)$ ,  $k \in \mathbb{N}$ , with  $k \geq K$  for some  $K > 0$ , and such that  $L(k)$  increases monotonically without bound. These solutions, which we will refer to as localized solutions, satisfy:*

$$u_{\ell,L}(x) = \begin{cases} u_f(x+L) + w_f^-(x+L;L), & x \leq -L \\ u_f(x+L) + w_f^+(x+L;L), & x \in [-L, 0] \\ u_b(x-L) + w_b^-(x-L;L), & x \in [0, L] \\ u_b(x-L) + w_b^+(x-L;L), & x \geq L \end{cases} \quad (3.1)$$

where  $u_f(x)$  and  $u_b(x)$  are also solutions to (2.1) that are independent of  $L$  and

satisfy  $\lim_{x \rightarrow -\infty} u_f(x) = 0$  and  $\lim_{x \rightarrow \infty} u_b(x) = 0$ . We also have

$$w_f^-(0; L) = w_f^+(0; L) \quad (3.2)$$

$$u_f(L; L) + w_f^-(L; L) = u_b(-L; L) + w_b^+(-L; L) \quad (3.3)$$

$$w_b^-(0; L) = w_b^+(0; L), \quad (3.4)$$

and there exist positive constants  $C$  and  $\eta$  such that

$$|w_f^-(x; L)| \leq Ce^{-\eta(L-x)}, \quad x \leq 0 \quad (3.5)$$

$$|w_f^+(x; L)| \leq Ce^{-\eta L}, \quad x \in [0, L] \quad (3.6)$$

$$|w_b^-(x; L)| \leq Ce^{-\eta L}, \quad x \in [-L, 0] \quad (3.7)$$

$$|w_b^+(x; L)| \leq Ce^{-\eta(L+x)}, \quad x \geq 0. \quad (3.8)$$

We then require the solutions  $u_f(x)$  and  $u_b(x)$  to relate to a single solution  $\gamma(x)$  as follows:

**Hypothesis 4.3.2.** *There exists a solution  $\gamma(x)$  of (2.1) and positive constants  $C$  and  $\eta$  such that the following holds uniformly in  $L = L(k)$ ,  $k \geq K$  as in Hypothesis 4.3.1:*

$$|u_f(L) - \gamma(0)| \leq Ce^{-\eta L} \quad (3.9)$$

$$|u_b(-L) - \gamma(0)| \leq Ce^{-\eta L}. \quad (3.10)$$

Moreover, there exists a constant  $c \in [0, 2\pi)$ , and positive constants  $C$  and  $\eta$ , all

independent of  $L$ , such that

$$|u_f(x) - \gamma(x + c)| \leq Ce^{-\eta x}, \quad x \geq 0 \quad (3.11)$$

$$|u_b(x) - \gamma(x - c)| \leq Ce^{\eta x}, \quad x \leq 0. \quad (3.12)$$

Finally,

$$|u_f(x)| \leq Ce^{\eta x}, \quad x \leq 0 \quad (3.13)$$

$$|u_b(x)| \leq Ce^{-\eta x}, \quad x \geq 0. \quad (3.14)$$

We will use the exponential closeness of  $u_f(L)$  and  $u_b(-L)$  to  $\gamma(0)$  in finding bounded solutions to (2.2) with  $u_*(x) = u_{\ell,L}(x)$ . We include the exponential approach so that we may take as our final two hypotheses the existence of exponential dichotomies associated to  $\gamma(x)$  and the trivial state, from which we deduce the existence of exponential dichotomies of the front and back.

**Remark 4.3.3.** *Since we no longer have dependence on  $\varphi_1$  and  $\varphi_2$ , we emphasize that the solutions  $u_f(x)$  and  $u_b(x)$  are not necessarily related by reversibility, though this possibility is not excluded. Indeed, we do not use or assume reversibility anywhere in this section.*

As mentioned already, these hypotheses are in fact satisfied in the setting of the previous chapter:

**Lemma 4.3.4.** *Suppose that we are in the setting of Section 3.3, so that Hypotheses 3.3.1–3.3.2 and the analogues of Hypotheses 3.2.1–3.2.3 are satisfied, and Theorem 3.2 holds. Denote by  $\hat{\gamma}(x)$ ,  $\hat{u}_f(x)$  and  $\hat{u}_b(x)$  the periodic, front, and back solutions introduced in Section 3.3. Fix  $\mu \in J$ ,  $\varphi_1^*, \varphi_2^* \in [0, 2\pi)$ , and  $m \in \{0, 1\}$ , with  $\mu =$*

$z(\varphi_1^*) = z(\varphi_2^*)$  and  $|z'(\varphi_1^*)|, |z'(\varphi_2^*)| \neq 0$ . Let  $\varphi_1, \varphi_2$  and  $L(\varphi_1, \varphi_2, k)$  be as defined in Theorem 3.2, and let  $u_1(x; \varphi_1, \varphi_2, k)$  be the localized solution associated to  $\hat{u}_f(x; \varphi_1)$ ,  $\hat{u}_b(x; \varphi_2)$  as given by Theorem 3.2. Further define  $\bar{\varphi} = (\varphi_2 - \varphi_1)/2$  and  $c = (\varphi_1 + \varphi_2)/2 \pmod{2\pi}$ . Then there exists  $K > 0$  such that Hypotheses 4.3.1 and 4.3.2 hold, with  $L = L(k)$  as given in Theorem 3.2,  $u_{\ell, L}(x) = u_1(x - \bar{\varphi}; \varphi_1, \varphi_2, k)$ ,  $u_f(x) = \hat{u}_f(x - \bar{\varphi}; \varphi_1)$ ,  $u_b(x) = \hat{u}_b(x - \bar{\varphi}; \varphi_2)$ , and  $\gamma(x) = \hat{\gamma}(x)$ .

**Remark 4.3.5.** As is clear from the following proof, the constant  $K > 0$  for which Hypotheses 4.3.1 and 4.3.2 hold may need to be larger than that for Theorem 3.2. The rate  $\eta > 0$  appearing in (3.5)–(3.8) is the same as that appearing in Theorem 3.2, and the constant  $C$  can be chosen independently of  $\mu, \varphi_1$  and  $\varphi_2$ . The  $\eta > 0$  appearing in Hypothesis 4.3.2 is bounded below by the  $\eta > 0$  given in Theorem 3.2.

**Proof.** (Lemma 4.3.4) Set  $L = L(k)$  as in Theorem 3.2, define  $\bar{\varphi} := (\varphi_2 - \varphi_1)/2$ , and let  $u_{\ell, L}(x) = u_1(x - \bar{\varphi}; \varphi_1, \varphi_2, k)$ ,  $u_f(x) = \hat{u}_f(x - \bar{\varphi}; \varphi_1)$ ,  $u_b(x) = \hat{u}_b(x - \bar{\varphi}; \varphi_2)$ . Since  $\varphi_1$  and  $\varphi_2$  are fixed, we generally suppress dependence on  $\varphi_1$  and  $\varphi_2$  going forward.

In order for (3.1) to hold, we define

$$w_f^-(x; L) := u_{\ell, L}(x - L) - u_f(x) = u_1(x - L - \bar{\varphi}; k) - \hat{u}_f(x - \bar{\varphi}) \quad (3.15)$$

and make analogous definitions for  $w_f^+(x; L)$  and  $w_b^\pm(x; L)$ . Then (3.2)–(3.4) are automatically satisfied due to the continuity of  $u_1$ . To avoid cluttered notation in the following, we write  $w_{f,b}^\pm(x) = w_{f,b}^\pm(x; L)$  and  $u_1(x) = u_1(x; k)$ , but dependence on  $k$  is, of course, important.

We now consider (3.5)–(3.8). First suppose that  $\bar{\varphi} > 0$ ; we can address the case  $\bar{\varphi} < 0$  by reversing the roles of  $u_f$  and  $u_b$  in the following.

By (3.15) in Theorem 3.2, we have

$$|u_1(x - L) - \hat{u}_f(x)| \leq Ce^{-\eta L} e^{\eta x}, \quad x \leq 0 \quad (3.16)$$

so that, since  $\bar{\varphi} > 0$ ,

$$|w_f^-(x)| = |u_1(x - L - \bar{\varphi}) - \hat{u}_f(x - \bar{\varphi})| \leq Ce^{-\eta L} e^{\eta x}, \quad x \leq 0 \quad (3.17)$$

also holds. Moreover, since  $\bar{\varphi} \leq 2\pi$ , it follows that

$$|w_f^+(x)| = |u_1(x - L - \bar{\varphi}) - \hat{u}_f(x - \bar{\varphi})| \leq Ce^{-\eta L}, \quad 0 \leq x \leq \bar{\varphi}. \quad (3.18)$$

Then from (3.16) in Theorem 3.2, we have

$$|u_1(x - L) - \hat{u}_f(x)| \leq Ce^{-\eta L}, \quad 0 \leq x \leq L \quad (3.19)$$

so that

$$|w_f^+(x)| = |u_1(x - L - \bar{\varphi}) - \hat{u}_f(x - \bar{\varphi})| \leq Ce^{-\eta L}, \quad \bar{\varphi} \leq x \leq L + \bar{\varphi} \quad (3.20)$$

and, as we will use momentarily,

$$|u_1(x - L - \bar{\varphi}) - \hat{u}_f(x - \bar{\varphi})| \leq Ce^{-\eta L}, \quad L \leq x \leq L + \bar{\varphi}. \quad (3.21)$$

Thus we have shown (3.5) and (3.6) hold. Now from (3.17) in Theorem 3.2 we have

$$|u_1(x + L) - \hat{u}_b(x)| \leq Ce^{-\eta L}, \quad -L \leq x \leq 0 \quad (3.22)$$

so that

$$|u_1(x + L - \bar{\varphi}) - \hat{u}_b(x - \bar{\varphi})| \leq Ce^{-\eta L}, \quad -L + \bar{\varphi} \leq x \leq \bar{\varphi} \quad (3.23)$$

To address  $|w_b^-(x)|$  on  $-L \leq x \leq -L + \bar{\varphi}$ , we note

$$\begin{aligned} |u_1(x + L - \bar{\varphi}) - \hat{u}_b(x - \bar{\varphi})| &\leq |u_1(x + L - \bar{\varphi}) - \hat{u}_f(x + 2L - \bar{\varphi})| \\ &\quad + |\hat{u}_f(x + 2L - \bar{\varphi}) - \gamma(x + L)| + |\gamma(x + L) - \hat{u}_b(x - \bar{\varphi})|. \end{aligned} \quad (3.24)$$

By (3.21), the first term on the right hand side is bounded by  $Ce^{-\eta L}$  for  $x \in [-L, -L + \bar{\varphi}]$ . We now recall (2.10) and (2.11) from Chapter 3:

$$|\hat{u}_f(x + \varphi_1) - \gamma(x)| \leq Ce^{-\eta(x + \varphi_1)}, \quad x \geq -\varphi_1 \quad (3.25)$$

$$|\hat{u}_b(x - \varphi_2) - \gamma(x)| \leq Ce^{\eta(x - \varphi_2)}, \quad x \leq \varphi_2 \quad (3.26)$$

where we have reformulated the relations slightly, and stated them for  $\varphi_1$  and  $\varphi_2$  for clarity. The second term in (3.24) is equivalent to  $|\hat{u}_f(x + L - \bar{\varphi}) - \gamma(x)|$  on  $0 \leq x \leq \bar{\varphi}$ , and since  $L - \bar{\varphi} = \varphi_1 + 2k\pi + O(e^{-\eta 2k\pi})$  and  $\gamma(x) = \gamma(x + 2k\pi)$ , we can rewrite this as

$$|\hat{u}_f(x + \varphi_1 + 2k\pi + O(e^{-\eta 2k\pi})) - \gamma(x + 2k\pi)| \quad (3.27)$$

Then Taylor expanding  $\hat{u}_f(x + \varphi_1 + 2k\pi + O(e^{-\eta 2k\pi}))$  about  $\hat{u}_f(x + \varphi_1 + 2k\pi)$ , we note that  $|\hat{u}'_f(x + \varphi_1 + 2k\pi)|$  is, for any  $\varphi_1$ , uniformly bounded in  $k \geq K$ ,  $K > 0$  sufficiently large, by a multiple of  $\sup_{x \in [0, 2\pi]} |\gamma'(x)|$ . So we conclude that

$$|\hat{u}_f(x + L - \bar{\varphi}) - \gamma(x)| \leq Ce^{-\eta 2k\pi} \leq Ce^{-\eta L} \quad (3.28)$$

uniformly in  $L = L(k)$ ,  $k \geq K$  with  $K > 0$  sufficiently large. Similarly, the last term in (3.24) is equivalent to  $|\gamma(x) - \hat{u}_b(x - L - \bar{\varphi})|$  on  $0 \leq x \leq \bar{\varphi}$  and we note  $\bar{\varphi} \leq \varphi_2$ . We then have  $-L - \bar{\varphi} = -\varphi_2 - 2k\pi - O(e^{-\eta 2k\pi})$  and by an analogous argument as above

$$|\hat{u}_f(x - L - \bar{\varphi}) - \gamma(x)| \leq Ce^{-\eta L}. \quad (3.29)$$

This then shows that (3.7) holds. As for (3.8), from (3.23) and  $\bar{\varphi} \leq 2\pi$  so that we can subsume  $e^{\eta 2\pi}$  into the constant, we have

$$|u_1(x + L - \bar{\varphi}) - \hat{u}_b(x - \bar{\varphi})| \leq C e^{-\eta(L+x)}, \quad 0 \leq x \leq \bar{\varphi} \quad (3.30)$$

Moreover, from (3.18) in Theorem 3.2 we have

$$|u_1(x + L) - \hat{u}_b(x)| \leq C e^{-\eta(L+x)}, \quad x \geq 0 \quad (3.31)$$

and again since  $\bar{\varphi} \leq 2\pi$ , we have

$$|u_1(x + L - \bar{\varphi}) - \hat{u}_b(x - \bar{\varphi})| \leq C e^{-\eta(L+x)}, \quad x \geq \bar{\varphi}. \quad (3.32)$$

As we remarked at the beginning, the preceding assumed that  $\bar{\varphi} > 0$ . If  $\bar{\varphi} < 0$ , we can reverse the arguments, starting with  $|w_b^+(x)|$ . Thus we conclude that  $|w_b^+(x)| \leq C e^{-\eta(L+x)}$  on  $x \geq 0$  directly from (3.18) in Theorem 3.2, as we did above for  $|w_f^-(x)|$  on  $x \leq 0$  using (3.15) in Theorem 3.2. For  $|w_b^-(x)|$ , we use (3.18) and (3.17) in Theorem 3.2 in an analogous fashion to the argument above for  $|w_f^+(x)|$ , and so on. If  $\bar{\varphi} = 0$ , as is the case for a symmetric localized solution, all the bounds follow immediately from Theorem 3.2 and the definition (3.15).

Finally, we show that Hypothesis 4.3.2 holds: we write

$$|u_f(L) - \gamma(0)| \leq |u_f(L) - u_f(2k\pi + \varphi_1 + \bar{\varphi})| + |u_f(2k\pi + \varphi_1 + \bar{\varphi}) - \gamma(0)| \quad (3.33)$$

First considering the first term on the right hand side, by definition  $2k\pi + \varphi_1 + \bar{\varphi} = L + O(e^{-\eta 2k\pi})$ , so we can Taylor expand about  $L$  and again note that  $|u'_f(L)|$  is bounded uniformly in  $L$  for any  $\varphi_1$  by a multiple of  $\sup_{x \in [0, 2\pi]} |\gamma'(x)|$ . Thus the first term is  $O(e^{-\eta 2k\pi}) = O(e^{-\eta L})$ . As for the second term,  $u_f(2k\pi + \varphi_1 + \bar{\varphi}) = \hat{u}_f(2k\pi + \varphi_1)$

and  $\gamma(0) = \gamma(2k\pi)$ , so that by (2.10), the second term is also  $O(e^{-\eta L})$ . Thus we have that for  $C, \eta > 0$ ,  $|u_f(L) - \gamma(0)| \leq Ce^{-\eta L}$  uniformly in  $L = L(k)$ ,  $k \geq K$  with  $K > 0$  sufficiently large. To show that (3.10) holds, we write

$$|u_b(-L) - \gamma(0)| \leq |u_b(-L) - u_b(-2k\pi - \varphi_2 + \bar{\varphi})| + |u_b(-2k\pi - \varphi_2 + \bar{\varphi}) - \gamma(0)| \quad (3.34)$$

and argue analogously. Finally, the remaining statements in Hypothesis 4.3.2 follow from the definition of  $u_f(x)$  and  $u_b(x)$  upon setting  $\tilde{c} = (\varphi_1 + \varphi_2)/2$ . As  $\tilde{c}$  is bounded and  $\gamma(x)$  is  $2\pi$  periodic, we can then replace  $\tilde{c}$  with  $c = (\varphi_1 + \varphi_2)/2 \pmod{2\pi}$ . ■

We now have two assumptions of the existence of exponential dichotomies for the eigenvalue problems associated to  $\gamma(x)$ , and the trivial solution at 0. These then imply exponential dichotomies for  $u_{f,b}(x)$  on  $\mathbb{R}^+$  and  $\mathbb{R}^-$ , which in turn imply exponential dichotomies for the localized solution on  $(-\infty, -L]$ ,  $[-L, 0]$ ,  $[0, L]$  and  $[L, \infty)$ . As noted below, these are natural assumptions for the PDE formulations we have in mind, but they of course depend on the form of the operator  $B$  in (2.2), and do not arise automatically from the set-up in Chapter 3. (Although inasmuch as the  $\lambda = 0$  case reduces to the problem studied in Chapter 3, we note that these hypotheses are compatible with our previous hypotheses on the spatial eigenvalues of the linearizations about the 0 solution and  $\gamma(x)$ .)

We first assume the existence of an exponential dichotomy of the eigenvalue problem (2.2) with  $u_*(x) = \gamma(x)$ .

**Hypothesis 4.3.6.** *The solution  $\gamma(x)$  of (2.1) is such that for any  $\lambda \in \Omega$ ,*

$$\dot{v} = [f_u(\gamma(x)) + \lambda B(\gamma(x))]v \quad (3.35)$$

*has an exponential dichotomy on  $\mathbb{R}$ . We denote these exponential dichotomies by*

$\Phi_\gamma^{s,u}(x, y; \lambda)$  and the associated projections by  $P_\gamma^{s,u}(x; \lambda) = \Phi_\gamma^{s,u}(x, x; \lambda)$ . The  $x$ -independent dimension  $\dim \operatorname{Rg}(P_\gamma^u(x, \lambda))$  is, for all  $\lambda \in \Omega$ , assumed to be equal to  $n$ , so that  $\dim \operatorname{Rg}(P_\gamma^s(x, \lambda)) = n$  as well.

Note that in the present context, our only assumptions on  $\gamma(x)$  are given in Hypotheses 4.3.2 and 4.3.6, and we do not use the particular assumptions on  $\gamma(x)$  given in Hypothesis 3.3.1 of Chapter 3.

Hypothesis 4.3.6 corresponds to the assumption that the operator corresponding to the linearization about the periodic solution  $\gamma(x)$  has no essential spectrum in the open right half plane; as a periodic solution, it has no point spectrum. The condition  $\dim \operatorname{Rg}(P_\gamma^u(x, \lambda)) = \dim \operatorname{Rg}(P_\gamma^s(x, \lambda)) = n$  is always satisfied for a reversible system, but see also Remark 4.3.8.

We finally require that the trivial solution has an exponential dichotomy on  $\mathbb{R}$ :

**Hypothesis 4.3.7.** *There exists a constant  $d > 0$  such that*

$$\dot{v} = [f_u(0) + \lambda B(0)]v \tag{3.36}$$

*has an exponential dichotomy on  $\mathbb{R}$  for all  $\lambda$  with  $\operatorname{Re} \lambda > -d$ . We denote these dichotomies by  $\Phi_0^{s,u}(x, y; \lambda)$  and the associated projections by  $P_0^{s,u}(x; \lambda)$ . The  $x$ -independent dimension  $\dim \operatorname{Rg}(P_0^u(x, \lambda))$  is, for all  $\lambda$  with  $\operatorname{Re} \lambda > -d$ , assumed to be equal to  $n$ , so that  $\dim \operatorname{Rg}(P_0^s(x, \lambda)) = n$  as well.*

Hypothesis 4.3.7 corresponds to the assumption that the essential spectrum of the operator corresponding to the linearization about the trivial solution is bounded away from 0 in the left half plane. For our immediate purposes we only need the existence of exponential dichotomies for  $\lambda \in \Omega$ , the open right half plane, but we

will use this stronger condition in Chapter 5.

Taken together, Hypotheses 4.3.6 and 4.3.7, along with Hypothesis 4.3.2 and the roughness theorem for exponential dichotomies (see Theorem 1.1, and Remark 1.1.2 in Appendix A.1), then imply that the front and back solutions have exponential dichotomies on  $\mathbb{R}^\pm$ . More precisely, for any  $\lambda \in \Omega$ ,

$$\dot{v} = [f_u(u_j(x)) + \lambda B(u_j(x))]v \quad (3.37)$$

with  $j = f, b$  has exponential dichotomies on  $\mathbb{R}^+$  and  $\mathbb{R}^-$ , which we can always choose to be locally analytic. We denote these dichotomies by  $\Phi_{j,+}^{s,u}(x, y; \lambda)$  and  $\Phi_{j,-}^{s,u}(x, y; \lambda)$  with  $j = f, b$ , where the subscripts  $+$  and  $-$  correspond to the dichotomies on  $\mathbb{R}^+$  and  $\mathbb{R}^-$ , respectively. We again denote the associated projections by  $P_{j,\pm}^{s,u}(x; \lambda) := \Phi_{j,\pm}^{s,u}(x, x; \lambda)$ . The dimension of the range of each of these projections is equal to  $n$ . This indicates that the operators corresponding to the linearizations about the front and back solutions have no essential spectrum in the open right half plane, but only isolated eigenvalues.

**Remark 4.3.8.** *In a general system it may happen that the range of the projection operator associated to each exponential dichotomy has dimension other than  $n$ , in contrast to the situation for a reversible system where this dimension must equal  $n$ . To account for this possibility, in the above hypotheses we could instead allow an arbitrary dimension,  $\dim \text{Rg}(P_\gamma^u(x, \lambda)) = i_\infty$ , so that  $\dim \text{Rg}(P_\gamma^s(x, \lambda)) = 2n - i_\infty$ . The dimension  $i_\infty$  is commonly referred to as the Morse index. If it happened that  $i_\infty \neq n$ , we would then have the additional requirement that the dimensions of the exponential dichotomy associated to the trivial solution is compatible with that of  $\gamma$ :*

$$\dim \text{Rg}(P_0^u(x, \lambda)) = \dim \text{Rg}(P_\gamma^u(x, \lambda)) = i_\infty$$

which would of course imply

$$\dim \operatorname{Rg}(P_0^s(x, \lambda)) = \dim \operatorname{Rg}(P_\gamma^s(x, \lambda)) = 2n - i_\infty.$$

This would then imply that the dimensions of the dichotomies associated with  $u_f$  and  $u_b$  on  $\mathbb{R}^\pm$  are compatible with each other and with the dichotomies associated to  $\gamma$  and the trivial solution. Our results are the same whether we allow an arbitrary dimension  $i_\infty$  and enforce the above compatibility condition, or take the dimension of the range of all projection operators to be  $n$ ; for simplicity, we make the latter choice.

We are now in a position to state the main result of this section:

**Theorem 4.1.** *Suppose Hypotheses 4.3.1, 4.3.2, 4.3.6 and 4.3.7 are satisfied, and define the functions*

$$D_f(\lambda) := \det (\operatorname{Rg} P_{f,-}^u(0; \lambda), \operatorname{Rg} P_{f,+}^s(0; \lambda)) \quad (3.38)$$

$$D_b(\lambda) := \det (\operatorname{Rg} P_{b,-}^u(0; \lambda), \operatorname{Rg} P_{b,+}^s(0; \lambda)). \quad (3.39)$$

Fix  $\lambda_* \in \Omega$  and suppose that for  $m_f, m_b \geq 0$  and for some  $\delta > 0$ ,

$$D_f(\lambda) = (\lambda - \lambda_*)^{m_f} + \mathcal{O}(|\lambda - \lambda_*|^{m_f+1}) \quad (3.40)$$

and

$$D_b(\lambda) = (\lambda - \lambda_*)^{m_b} + \mathcal{O}(|\lambda - \lambda_*|^{m_b+1}) \quad (3.41)$$

for  $\lambda \in U_\delta(\lambda_*)$ , the ball of radius  $\delta$  centered at  $\lambda_*$ . Then we may define an analytic function  $D_{\ell,L}(\lambda)$  such that there exists a  $\hat{\delta}$  sufficiently small, with  $\delta > \hat{\delta} > 0$ , and an  $L_* > 0$  sufficiently large, such that the following hold uniformly in  $L \geq L_*$ :

(i)  $D_{\ell,L}(\lambda)$  has precisely  $m_f + m_b$  roots, counted with multiplicity, in  $U_{\delta}(\lambda_*)$ . These values of  $\lambda$  are  $O(e^{-\eta L})$  close to  $\lambda_*$ , with  $\eta > 0$ .

(ii) The system

$$\dot{v} = [f_u(u_{\ell,L}(x)) + \lambda B(u_{\ell,L}(x))] v, \quad (3.42)$$

has a bounded, nontrivial solution at  $\lambda \in U_{\delta}(\lambda_*)$  if and only if  $D_{\ell,L}(\lambda) = 0$ .

The function  $D_{\ell,L}(\lambda)$  is defined in (3.76).

**Proof.** We will show that we have a bounded, nontrivial solution to (3.42) if and only if  $D_{\ell,L}(\lambda) = 0$ , where  $D_{\ell,L}(\lambda)$  is an analytic function of the form

$$D_{\ell,L}(\lambda) = (D_f(\lambda) + O(e^{-\eta L}))(D_b(\lambda) + O(e^{-\eta L})) + O(e^{-2\eta L}). \quad (3.43)$$

We begin by noting that using (3.1), we can solve the eigenvalue problem (3.42) in pieces by solving the equations

$$\dot{v}_f^- = \left[ f_u(u_f(x) + w_f^-(x)) + \lambda B(u_f(x) + w_f^-(x)) \right] v_f^-, \quad x \leq 0 \quad (3.44)$$

$$\dot{v}_f^+ = \left[ f_u(u_f(x) + w_f^+(x)) + \lambda B(u_f(x) + w_f^+(x)) \right] v_f^+, \quad x \in [0, L] \quad (3.45)$$

$$\dot{v}_b^- = \left[ f_u(u_b(x) + w_b^-(x)) + \lambda B(u_b(x) + w_b^-(x)) \right] v_b^-, \quad x \in [-L, 0] \quad (3.46)$$

$$\dot{v}_b^+ = \left[ f_u(u_b(x) + w_b^+(x)) + \lambda B(u_b(x) + w_b^+(x)) \right] v_b^+, \quad x \geq 0 \quad (3.47)$$

and then constructing our solution as

$$v(x) = \begin{cases} v_f^-(x+L), & x \leq -L \\ v_f^+(x+L), & x \in [-L, 0] \\ v_b^-(x-L), & x \in [0, L] \\ v_b^+(x-L), & x \geq L. \end{cases} \quad (3.48)$$

Thus we have a bounded solution to (3.42) if and only if we have solutions to (3.44)–(3.47) along with the matching conditions

$$v_f^+(L) - v_b^-(-L) = 0 \quad (3.49)$$

$$v_f^+(0) - v_f^-(0) = 0 \quad (3.50)$$

$$v_b^+(0) - v_b^-(0) = 0. \quad (3.51)$$

We fix  $\lambda_* \in \Omega$  as in the Theorem statement. By the existence of exponential dichotomies for (3.37) and the roughness theorem for exponential dichotomies (again see Appendix A.1), we have exponential dichotomies for each equation (3.44)–(3.47), which can be chosen so that they depend analytically on  $\lambda \in U_\delta(\lambda_*)$  for  $\delta > 0$  small.

That is, we have

$$\begin{aligned} |\Phi_{\ell(f,L,-)}^s(x,y;\lambda)| &\leq Ce^{-\eta|x-y|}, \quad x \geq y, & |\Phi_{\ell(f,L,-)}^u(x,y;\lambda)| &\leq Ce^{-\eta|x-y|}, \quad x \leq y, \quad x, y \leq 0 \\ |\Phi_{\ell(f,L,+)}^s(x,y;\lambda)| &\leq Ce^{-\eta|x-y|}, \quad x \geq y, & |\Phi_{\ell(f,L,+)}^u(x,y;\lambda)| &\leq Ce^{-\eta|x-y|}, \quad x \leq y, \quad x, y \in [0, L] \\ |\Phi_{\ell(b,L,-)}^s(x,y;\lambda)| &\leq Ce^{-\eta|x-y|}, \quad x \geq y, & |\Phi_{\ell(b,L,-)}^u(x,y;\lambda)| &\leq Ce^{-\eta|x-y|}, \quad x \leq y, \quad x, y \in [-L, 0] \\ |\Phi_{\ell(b,L,+)}^s(x,y;\lambda)| &\leq Ce^{-\eta|x-y|}, \quad x \geq y, & |\Phi_{\ell(b,L,+)}^u(x,y;\lambda)| &\leq Ce^{-\eta|x-y|}, \quad x \leq y, \quad x, y \geq 0 \end{aligned} \quad (3.52)$$

We denote the associated projections  $P_{\ell(j,L,\pm)}^{s,u}(x;\lambda) := \Phi_{\ell(j,L,\pm)}^{s,u}(x,x;\lambda)$ ,  $j = f, b$ .

Moreover, as a consequence of Hypothesis 4.3.6, we have that

$$|P_{\ell(f,L,+)}^u(L; \lambda) - P_\gamma^u(0; \lambda)| \leq Ce^{-\eta L} \quad (3.53)$$

$$|P_{\ell(b,L,-)}^s(-L; \lambda) - P_\gamma^s(0; \lambda)| \leq Ce^{-\eta L}. \quad (3.54)$$

We now let  $a := (a_f^+, a_b^-) \in V_a$ ,  $b := (b_f^-, b_f^+, b_b^-, b_b^+) \in V_b$  and  $\lambda \in V_\lambda$ , where the spaces  $V_a, V_b, V_\lambda$  are defined as follows:

$$\begin{aligned} V_a &:= \text{Rg } P_\gamma^u(0; \lambda_*) \oplus \text{Rg } P_\gamma^s(0; \lambda_*) \\ V_b &:= (\text{Rg } P_{\ell(f,L,-)}^u(0; \lambda_*) \times \text{Rg } P_{\ell(f,L,+)}^s(0; \lambda_*)) \\ &\quad \times (\text{Rg } P_{\ell(b,L,-)}^u(0; \lambda_*) \times \text{Rg } P_{\ell(b,L,+)}^s(0; \lambda_*)) \\ V_\lambda &:= U_\delta(\lambda_*) \subset \mathbb{C}, \end{aligned}$$

and where  $V_a$  and  $V_b$  are endowed with the maximum norm over components.

For  $\delta$  sufficiently small and  $L > L_*$  sufficiently large, we can then write solutions to the eigenvalue problem (3.2) for the localized structure  $u_{\ell,L}$  as

$$v_f^-(x) = \Phi_{\ell(f,L,-)}^u(x, 0; \lambda) b_f^- \quad (3.55)$$

$$v_f^+(x) = \Phi_{\ell(f,L,+)}^s(x, 0; \lambda) b_f^+ + \Phi_{\ell(f,L,+)}^u(x, L; \lambda) a_f^+ \quad (3.56)$$

$$v_b^-(x) = \Phi_{\ell(b,L,-)}^s(x, -L; \lambda) a_b^- + \Phi_{\ell(b,L,-)}^u(x, 0; \lambda) b_b^- \quad (3.57)$$

$$v_b^+(x) = \Phi_{\ell(b,L,+)}^s(x, 0; \lambda) b_b^+, \quad (3.58)$$

where these are defined on  $(-\infty, 0], [0, L], [-L, 0]$  and  $[0, \infty)$ , respectively. Clearly any solution of (3.55)–(3.58) and the matching conditions (3.49)–(3.51) with  $a$  and  $b$  not both 0 will be a nontrivial, bounded solution to (3.42). On the other hand, all bounded solutions to (3.42) can be found as solutions to (3.55)–(3.58)

and (3.49)–(3.51) provided (i)  $\delta$  is sufficiently small such that  $\text{Rg } P_{\ell(f,L,-)}^s(0; \lambda) \cap \text{N } P_{\ell(f,L,-)}^s(0; \lambda_*) = 0$  and similarly for the other projections operating on  $V_b$ , which is guaranteed to hold for some  $\delta > 0$  by the analytic dependence of the exponential dichotomies on  $\lambda$  near  $\lambda_*$ , and (ii)  $\delta$  is sufficiently small and  $L_*$  is sufficiently large such that  $\text{Rg } P_{\ell(f,L,+)}^u(L; \lambda) \cap \text{N } P_\gamma^u(0; \lambda_*) = 0$ , and similarly  $\text{Rg } P_{\ell(b,L,-)}^s(-L; \lambda) \cap \text{N } P_\gamma^s(0; \lambda_*) = 0$ , which holds again by analytic dependence of the exponential dichotomies, along with the relations (3.53) and (3.54).

We now use the matching conditions (3.49)–(3.51) to solve for  $a$  and  $b$ . We begin by using the first matching condition (3.49) to solve for  $a$  in terms of  $b$ .

**Lemma 4.3.9.** *There exists an  $L_*$  such that for all  $L > L_*$ , the following holds uniformly in  $L$ . There exists an operator  $A_1 : V_\lambda \times V_b \rightarrow V_a$  such that  $v(x)$  as given by (3.55)–(3.58) with  $a = A_1(\lambda)b$  solves (3.49) for any  $b$  and  $\lambda$ .  $A_1$  is analytic in  $\lambda$  and linear in  $b$ , and satisfies*

$$|A_1(\lambda)b| \leq Ce^{-\eta L}|b|. \quad (3.59)$$

**Proof.** Substituting from (3.55)–(3.58) into (3.49) gives us:

$$\begin{aligned} 0 &= \Phi_{\ell(f,L,+)}^s(L, 0; \lambda)b_f^+ + \Phi_{\ell(f,L,+)}^u(L, L; \lambda)a_f^+ - \Phi_{\ell(b,L,-)}^s(-L, -L; \lambda)a_b^- - \Phi_{\ell(b,L,-)}^u(-L, 0; \lambda)b_b^- \\ &= a_f^+ - a_b^- + (P_{\ell(f,L,+)}^u(L; \lambda) - P_\gamma^u(0; \lambda))a_f^+ + (P_\gamma^s(0; \lambda) - P_{\ell(f,L,+)}^s(L; \lambda))a_b^- \\ &\quad + \Phi_{\ell(f,L,+)}^s(L, 0; \lambda)b_f^+ - \Phi_{\ell(b,L,-)}^u(-L, 0; \lambda)b_b^-. \end{aligned} \quad (3.60)$$

We then define

$$\begin{aligned} F_1(\lambda)(a, b) &:= (P_{\ell(f,L,+)}^u(L; \lambda) - P_\gamma^u(0; \lambda))a_f^+ + (P_\gamma^s(0; \lambda) - P_{\ell(f,L,+)}^s(L; \lambda))a_b^- \\ &\quad + \Phi_{\ell(f,L,+)}^s(L, 0; \lambda)b_f^+ - \Phi_{\ell(b,L,-)}^u(-L, 0; \lambda)b_b^- \end{aligned} \quad (3.61)$$

so that clearly  $F_1(\lambda)(a, b)$  is analytic in  $\lambda$  and linear in  $a$  and  $b$ . Moreover, from (3.53) and (3.54) and definition of the dichotomies, i.e., the decay of  $\Phi_{\ell(f,L,+)}^s(x, y; \lambda)$  on  $x \geq y$  and  $\Phi_{\ell(b,L,-)}^u(x, y; \lambda)$  on  $x \leq y$ , we have

$$|F_1(\lambda)(a, b)| \leq Ce^{-\eta L}(|a| + |b|). \quad (3.62)$$

We further define the map  $J$  as

$$\begin{aligned} J : V_a &\rightarrow \mathbb{C}^{2n} \\ (a_f^+, a_b^-) &\mapsto a_f^+ - a_b^-, \end{aligned} \quad (3.63)$$

and since  $V_a = \text{Rg } P_\gamma^u(0; \lambda_*) \oplus \text{Rg } P_\gamma^s(0; \lambda_*) = \mathbb{C}^{2n}$ , we have that  $J$  is a linear isomorphism and  $\|J\| \leq C$ . Then we can rewrite (3.60) as

$$(J + F_1(\lambda)I_1)a = F_1(\lambda)(0, b), \quad (3.64)$$

where  $I_1 a := (a, 0)$ . By (3.62), for  $L \geq L_*$  with  $L_*$  sufficiently large,  $(J + F_1(\lambda)I_1)$  is invertible so that we have the solution operator

$$a = -(J + F_1(\lambda)I_1)^{-1}F_1(\lambda)(0, b) =: A_1(\lambda)b, \quad (3.65)$$

Finally, again from (3.62) we have

$$|A_1(\lambda)b| \leq Ce^{-\eta L}|b|, \quad (3.66)$$

which completes the proof. ■

Turning now to the second matching condition  $v_f^+(0) - v_f^-(0) = 0$ , we have

$$\begin{aligned} 0 &= \Phi_{\ell(f,L,+)}^s(0, 0; \lambda)b_f^+ + \Phi_{\ell(f,L,+)}^u(0, L; \lambda)a_f^+ - \Phi_{\ell(f,L,-)}^u(0, 0; \lambda)b_f^- \\ &= P_{\ell(f,L,+)}^s(0; \lambda)b_f^+ - P_{\ell(f,L,-)}^u(0; \lambda)b_f^- + \Phi_{\ell(f,L,+)}^u(0, L; \lambda)(A_1(\lambda)b)_f^+, \end{aligned} \quad (3.67)$$

where we have defined  $(A_1(\lambda)b)_f^+$  to be the component of  $A_1(\lambda)b$  in  $\text{Rg } P_\gamma^u(0; \lambda_*)$ . We observe that by (3.52) and (3.59),

$$\Phi_{\ell(f,L,+)}^u(0, L; \lambda)(B(\lambda)b)_f^+ = O(e^{-2\eta L}|b|) \quad (3.68)$$

uniformly in  $\lambda$  near  $\lambda_*$ .

Similarly, from the third matching condition  $v_b^+(0) - v_b^-(0) = 0$ , we have

$$\begin{aligned} 0 &= \Phi_{\ell(b,L,-)}^s(0, 0; \lambda)b_b^+ - \Phi_{\ell(b,L,-)}^u(0, 0; \lambda)b_b^- - \Phi_{\ell(b,L,-)}^s(0, -L; \lambda)(A_1(\lambda)b)_b^- \\ &= P_{\ell(b,L,-)}^s(0; \lambda)b_b^+ - P_{\ell(b,L,-)}^u(0; \lambda)b_b^- - \Phi_{\ell(b,L,-)}^s(0, -L; \lambda)(A_1(\lambda)b)_b^-, \end{aligned} \quad (3.69)$$

where  $(A_1(\lambda)b)_b^-$  is the component of  $A_1(\lambda)b$  in  $\text{Rg } P_\gamma^s(0; \lambda_*)$ . From (3.52) and (3.59), we again have

$$\Phi_{\ell(b,L,-)}^s(0, -L; \lambda)(A_1(\lambda)(b))_b^- = O(e^{-2\eta L}|b|) \quad (3.70)$$

uniformly in  $\lambda$  near  $\lambda_*$ .

We have a nontrivial solution at  $\lambda$  near  $\lambda_*$  if the conditions (3.67) and (3.69) hold

for  $b \neq 0$ . We can rewrite the two conditions as:

$$\begin{aligned} \begin{pmatrix} 0 \\ 0 \end{pmatrix} &= \left[ \begin{pmatrix} -P_{\ell(f,L,-)}^u(0; \lambda) & P_{\ell(f,L,+)}^s(0; \lambda) & 0 & 0 \\ 0 & 0 & -P_{\ell(b,L,-)}^u(0; \lambda) & P_{\ell(b,L,+)}^s(0; \lambda) \end{pmatrix} \right. \\ &\quad \left. + \begin{pmatrix} \Phi_{\ell(f,L,+)}^u(0, L; \lambda) & -\Phi_{\ell(b,L,-)}^s(0, -L; \lambda) \end{pmatrix} A_1(\lambda) \right] b \\ &=: [P_L(\lambda) + R_L(\lambda)] b. \end{aligned} \tag{3.71}$$

We note that these matrices are square, as we are mapping from  $V_b$  with  $4n$  complex components (for general Morse indices,  $i_\infty + (2n - i_\infty) + i_\infty + (2n - i_\infty) = 4n$ ) to  $\mathbb{C}^{2n} \times \mathbb{C}^{2n}$ . From (3.68) and (3.70),

$$R_L(\lambda) = O(e^{-2\eta L}), \tag{3.72}$$

uniformly in  $\lambda$  near  $\lambda_*$ .

We will then have a nontrivial solution to (3.44)–(3.47) along with the matching conditions (3.49)–(3.51) at  $\lambda$  near  $\lambda_*$  provided that we can find  $b \in V_b$ ,  $b \neq 0$  such that  $(P_L(\lambda) + R_L(\lambda))b = 0$ . Thus we define  $\hat{P}_{\ell(f,L,-)}^u(0; \lambda)$  as  $P_{\ell(f,L,-)}^u(0; \lambda)$  restricted to  $\text{Rg } P_{\ell(f,L,-)}^u(0; \lambda_*)$ :

$$\hat{P}_{\ell(f,L,-)}^u(0; \lambda) := P_{\ell(f,L,-)}^u(0; \lambda) \Big|_{\text{Rg } P_{\ell(f,L,-)}^u(0; \lambda_*)} \tag{3.73}$$

and similarly for the other projection operators. We further define

$$\hat{P}_L(\lambda) = \begin{pmatrix} -\hat{P}_{\ell(f,L,-)}^u(0; \lambda) & \hat{P}_{\ell(f,L,+)}^s(0; \lambda) & 0 & 0 \\ 0 & 0 & -\hat{P}_{\ell(b,L,-)}^u(0; \lambda) & \hat{P}_{\ell(b,L,+)}^s(0; \lambda) \end{pmatrix} \tag{3.74}$$

and

$$\hat{R}_L(\lambda) = R_L(\lambda) \Big|_{V_b}. \quad (3.75)$$

We thus define

$$D_{\ell,L}(\lambda) := \det(\hat{P}_L(\lambda) + \hat{R}_L(\lambda)) \quad (3.76)$$

so that we have a nontrivial solution of (3.42) at  $\lambda$  near  $\lambda_*$  if and only if

$$D_{\ell,L}(\lambda) = 0. \quad (3.77)$$

Now since  $\hat{P}_L(\lambda)$  and  $\hat{R}_L(\lambda)$  are analytic, as is the determinant, we can write this as

$$\det \left( \hat{P}_L(\lambda) \right) + \tilde{R}_L(\lambda) = 0, \quad (3.78)$$

where

$$\tilde{R}_L(\lambda) = O \left( |\hat{R}_L(\lambda)| \right) = O(e^{-2\eta L}), \quad (3.79)$$

and we clarify that the first equality is meant asymptotically as  $\lambda \rightarrow \lambda_*$  and the second as  $L \rightarrow \infty$ , so that taken together there exists a  $C$  which does not depend on  $\lambda$  or  $L$  such that for  $\lambda \in U_\delta$  with  $\delta$  sufficiently small and  $L > L_*$ , with  $L_*$  sufficiently large,

$$\tilde{R}_L(\lambda) \leq C e^{-2\eta L}. \quad (3.80)$$

Focusing then on  $\det(\hat{P}_L(\lambda))$ , we have

$$\det(\hat{P}_L(\lambda)) = \det \left( \begin{array}{cc} -\hat{P}_{\ell(f,L,-)}^u(0; \lambda) & \hat{P}_{\ell(f,L,+)}^s(0; \lambda) \end{array} \right) \det \left( \begin{array}{cc} -\hat{P}_{\ell(b,L,-)}^u(0; \lambda) & \hat{P}_{\ell(b,L,-)}^s(0; \lambda) \end{array} \right) \quad (3.81)$$

where again the hats indicate that the projections are restricted to the range of the

corresponding projection with  $\lambda = \lambda_*$ . But we note that

$$\operatorname{Rg} P_{\ell(f,L,-)}^u(0; \lambda) \Big|_{\operatorname{Rg} P_{\ell(f,L,-)}^u(0; \lambda_*)} \rightarrow \operatorname{Rg} P_{\ell(f,L,-)}^u(0; \lambda) \quad (3.82)$$

is an isomorphism with uniform bound in  $\lambda$  near  $\lambda_*$ , and similarly for the other projection operators. So then we have a nontrivial solution if and only if

$$\det \left( \operatorname{Rg} P_{\ell(f,L,-)}^u(0; \lambda), \operatorname{Rg} P_{\ell(f,L,+)}^s(0; \lambda) \right) \det \left( \operatorname{Rg} P_{\ell(b,L,-)}^u(0; \lambda), \operatorname{Rg} P_{\ell(b,L,+)}^s(0; \lambda) \right) + \tilde{R}_L(\lambda) = 0. \quad (3.83)$$

Now since we also have that  $|P_{\ell(f,L,+)}^s(0; \lambda) - P_{f,+}^s(0; \lambda)| \leq C e^{-\eta L}$ , and analogously for projections associated with the other exponential dichotomies, we have

$$\begin{aligned} 0 &= \left( \det \left( \operatorname{Rg} P_{f,+}^s(0; \lambda), \operatorname{Rg} P_{f,-}^u(0; \lambda) \right) + O(e^{-\eta L}) \right) \left( \det \left( \operatorname{Rg} P_{b,-}^s(0; \lambda), \operatorname{Rg} P_{b,+}^u(0; \lambda) \right) + O(e^{-\eta L}) \right) \\ &\quad + O(e^{-2\eta L}). \end{aligned} \quad (3.84)$$

We note that by the definitions (3.40) and (3.41), our requirement can then be written

$$D_\ell(\lambda) = (D_f(\lambda) + O(e^{-\eta L})) (D_b(\lambda) + O(e^{-\eta L})) + O(e^{-2\eta L}) = 0. \quad (3.85)$$

Since, by assumption,

$$D_f(\lambda) = (\lambda - \lambda_*)^{m_f} + O(|\lambda - \lambda_*|^{m_f+1}) \quad (3.86)$$

and

$$D_b(\lambda) = (\lambda - \lambda_*)^{m_b} + O(|\lambda - \lambda_*|^{m_b+1}) \quad (3.87)$$

hold for  $\lambda \in U_\delta(\lambda_*)$ , we can use Rouché's Theorem to complete our proof:

**Lemma 4.3.10.** *Suppose that (3.86) and (3.87) hold for  $\lambda \in U_{\delta_0}(\lambda_*)$  and  $D_{\ell,L}(\lambda)$  is as defined in (3.76) for  $\lambda \in U_{\delta_1}(\lambda_*)$ . Then there exists a  $\hat{\delta}$  satisfying  $\min\{\delta_0, \delta_1\} > \hat{\delta} > 0$  such that for  $L_* > 0$  sufficiently large,  $D_{\ell,L}(\lambda)$  has exactly  $m_f + m_b$  zeroes in  $U_{\hat{\delta}}(\lambda_*)$ , uniformly in  $L \geq L_*$ , which are  $O(e^{-\eta L/f(m_f, m_b)})$  close to  $\lambda_*$ , with  $f(m_f, m_b) = \max\{m_f, m_b\} + \epsilon$  and  $\epsilon > 0$  arbitrarily small.*

**Proof.** Rouché's theorem can be stated as follows: Let  $K \subset \mathbb{C}$  a closed, bounded region with  $\partial K$  a simple closed contour, and suppose  $f, g : K \rightarrow \mathbb{C}$  are analytic with

$$|f(z) - g(z)| < |f(z)| + |g(z)| \quad (3.88)$$

on  $\partial K$ . Then  $f$  and  $g$  have the same number of zeros in  $K$ , counted with multiplicity.

In the present case, working from the expression for  $D_{\ell,L}(\lambda)$  given in (3.85), we let  $z = \lambda - \lambda_*$ , and define

$$\begin{aligned} f(z) &= z^{m_f+m_b} \\ g(z) &= z^{m_f+m_b} + O(z^{m_f+m_b+1}) + O(e^{-\eta L}(z^{m_f} + z^{m_b})) + O(e^{-2\eta L}) \end{aligned} \quad (3.89)$$

with  $K = B_r(0)$  for some  $r > 0$ . We wish to find the smallest  $r$  such that  $f$  and  $g$  have the same number of zeros in  $K$ . We require

$$\begin{aligned} O(r^{m_f+m_b+1}) + O(e^{-\eta L}(r^{m_f} + r^{m_b})) + O(e^{-2\eta L}) &< 2r^{m_f+m_b} - O(r^{m_f+m_b+1}) \\ &- O(e^{-\eta L}(r^{m_f} + r^{m_b})) - O(e^{-2\eta L}) \end{aligned} \quad (3.90)$$

or

$$O(e^{-2\eta L}) < 2r^{m_f+m_b} (1 - O(r) - O(e^{-\eta L}(r^{-m_b} + r^{-m_f}))) \quad (3.91)$$

In other words, for  $L_*$  sufficiently large, there exists a  $C$  such that we can write the

requirement as

$$Ce^{-2\eta L} < 2r^{m_f+m_b} (1 - Cr - Ce^{-\eta L}(r^{-m_b} + r^{-m_f})). \quad (3.92)$$

Then setting  $r = C^{-1}e^{-\eta L/f(m_f, m_b)}$ , where  $f(m_f, m_b)$  is a function to be determined, we require  $\frac{m_f+m_b}{f(m_f, m_b)} \leq 1$  as well as  $\frac{m_f}{f(m_f, m_b)} < \frac{1}{2}$  and  $\frac{m_b}{f(m_f, m_b)} < \frac{1}{2}$ , where we require strict inequalities to ensure the second factor in (3.92) can be made arbitrarily close to 1 without requiring dependence of the constant on  $m_f$  or  $m_b$ . Thus we need  $f(m_f, m_b) > 2 \max\{m_f, m_b\}$ , and so we conclude that  $r = O(e^{-\eta L/f(m_f, m_b)})$ , where  $f(m_f, m_b) = 2 \max\{m_f, m_b\} + \epsilon$ , where  $\epsilon > 0$ . ■

This completes the proof of Theorem 4.1. ■

**Remark 4.3.11.** *We expect that the algebraic multiplicity of  $\lambda$  considered as an eigenvalue of the PDE problem associated to (3.42) (in other words, the multiplicity of  $\lambda$  as an eigenvalue of  $\mathcal{T}(\lambda)$ , see Appendix B) should be equal to the multiplicity of  $\lambda$  as a root of  $D_{\ell, L}(\lambda, 0)$ . We refer to [55, Section 4 and Appendix B] for related computations. We have not, however, carried this through explicitly.*

## 4.4 The translation eigenvalue at $\lambda = 0$

Having shown that the exponential closeness of eigenvalues of the localized solution to those of the front and back in the right half plane, we now discuss the situation at  $\lambda = 0$ . As mentioned initially, provided the front and back have simple eigenvalues at  $\lambda = 0$  in an appropriate sense, we expect that the eigenvalue of the localized solution at  $\lambda = 0$  will also be simple. This is in contrast to the case for localized

solutions constructed from gluing together fronts and backs connecting stable rest points (in the PDE sense), where two eigenvalues arise near  $\lambda = 0$  [1, 47, 55].

To appreciate the importance of this distinction, consider that if there were two eigenvalues for the localized solution arising from  $\lambda = 0$ , we would only be able to locate one at  $\lambda = 0$  by translation invariance, and we would then need to track the other. While our results above show that asymptotically in  $L$  there can be no eigenvalues in the right half plane, for any finite value of  $L$ , it is possible that this second eigenvalue arising from  $\lambda = 0$  could lie near 0 in the right half plane. As we will see, this does not happen, and in each of the numerical examples presented in Section 4.6 below, we indeed observe a single eigenvalue at  $\lambda = 0$ .

Heuristically, we can appreciate the difference between localized periodic and localized monotone solutions by arguing as follows: in both cases, the eigenvalue at  $\lambda = 0$  for the front (and back) will correspond to the derivative of the front solution, existing due to translation invariance. However, in the monotone pulse case, this function will be localized around the front and back interfaces, so that we can connect the front and back interfaces to produce two different eigenfunctions; if the front and back both return to the same rest state so that the pulse represents a homoclinic solution, then we will have an even and an odd eigenfunction. The odd solution will remain at  $\lambda = 0$  as it corresponds to the  $x$ -derivative of the localized solution, while the even solution will exist near  $\lambda = 0$ , but its position still needs to be tracked. In contrast, the derivative of the front and back corresponding to a localized periodic solution will still be periodic, rather than localized at the interfaces. We then lose the freedom to construct two different eigenfunctions, as the phases of the two eigenfunctions must match in the middle. Thus we can only realize one eigenfunction, corresponding to the derivative of the localized solution, which we know must lie at  $\lambda = 0$ .

Alternatively, we can argue in terms of functions spaces: since the front and back are both asymptotically periodic in one direction, the translation eigenfunction with eigenvalue zero corresponding to the derivative of each with respect to  $x$  is not properly an eigenfunction in a space of bounded functions. This of course is reflected in the fact that 0 is contained in the essential spectrum of the front and back. Thus it is only by matching these two putative eigenfunctions together that we realize a true eigenfunction of the localized solution in a space of bounded functions. Again since the functions are not exponentially small at the matching point, there is only one way in which this function can be constructed, and in particular it must correspond to the eigenfunction at  $\lambda = 0$  given by the  $x$ -derivative of the localized solution. All of these arguments will be made precise in Chapter 5, where we extend the Evans function of the front analytically across  $\lambda = 0$ .

## 4.5 Special case: simple eigenvalue of the front

As mentioned at the outset, additional information about the eigenvalues and eigenfunctions associated to localized solutions may be obtained by following a slightly different but closely related strategy to that employed in Section 4.3. In particular, in the case of a simple eigenvalue of the front we have the following result:

**Theorem 4.2.** *There exists an  $L_* > 0$  such that the following holds uniformly in  $L > L_*$ . There exists a small  $\delta > 0$  such that (3.42) has a bounded, nonzero solution for  $\lambda \in U_\delta(\lambda_*)$  if and only if*

$$-\langle \psi_*(L), P_\gamma^u(0; \lambda_*) v_{f_*}(L) \rangle - (\lambda - \lambda_*)M + R(\lambda - \lambda_*) = 0 \quad (5.1)$$

where

$$M = \int_{-\infty}^{\infty} \langle \psi_*(s), B(u_f(s))v_{f*}(s) \rangle ds \quad (5.2)$$

and  $R$  is analytic in  $\lambda - \lambda_*$  and satisfies

$$|R(\lambda - \lambda_*)| \leq C \left( e^{-\alpha L_*} \left( \sup_{s \geq L_*} |B(u_f(s))v_{f*}(s)| + |v_{f*}(L_*)| + e^{-\eta L_*} + |\lambda - \lambda_*| \right) + e^{-\eta L_*} \right) \quad (5.3)$$

Here  $v_{f*}(x)$  is the eigenfunction associated with the eigenvalue  $\lambda_*$  of the front  $u_f(x)$  at  $\lambda_*$ , i.e., the unique bounded solution to

$$\dot{v} = [f_u(u_f(x)) + \lambda B(u_f(x))] v \quad (5.4)$$

at  $\lambda_*$ , while  $\psi_*$  is the unique bounded solution of the adjoint equation

$$\dot{w} = -[f_u(u_f(x)) + \lambda B(u_f(x))]^* w \quad (5.5)$$

at  $\lambda_*$ , and we assume that the eigenvalue problem associated to the back has no nontrivial bounded solution at  $\lambda_*$ . Of course, the same result would hold with the conditions on the front and back switched. Since the proof is rather long and we already have a general result in Theorem 4.1, we refer to Appendix C for the complete set-up and proof of Theorem 4.2.

## 4.6 Numerical results

In this section we illustrate our results numerically, using the Swift–Hohenberg equation. In particular, we will examine the stripe and spot pattern of the cubic-quintic

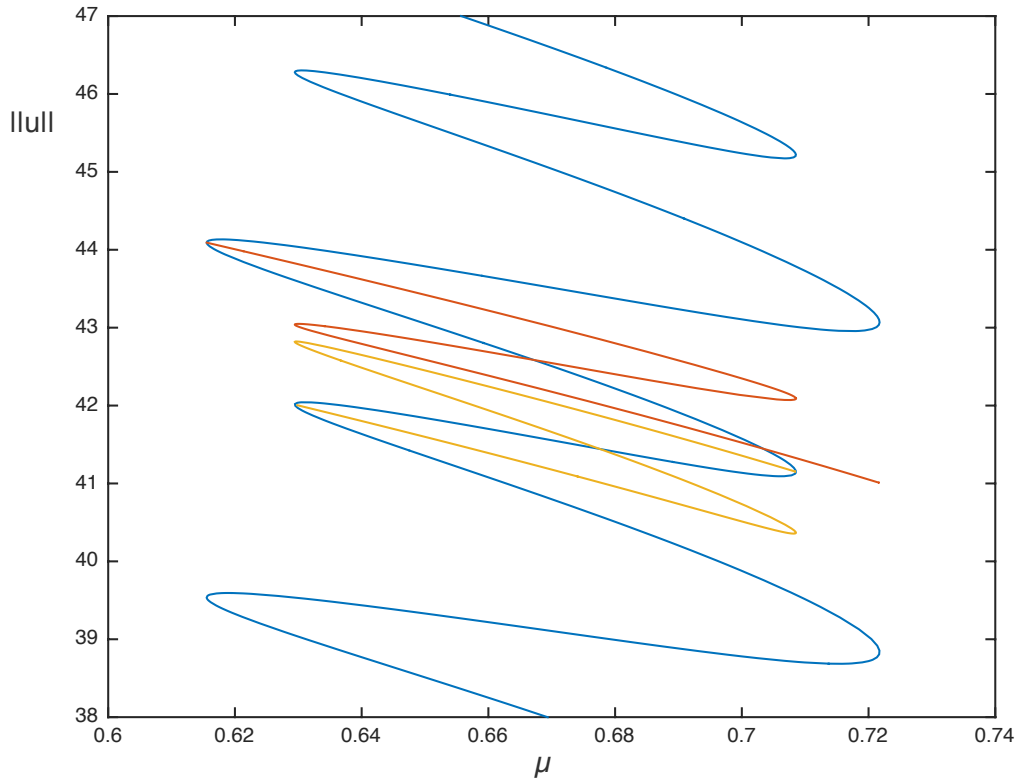


**Figure 4.2:** Selected branches in the bifurcation diagram for stripe and spot patterns, showing the three branches of solutions whose spectra will be analyzed in the following: symmetric (blue), asymmetric cross-connecting (orange) and asymmetric self-connecting (yellow). See also Figure 3.3.

Swift–Hohenberg equation. We note that spectral computations for these equations have been published previously in [3].

Bifurcation diagrams were computed via numerical continuation in MATLAB, as described in Section 3.4 above. Operators were again computed using spectral differentiation matrices in the periodic  $y$ -direction, and centered finite differences in the  $x$ -direction, with  $n_y = 8$  Fourier modes and  $n_x = 800$  equidistant points, with boundary conditions and domains as indicated below. The built-in MATLAB routine `eigs` with initial shift `sigma = 0.5` was used to compute the 20 largest eigenvalues of the operator linearized about each solution along a branch, with operator boundary conditions as indicated.

We first recall the bifurcation structure of these patterns, which was shown in Figures 3.3 and 3.4, along with particular solution profiles. Figure 4.2 shows an  $\mathcal{R}$ -symmetric branch, along with one cross-connecting and one self-connecting asymmetric branch. Note that the cross-connecting branch ends at a  $\kappa\mathcal{R}$ -symmetric branch (not shown). All information necessary for constructing its bifurcation structure is contained in the  $\mathcal{R}$ -symmetric branch.

### 4.6.1 Symmetric localized solutions

We begin by confirming that the multiplicity of eigenvalues is as expected. In Figure 4.3 we show the eigenvalues computed along one period of the symmetric snaking branch, computed with Neumann boundary conditions on the domain  $[-50, 50] \times [0, \pi]$ . Along the  $x$ -axis we plot the cumulative change in the parameter  $\mu$ , while the  $y$ -axis shows the real part of  $\lambda$ , which is in fact just  $\lambda$  in this case; all the eigenvalues are real as the operator  $\mathcal{L}$  is self-adjoint.

In Figure 4.4 we again show the eigenvalues for the symmetric localized solution, along with an overlay of the eigenvalues of a “front” solution computed on the domain  $[0, 50] \times [0, \pi]$ , again with Neumann boundary conditions. Of course, as soon as we begin computing on a bounded domain, we are effectively computing a localized solution. Our aim here is thus to illustrate that the correspondences and multiplicities are as expected, and we do not claim or attempt a test of exponential closeness. We indeed observe a single eigenvalue for the front with  $\text{Re } \lambda > 0$  giving rise to two such eigenvalues for the symmetric localized solution, which correspond to saddle node and pitchfork bifurcations. The eigenvalue of the symmetric localized solution at  $\lambda = 0$  is simple. In Figure 4.5, we focus on the eigenvalues with largest real part.

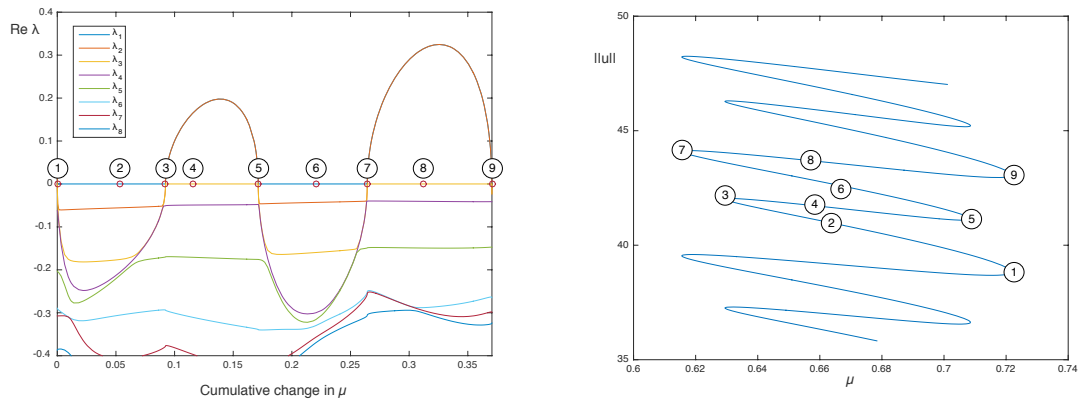


**Figure 4.3:** Left: Eigenvalues for symmetric localized solutions along one period of the  $\mathcal{R}$ -symmetric snaking branch, with  $\text{Re } \lambda$  plotted as a function of the cumulative change in  $\mu$ . Note there are two eigenvalues for the symmetric localized solution with  $\lambda > 0$ , corresponding to saddle node and pitchfork bifurcations, while the eigenvalue at  $\lambda = 0$  is simple. Right: the bifurcation diagram for  $\mathcal{R}$ -symmetric localized solutions, with corresponding points on the eigenvalue diagram as indicated. Note that a point on the bifurcation diagram at right corresponds to a vertical slice in the eigenvalue plot at left.

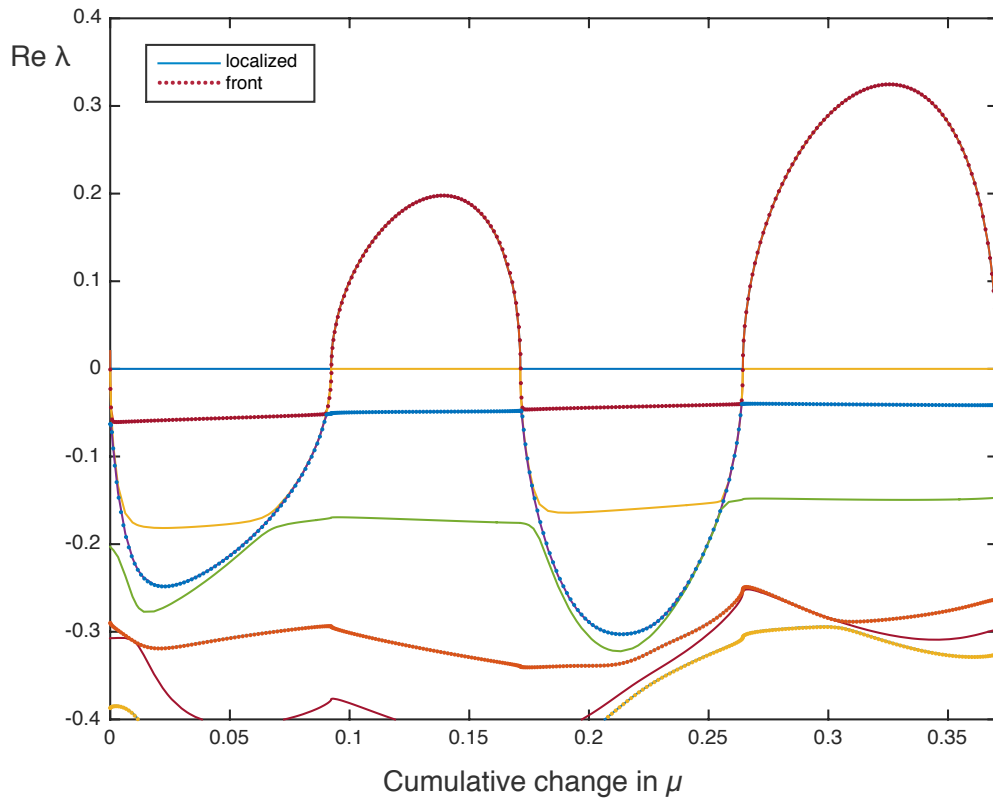


**Figure 4.4:** Eigenvalues for symmetric localized solutions (solid), as shown in Figure 4.3, along with eigenvalues for corresponding fronts (dots) overlaid along one period of a snaking branch.

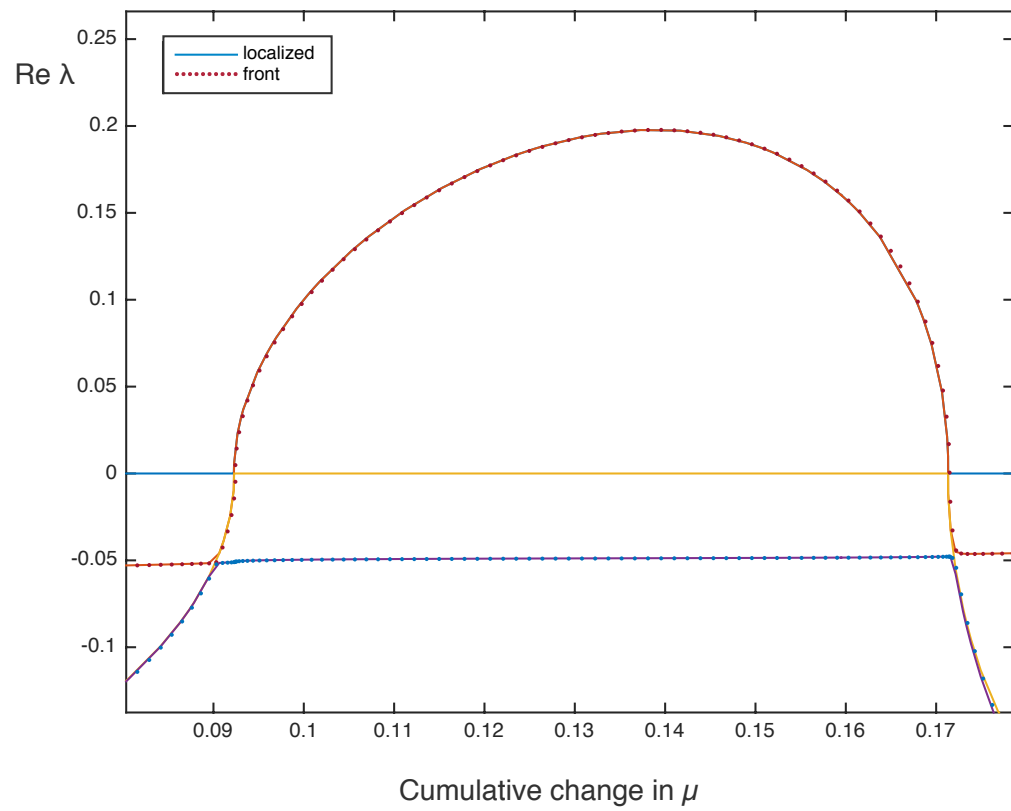


**Figure 4.5:** Detail of the top left quadrant of Figure 4.4, focusing on the leading eigenvalues for the first unstable portion of the symmetric branch.

### 4.6.2 Asymmetric localized solutions

Focusing now on the asymmetric localized solutions, we consider both a cross-connecting and self-connecting branch, both of which were depicted in Figure 4.2. We begin in Figure 4.6 with eigenvalues of the cross-connecting branch of asymmetric localized solutions, with correspondences to the bifurcation diagram as indicated. In Figure 4.7 we again show these eigenvalues, along with an overlay of the eigenvalues for the corresponding “front” and “back” solutions as described above. Here we find that one unstable eigenvalue arises from the front, and the other from the back, so that each is simple for the localized structure. In Figure 4.8 we show a detail of Figure 4.7, focusing on the leading eigenvalues. We observe that the number of eigenvalues with  $\text{Re } \lambda > 0$ , changes from one to two and back to one, so that the localized solutions are unstable along the entire branch.

In Figure 4.9 we show eigenvalues for the self-connecting branch of asymmetric localized solutions, again with correspondence to the bifurcation diagram as indicated. In Figure 4.10 we repeat these eigenvalues, along with an overlay of the eigenvalues for the corresponding “front” and “back” solutions. We once again find that one unstable eigenvalue arises from the front and one from the back, so that both are simple. However, in contrast to the cross-connecting branch which has two unstable eigenvalues in the middle section, the middle section of the self-connecting branch has no unstable eigenvalues, as it arises from two stable front (back) solutions. In Figure 4.11 we show a detail of Figure 4.7, focusing on the leading eigenvalues.

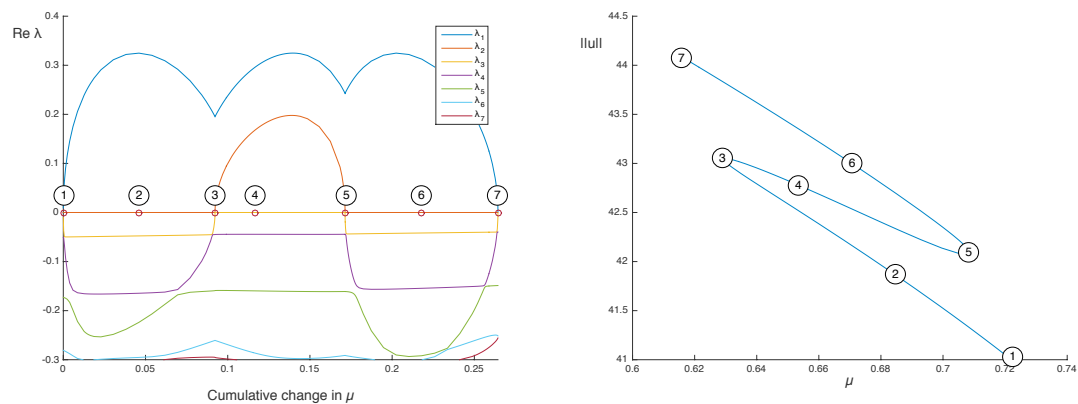


**Figure 4.6:** Left: Eigenvalues for asymmetric localized solutions along a cross-connecting branch, with  $\text{Re } \lambda$  plotted as a function of the cumulative change in  $\mu$ . Note that each of the eigenvalues with  $\lambda > 0$  is simple, as is the eigenvalue at  $\lambda = 0$ . Right: the bifurcation diagram for the cross-connecting asymmetric localized solutions repeated from Figure 4.2, with corresponding points on the eigenvalue diagram as indicated. Note that a point on the bifurcation diagram at right corresponds to a vertical slice in the eigenvalue plot at left.

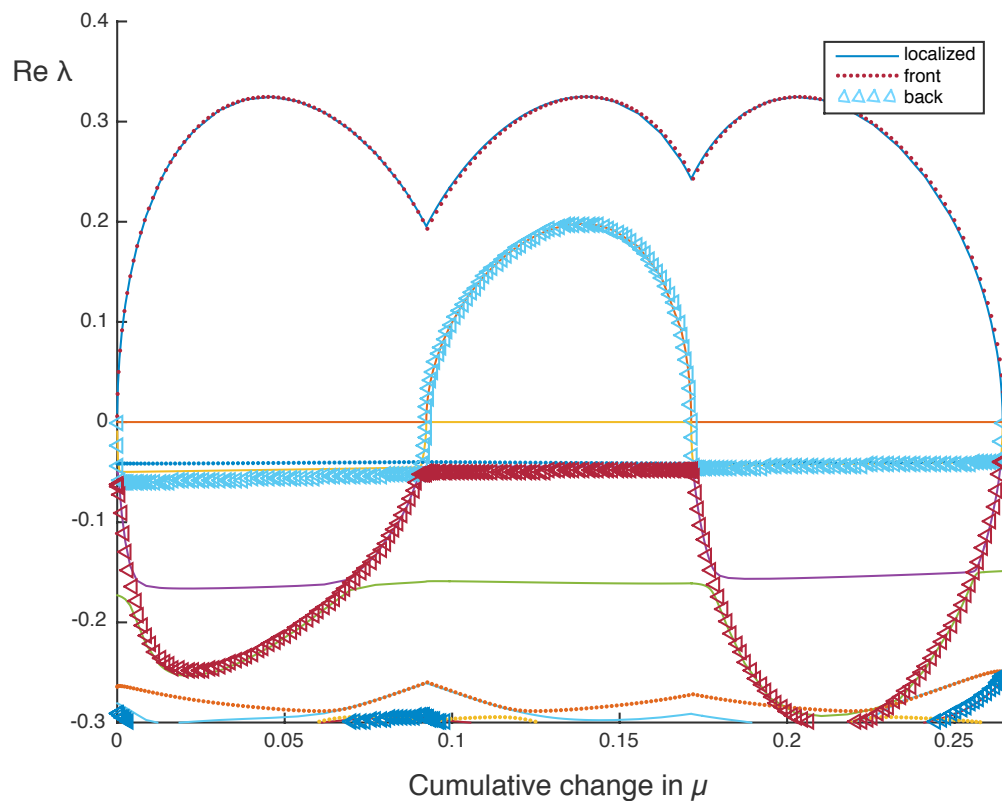


**Figure 4.7:** Eigenvalues for asymmetric localized solutions along a cross-connecting branch (solid), with eigenvalues for corresponding fronts (dots) and backs (triangles) overlaid. Note that one unstable eigenvalue arises from the front, and the other from the back, so that each is simple.

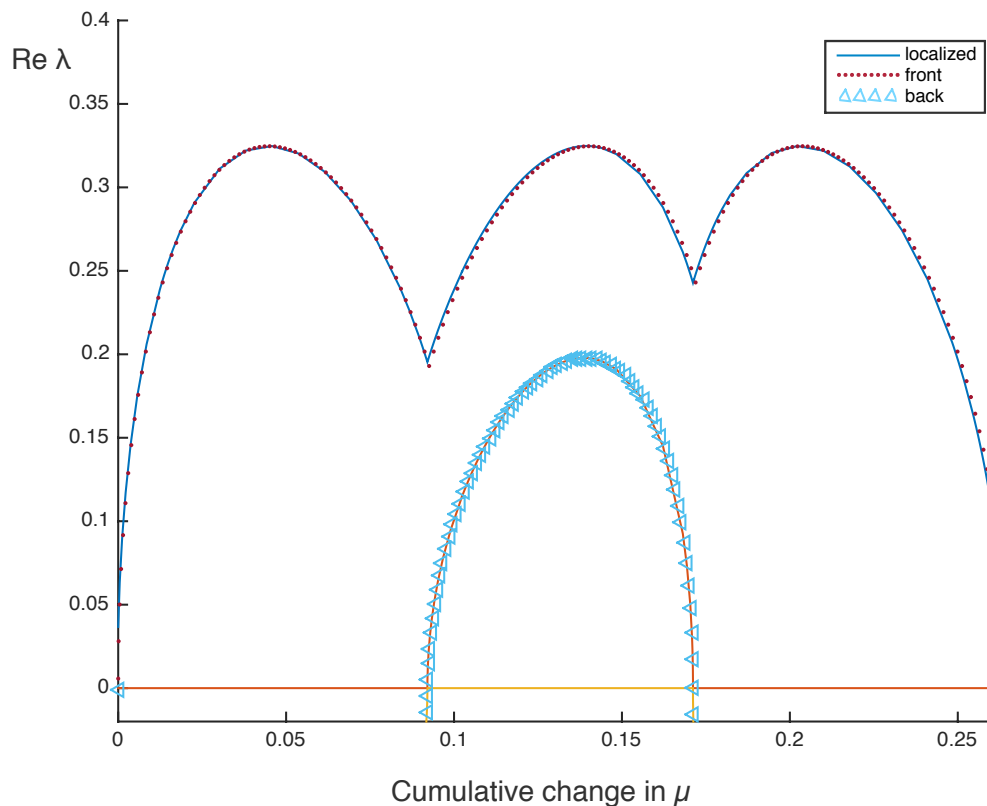


**Figure 4.8:** Detail of Figure 4.7, focusing on the leading eigenvalues.

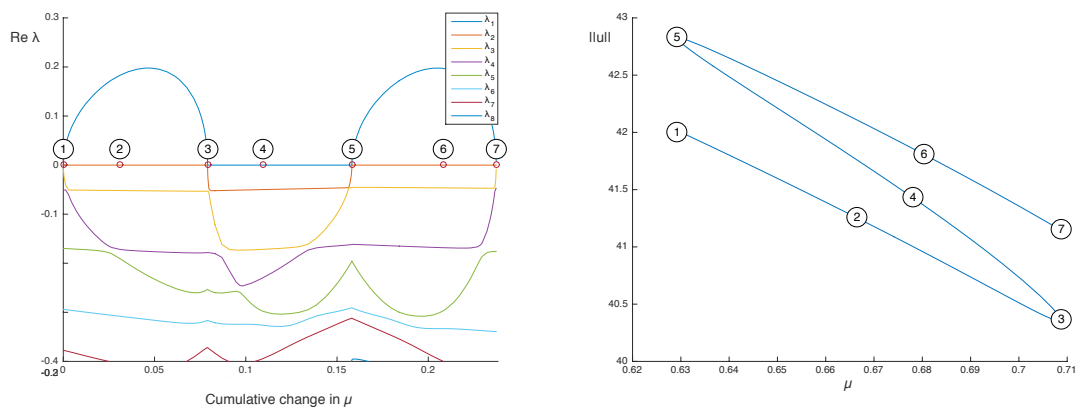


**Figure 4.9:** Left: Eigenvalues for asymmetric localized solutions along a self-connecting branch, with  $\text{Re } \lambda$  plotted as a function of the cumulative change in  $\mu$ . Note that each unstable eigenvalue is simple, as is the eigenvalue at  $\lambda = 0$ . Right: the bifurcation diagram for the cross-connecting asymmetric localized solutions repeated from Figure 4.2, with corresponding points on the eigenvalue diagram as indicated. Note that a point on the bifurcation diagram at right corresponds to a vertical slice in the eigenvalue plot at left.

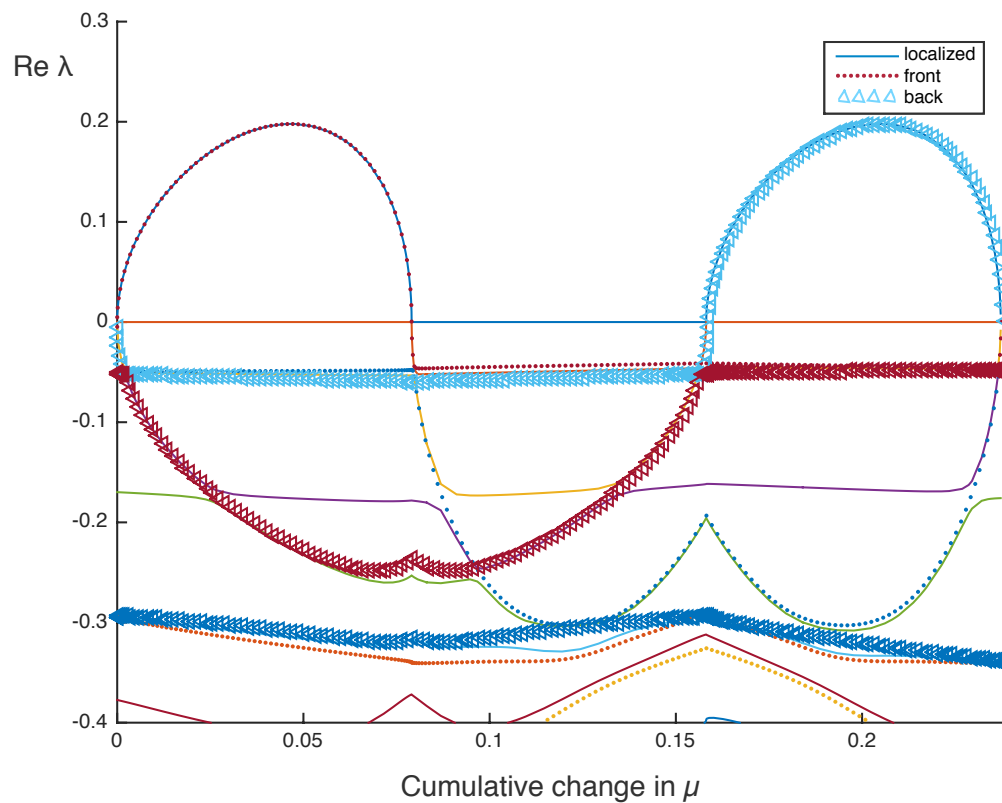


**Figure 4.10:** Eigenvalues for asymmetric localized solutions along self-connecting branch (solid), with eigenvalues for corresponding fronts (dots) and backs (triangles) overlaid. Note that one unstable eigenvalue arises from the front, and the other from the back, so that each is simple. Both the front and the back are stable in the middle section, so that the asymmetric localized solution is as well for these parameter values.

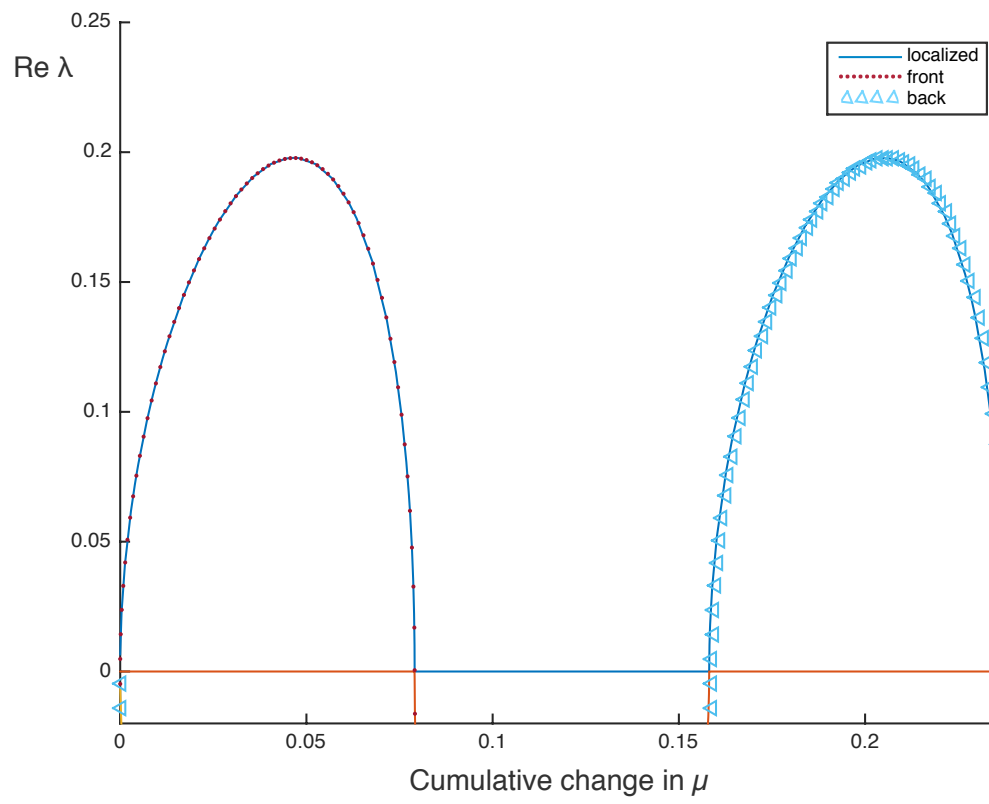


**Figure 4.11:** Detail of Figure 4.10, focusing on the leading eigenvalues.

## CHAPTER FIVE

---

# Embedded Eigenvalues and the Spectrum of Fronts

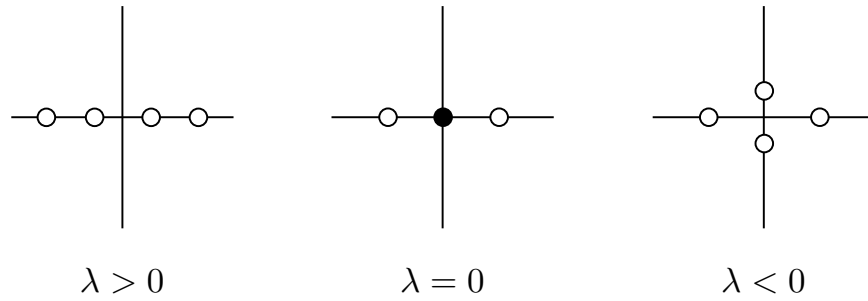


**Figure 5.1:** Spatial (Floquet) eigenvalues for the ODE corresponding to the PDE eigenvalue problem for the periodic solution. The white dots indicate simple eigenvalues, while the black dot corresponds to two eigenvalues at the origin. The three panels indicate the spatial eigenvalues as  $\lambda$  moves through zero along the real axis; see also Figure 5.2 for depictions in the entire complex plane. Note that these are the four eigenvalues with smallest real part; for higher dimensional systems, we assume that the real part of the remaining eigenvalues is uniformly bounded away from the four shown here.

## 5.1 Introduction

As noted in Chapter 4, our techniques require some modification when we reach  $\lambda = 0$ , as at this point we lose the exponential dichotomies for the periodic solution, and thus for the front. Indeed, we make a specific assumption about the way in which we lose the exponential dichotomy of the periodic solutions  $\gamma(x)$ , which in this chapter will be referred to as  $u_p(x)$ , since we reserve  $\gamma$  for use in the analytic extension of the Evans function, where we set  $\gamma^2 = \lambda$  according to standard notation. In particular, we assume that the Floquet spectrum of the periodic orbit is as depicted in Figure 5.1: as  $\lambda$  decreases through zero along the real axis, the two weakest spatial eigenvalues collide at zero as  $\lambda$  reaches zero, and then move onto the imaginary axis for  $\lambda < 0$ . The picture at  $\lambda = 0$  is consistent with the set-up in Chapter 3.

The key point is in some sense the assumption that the spatial eigenvalues move onto the imaginary axis as  $\lambda$  crosses through zero along the real axis, which we show in Section 5.3.1 occurs generically for PDEs supporting a family of periodic solutions;

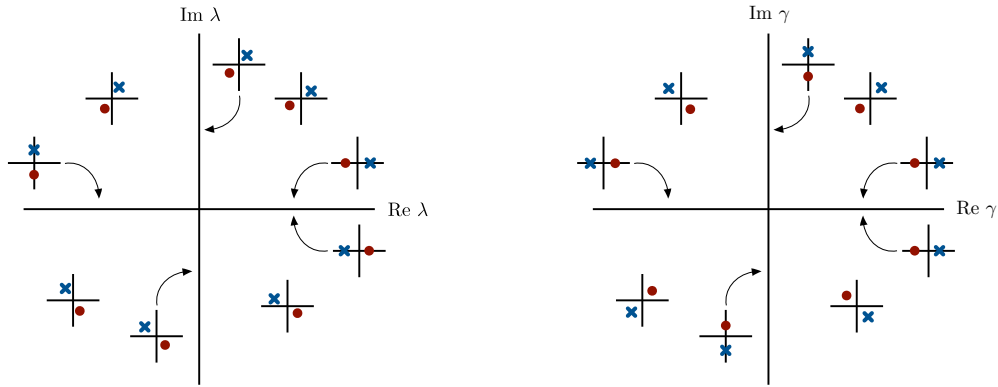


**Figure 5.2:** Left: A (necessarily) unsuccessful attempt to label the spatial eigenvalues closest to the origin consistently as functions of  $\lambda$ . Right: A successful rendering of the spatial eigenvalues as functions of  $\gamma$ , where  $\gamma^2 = \lambda$ . Note that  $\gamma$  forms a two-fold cover of  $\lambda$ .

if the spatial eigenvalues depended analytically on  $\lambda$ , they would generically move through each other after colliding at the origin, and continue along the real ( $\nu$ ) axis. However, here the leading eigenvalues go as  $\pm\sqrt{\lambda}$ , so that an analytic description of their associated eigenvectors necessitates the introduction of  $\gamma^2 = \lambda$ . In Figure 5.2 we show the impossibility of labeling the spatial eigenvalues consistently as functions of  $\lambda$ , as well as a successful labeling when we consider the eigenvalues as functions of  $\gamma$  rather than  $\lambda$ . We note that a consistent labeling is possible when restricted to the right half  $\lambda$  plane, which is the domain of the standard Evans function for the front.

As mentioned, our introduction of the extended Evans function is partially motivated by our desire to analyze the case  $\lambda = 0$  in the stability problem for localized systems. Having set up the extended Evans function in Section 5.4, we prove in Section 5.5 that the eigenvalue at  $\lambda = 0$  is simple, first in the special case of a symmetric localized solution, and then for general localized solutions.

Our analysis of the extended Evans function is further motivated by the appearance of the numerically computed spectra in Figure 4.3, and seen previously in [8]

and [3]. The results in [31, 32] suggest that, upon reaching the essential spectrum, an eigenvalue should generically move onto the Riemann sheet with  $\operatorname{Re} \gamma < 0$ . It would therefore correspond to a resonance pole rather than genuine eigenvalue, and should no longer be visible in spectral computations. However, as seen in Figure 4.3, for example, the saddle node and pitchfork eigenvalues can indeed be tracked as they move through the essential spectrum. We describe in Section 5.6 how this phenomenon arises under the conditions hypothesized here, but a complete description of the PDE or ODE systems which do (or do not) support such behavior is not yet available.

Before we can begin our construction of the extended Evans function, Section 5.2 contains preparatory material necessary to treat the asymptotically periodic systems we have in mind, i.e., eigenvalue problems for fronts that exponentially approach periodic solutions. We note that our treatment of the extended Evans function most closely follows [31, 32], though the use of the Evans function within the essential spectrum dates back to [50]. We finally note that the following results are for finite dimensional ODE systems, corresponding to PDE problems posed on the real line. We believe that our arguments may be generalizable to ODEs posed on infinite dimensional Hilbert spaces, but the extension to general Banach spaces is not clear.

## 5.2 Preliminaries

Suppose we have a system of the form

$$u_x = A(x, \lambda)u, \tag{2.1}$$

where  $x \in \mathbb{R}$ ,  $\lambda \in \mathbb{C}$ ,  $u \in \mathbb{C}^n$  and  $A(\cdot, \lambda) : \mathbb{C} \mapsto C^0(\mathbb{R}, \mathbb{C}^{n \times n})$  is analytic in  $\lambda$ . Further suppose

$$\lim_{x \rightarrow -\infty} A(x, \lambda) = A_-(\lambda) \quad (2.2)$$

$$\lim_{x \rightarrow +\infty} A(x, \lambda) = A_{per}(x, \lambda), \quad (2.3)$$

so that  $A_-$  is a constant coefficient matrix with respect to  $x$  and  $A_{per}(x, \lambda) = A_{per}(x+p, \lambda)$  for each  $x$ , with fixed  $p > 0$ . In fact, we will suppose that the approach is exponential, i.e.,

$$|A(x, \lambda) - A_-(\lambda)| \leq C e^{\eta x}, \quad x \leq 0 \quad (2.4)$$

$$|A(x, \lambda) - A_{per}(x, \lambda)| \leq C e^{-\eta x}, \quad x \geq 0 \quad (2.5)$$

for  $C, \eta > 0$ , uniformly in  $\lambda \in \Omega \subset \mathbb{C}$ ,  $\Omega$  compact. This is, of course, motivated by the eigenvalue problem for fronts, but we first address it as a general problem.

We wish to show that we can write solutions to (2.1) as  $u = P_{\pm} v$  where  $P_{\pm} = P_{\pm}(x, \lambda)$  are defined on  $x \geq 0$  and  $x \leq 0$  respectively,  $P_{\pm}(\cdot, \lambda) : \mathbb{C} \mapsto C^0[0, \pm\infty)$  are analytic, and  $v$  satisfies

$$v_x = A_-(\lambda)v, \quad x \leq 0 \quad (2.6)$$

$$v_x = A_{per}(x, \lambda)v, \quad x \geq 0. \quad (2.7)$$

For  $x \leq 0$  this is a standard application of the conjugation lemma, a corollary of the gap lemma [21, 30]. For  $x \geq 0$  we need to modify the proof of the constant coefficient version for the periodic case. Before we proceed, we first need to establish analyticity of the Floquet representations of periodic linear systems depending

analytically on  $\lambda$ .

### 5.2.1 Analyticity of Floquet representation

Since we will be working with periodic systems, we naturally expect to employ Floquet theory. Of course it is well-known that for each value of  $\lambda$ , the system

$$u_x = A_{per}(\lambda, x)u$$

will have a general solution

$$u(x) = S(x, \lambda)e^{R(\lambda)x}u_0.$$

However, in order to obtain the analyticity necessary for our later results, we will require analyticity of the matrix  $R(\lambda)$ . It is not immediately clear from standard proofs of the existence of a Floquet representation (e.g., [10, 23]) that this is possible. Therefore, we first show in Lemma 5.2.1 that such a construction is possible. We use this result in proving periodic versions of the gap lemma and conjugation lemma.

**Lemma 5.2.1. (Analyticity of Floquet Representation)** *Suppose  $A(x, \lambda) = A(x + p, \lambda)$  for each  $x \in \mathbb{R}$ , with fixed  $p > 0$ , and that for fixed  $\lambda_0 \in \mathbb{C}$ ,  $A(\cdot, \lambda) : \mathbb{C} \mapsto C^0(\mathbb{R}, \mathbb{C}^{n \times n})$  is analytic in  $\lambda$  near  $\lambda_0$ . If  $\Psi(x, \lambda)$  is a fundamental matrix solution of*

$$u_x = A(x, \lambda)u,$$

*then  $\Psi(x, \lambda)$  has a representation*

$$\Psi(x, \lambda) = S(x, \lambda)e^{R(\lambda)x}, \tag{2.8}$$

with  $S(x + p, \lambda) = S(x, \lambda)$  for all  $x$ , and  $S(\cdot, \lambda)$  and  $R(\lambda)$  analytic in  $\lambda$  near  $\lambda_0$ .

**Proof.** We begin as usual, noting that if  $\Psi(x, \lambda)$  is a fundamental matrix solution then so is  $\Psi(x + p, \lambda)$ , so that there exists a nonsingular matrix  $C(\lambda)$ , analytic in  $\lambda$  and constant in  $x$ , such that

$$\Psi(x + p, \lambda) = \Psi(x, \lambda)C(\lambda).$$

Now we wish to show that we can construct a matrix  $R(\lambda)$ , analytic in  $\lambda$ , such that

$$e^{R(\lambda)p} = C(\lambda). \quad (2.9)$$

We start by writing  $C = C(\lambda_0)$ , so that

$$C(\lambda) = C + \sum_{k=1}^{\infty} \frac{(\lambda - \lambda_0)^k}{k!} \frac{\partial^k}{\partial \lambda^k} C|_{\lambda_0} =: C + (\lambda - \lambda_0)D(\lambda), \quad (2.10)$$

where  $|D(\lambda)| \leq M$  uniformly in some neighborhood of  $\lambda_0$ .

We first establish the result for  $C = J$  a single Jordan block with the particular form

$$J = \begin{pmatrix} \tilde{\lambda} & \epsilon & & 0 \\ & \tilde{\lambda} & \epsilon & \\ & & \ddots & \ddots \\ & & & \ddots & \epsilon \\ 0 & & & & \tilde{\lambda} \end{pmatrix}, \quad (2.11)$$

with  $J \in \mathbb{C}^{m \times m}$  and where we may choose  $\epsilon$  as small as we like. Given  $C$  in the form

(2.11) and using (2.10), we have

$$C(\lambda) = \tilde{\lambda} \left( I + \frac{1}{\tilde{\lambda}} (N + (\lambda - \lambda_0)D(\lambda)) \right),$$

where  $N$  has  $\epsilon$  above the diagonal and 0 everywhere else. Defining

$$\tilde{N}(\lambda) := N + (\lambda - \lambda_0)D(\lambda),$$

we choose  $\epsilon$  so that  $|N| < 1/2|\tilde{\lambda}|$  and then fix  $|\lambda - \lambda_0|$  sufficiently small so that  $|(\lambda - \lambda_0)D(\lambda)| < 1/2|\tilde{\lambda}|$ , which is possible since  $|D(\lambda)| \leq M$  uniformly in some neighborhood of  $\lambda_0$ . Thus

$$|\tilde{N}(\lambda)| \leq |N| + |(\lambda - \lambda_0)D(\lambda)| < \frac{1}{|\tilde{\lambda}|}.$$

We now write

$$\ln C(\lambda) = (\ln \tilde{\lambda})I + \sum_{j=1}^{\infty} \frac{(-1)^{j+1}}{j} \left( \frac{\tilde{N}(\lambda)}{\tilde{\lambda}} \right)^j,$$

which holds since  $|\tilde{N}(\lambda)/\tilde{\lambda}| < 1$ . Thus our desired matrix  $R(\lambda)$  in the special case  $C = J$  is given by

$$R(\lambda) = \frac{1}{p} \left( (\ln \tilde{\lambda})I + \sum_{j=1}^{\infty} \frac{(-1)^{j+1}}{j} \left( \frac{\tilde{N}(\lambda)}{\tilde{\lambda}} \right)^j \right)$$

and we can see from the above that this is indeed analytic.

Now suppose that  $C$  is of general form, and let  $P(\epsilon)$  be such that

$$P^{-1}(\epsilon)CP(\epsilon) = \begin{pmatrix} J_1 & & 0 \\ & \ddots & \\ 0 & & J_r \end{pmatrix},$$

where each  $J_k$  has the form (2.11) for an appropriate  $\tilde{\lambda}_k$ . We now have

$$\begin{aligned} P^{-1}(\epsilon)C(\lambda)P(\epsilon) &= P^{-1}(\epsilon)CP(\epsilon) + (\lambda - \lambda_0)P^{-1}(\epsilon)D(\lambda)P(\epsilon) \\ &= \begin{pmatrix} J_1 & & 0 \\ & \ddots & \\ 0 & & J_r \end{pmatrix} + \begin{pmatrix} \hat{D}_1 & & 0 \\ & \ddots & \\ 0 & & \hat{D}_r \end{pmatrix} + \hat{D}, \end{aligned} \quad (2.12)$$

where we have split the matrix  $(\lambda - \lambda_0)P^{-1}(\epsilon)D(\lambda)P(\epsilon)$  into blocks  $\hat{D}_1, \dots, \hat{D}_r$  corresponding to the size of the blocks  $J_1, \dots, J_r$ , while  $\hat{D}$  consists of all remaining entries after subtracting these blocks. Dependence on  $\epsilon, \lambda, \lambda_0$  has been suppressed for notational convenience.

We have shown above that for each block problem  $J_k + \hat{D}_k$  we have  $\hat{R}_k(\lambda)$  analytic so that  $e^{\hat{R}_k(\lambda)P} = J_k + \hat{D}_k$  (where  $\epsilon$  is first chosen so that  $|N_k| < 1/2 \min_k |\tilde{\lambda}_k|$ , so that  $P := P(\epsilon)$  is fixed, and  $\lambda$  is then constrained by appropriately defined  $\hat{M}_k$  and  $\tilde{\lambda}_k$ ). By basic properties of the exponential, if we define  $\hat{R}(\lambda)$  composed of the blocks  $\hat{R}_k(\lambda)$ , then  $e^{\hat{R}(\lambda)P} = \text{diag}[e^{\hat{R}_1(\lambda)P}, \dots, e^{\hat{R}_r(\lambda)P}]$  so that  $e^{\hat{R}(\lambda)P}$  is equal to the first two terms on the right hand side of (2.12).

It now remains to show that given  $\hat{R}(\lambda)$  analytic such that  $e^{\hat{R}(\lambda)P} = \hat{C}(\lambda)$ , there exists  $R^*(\lambda)$  analytic such that  $e^{R^*(\lambda)P} = \hat{C}(\lambda) + \hat{D}(\lambda)$ . We write

$$\hat{C}(\lambda) + \hat{D}(\lambda) = \hat{C}(\lambda)(I + \hat{C}^{-1}(\lambda)\hat{D}(\lambda)),$$

and claim

$$\ln(\hat{C}(\lambda) + \hat{D}(\lambda)) = \hat{R}(\lambda) + \sum_{j=1}^{\infty} \frac{(-1)^{j+1}}{j} \left( \hat{C}^{-1}(\lambda)\hat{D}(\lambda) \right)^j. \quad (2.13)$$

Since  $\hat{C}(\lambda)$  is nonsingular,  $\hat{C}^{-1}(\lambda)$  is well-defined and  $|\hat{C}^{-1}(\lambda)| < \hat{M}$  uniformly for

$\lambda$  in some neighborhood of  $\lambda_0$ . So then choosing  $|\lambda - \lambda_0|$  sufficiently small so that  $|\hat{C}^{-1}(\lambda)\hat{D}(\lambda)| < 1$ , and still respecting the constraints required for the definition of  $\hat{R}(\lambda)$ , (2.13) holds and we have  $R^*(\lambda)$  analytic as desired. In summary, setting

$$R(\lambda) = \frac{1}{p}P \left( \hat{R}(\lambda) + \sum_{j=1}^{\infty} \frac{(-1)^{j+1}}{j} \left( \hat{C}^{-1}(\lambda)\hat{D}(\lambda) \right)^j \right) P^{-1}, \quad (2.14)$$

$R(\lambda)$  is well-defined, analytic and satisfies (2.9).

We now conclude in the standard fashion. We define  $S(x, \lambda) = \Psi(x, \lambda)e^{-R(\lambda)x}$ , so that  $S(x + p, \lambda) = \Psi(x + p, \lambda)e^{-R(\lambda)(x+p)} = \Psi(x, \lambda)e^{R(\lambda)p}e^{-R(\lambda)p}e^{-R(\lambda)x} = S(x, \lambda)$ , and  $S$  is clearly analytic in  $\lambda$ . ■

## 5.2.2 Gap and conjugation lemmas with periodic coefficients

Having shown that an analytic Floquet construction is possible, we now proceed with periodic analogues of the gap and conjugation lemmas.

**Lemma 5.2.2. (Gap Lemma with Periodic Coefficients, cf [21, 30])** *Suppose that we are in the setting described above, and in particular that (2.5) holds for the system (2.1). Further suppose that associated to the system*

$$v_x = A_{per}(\lambda, x)v \quad (2.15)$$

*is a Floquet representation of the evolution*

$$\Phi(x, \lambda) = S(x, \lambda)e^{R(\lambda)x}. \quad (2.16)$$

*If  $v_*(\lambda)$  is an eigenvector of  $R(\lambda)$  with eigenvalue  $\nu(\lambda)$ , then there exists a solution*

of (2.1) of the form

$$u(x, \lambda) = e^{\nu(\lambda)x} S(x, \lambda) v(x, \lambda) \quad (2.17)$$

where  $v$  is  $C^1$  in  $x$  and locally analytic in  $\lambda$ , and for any fixed  $\tilde{\eta} < \eta$  satisfies

$$v(x, \lambda) = v_*(\lambda) + O(e^{-\tilde{\eta}x} |S^{-1}(\lambda)| |S(\lambda)| |v_*(\lambda)|), \quad x \geq 0. \quad (2.18)$$

**Proof.** Suppressing the  $\lambda$  dependence and letting  $u(x) = e^{\nu x} S(x) v(x)$ , we find that (2.1) is equivalent to

$$v_x = (R - \nu I)v + \Theta(x)v, \quad (2.19)$$

where

$$\Theta(x) = \Theta(x, \lambda) := S^{-1}(x, \lambda)(A(x, \lambda) - A_{per}(x, \lambda))S(x) = O(e^{-\eta x} |S^{-1}(\lambda)| |S(\lambda)|), \quad x \geq 0. \quad (2.20)$$

To see this, we argue as follows: substitution immediately yields

$$[\nu e^{\nu x} S(x) + e^{\nu x} S_x(x)] v + e^{\nu x} S(x) v_x = A e^{\nu x} S(x) v$$

which we rewrite as

$$S(x) v_x = A(x) S(x) v - \nu S(x) v - S_x(x) v.$$

It is always true for a Floquet representation that  $A_{per}(x) S(x) = S_x(x) + S(x) R$ , as can be checked by differentiation. Consequently, subtracting and adding  $S(x) R v$  to

the above, we have

$$S(x)v_x = A(x)S(x)v - \nu S(x)v - A_{per}S(x)v + S(x)Rv$$

or

$$S(x)v_x = S(x)(R - \nu I)v + (A(x) - A_{per}(x))S(x)v$$

so that

$$v_x = (R - \nu I)v + [S^{-1}(x)(A(x) - A_{per}(x))S(x)]v$$

as was claimed.

We now choose  $\eta_1$  with  $\tilde{\eta} < \eta_1 < \eta$  such that there is a gap between the spectrum of  $R$  and  $\nu - \eta_1$ , i.e.,  $|\operatorname{Re}(\operatorname{spec} R - (\nu - \eta_1))| > 0$ . Then fixing a point  $\lambda = \lambda_*$ , we can define for all  $\lambda$  in a neighborhood of  $\lambda_*$  the spaces  $E^s(\lambda)$  and  $E^u(\lambda)$  corresponding to generalized eigenspaces of the eigenvalues of  $R$  with real part less than  $\nu - \eta_1$  and greater than  $\nu - \eta_1$ , respectively. Associated to these spaces we have projections  $P^u(\lambda)$  and  $P^s(\lambda)$  analytic in  $\lambda$  such that

$$|e^{(R-\nu I)x}P^u| \leq Ce^{-\eta_1 x}, \quad x \leq 0, \quad |e^{(R-\nu I)x}P^s| \leq Ce^{-\eta_1 x}, \quad x \geq 0. \quad (2.21)$$

We wish to find a solution  $v(x, \lambda)$  to (2.19) satisfying (2.18). As can be understood by consideration of the above projections with the evolution operator, we define the map  $\mathcal{T}$  by

$$\mathcal{T}v(x) = v_* + \int_M^x e^{(R-\nu I)(x-y)}P^s\Theta(y)v(y)dy - \int_x^\infty e^{(R-\nu I)(x-y)}P^u\Theta(y)v(y)dy. \quad (2.22)$$

From this we see that, for any  $v_1(x)$  and  $v_2(x)$ , we have the bound

$$\begin{aligned} |\mathcal{T}v_1 - \mathcal{T}v_2|_{(x)} &\leq \left( \int_M^x e^{-\eta(x-y)} e^{-\eta y} dy + \int_x^\infty e^{-\eta(x-y)} e^{-\eta y} dy \right) C |S^{-1}| |S| |v_1 - v_2|_\infty \\ &= C \frac{e^{-\eta_1(x-M)} e^{-\eta M}}{\eta - \eta_1} |S^{-1}| |S| |v_1 - v_2|_\infty. \end{aligned} \quad (2.23)$$

So for  $\lambda$  in a compact neighborhood and  $M$  sufficiently large, the terms preceding  $|v_1 - v_2|_\infty$  in (2.23) will be strictly less than 1, so that  $\mathcal{T}$  is a contraction mapping on  $L^\infty[M, \infty)$ . Thus we have a unique solution  $\bar{v} \in L^\infty[M, \infty)$  to  $v = \mathcal{T}v$ . Since this solution may be obtained iteratively starting with  $v_0 = 0$ , it is analytic in  $\lambda$  as the uniform limit of analytic iterates. By differentiating, we can see that  $\bar{v}$  a bounded solution of (2.19), so that with  $v(x, \lambda) = \bar{v}(x, \lambda)$ , (2.17) is a solution of (2.1) on  $[M, \infty)$ . Furthermore, letting  $v_1 = \bar{v}$  and  $v_2 = 0$  in the above, we have

$$|\bar{v} - v_*| = |\mathcal{T}\bar{v} - \mathcal{T}0| \leq C e^{-\tilde{\eta}x} |S^{-1}| |S| |\bar{v}| \leq C e^{-\tilde{\eta}x} |S^{-1}| |S| |v_*| \quad (2.24)$$

so that (2.18) holds. This bound, as well as analyticity, extends to  $x \geq 0$  by considering the initial value problem at  $x = M$ . ■

**Corollary 5.2.3. (Conjugation Lemma with Periodic Coefficients, cf [46])**

*Suppose that (2.5) holds for the system (2.1), and fix  $0 < \tilde{\eta} < \eta$ ,  $\lambda_0 \in \Omega$ . Then there exists locally to  $\lambda_0$  an invertible transformation  $P(x, \lambda)$ ,  $x \geq 0$ , which is analytic in  $\lambda$ , such that*

$$|P(x, \lambda) - I| \leq C e^{-\tilde{\eta}x}, \quad (2.25)$$

*and under the transformation  $u = P(x, \lambda)v$ , (2.1) becomes*

$$v_x = A_{per}(x, \lambda)v, \quad x \geq 0. \quad (2.26)$$

**Proof.** Let  $u = P(x, \lambda)v$  and suppose (2.26) holds. Substituting into (2.1) we have

$$P_x(x, \lambda)v + P(x, \lambda)A_{per}(x, \lambda)v = AP(x, \lambda)v,$$

so we wish to find  $P$  such that

$$P_x = AP - PA_{per} =: \mathcal{A}P. \quad (2.27)$$

We note  $\mathcal{A}$  is such that  $\lim_{x \rightarrow \infty} \mathcal{A} = \mathcal{A}_{per}$ , where  $\mathcal{A}_{per}P := A_{per}P - PA_{per}$ , and the convergence is with exponential rate  $\eta$  as before. Moreover we see that  $\mathcal{A}_{per}$  has eigenvalue, eigenvector pair  $0, I$  for every  $\lambda$ . If we write a Floquet representation associated to  $\mathcal{A}_{per}$  as

$$\Phi(x, \lambda) = \hat{S}(x, \lambda)e^{\hat{R}(\lambda)x}, \quad (2.28)$$

then  $\mathcal{A}_{per}I = 0$  implies  $\hat{S}(x, \lambda)e^{\hat{R}(\lambda)x}I = I$ . This holds if  $0, I$  is an eigenvalue, eigenvector pair for  $\hat{R}(\lambda)$  (and  $\hat{S}(x)$  has eigenvalue, eigenvector pair  $1, I$ ). More generally,  $\hat{R}$  may have eigenvalue  $\alpha \in \mathbb{C}$  with eigenvector  $I$ , while  $\hat{S}(x)$  is of the form  $e^{-\alpha x}$ ; since  $\hat{S}(x)$  is periodic,  $\alpha$  must be pure imaginary. From Lemma 5.2.2 we then have for  $k \in \mathbb{R}$  the solution  $P = e^{ikx}e^{-ikx}(I + O(e^{-\tilde{\eta}x}|e^{ikx}||e^{-ikx}||I|)) = I + O(e^{-\tilde{\eta}x})$ , which is as desired. ■

**Remark 5.2.4.** *Note that we can in fact conjugate the system (2.1) for  $x \geq 0$  to the constant coefficient system*

$$w_x = R(\lambda)w \quad (2.29)$$

*via the relation  $u = P(x, \lambda)S(x, \lambda)w$ , where  $R(\lambda)$  and  $S(x, \lambda)$  are associated to  $A_{per}(x, \lambda)$  and  $P$  again satisfies (2.25). That these two formulations are equivalent*

can be seen by letting  $v = S(x, \lambda)w$  so that

$$\begin{aligned}
 v_x &= S_x(x, \lambda)w + S(x, \lambda)w_x \\
 &= S_x(x, \lambda)w + S(x, \lambda)R(\lambda)w \\
 &= (S_x(x, \lambda) + S(x, \lambda)R(\lambda))S^{-1}(x, \lambda)v \\
 &= A_{per}(x, \lambda)S(x, \lambda)S^{-1}(x, \lambda)v \\
 &= A_{per}(x, \lambda)v.
 \end{aligned}$$

### 5.3 Hypotheses and motivations

Having established the necessary technical tools, we now turn to our specific problem.

We will once again consider

$$u_x = f(u, \mu) \tag{3.1}$$

with  $u \in \mathbb{R}^{2n}$  and  $\mu \in \mathbb{R}$ , and the eigenvalue problems

$$v_x = [f_u(u_*(x), \mu) + \lambda B]v \tag{3.2}$$

with  $v \in \mathbb{C}^{2n}$ ,  $\lambda \in \mathbb{C}$  and  $B \in \mathbb{R}^{2n \times 2n}$ , and  $u_*(x)$  a particular solution of (3.1). Note that, for simplicity, we take  $B$  to be a fixed matrix in this chapter.

In order to address the behavior of the saddle node eigenvalues along snaking branches, we will assume that all hypotheses from Chapter 3, in particular Section 3.3, hold here for the system (3.1). We recall that under these hypotheses we have a reversible, conservative system such that the origin is hyperbolic and there exists a family of symmetric periodic orbits depending smoothly on  $\mu$ . Again we remark that the periodic solutions will be denoted by  $u_p(x, \mu)$  or simply  $u_p(x)$  in this

chapter, as we will employ the standard notation  $\gamma^2 = \lambda$ . We also have conditions on the intersection of the stable manifold from the origin  $W^s(0, \mu)$  and the strong unstable fibers of the periodic orbit  $W^{uu}(\gamma(\varphi, \mu), \mu)$  as detailed in Hypothesis 3.3.2.

As in Chapter 4, we initially fix  $\mu$  and address a particular family of localized solutions  $u_{\ell,L}$  associated to a front  $u_f(x)$  with phase  $\varphi_1^*$  and back  $u_b(x)$  with phase  $\varphi_2^*$ , and  $z(\varphi_1^*), z(\varphi_2^*) \neq 0$ , and  $m \in \{0, 1\}$  fixed as in Theorem 3.2. We will reintroduce  $\mu$  in analyzing the behavior of the saddle node eigenvalue near the essential spectrum of the periodic orbits.

In the following we will give results on symmetric and asymmetric localized solutions, and we will use reversibility to relate assumptions on the form of exponentially decaying solutions of the eigenvalue problem for the back, expressed in the transformed coordinate system, to analogous assumptions for the front (though we note that reversibility is otherwise not essential for the general result). We note that the parameterizations for Chapters 3 and 4 match for symmetric localized solutions with  $m = 0$ , but there is a shift of  $\pi$  for  $m = 1$ .

In the present setting the most convenient parameterization will be that of Chapter 4 shifted by  $m\pi$ ; more precisely if  $\tilde{u}_{\ell,L}(x)$ ,  $\tilde{u}_f(x)$  and  $\tilde{u}_b(x)$  are the solutions from Chapter 4, in the present chapter we set  $u_{\ell,L}(x) = \tilde{u}_{\ell,L}(x + m\pi)$ ,  $u_f(x) = \tilde{u}_f(x + m\pi)$  and  $u_b(x) = \tilde{u}_b(x + m\pi)$ . This is equivalent to using  $\tilde{\varphi} = (\varphi_2^* - \varphi_1^*)/2$  in place of  $\bar{\varphi} = (\varphi_2 - \varphi_1)/2$  in the transformation described in Lemma 4.3.4.

With the above definitions, the parameterization for symmetric localized solutions exactly matches that of Chapter 3 whether  $m = 0$  or  $m = 1$ . However, asymmetric solutions are shifted by the phase differential from either 0 or  $\pi$  depending on whether  $m = 0$  or  $m = 1$ . Matching will therefore be done either in the 0 or  $\pi$

phase of the periodic solution depending upon whether  $m = 0$  or  $m = 1$ . Note that we could have used the same parameterization in Chapter 4, in which case we would have set  $V_a = \text{Rg } P_\gamma^u(m\pi; \lambda_*) \oplus \text{Rg } P_\gamma^s(m\pi; \lambda_*)$  in the proof of Theorem 4.1. In the present case we will use the conjugation lemma to move into a constant coefficient framework, but we will still have a matching condition which carries  $x$ -dependence via the periodic Floquet matrix.

We finally suppose that Hypothesis 4.3.7 continues to hold: the essential spectrum of the trivial solution is bounded away from the imaginary axis in the left half plane.

We are interested in writing down the Evans function for the eigenvalue problem associated to the front

$$v_x = [f_u(u_f(x)) + \lambda B]v =: A_f(x, \lambda)v \quad (3.3)$$

using information about the periodic orbits

$$v_x = [f_u(u_p(x)) + \lambda B]v =: A_p(x, \lambda)v. \quad (3.4)$$

We have

$$|u_f(x + \varphi_1^*) - u_p(x)| \leq Ce^{-\eta x}, \quad x \geq 0 \quad (3.5)$$

so that

$$|A_f(x + \varphi_1^*, \lambda) - A_p(x, \lambda)| \leq Ce^{-\eta x}, \quad x \geq 0 \quad (3.6)$$

uniformly in  $\lambda$  near 0.

In the case  $\varphi_1 \neq \varphi_2$  we will also be interested in the eigenvalue problem for the

back, given by

$$v_x = [f_u(u_b(x)) + \lambda B]v =: A_b(x, \lambda)v \quad (3.7)$$

where we know

$$|u_b(x - \varphi_2^*) - u_p(x)| \leq Ce^{\eta x}, \quad x \leq 0$$

so that

$$|A_b(x - \varphi_2^*, \lambda) - A_p(x, \lambda)| \leq Ce^{\eta x}, \quad x \leq 0$$

uniformly in  $\lambda$  near 0.

In Chapter 4 we did not use the periodicity of the solutions  $u_p(x)$ , which is reasonable given that the result of adding eigenvalues with multiplicity is known for monotone pulse solutions. The periodicity of  $u_p(x)$  will, however, play a crucial role in the following. Our next Hypothesis is consistent with Hypothesis 4.3.6 in Chapter 4, but explicitly specifies the way in which the exponential dichotomies are lost at  $\lambda = 0$ .

**Hypothesis 5.3.1.** *There exists  $\delta > 0$  such that, for  $\lambda \in U_\delta(0)$ , the eigenvalue problem*

$$v_x = [f_u(u_p(x)) + \lambda B]v. \quad (3.8)$$

*has associated Floquet matrices  $S(x, \lambda)$  and  $R(\lambda)$ , chosen analytically for some neighborhood of  $\lambda = 0$ , which we take without loss of generality to include  $U_\delta(0)$ , and there exists a  $V(\lambda)$ , analytic and invertible for  $\lambda \in U_\delta(0)$ , such that  $V^{-1}(\lambda)R(\lambda)V(\lambda) =$*

$J(\lambda)$ , where

$$J(\lambda) = \left( \begin{array}{cc|ccc} 0 & 1 & 0 & \cdots & 0 \\ \lambda & 0 & 0 & \cdots & 0 \\ \hline 0 & 0 & & & \\ \vdots & \vdots & & D(\lambda) & \\ 0 & 0 & & & \end{array} \right) \quad (3.9)$$

and  $D(\lambda)$  is a diagonal matrix such that at  $\lambda = 0$  all entries are real and bounded away from zero by  $\alpha > 0$ . We denote by  $\pm\alpha(\lambda)$  the entries of  $D(\lambda)$  with smallest real part at  $\lambda = 0$  and we assume that these are further bounded away in real part from the remaining entries by some  $\eta > 0$ .

In other words, we assume the dispersion relation  $d(\nu, \lambda) = \det(R(\lambda) - \nu I)$  for  $\nu \in i\mathbb{R}$  has a double root at  $(\nu, \lambda) = (0, 0)$  with  $d_\nu(0, 0) = 0$ . We do not actually need the matrix  $D$  to be diagonal, only that the leading stable and unstable eigenvalues at  $\lambda = 0$  are simple and bounded away from zero and the rest of the spectrum, as we supposed in Hypothesis 3.3.1.

Further hypotheses dictating the order of the roots of the Evans function of the front will be given in Sections 5.5 and 5.6, once we have written down the Evans function in Section 5.4.

To motivate our set-up, in the following subsection we show that Hypothesis 5.3.1 is generically satisfied for a reversible PDE system supporting a family of symmetric stationary periodic solutions.

### 5.3.1 A PDE system

Loosely stated, we will show that Hypothesis 5.3.1 holds generically for the ODE eigenvalue problem arising from a reversible and/or conservative PDE supporting a stationary periodic solution, where we assume that the operator  $\mathcal{L}_{per}$  associated to the linearization about the periodic solution has a simple eigenvalue at  $\lambda = 0$ .

We consider a PDE of the form

$$U_t = \mathcal{A}(\partial_x)U + \mathcal{N}(U), \quad x \in \mathbb{R}, \quad U \in \mathcal{X}, \quad \mu \in \mathbb{R} \quad (3.10)$$

where  $\mathcal{A}(\cdot)$  is a vector-valued polynomial,  $\mathcal{X}$  is a Banach space of functions  $U(x)$  so that  $\mathcal{A}(\partial_x) : \mathcal{X} \rightarrow \mathcal{X}$  is closed and densely defined, and  $\mathcal{N} : \mathcal{X} \times \mathbb{R} \rightarrow \mathcal{X}$  is some nonlinearity defined via pointwise evaluation of  $U$  and possibly derivatives of  $U$ . We further consider the corresponding ODE

$$u_x = f(u) \quad (3.11)$$

with  $u = (U, U_x, \dots)^T \in \mathbb{R}^n$ .

We suppose that (3.10) has a stationary solution  $Q_{per}(x + p) = Q_{per}(x)$  for all  $x$ , and we define  $q_{per}(x) := (Q_{per}(x), \partial_x Q_{per}(x), \dots)^T \in \mathbb{R}^n$ . We further define the linearized operator

$$\mathcal{L}_{per} := \mathcal{A}(\partial_x)U + \partial_U \mathcal{N}(Q_{per}(x))U. \quad (3.12)$$

with the associated ODE eigenvalue problem

$$u_x = [f_u(q_{per}(x)) + \lambda B]u \quad (3.13)$$

We now assume that our system is reversible:

**Hypothesis 5.3.2.** (3.10) is symmetric under  $x \mapsto -x$ , so that if  $U(x)$  is a solution, so is  $U(-x)$ .

This generically implies our next hypothesis, that the system (3.10) admits not only the stationary solution  $Q_{per}(x)$ , but a family of periodic stationary solutions  $Q_{per}(x; \epsilon)$ ; see [62] or [16]. We state this as a separate hypothesis for clarity, and note that conservative ODE systems, corresponding to variational PDE systems also generically support families of periodic solutions; again see [62].

**Hypothesis 5.3.3.** There exists a family of symmetric spatially periodic solutions  $Q_{per}(x; \epsilon)$  to (3.10) for  $\epsilon$  not necessarily small, with  $Q_{per}(x) =: Q_{per}(x; \epsilon_0)$ , and  $Q_{per}(x + T(\epsilon); \epsilon) = Q_{per}(x; \epsilon)$ ,  $T(\epsilon) > 0$  for all  $x$  and  $\epsilon$  in a neighborhood of  $\epsilon_0$ .

We define  $q_{per}(x; \epsilon_0) := (Q_{per}(x; \epsilon_0), \partial_x Q_{per}(x; \epsilon_0), \dots)^T \in \mathbb{R}^n$ . Our final hypothesis concerns the operator  $\mathcal{L}_{per}$  defined in (3.2), which we emphasize is associated to the periodic orbit  $Q_{per}(x; \epsilon_0)$ .

**Hypothesis 5.3.4.**  $\lambda = 0$  is simple as an eigenvalue of  $\mathcal{L}_{per}$ .

We note that this implies  $N(\mathcal{L}_{per}) = \text{span}\{\partial_x Q_{per}(x; \epsilon_0)\}$  since substituting  $Q_{per}(x) = Q_{per}(x; \epsilon_0)$  for  $U(x, t)$  in (3.10) and differentiating with respect to  $x$  yields

$$0 = \mathcal{A}(\partial_x) \partial_x Q_{per}(x) + \mathcal{N}(Q_{per}(x)) \partial_x Q_{per}(x) = \mathcal{L}_{per} \partial_x Q_{per}(x). \quad (3.14)$$

Similarly, (3.13) with  $\lambda = 0$  has solution  $\partial_x q_{per}(x; \epsilon_0)$ .

**Lemma 5.3.5.** Suppose that Hypotheses 5.3.2–5.3.4 hold. Then Hypothesis 5.3.1 holds for the linearization of (3.11) about  $q_{per}(x; \epsilon_0)$ , with the entry  $\lambda$  appearing in

the second row, first column of  $J$  replaced by  $a\lambda$  for  $a \neq 0$ , and the form of  $D$  holding generically for a reversible system.

**Proof.** We first show that Hypothesis 5.3.4 implies that the period  $T(\epsilon)$  of the solutions  $q_{per}(x; \epsilon)$  satisfies  $\frac{d}{d\epsilon}T(\epsilon_0) \neq 0$ . We introduce  $y = x/T(\epsilon)$  so that

$$u_y = T(\epsilon)f(u).$$

Differentiating this with respect to  $\epsilon$  yields

$$\begin{aligned} \partial_\epsilon u_y &= \frac{d}{d\epsilon}T(\epsilon)f(u) + T(\epsilon)f_u(u)\partial_\epsilon u \\ &= \frac{\frac{d}{d\epsilon}T(\epsilon)}{T(\epsilon)}u_y + T(\epsilon)f_u(u)\partial_\epsilon u \end{aligned} \quad (3.15)$$

Letting  $u_* = q_{per}(x; \epsilon_0)$  and writing  $v = \partial_\epsilon u_*$ , we then have

$$v' = \frac{\frac{d}{d\epsilon}T(\epsilon_0)}{T(\epsilon_0)}u'_* + T(\epsilon_0)f_u(u_*)v, \quad (3.16)$$

where  $' = \frac{d}{dy}$ . Then  $\frac{d}{d\epsilon}T(\epsilon_0) \neq 0$  or we would have a second solution  $v = \partial_\epsilon q_{per}$  of (3.13) with  $\lambda = 0$ , contradicting  $\lambda = 0$  simple as an eigenvalue of  $\mathcal{L}_{per}$ .

We now show that the Floquet exponent matrix  $R(0)$  associated to (3.13) with  $\lambda = 0$  has a two dimensional Jordan block with Floquet exponent  $\nu = 0$ .

Writing  $\Phi(x, y)$  for the 1-periodic flow associated to  $v' = T(\epsilon_0)f_u(u_*)v$ , we use

variation of constants to find a 1-periodic solution  $v(x)$  to (3.16):

$$\begin{aligned}
 v(x) &= \Phi(x, 0)v(0) + \int_0^x \Phi(x, y) \frac{d}{d\epsilon} \frac{T(\epsilon_0)}{T(\epsilon_0)} u'_*(y) dy \\
 &= \Phi(x, 0)v(0) + \frac{d}{d\epsilon} \frac{T(\epsilon_0)}{T(\epsilon_0)} \int_0^x u'_*(x) dy \\
 &= \Phi(x, 0)v(0) + \frac{d}{d\epsilon} \frac{T(\epsilon_0)}{T(\epsilon_0)} u'_*(x)x.
 \end{aligned}$$

Then

$$v(0) = v(1) = \Phi(1, 0)v(0) + \frac{d}{d\epsilon} \frac{T(\epsilon_0)}{T(\epsilon_0)} u'_*(0)$$

so

$$\Phi(1, 0)v(0) = v(0) - \frac{d}{d\epsilon} \frac{T(\epsilon_0)}{T(\epsilon_0)} u'_*(0).$$

Thus  $e^{R(0)}$  has a block of the form  $\begin{pmatrix} 1 & c \\ 0 & 1 \end{pmatrix}$ ,  $c \neq 0$ , so that  $R(0)$  has a block of the form  $\begin{pmatrix} 0 & 1 \\ 0 & 0 \end{pmatrix}$  under an appropriate coordinate transformation.

We can then assume generically that all remaining Floquet exponents are nonzero and distinct, so that there exists an invertible matrix  $V = V(0)$  such that

$$V^{-1}R(0)V = \left( \begin{array}{cc|ccc} 0 & 1 & 0 & \cdots & 0 \\ 0 & 0 & 0 & \cdots & 0 \\ \hline 0 & 0 & & & \\ \vdots & \vdots & & D & \\ 0 & 0 & & & \end{array} \right)$$

for  $D$  diagonal.

We now show that for  $\lambda \neq 0$ , the entry in the second row, first column of the Jordan block will be of the form  $a\lambda + O(\lambda^2)$ , for  $a \neq 0$ .

Considering the upper left block of the matrix  $V^{-1}R(0)V =: \tilde{R}(0)$ , we denote (with a small abuse of notation)  $N(\tilde{R}(0)) = \text{Rg}(\tilde{R}(0))$  by  $u_*$  and  $N(\tilde{R}(0)^T) = \text{Rg}(\tilde{R}(0)^T)$  by  $\psi_*$ , so that  $\langle \psi_*, u_* \rangle = 0$  and  $\langle \psi_*, u_\epsilon \rangle \neq 0$ .

Now considering the eigenvalue problem for  $\lambda \neq 0$ , we write

$$v = [A(y) + \lambda B]v \quad (3.17)$$

and look for a solution of the form  $v(y) = u_*(y) + \lambda w(y)$ , where we wish to show  $\langle \psi_*(1), v(1) \rangle = a\lambda$  with  $a \neq 0$ .

Since  $u_*(y)$  satisfies  $v_y = A(y)v$ , we have

$$w = [A(y) + \lambda B]w(y) + Bu_* \quad (3.18)$$

Moreover, at  $\lambda = 0$  we have

$$w = A(y)w(y) + Bu_* \quad (3.19)$$

so that using the variation of constants formula, we have

$$w(y) = \Phi(y, 0)w(0) + \int_0^y \Phi(y, x)Bu_*(x)dx \quad (3.20)$$

Thus

$$\begin{aligned}\langle \psi_*(1), w(1) \rangle &= \langle \psi_*(1), \Phi(1, 0)w(0) + \int_0^1 \Phi(1, x)Bu_*(x)dx \rangle \\ &= \langle \psi_*(1), \Phi(1, 0)w(0) \rangle + \int_0^1 \langle \psi_*(x), Bu_*(x) \rangle dx.\end{aligned}\quad (3.21)$$

Now writing  $w(0)$  generically as  $w(0) = \alpha u_*(0) + \beta u_\epsilon(0)$ , we have

$$\Phi(1, 0)w(0) = \alpha u_*(0) + \beta(u_\epsilon(0) + u_*(0)) \quad (3.22)$$

so that

$$\langle \psi_*(1), \Phi(1, 0)w(0) \rangle = \langle \psi_*(1), \beta u_\epsilon(0) \rangle. \quad (3.23)$$

Thus with  $v(1) = u_*(1) + \lambda w(1)$ , we have

$$\begin{aligned}\langle \psi_*(1), v(1) \rangle &= \lambda \langle \psi_*(1), w(1) \rangle \\ &= \lambda \left( \beta \langle \psi_*(1), u_\epsilon(0) \rangle + \int_0^1 \langle \psi_*(x), Bu_*(x) \rangle dx \right)\end{aligned}\quad (3.24)$$

Now the first part of the expression multiplying  $\lambda$  is zero only if  $\beta = 0$ , while the second part is nonzero as  $\lambda = 0$  is a simple eigenvalue by Hypothesis 5.3.4. Thus we indeed have  $\langle \psi_*(1), v(1) \rangle = a\lambda$  with  $\lambda \neq 0$ , as desired.  $\blacksquare$

## 5.4 The extended Evans function

We will focus in the following on the system in  $\mathbb{R}^4$ . In fact, for the purpose of analyzing possible eigenvalues of the localized solution at  $\lambda = 0$ , the 2x2 center space would be sufficient. However, we will need the four dimensional space to understand the behavior of the saddle node, and so we work in four dimensions from

the outset. Of course, eigenvalues associated with faster modes may play a role in additional bifurcations, but we will not concern ourselves with these here. Explicitly, we then have

$$J(\lambda) = \begin{pmatrix} 0 & 1 & 0 & 0 \\ \lambda & 0 & 0 & 0 \\ 0 & 0 & -\alpha(\lambda) & 0 \\ 0 & 0 & 0 & \alpha(\lambda) \end{pmatrix}. \quad (4.1)$$

We now invoke the periodic conjugation lemma with  $\tilde{\eta}$  satisfying  $\eta > \tilde{\eta} > 0$  fixed, so that solutions to (3.3) are given by

$$v(x) = P(x, \lambda)S(x, \lambda)V(\lambda)w(x) \quad (4.2)$$

where  $w(x)$  solves

$$w_x = J(\lambda)w \quad (4.3)$$

and  $P(x, \lambda) = I + O(e^{-\tilde{\eta}x})$ .

We observe that the eigenvectors of  $J(\lambda)$  are

$$\begin{pmatrix} 1 \\ -\sqrt{\lambda} \\ 0 \\ 0 \end{pmatrix}, \begin{pmatrix} 1 \\ \sqrt{\lambda} \\ 0 \\ 0 \end{pmatrix}, \begin{pmatrix} 0 \\ 0 \\ 1 \\ 0 \end{pmatrix}, \begin{pmatrix} 0 \\ 0 \\ 0 \\ 1 \end{pmatrix} \quad (4.4)$$

with eigenvalues  $-\sqrt{\lambda}, \sqrt{\lambda}, -\alpha(\lambda), \alpha(\lambda)$ . We therefore introduce  $\gamma^2 = \lambda$  so that we arrive at a coordinate system which is analytic in  $\gamma$ .

We define  $\hat{D}(\gamma)$  to be the diagonal matrix with entries  $-\gamma, \gamma, -\alpha(\gamma^2), \alpha(\gamma^2)$ , and

define  $V_1(\gamma)$  and  $V_1^{-1}(\gamma)$  such that  $V_1(\gamma)\hat{D}(\gamma)V_1^{-1}(\gamma) = J(\lambda)$ :

$$V_1(\lambda) = \begin{pmatrix} 1 & 1 & 0 & 0 \\ -\gamma & \gamma & 0 & 0 \\ 0 & 0 & 1 & 0 \\ 0 & 0 & 0 & 1 \end{pmatrix}, \quad V_1^{-1}(\gamma) = \begin{pmatrix} \frac{1}{2} & -\frac{1}{2\gamma} & 0 & 0 \\ \frac{1}{2} & \frac{1}{2\gamma} & 0 & 0 \\ 0 & 0 & 1 & 0 \\ 0 & 0 & 0 & 1 \end{pmatrix}.$$

We note that we have a singularity (a pole of order 1) at  $\gamma = 0$ , but we emphasize that this will not present a problem as our goal is not to write  $V_1(\gamma)$  analytic in  $\gamma$  but rather to ensure that the Evans function is analytic in  $\gamma$ , i.e., that we are able to choose analytic basis functions.

For future reference, we also record that the evolution of (4.3) is given by

$$e^{J(\lambda)x} = \begin{pmatrix} \frac{1}{2}(e^{-\gamma x} + e^{\gamma x}) & \frac{1}{2\gamma}(-e^{-\gamma x} + e^{\gamma x}) & 0 & 0 \\ \frac{\gamma}{2}(-e^{-\gamma x} + e^{\gamma x}) & \frac{1}{2}(e^{-\gamma x} + e^{\gamma x}) & 0 & 0 \\ 0 & 0 & e^{-\alpha(\gamma^2)x} & 0 \\ 0 & 0 & 0 & e^{\alpha(\gamma^2)x} \end{pmatrix} \quad (4.5)$$

$$= \begin{pmatrix} \cosh(\gamma x) & \frac{1}{\gamma} \sinh(\gamma x) & 0 & 0 \\ \gamma \sinh(\gamma x) & \cosh(\gamma x) & 0 & 0 \\ 0 & 0 & e^{-\alpha(\gamma^2)x} & 0 \\ 0 & 0 & 0 & e^{\alpha(\gamma^2)x} \end{pmatrix} \quad (4.6)$$

We note that  $\cosh(\gamma x) = 1 + O(\gamma^2 x^2)$ , while  $\sinh(\gamma x) = x\gamma + O(\gamma^3 x^3)$ . Moreover, since  $\cosh(x)$  is even and  $\sinh(x)$  is odd, their power series contain only even and odd terms respectively, so that  $\gamma \sinh(\gamma x)$  and  $\frac{1}{\gamma} \sinh(\gamma x)$  both have only even terms. Thus  $e^{J(\lambda)x}$  is in fact analytic in  $\gamma^2 = \lambda$ , as of course it must be.

Now referring to the columns of  $V_1$  by  $v_1, \dots, v_4$ , the stable subspace for the periodic orbits in the transformed system is then spanned by the first and third of these vectors, and the unstable subspace by the second and fourth, i.e.,

$$E_p^s(\gamma) = \text{span} \{v_1, v_3\}, \quad E_p^u(\gamma) = \text{span} \{v_2, v_4\}. \quad (4.7)$$

We then fix  $x = x_0 > 0$  so that in our transformed coordinate system we have the extended Evans function

$$D_f(\gamma) = \det(E_{f,-}^u(x_0, \gamma), E_p^s(\gamma)). \quad (4.8)$$

We note that for  $\text{Re } \gamma > 0$ , with  $\gamma$  such that the transformations  $P(x_0, \lambda), S(x_0, \lambda)$  and  $V(\lambda)$  are analytic and invertible, the roots of (4.8) and the standard Evans function in  $\lambda$  are in one-to-one correspondence.

We now write (4.8) generically as

$$D_f(\gamma) = \begin{vmatrix} f_1 & g_1 & 1 & 0 \\ f_2 & g_2 & -\gamma & 0 \\ f_3 & g_3 & 0 & 1 \\ f_4 & g_4 & 0 & 0 \end{vmatrix} = \gamma(f_4g_1 - f_1g_4) + f_4g_2 - f_2g_4 \quad (4.9)$$

where all  $f_i, g_i$  are functions of  $\gamma$ , which are analytic in  $\lambda = \gamma^2$ , and  $f$  and  $g$  are linearly independent.

## 5.5 The eigenvalue at $\lambda = 0$

We remark at the outset that, although the Evans function of the front loses analyticity in  $\lambda$  at  $\lambda = 0$ , the Evans function of the localized solution must in fact be analytic for all  $\lambda$  with  $\operatorname{Re} \lambda > -d$  as in Hypothesis 4.3.7, i.e., for all  $\lambda$  to the right of  $\Sigma_{ess}^0$ . This may be seen in any number of equivalent ways, but essentially follows from the fact that the localized solution is asymptotically a constant coefficient problem, so that its essential spectrum is given by  $\Sigma_{ess}^0$ , and the Evans function is analytic in any connected component of the complex plane that does not include essential spectrum, i.e.,  $\Omega \subset \mathbb{C} \setminus \Sigma_{ess}$ ; see Appendix B.

We show in the following that, given simple roots of the front and back at  $\gamma = 0$ , the only eigenvalue for the localized solution in the closed right half plane will be at  $\lambda = 0$ . We provide proofs here for the symmetric localized solutions, and also for general localized solutions. Note that the symmetric localized solutions are also covered by the latter proof. We remark that, in some sense, we can think of these results as saying that a simple root in  $\gamma$  for both the front and back corresponds to a  $\gamma^2$  root for the localized solution, and therefore a simple root in  $\lambda$ .

We first impose assumptions to ensure a simple root of the front. Thinking of the vector  $f$  in (4.9) as corresponding to the translation eigenvector motivates the following assumptions on the form of  $E_{f,-}^u(\gamma)$  in our transformed coordinate system:

**Hypothesis 5.5.1.** *The components  $f_2$  and  $f_4$  of  $E_{f,-}^u(x_0, \gamma)$  vanish at 0:  $f_2(0) = f_4(0) = 0$ , while  $f_1(0) \neq 0$  and  $g_4(0) \neq 0$ .*

We remark that  $f_1(0) \neq 0$  corresponds to the fact that the translation eigenvalue at 0 is given by the derivative of the front, so that it has a nonzero component in

this direction. Given this and the linear independence of  $f$  and  $g$ , we replace  $f$  by  $\tilde{g} = g - \frac{g_1}{f_1}f$  so that  $\tilde{g}_1 = 0$ . Since  $f_4(0) = 0$ , we continue to have  $\tilde{g}_4(0) \neq 0$ . We drop the tildes going forward.

Now given Hypothesis 5.5.1, we see that for  $\gamma \in U_\delta(0)$ ,

$$D_f(\gamma) = -\gamma f_1(0)g_4(0) + \gamma^2 \left( \frac{d}{d\gamma^2}f_4(0)\frac{d}{d\gamma^2}g_2(0) - \frac{d}{d\gamma^2}f_2(0)\frac{d}{d\gamma^2}g_4(0) \right) + \mathcal{O}(\gamma^3).$$

Thus we have a simple root of  $D_f(\gamma)$  at  $\gamma = 0$ .

In the case that  $u_f(x) \neq \mathcal{R}u_b(-x)$ , we have the analogous hypothesis for  $u_b(x)$ :

**Hypothesis 5.5.2.** *The components  $f_2^+$  and  $f_3^+$  of  $E_{b,+}^u(-x_0, \gamma)$  vanish at 0:  $f_2^+(0) = f_3^+(0) = 0$ , while  $f_1^+(0) \neq 0$  and  $g_3^+(0) \neq 0$ .*

We note that Hypothesis 5.5.2 asserts the same structure as Hypothesis 5.5.1, upon employing the action of the reverser  $\mathcal{R}$ . We then have

$$\begin{aligned} D_b(\gamma) &= \det(E_p^u(\gamma), E_{b,+}^s(-x_0, \gamma)) = \begin{vmatrix} 1 & 0 & f_1^+ & 0 \\ \gamma & 0 & f_2^+ & g_2^+ \\ 0 & 0 & f_3^+ & g_3^+ \\ 0 & 1 & f_4^+ & g_4^+ \end{vmatrix} \\ &= \gamma f_1^+ g_3^+ + \gamma^2 (\hat{f}_3^+ g_2^+ - \hat{f}_2^+ g_3^+) + \mathcal{O}(\gamma^3) \end{aligned}$$

so that we have a simple root of  $D_b(\gamma)$  at  $\gamma = 0$ .

### 5.5.1 Special case: symmetric localized solutions

For symmetric localized solutions, rather than defining the Evans function separately for the front and back and employing a matching argument, we define “even” and “odd” Evans functions for the localized solutions by replacing the stable forward space with the spaces  $\text{Fix } \mathcal{R}$  and  $\text{Fix } (-\mathcal{R})$ . In particular, we consider the spaces  $\text{Fix } \mathcal{R}$  and  $\text{Fix } (-\mathcal{R})$  at the center of the symmetric localized solutions, and pull them back under the flow of (4.3) to the point  $x_0$  where we wrote down the Evans function of the front.

**Theorem 5.1.** *Under the hypotheses in Section 3.3, along with Hypotheses 4.3.7, 5.3.1 and 5.5.1, there exists an  $L_* > 0$  such that the following holds uniformly in  $L > L_*$ : there exists a  $\hat{\delta} > 0$  such that*

$$v_x = [f_u(u_{\ell,L}(x)) + \lambda B]v \quad (5.1)$$

with  $u_{\ell,L}(0) \in \text{Fix } \mathcal{R}$  has a nontrivial bounded solution at  $\lambda = 0$  given by  $v(x) = \partial_x u_{\ell,L}(x)$ , and (5.1) has no other nontrivial bounded solutions for

$$\lambda \in U_{\hat{\delta}}(0) \cap \{\lambda : \text{Re } \lambda \geq 0\}.$$

**Remark 5.5.3.** *As seen in the following proof, there will be solutions approaching the imaginary  $\lambda$  axis from  $\text{Re } \lambda < 0$  with increasing  $L$ , but we are able to distinguish these from solutions with  $\text{Re } \lambda \geq 0$ , so that we have a uniform result in  $L$ . The result in fact holds on the set  $S_\gamma := \{\gamma = r(1 + di) : r, d \in \mathbb{R}, r \geq 0, |d| \leq C\}$  where  $C$  is any bounded constant, corresponding to the complex  $\lambda$  plane less the sector bounded by rays at approximately  $-C \pm 2i$  (precisely,  $-C + \frac{1}{C} \pm 2i$ ), and encompassing the negative real  $\lambda$  axis (see Figure 5.3). However, the allowable size of  $\hat{\delta}$  will decrease with increasing  $C$ , and the result for  $\text{Re } \lambda \geq 0$  is sufficient.*

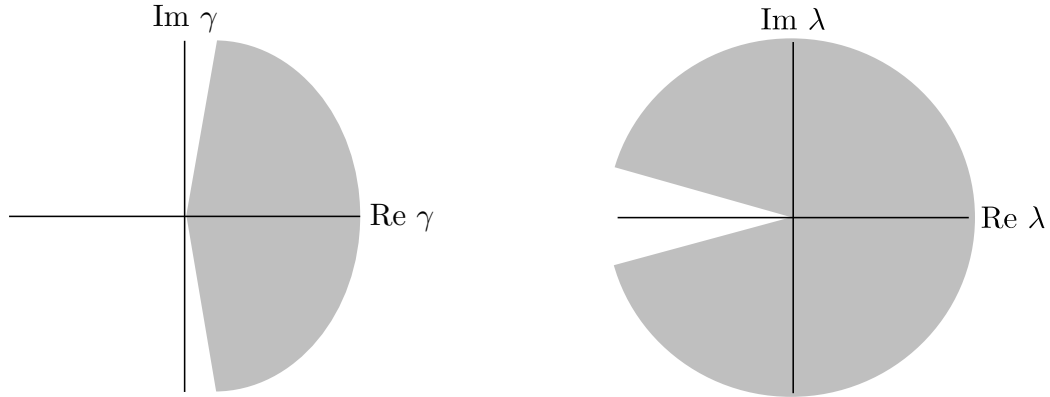


**Figure 5.3:** Schematic depiction of the regions the complex  $\gamma$  and  $\lambda$  planes where we have a simple root in  $\lambda$  near zero. In the proof of Theorem 5.1, we use the region  $S_\gamma := \{\gamma = r(1 + di) : r, d \in \mathbb{R}, r \geq 0, |d| \leq C\}$  with  $C = 2$ .

**Proof.** (Theorem 5.1) We first observe that in the transformed coordinate system corresponding to linearization about the symmetric periodic orbit  $u_p(x)$ , we have

$$\text{Fix } (-\mathcal{R}) = \text{span} \left\{ \begin{pmatrix} 1 \\ 0 \\ 0 \\ 0 \end{pmatrix}, \begin{pmatrix} 0 \\ 0 \\ 1 \\ -1 \end{pmatrix} \right\}, \quad \text{Fix } \mathcal{R} = \text{span} \left\{ \begin{pmatrix} 0 \\ 1 \\ 0 \\ 0 \end{pmatrix}, \begin{pmatrix} 0 \\ 0 \\ 1 \\ 1 \end{pmatrix} \right\}.$$

We will refer to  $\text{Fix } (-\mathcal{R})$  and  $\text{Fix } \mathcal{R}$  as odd and even subspaces, respectively.

Now we recall that  $|u_{\ell,L}(x-L) - u_f(x)| \leq Ce^{-\eta L}$  uniformly in  $L$  for all  $x \leq L$ . Since the  $x_0$  at which we wrote our coordinate system is fixed, we take  $L$  large so that  $L > x_0$  and we have

$$E_{\ell,L,-}^u(x_0, \gamma) = E_{f,-}^u(x_0, \gamma) + O(e^{-\eta L}).$$

We may in fact take  $L - x_0 = L$  without loss of generality, so that pulling back

Fix  $(-\mathcal{R})$  for time or distance  $L$  under the flow given in (4.6), we have

$$\begin{pmatrix} \cosh(\gamma L) \\ -\gamma \sinh(\gamma L) \\ 0 \\ 0 \end{pmatrix}, \begin{pmatrix} 0 \\ 0 \\ e^{\alpha(\gamma^2)L} \\ -e^{-\alpha(\gamma^2)L} \end{pmatrix}$$

which we normalize as

$$\begin{pmatrix} \cosh(\gamma L) \\ -\gamma \sinh(\gamma L) \\ 0 \\ 0 \end{pmatrix}, \begin{pmatrix} 0 \\ 0 \\ 1 \\ -e^{-2\alpha(\gamma^2)L} \end{pmatrix}.$$

Thus the Evans function of the symmetric localized solution with odd boundary condition in the middle is given by

$$\begin{aligned} D_{\text{odd},L}(\gamma) &= \begin{vmatrix} f_1 & 0 & \cosh(\gamma L) & 0 \\ \gamma^2 \hat{f}_2 & g_2 & -\gamma \sinh(\gamma L) & 0 \\ f_3 & g_3 & 0 & 1 \\ \gamma^2 \hat{f}_4 & g_4 & 0 & -e^{-2\alpha(\gamma^2)L} \end{vmatrix} + O(e^{-\eta L}) \\ &= - \begin{vmatrix} f_1 & 0 & \cosh(\gamma L) \\ \gamma^2 \hat{f}_2 & g_2 & -\gamma \sinh(\gamma L) \\ \gamma^2 \hat{f}_4 & g_4 & 0 \end{vmatrix} - e^{-2\alpha(\gamma^2)L} \begin{vmatrix} f_1 & 0 & \cosh(\gamma L) \\ \gamma^2 \hat{f}_2 & g_2 & -\gamma \sinh(\gamma L) \\ f_3 & g_3 & 0 \end{vmatrix} + O(e^{-\eta L}) \\ &= \gamma^2 \left( \frac{\sinh(\gamma L)}{\gamma} f_1 g_4 - \cosh(\gamma L) (\hat{f}_2 g_4 - \hat{f}_4 g_2) \right. \\ &\quad \left. \dots - e^{-2\alpha(\gamma^2)L} \left( \cosh(\gamma L) (\hat{f}_2 g_3 - f_3 g_2) - \frac{\sinh(\gamma L)}{\gamma} f_1 g_3 \right) \right) + O(e^{-\eta L}) \end{aligned} \tag{5.2}$$

where  $f_i, g_i$  are evaluated at  $\gamma = 0$ , and  $\hat{f}_i = 2\frac{d}{d\gamma^2}f_i(0), i = 2, 4$ . We note that, as the determinant of vectors that depend analytically on  $\lambda$ ,  $D_{\text{odd},L}(\gamma)$  is in fact analytic in  $\gamma^2 = \lambda$ , as we knew *a priori* it should be. We now wish to show that we have a unique root near  $\lambda = 0$  for  $\text{Re } \lambda \geq 0$ . We can then conclude that we in fact have a root at  $\lambda = 0$ , since direct substitution confirms that  $v(x) = \partial_x u_{\ell,L}(x)$  is a solution of (5.1) with  $\lambda = 0$ .

We will consider the set  $S_\gamma = \{\gamma = r(1 + di) : r, d \in \mathbb{R}, r \geq 0, |d| \leq 2\}$ , so that defining  $S_\lambda := \{\lambda : \lambda = \gamma^2, \gamma \in S_\gamma\}$ , we have  $\{\lambda : \text{Re } \lambda \geq 0\} \subset S_\lambda$ .

We now rewrite the factor following  $\gamma^2$  in (5.2) as

$$(a_1 + a_2 e^{-\alpha(\gamma^2)L}) \frac{\sinh(\gamma L)}{\gamma} + (b_1 + b_2 e^{-\alpha(\gamma^2)L}) \cosh(\gamma L) =: F(\gamma, L) \quad (5.3)$$

We first note that  $\text{Re } \alpha(\lambda) > 0$  for all  $\lambda \in U_\delta(0)$  so that  $e^{-2\alpha(\gamma^2)L}$  is strictly decreasing in  $L$ . Additionally,  $\lim_{\gamma \rightarrow 0} F(\gamma, L) = (a_1 + a_2 e^{-\alpha(\gamma^2)L})L + (b_1 + b_2 e^{-\alpha(\gamma^2)L})$ , so that as  $L$  increases, this is approximately  $a_1 L$  and therefore bounded below in modulus (note  $a_1 = f_1 g_4$ , and recall that both  $f_1$  and  $g_4$  are nonzero by assumption.) We now consider  $F(\gamma, L)$  for  $|\gamma L| < 1$  and  $|\gamma L| \geq 1$  separately, with  $\gamma \in S_\gamma \setminus \{0\}$ .

Writing  $y = \gamma L$  and first considering  $|y| < 1$ , we have

$$\left| L(a_1 + a_2 e^{-\alpha(\gamma^2)L}) \frac{e^y - e^{-y}}{2y} \right| > \left| (b_1 + b_2 e^{-\alpha(\gamma^2)L}) \frac{e^y + e^{-y}}{2} \right| \quad (5.4)$$

uniformly in  $L$  for  $L$  sufficiently large, since  $(e^y - e^{-y})/y = 1 + O(y^2)$  and also  $e^y + e^{-y} = 1 + O(y^2)$ .

On the other hand, for  $|y| \geq 1$ , we have

$$\left| (a_1 + a_2 e^{-\alpha(\gamma^2)L})(e^y - e^{-y}) \right| > \left| \gamma(b_1 + b_2 e^{-\alpha(\gamma^2)L})(e^y + e^{-y}) \right| \quad (5.5)$$

uniformly in  $L$  for  $L$  sufficiently large, provided that

$$|\gamma| \leq \frac{|a_1|}{2|b_1|} \left( \frac{1 - e^{-2/\sqrt{5}}}{1 + e^{-2/\sqrt{5}}} \right) =: \tilde{\delta} \quad (5.6)$$

where the  $\sqrt{5}$  comes from  $\sqrt{1 + d^2}$  with  $d = 2$ , and we note  $(1 - e^{-2/\sqrt{5}})/(1 + e^{-2/\sqrt{5}}) \approx 0.42$ . We have assumed  $b_1 \neq 0$ ; if  $b_1 = 0$ , then we have

$$\left| (a_1 + a_2 e^{-\alpha(\gamma^2)L})(e^y - e^{-y}) \right| > \left| \gamma(b_2 e^{-\alpha(\gamma^2)L})(e^y + e^{-y}) \right| \quad (5.7)$$

uniformly in  $L$  for  $L$  sufficiently large, for all  $\gamma$ .

In summary, we have shown that  $F(\gamma, L)$  is uniformly bounded below in modulus for  $L > L_*$ , with  $\gamma \in U_{\tilde{\delta}}(0) \cap S_\gamma \setminus \{0\}$ , with  $\tilde{\delta}$  as in (5.6). Since the remaining term in (5.2) is  $O(e^{-\eta L})$ , we can then conclude the existence of a unique root  $\lambda$  for  $\lambda \in S_\lambda \cap U_{\tilde{\delta}}(0)$ , which as noted above implies a unique root at  $\lambda = 0$  for  $\lambda \in \{\lambda : \operatorname{Re} \lambda \geq 0\} \cap U_{\tilde{\delta}}(0)$ .

We now turn to the Evans function for a symmetric localized solution with even boundary condition in the middle. Pulling back  $\operatorname{Fix} \mathcal{R}$ , we have

$$\begin{pmatrix} -\frac{1}{\gamma} \sinh(\gamma L) \\ \cosh(\gamma L) \\ 0 \\ 0 \end{pmatrix}, \begin{pmatrix} 0 \\ 0 \\ e^{\alpha(\gamma^2)L} \\ e^{-\alpha(\gamma^2)L} \end{pmatrix}$$

Due to the form of  $\sinh(x)$ , we see that  $\frac{1}{\gamma}$  will not pose a problem and we leave this as is, and renormalize as

$$\begin{pmatrix} -\frac{1}{\gamma} \sinh(\gamma L) \\ \cosh(\gamma L) \\ 0 \\ 0 \end{pmatrix}, \begin{pmatrix} 0 \\ 0 \\ 1 \\ e^{-2\alpha(\gamma^2)L} \end{pmatrix}$$

so that

$$\begin{aligned} D_{\text{even},L}(\gamma) &= \begin{vmatrix} f_1 & 0 & -\frac{1}{\gamma} \sinh(\gamma L) & 0 \\ \gamma^2 \hat{f}_2 & g_2 & \cosh(\gamma L) & 0 \\ f_3 & g_3 & 0 & 1 \\ \gamma^2 \hat{f}_4 & g_4 & 0 & e^{-2\alpha(\gamma^2)L} \end{vmatrix} + O(e^{-\eta L}) \\ &= - \begin{vmatrix} f_1 & 0 & -\frac{1}{\gamma} \sinh(\gamma L) \\ \gamma^2 \hat{f}_2 & g_2 & \cosh(\gamma L) \\ \gamma^2 \hat{f}_4 & g_4 & 0 \end{vmatrix} + e^{-2\alpha(\gamma^2)L} \begin{vmatrix} f_1 & 0 & -\frac{1}{\gamma} \sinh(\gamma L) \\ \gamma^2 \hat{f}_2 & g_2 & \cosh(\gamma L) \\ f_3 & g_3 & 0 \end{vmatrix} \\ &= \gamma \sinh(\gamma L)(\hat{f}_2 g_4 - \hat{f}_4 g_2) + \cosh(\gamma L) f_1 g_4 \\ &\quad + e^{-2\alpha(\gamma^2)L} \left( -\gamma \sinh(\gamma L)(\hat{f}_2 g_3 - f_3 g_2) + \cosh(\gamma L) f_1 g_3 \right) + O(e^{-\eta L}). \end{aligned}$$

As before, we write the terms preceding the  $O(e^{-\eta L})$  term as

$$(a_1 + a_2 e^{-2\alpha(\gamma^2)L}) \gamma \sinh(\gamma L) + (b_1 + b_2 e^{-2\alpha(\gamma^2)L}) \cosh(\gamma L). \quad (5.8)$$

Note that at  $\gamma = 0$ , (5.8) reduces to  $b_1 + b_2 e^{-2\alpha(0)L}$ , which is nonzero uniformly in  $L$  for  $L$  sufficiently large, since  $b_1 = f_1 g_4$  is nonzero by hypothesis. We now consider  $\gamma \in S_\gamma$  as defined above, and setting  $y = \gamma L$  we have

$$(b_1 + b_2 e^{-2\alpha(\gamma^2)L})(e^y + e^{-y}) > \gamma(a_1 + a_2 e^{-2\alpha(\gamma^2)L}) \gamma(e^y - e^{-y}) \quad (5.9)$$

uniformly in  $L$  for  $L$  sufficiently large, provided that

$$|\gamma| < \frac{|b_1|}{2|a_1|} =: \tilde{\delta}_2, \quad (5.10)$$

where we could have obtained a looser bound by including the ratio of the exponentials, and an addition of  $\epsilon$  rather than the factor of 2 in the denominator would have sufficed. Here we note  $b_1 = f_1 g_4$  is nonzero by hypothesis, and we have assumed  $a_1 \neq 0$ ; if  $a_1 = 0$  then we in fact have the inequality (5.9) uniformly in  $L$  sufficiently large for all  $\gamma$ .

Since the remaining term is  $O(e^{-\eta L})$ , we conclude that  $D_{\text{even},L}(\gamma)$  is bounded away from 0 uniformly in  $L > L_*$  for  $\gamma \in S_\gamma \cap U_{\tilde{\delta}_2}(0)$  and therefore for  $\lambda \in \{\lambda : \text{Re } \lambda \geq 0\} \cap U_{\tilde{\delta}}(0)$ . ■

## 5.5.2 General localized solutions

Turning our attention to the general case, covering both symmetric and asymmetric solutions, we will proceed in the spirit of Theorem 4.1 in Chapter 4. However, in this case we will use the conjugation lemma to move into the coordinate system of the wave train, taking advantage of the analytic splitting in  $\gamma$  coordinates.

We again remark that these results do not require reversibility; however, the presence of a reverser makes the assumptions enforcing existence of a simple eigenvalue of the back completely analogous to the assumption for the front, whereas in the absence of reversibility, the assumptions on the front and back would differ in form.

**Theorem 5.2.** *Under the hypotheses in Section 3.3, along with Hypotheses 4.3.7, 5.3.1, 5.5.1 and 5.5.2, there exists an  $L_* > 0$  such that the following holds uniformly*

in  $L > L_*$ : there exists a  $\hat{\delta} > 0$  such that

$$v_x = [f_u(u_{\ell,L}(x)) + \lambda B]v \quad (5.11)$$

has a nontrivial bounded solution at  $\lambda = 0$  given by  $v(x) = \partial_x u_{\ell,L}(x)$ , and has no other nontrivial bounded solutions for  $\lambda \in U_{\hat{\delta}}(0) \cap \{\lambda : \operatorname{Re} \lambda \geq 0\}$ .

**Proof.** We first fix  $\tilde{\eta}$  such that  $\eta > \tilde{\eta} > 0$  and apply the conjugation lemma at  $x_0$  for the front and  $-x_0$  for the back, where  $x_0$  is chosen without loss of generality to be the same for the front and back, and such that if  $P_f(x, \lambda)$  and  $P_b(x, \lambda)$  are the transformations for the front and back respectively, then  $|P_f(x_0, \lambda) - I| \ll 1$  and  $|P_b(-x_0, \lambda) - I| \ll 1$ .

For convenience in the following, we let  $\tilde{L}$  be the original  $L$  corresponding to half the solution length, and define  $L = \tilde{L} - x_0$ . We then define solutions to (5.11) in pieces as

$$v(x) = \begin{cases} v_{\ell}^{-}(x + L), & x \leq -L \\ T_1(x + L, \lambda)v_p^{-}(x + L), & x \in [-L, 0] \\ T_2(x - L, \lambda)v_p^{+}(x - L), & x \in [0, L] \\ v_{\ell}^{+}(x - L), & x \geq L, \end{cases} \quad (5.12)$$

along with the matching conditions

$$T_1(L, \lambda)v_p^{-}(L) = T_2(-L, \lambda)v_p^{+}(-L) \quad (5.13)$$

$$v_p^{-}(0) = T_1^{-1}(0, \lambda)v_{\ell}^{-}(0) \quad (5.14)$$

$$v_p^{+}(0) = T_2^{-1}(0, \lambda)v_{\ell}^{+}(0), \quad (5.15)$$

where  $v_{\ell}^{-}(x)$ ,  $v_p^{-}(x)$ ,  $v_p^{+}(x)$ ,  $v_{\ell}^{+}(x)$  are defined for  $x \in (-\infty, 0]$ ,  $[0, L]$ ,  $[-L, 0]$  and  $[0, \infty)$ ,

respectively, and where  $T_1(x, \lambda) := P_f(x + x_0, \lambda)S(x + x_0, \lambda)V(\lambda)$  on  $x \geq 0$  and  $T_2(x, \lambda) := P_b(x - x_0, \lambda)S(x - x_0, \lambda)V(\lambda)$  on  $x \leq 0$  with  $P_f$  and  $P_b$  the transformations from the conjugation lemma applied to the front and back, respectively. We note that since  $P_b^{-1}(-\tilde{L}, \lambda)P_f(\tilde{L}, \lambda) = I + O(e^{-\tilde{\eta}\tilde{L}})$  and  $S^{-1}(-\tilde{L}, \lambda)S(\tilde{L}, \lambda) = I + O(e^{-\tilde{\eta}\tilde{L}})$ , we have that

$$T_2^{-1}(-L, \lambda)T_1(L, \lambda) = I + O(e^{-\tilde{\eta}L}). \quad (5.16)$$

We let  $a_-^c \in E_p^c(\gamma)$ ,  $a_-^u \in E_p^u(\gamma)$  and  $a_-^s \in E_p^s(\gamma)$ , and define  $a_+^c$ ,  $a_+^u$  and  $a_+^s$  analogously. We further let  $b_-^u \in E_{f,-}^u(x_0, \gamma)$  and  $b_+^s \in E_{b,+}^s(-\tilde{x}_0, \gamma)$ .

We then have the expressions

$$v_\ell^-(x) = \Phi_{\ell,-}^u(x, 0; \lambda)T_1(0, \lambda)b_-^u \quad (5.17)$$

$$v_p^-(x) = \Phi_p^c(x, L; \gamma)a_-^c + \Phi_p^s(x, 0; \gamma)a_-^s + \Phi_p^u(x, L; \gamma)a_-^u \quad (5.18)$$

$$v_p^+(x) = \Phi_p^c(x, -L; \gamma)a_+^c + \Phi_p^s(x, -L; \gamma)a_+^s + \Phi_p^u(x, 0; \gamma)a_+^u \quad (5.19)$$

$$v_\ell^+(x) = \Phi_{\ell,+}^s(x, 0; \lambda)T_2(0, \lambda)b_+^s \quad (5.20)$$

where  $\Phi_\ell^{s,u}(x, y; \lambda)$  are evolution operators for (5.11) and  $\Phi_p^{c,s,u}(x, y; \gamma)$  are evolution operators for (4.3).

We begin with the first matching condition

$$\begin{aligned} T_1(L, \lambda)v_p^-(L) &= T_2(-L, \lambda)v_p^+(-L) \\ T_2^{-1}(-L, \lambda)T_1(L, \lambda)(a_-^c + O(e^{-\eta L})a_-^s + a_-^u) &= a_+^c + a_+^s + O(e^{-\eta L})a_+^u \end{aligned} \quad (5.21)$$

so that invoking (5.16) and comparing subspaces, we have

$$\begin{aligned}
a_-^c &= a_+^c + O(e^{-\tilde{\eta}L})a \\
O(e^{-\eta L})a_-^s &= a_+^s + O(e^{-\tilde{\eta}L})a \\
a_-^u &= O(e^{-\eta L})a_+^u + O(e^{-\tilde{\eta}L})a,
\end{aligned} \tag{5.22}$$

where  $a := (a_-^c, a_-^s, a_+^u)$ .

Turning to the second and third matching conditions, we note that

$$\text{Rg}(T_1^{-1}(0, \lambda)P_{\ell,-}^u(0, \gamma)T_1(0, \lambda)) = E_{f,-}^u(x_0, \gamma) + O(e^{-\eta L}) \tag{5.23}$$

and similarly

$$\text{Rg}(T_2^{-1}(0, \lambda)P_{\ell,+}^s(0, \gamma)T_2(0, \lambda)) = E_{b,+}^u(-x_0, \gamma) + O(e^{-\eta L}). \tag{5.24}$$

Thus we can write

$$T_1^{-1}(0, \lambda)v_{\ell}^-(0) = b_1^- f^- + b_2^- g^- + O(e^{-\eta L})b^-, \tag{5.25}$$

and

$$T_2^{-1}(0, \lambda)v_{\ell}^+(0) = b_1^+ f^+ + b_2^+ g^+ + O(e^{-\eta L})b^+, \tag{5.26}$$

where  $f^-, g^-$  are as in Hypothesis 5.5.1, and  $f^+, g^+$  are as in Hypothesis 5.5.2.

The second matching condition can then be written as

$$\begin{aligned}
0 &= v_p^-(0) - T_1^{-1}(0, \lambda)v_\ell^-(0) \\
&= \Phi_p^c(0, L; \gamma)a_-^c + a_-^s + \Phi_p^u(0, L; \gamma)a_-^u + O(e^{-\tilde{\eta}L})a - b_1^- f^- - b_2^- g^- + O(e^{-\eta L})b^- \\
&= \begin{pmatrix} \cosh(\gamma L) & -\frac{1}{\gamma} \sinh(\gamma L) \\ -\gamma \sinh(\gamma L) & \cosh(\gamma L) \end{pmatrix} \begin{pmatrix} a_1^c \\ a_2^c \end{pmatrix} + a_-^s + O(e^{-2\eta L})a_+^u \\
&\quad - b_1^- f^- - b_2^- g^- + O(e^{-\eta L})b^- + O(e^{-\tilde{\eta}L})a
\end{aligned} \tag{5.27}$$

Similarly, the third matching condition can be written as

$$\begin{aligned}
0 &= v_p^+(0) - T_2^{-1}(0, \lambda)v_\ell^+(0) \\
&= \Phi_p^c(0, -L; \gamma)a_+^c + \Phi_p^s(0, -L; \gamma)a_+^s + a_+^u + O(e^{-\tilde{\eta}L})a - b_1^+ f^+ - b_2^+ g^+ + O(e^{-\eta L})b^+ \\
&= \begin{pmatrix} \cosh(\gamma L) & \frac{1}{\gamma} \sinh(\gamma L) \\ \gamma \sinh(\gamma L) & \cosh(\gamma L) \end{pmatrix} \begin{pmatrix} a_1^c \\ a_2^c \end{pmatrix} + O(e^{-2\eta L})a_-^s + a_+^u \\
&\quad - b_1^+ f^+ - b_2^+ g^+ + O(e^{-\eta L})b^+ + O(e^{-\tilde{\eta}L})a
\end{aligned} \tag{5.28}$$

Thus defining  $b := (b^-, a, b^+) = (b_1^-, b_2^-, a_1^c, a_2^c, a_-^s, a_+^u, b_1^+, b_2^+)$ , (5.27) and (5.28)

together show that we have a solution for  $b \neq 0$  if and only if

$$0 = \begin{vmatrix} f_1^- & 0 & \cosh(\gamma L) & -\frac{1}{\gamma} \sinh(\gamma L) & 0 & 0 & 0 & 0 \\ \gamma^2 f_2^- & g_2^- & -\gamma \sinh(\gamma L) & \cosh(\gamma L) & 0 & 0 & 0 & 0 \\ f_3^- & g_3^- & 0 & 0 & 1 & 0 & 0 & 0 \\ \gamma^2 f_4^- & g_4^- & 0 & 0 & 0 & O(e^{-2\eta L}) & 0 & 0 \\ 0 & 0 & \cosh(\gamma L) & \frac{1}{\gamma} \sinh(\gamma L) & 0 & 0 & f_1^+ & 0 \\ 0 & 0 & \gamma \sinh(\gamma L) & \cosh(\gamma L) & 0 & 0 & \gamma^2 f_2^+ & g_2^+ \\ 0 & 0 & 0 & 0 & O(e^{-2\eta L}) & 0 & \gamma^2 f_3^+ & g_3^+ \\ 0 & 0 & 0 & 0 & 0 & 1 & f_4^+ & g_4^+ \end{vmatrix} + O(e^{-\tilde{\eta}L})$$

(5.29)

We will not explicitly track the  $O(e^{-2\eta L})$  terms in the following, but we will write them separately from the  $O(e^{-\tilde{\eta}L})$  terms as they also include sinh and cosh terms;

we will reintroduce these terms in the final analysis. Thus we have

$$\begin{aligned}
0 &= \begin{vmatrix} f_1^- & 0 & \cosh(\gamma L) & -\frac{1}{\gamma} \sinh(\gamma L) & 0 & 0 \\ \gamma^2 f_2^- & g_2^- & -\gamma \sinh(\gamma L) & \cosh(\gamma L) & 0 & 0 \\ \gamma^2 f_4^- & g_4^- & 0 & 0 & 0 & 0 \\ 0 & 0 & \cosh(\gamma L) & \frac{1}{\gamma} \sinh(\gamma L) & f_1^+ & 0 \\ 0 & 0 & \gamma \sinh(\gamma L) & \cosh(\gamma L) & \gamma^2 f_2^+ & g_2^+ \\ 0 & 0 & 0 & 0 & \gamma^2 f_3^+ & g_3^+ \end{vmatrix} + O(e^{-2\eta L}) + O(e^{-\bar{\eta} L}) \\
&= -f_1^- g_4^- \begin{vmatrix} -\gamma \sinh(\gamma L) & \cosh(\gamma L) & 0 & 0 \\ \cosh(\gamma L) & \frac{1}{\gamma} \sinh(\gamma L) & f_1^+ & 0 \\ \gamma \sinh(\gamma L) & \cosh(\gamma L) & \gamma^2 f_2^+ & g_2^+ \\ 0 & 0 & \gamma^2 f_3^+ & g_3^+ \end{vmatrix} \\
&+ \gamma^2 (f_2^- g_4^- - f_4^- g_2^-) \begin{vmatrix} \cosh(\gamma L) & -\frac{1}{\gamma} \sinh(\gamma L) & 0 & 0 \\ \cosh(\gamma L) & \frac{1}{\gamma} \sinh(\gamma L) & f_1^+ & 0 \\ \gamma \sinh(\gamma L) & \cosh(\gamma L) & \gamma^2 f_2^+ & g_2^+ \\ 0 & 0 & \gamma^2 f_3^+ & g_3^+ \end{vmatrix} + O(e^{-2\eta L}) + O(e^{-\bar{\eta} L}) \\
&= f_1^- g_4^- f_1^+ g_3^+ \begin{vmatrix} -\gamma \sinh(\gamma L) & \cosh(\gamma L) \\ \gamma \sinh(\gamma L) & \cosh(\gamma L) \end{vmatrix} + \gamma^2 f_1^- g_4^- (f_3^+ g_2^+ - f_2^+ g_3^+) \begin{vmatrix} -\gamma \sinh(\gamma L) & \cosh(\gamma L) \\ \cosh(\gamma L) & \frac{1}{\gamma} \sinh(\gamma L) \end{vmatrix} \\
&- \gamma^2 (f_2^- g_4^- - f_4^- g_2^-) f_1^+ g_3^+ \begin{vmatrix} \cosh(\gamma L) & -\frac{1}{\gamma} \sinh(\gamma L) \\ \gamma \sinh(\gamma L) & \cosh(\gamma L) \end{vmatrix} \\
&+ \gamma^4 (f_2^- g_4^- - f_4^- g_2^-) (f_2^+ g_3^+ - f_3^+ g_2^+) \begin{vmatrix} \cosh(\gamma L) & -\frac{1}{\gamma} \sinh(\gamma L) \\ \cosh(\gamma L) & \frac{1}{\gamma} \sinh(\gamma L) \end{vmatrix} + O(e^{-2\eta L}) + O(e^{-\bar{\eta} L}) \\
&= -\gamma \sinh(2\gamma L) f_1^- g_4^- f_1^+ g_3^+ - \gamma^2 \cosh(2\gamma L) (f_1^- g_4^- (f_3^+ g_2^+ - f_2^+ g_3^+) + (f_2^- g_4^- - f_4^- g_2^-) f_1^+ g_3^+) \\
&+ \gamma^3 \sinh(2\gamma L) (f_2^- g_4^- - f_4^- g_2^-) (f_2^+ g_3^+ - f_3^+ g_2^+) + O(e^{-2\eta L}) + O(e^{-\bar{\eta} L}) \quad (5.30)
\end{aligned}$$

Note that all of the above terms are analytic in  $\gamma^2 = \lambda$ . We now have an expression which is almost precisely the same as that analyzed in Theorem 5.1. In particular, we have a leading term of the form

$$\gamma^2 \left( (a_1 + O(e^{-2\eta L})) \frac{\sinh(\gamma L)}{\gamma} + (b_1 + O(e^{-2\eta L})) \cosh(\gamma L) \right). \quad (5.31)$$

The arguments for  $\gamma \in U_{\delta}(0) \cap S_{\gamma} \setminus \{0\}$  with  $S_{\gamma} = \{\gamma = r(1 + di) : r, d \in \mathbb{R}, r \geq 0, |d| \leq 2\}$  then follow exactly as in Theorem 5.1 for the odd boundary condition, and we conclude that we have a simple root in  $\lambda$  for  $\lambda \in U_{\delta}(0) \cap \{\lambda : \operatorname{Re} \lambda \geq 0\}$ . As before we know that this root must lie at  $\lambda = 0$ .  $\blacksquare$

## 5.6 The behavior of the saddle node eigenvalue

Returning to the Evans function before we made any assumptions on  $f$  or  $g$ , we have

$$D_f(\gamma) = f_4 g_2 - \gamma f_1 g_4 + \gamma f_4 g_1 \quad (6.1)$$

We now reintroduce the  $\mu$  independence, but we note that the appropriate way to do this is to allow dependence on  $\varphi$ , as the snaking phenomenon reflects the fact that solutions will not be unique in  $\mu$ , and the saddle node of course corresponds to a turning back in  $\mu$ . Recall that we assumed in Hypothesis 3.3.2 that  $z : S^1 \rightarrow \mathring{J}$  is a smooth function. We further observe that since we are presently interested in the behavior of saddle nodes for the front,  $z(\varphi) = \mu$  is an *exact* relationship, and there is no exponential correction necessary.

Thus we now assume that the vectors  $f$  and  $g$ , and consequently their components, depend analytically on  $\gamma^2$ , and smoothly on  $\varphi$ . We take  $\varphi = 0$  to correspond

to a particular saddle node; our aim in the following is to understand what scenarios lead to the saddle node eigenvalue moving from  $\operatorname{Re} \lambda > 0$  to  $\operatorname{Re} \lambda < 0$ , corresponding to movement from  $\gamma \in \mathbb{R}$  to  $\gamma \in i\mathbb{R}$ . We note that to complete this analysis we need to show parameter-dependent versions of the lemmas proved in Section 5.2, but we do not anticipate difficulties in the extensions.

We first note that there are generically four ways to enforce the existence of a translation eigenvalue at 0 for all  $\varphi$  near 0:

$$(i) \quad f_2 = f_4 = 0$$

$$(ii) \quad f_2 = g_2 = 0$$

$$(iii) \quad f_4 = g_4 = 0$$

$$(iv) \quad f_4 g_2 - f_2 g_4 = 0 \quad (\text{and } f_2, f_4, g_2, g_4 \neq 0)$$

where in all cases we list the values of individual components at  $(0, \varphi)$ , for all  $\varphi$  near 0. The first case is the one we assumed in the preceding analysis, and it is the only one that requires the participation of only one of the two vectors (the case  $g_2 = g_4 = 0$  is of course equivalent since the designations  $f$  and  $g$  were arbitrary).

We then have the following leading order expansions for  $D_f$  in  $\gamma$  near 0 in each of the above cases:

$$(i) \quad D_f(\gamma, \varphi) = -\gamma f_1 g_4$$

$$(ii) \quad D_f(\gamma, \varphi) = \gamma(f_4 g_1 - f_1 g_4)$$

$$(iii) \quad D_f(\gamma, \varphi) = \gamma^2((\partial_\lambda f_4)g_2 - f_2(\partial_\lambda g_4))$$

$$(iv) D_f(\gamma, \varphi) = \gamma(f_4 g_1 - f_1 g_4)$$

where again all terms are evaluated at  $(0, \varphi)$ , and in (iii) we assume that the terms of next lowest order are nonzero. Thus we see cases (i), (ii) and (iv) all correspond to simple roots, whereas . Note that in (iii) we will still have higher order terms in odd powers of  $\gamma$  so that (iii) is analytic only in  $\lambda$ . Moreover, while (ii) and (iv) agree to first order, they will differ in their second order terms, as the latter will include  $(\partial_\lambda f_4)g_2 - f_2(\partial_\lambda)g_4$ .

We now focus our attention on the case (i) as the most relevant to our situation, and detail the impacts of additional assumptions at  $\varphi = 0$ . We assume in all cases that  $f_2(0, \varphi) = f_4(0, \varphi) = 0$  and  $\partial_\lambda f_2(0, \varphi), \partial_\lambda f_4(0, \varphi) \neq 0$  for all  $\varphi$  near zero, plus the following, where in all cases we assume the next lowest order term is nonzero:

$$(a) g_4(0, 0) = 0$$

Then we have

$$D_f(\gamma, \varphi) = -\gamma(\varphi f_1 \partial_\varphi g_4 - \gamma \partial_\lambda f_4 g_2 + O(\gamma^2 + \varphi^2)),$$

where here and in all following expressions, coefficients are evaluated at  $(0, 0)$ .

Thus near  $(\gamma, \varphi) = (0, 0)$  we have roots at  $\gamma = 0$  and

$$\gamma = \varphi \left( \frac{f_1(\partial_\varphi g_4)}{(\partial_\lambda f_4)g_2} \right) + O(\varphi^2).$$

$$(b) f_1(0, 0) = 0$$

$$D_f(\gamma, \varphi) = -\gamma \left( \varphi(\partial_\varphi f_1)g_4 - \gamma((\partial_\lambda f_4)g_2 - (\partial_\lambda f_2)g_4) + O(\gamma^2 + \varphi^2) \right)$$

so that we have roots at  $\gamma = 0$  and

$$\gamma = \varphi \left( \frac{(\partial_\varphi f_1)g_4}{(\partial_\lambda f_4)g_2 - (\partial_\lambda f_2)g_4} \right) + O(\varphi^2)$$

(c)  $g_4(0, 0) = 0$  and  $g_2(0, 0) = 0$

$$\begin{aligned} D_f(\gamma, \varphi) = & -\gamma \left( \varphi f_1(\partial_\varphi g_4) - \gamma^2 ((\partial_\lambda f_4)g_1 - f_1(\partial_\lambda g_4)) \right) \\ & - \varphi \gamma ((\partial_\lambda f_4)(\partial_\varphi f_2) - (\partial_\lambda f_2)(\partial_\varphi g_4)) + O(\varphi^2 + \varphi\gamma^2 + \gamma^3) \end{aligned}$$

so that we have roots at  $\gamma = 0$  and

$$\gamma = \pm \sqrt{\varphi \left( \frac{f_1(\partial_\varphi g_4)}{(\partial_\lambda f_4)g_1 - f_1(\partial_\lambda g_4)} \right)} + O(\varphi)$$

(d)  $f_1(0, 0) = 0$  and  $(\partial_\lambda f_4)g_2 - (\partial_\lambda f_2)g_4 = 0$  (but  $g_2, g_4 \neq 0$ )

$$D_f(\gamma, \varphi) = -\gamma \left( \varphi(\partial_\varphi f_1)g_4 - \gamma^2 ((\partial_\lambda f_4)g_1 - (\partial_\lambda f_1)g_4) + O(\varphi^2 + \varphi\gamma^2 + \gamma^3) \right)$$

so that we have roots at  $\gamma = 0$  and

$$\gamma = \pm \sqrt{\varphi \left( \frac{(\partial_\varphi f_1)g_4}{(\partial_\lambda f_4)g_1 - (\partial_\lambda f_1)g_4} \right)} + O(\varphi)$$

(e) We can also arrange to have roots at  $\gamma = 0$  and  $\gamma = O(\varphi^2)$ , e.g., via  $g_4(0, 0) = \partial_\varphi g_4(0, 0) = 0$ .

Cases (a) and (b), in which we have a root at  $\gamma = O(\varphi)$ , would in some sense seem the most generic, as they require the fewest assumptions. We note that in both these cases the single  $O(\varphi)$  root moves from  $\text{Re } \gamma > 0$  to  $\text{Re } \gamma < 0$  as  $\varphi$  moves from positive to negative, thus becoming a resonance pole.

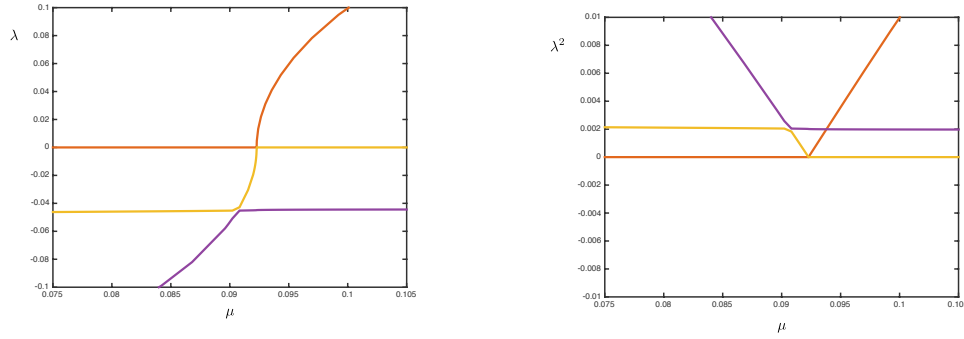


**Figure 5.4:** Numerical illustration of the scaling  $\mu \propto \lambda^2$  of the saddle node eigenvalue along a branch of asymmetric stripes and spots solutions in the planar cubic–quintic Swift–Hohenberg equation. *Left:*  $\lambda$  plotted as a function of the cumulative change in  $\mu$ . *Right:*  $\lambda^2$  plotted as a function of the cumulative change in  $\mu$ . This particular point corresponds to point 3 in Figure 4.6; we observe the same scaling at all saddle node crossings for both symmetric and asymmetric branches.

Case (c), which requires two assumptions, i.e., that  $g_4(0, 0) = 0$  and  $g_2(0, 0) = 0$ , in fact corresponds to only one additional assumption in the case that we have a conservative system; since  $f_2$  and  $g_2$  correspond to the direction of changing energy, we must in fact have  $f_2(0, \varphi) = g_2(0, \varphi) = 0$ . This is also consistent what we see numerically for the Swift–Hohenberg equation: as  $\varphi$  decreases through zero, the saddle node eigenvalue with  $\text{Re } \gamma > 0$  meets a resonance pole with  $\text{Re } \gamma < 0$  and both move onto the imaginary  $\gamma$  axis. The scaling given here is also consistent with the  $\mu \propto \lambda^2$  seen numerically ( $\varphi^2 \propto \mu$  near the saddle node implies that for scenario (c),  $\gamma \propto \mu^{1/4}$ , or  $\lambda^2 \propto \mu$ ). See Figure 5.4 for numerical confirmation along an asymmetric branch in the planar Swift–Hohenberg equation.

Some simplification of the expression for the root in case (c) is possible: using the linear independence of  $f$  and  $g$ , we may set  $g_1 = 0$  using  $f_1 \neq 0$  and subtracting  $(g_1/f_1)f$  from  $g$ . Since we assumed  $f_2(0, \varphi) = f_4(0, \varphi) = 0$ , we will not destroy the zeros at  $g_2(0, 0)$  and  $g_4(0, 0)$  by this procedure, so that we do not need any additional

assumptions on our redefined  $g$  to obtain the simplified expression

$$\gamma = \pm i \sqrt{\varphi \left( \frac{\partial_\varphi g_4}{\partial_\lambda g_4} \right)} + O(\varphi). \quad (6.2)$$

Case (d) supports the same behavior of the saddle nodes, but it does not appear to fit with the assumption that  $f$  corresponds to the translation eigenfunction. The scenario described in (e) corresponds to a situation in which all solutions are unstable, as roots exist for  $\lambda$  in the right half plane for all  $\varphi$ .

Another situation in which we observe similar behavior of the roots is case (ii) above, i.e.,  $f_2(0, \varphi) = g_2(0, \varphi) = 0$ , which we again note corresponds to a conservative system, with the additional assumptions  $f_4(0, 0) = g_4(0, 0) = 0$ . In this instance we have

$$D_f(\gamma, \varphi) = \gamma \left( \varphi \left( (\partial_\varphi f_4) g_1 - f_1(\partial_\varphi g_4) \right) - \gamma^2 \left( f_1(\partial_\lambda g_4) - (\partial_\lambda f_4) g_1 \right) + O(\varphi\gamma + \varphi^2) \right)$$

leading to nonzero roots at

$$\gamma = \pm \sqrt{\varphi \left( \frac{(\partial_\varphi f_4) g_1 - f_1(\partial_\varphi g_4)}{f_1(\partial_\lambda g_4) - (\partial_\lambda f_4) g_1} \right)} + O(\varphi).$$

Using the same procedure as above, this too simplifies to the form (6.2).

We finally note that we have not yet taken into account all the properties of the extended Evans function which arise when operating in  $\gamma$  while some components making up the Evans function are analytic in  $\lambda$ . In the nonlinear Schrödinger equation studied in [31, 32], all solutions comprising the extended Evans functions formed there were analytic only in  $\gamma$ .

In particular, we first consider why a simple root of the Evans function away from zero at  $\gamma_*$  should be accompanied by a second root at  $-\gamma_*$  (both for the same  $\varphi_*$ ). We write down the Evans function explicitly as

$$D_f(\gamma_*) = f_4g_2 - f_2g_4 + \gamma_*(f_4g_1 - f_1g_4),$$

where  $f_i = f_i(\gamma_*)$ , and similarly for  $g$ . If we suppose that  $f$  corresponds to the translation eigenfunction so that the  $f_i$  are generically nonzero away from  $\gamma = 0$ , the root must be enforced by  $g$ , and we then require (note  $\gamma_*$  is nonzero by assumption, so all four leading order terms in the above must vanish)

$$(i) \quad g_i(\gamma_*) = 0, \quad i = 1, 2, 4$$

$$(ii) \quad \frac{d}{d\gamma}g_i(\gamma_*) \neq 0, \quad i = 1, 2, 4$$

Note that for  $\gamma_*$  near 0, if we are in the setting above we may assume that  $f_1 \neq 0$ , so that the assumption  $g_1 = 0$  is . In any event, under the above assumptions we have  $D_f(\gamma_*) = 0$  and for  $\gamma$  sufficiently near  $\gamma_*$ , we have

$$D_f(\gamma) = (\gamma - \gamma_*)(f_4g'_2 - f_2g'_4) + \gamma(\gamma - \gamma_*)(f_4g'_1 - f_1g'_4) \quad (6.3)$$

where all  $f_i, g'_i$  are evaluated at  $\gamma_*$ , and  $' = \frac{d}{d\gamma}$ . This root is indeed simple, as shown by the calculation

$$(\gamma - \gamma_*)a + \gamma(\gamma - \gamma_*)b - \gamma_*(\gamma - \gamma_*)b + \gamma_*(\gamma - \gamma_*)b = (\gamma - \gamma_*)(a + \gamma_*b) + (\gamma - \gamma_*)^2b$$

Moreover, since  $g$  is analytic in  $\lambda$ , i.e., we have  $g(\gamma) = \hat{g}(\gamma^2)$ , where  $\hat{g}$  is an analytic function in  $\gamma$ , we also have  $g_i(-\gamma_*) = 0, i = 1, 2, 4$  by the above, so that we also have a simple root at  $D(\gamma_*)$ . Thus any roots away from zero will always come in

pairs, and if one is such that  $\operatorname{Re} \gamma > 0$ , then the other will have  $\operatorname{Re} \gamma < 0$ , so that we have an eigenvalue, resonance pole pair. Of course this also means that if one lies in  $i\mathbb{R}$  then the other does as well, and they will always lie on top of each other in the  $\gamma^2 = \lambda$  plane.

In conclusion, the numerical effects seen in Figure 4.3, as well as previously in [8, Figure 10] and [3, Figure 14], for example, are consistent with the situation described here by case (i)(c), both in general form and in particular scaling. However, this analysis still leaves unanswered questions, for example regarding the precise role of the translation eigenvalue, and the impact of perturbations breaking translation symmetry. We will continue to explore this phenomenon numerically and analytically in future work.

## CHAPTER SIX

---

# Predicting the Effects of Perturbations

## 6.1 Introduction

As we have seen, one characteristic common to many snaking systems is spatial reversibility. Often, such systems are also variational, and some are invariant under an additional  $\mathbb{Z}_2$  symmetry corresponding, for example, to symmetry in the midplane of a fluid system. Here we are interested in how the structure of snaking diagrams changes when reversibility, variational structure, or  $\mathbb{Z}_2$  symmetries, if present, are broken, either individually or jointly, by adding perturbative terms to the governing equation. The effects of breaking reversibility were recently explored analytically in [7, 37, 59], while numerical studies of perturbations that break variational structure and  $\mathbb{Z}_2$  symmetry were carried out recently in [26]. Generally speaking, breaking reversibility or symmetry leads to a rearrangement of bifurcation branches, while breaking the variational structure leads to patterns that drift with nonzero speed.

In this Chapter, we show that perturbative terms breaking symmetry or variational structure affect solution profiles and overall bifurcation structure in ways which are fully predictable analytically. By evaluating scalar products involving only solutions of the unperturbed system and perturbative terms evaluated at unperturbed solutions, we are able to predict which of many topologically distinct bifurcation diagrams will emerge upon introduction of perturbative terms, as well as the drift speeds of asymmetric solutions where appropriate. We confirm these predictions numerically for various perturbations to the cubic-quintic Swift–Hohenberg system both on the line and in the plane:

$$u_t = -(1 + \Delta)^2 u - \mu u + \nu u^3 - u^5. \quad (1.1)$$

Though we use the Swift–Hohenberg equation to demonstrate our results numeri-

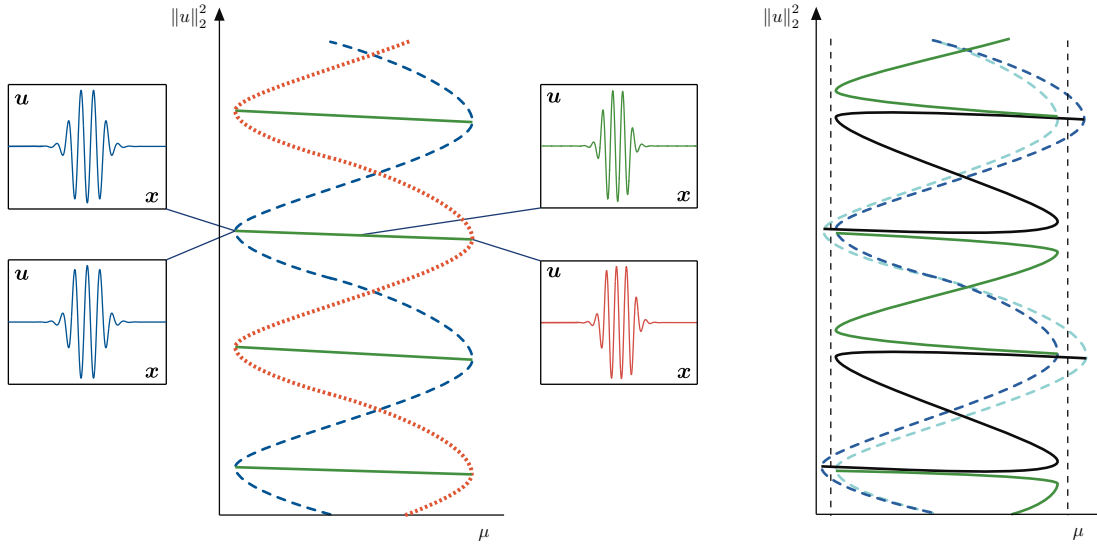


**Figure 6.1:** *Left:* Schematic of the bifurcation diagram for the unperturbed system (1.2) with  $\varepsilon = 0$ , with illustrative solution profiles. The dashed dark blue snaking branch consists of two branches of even parity solutions, while the dotted orange branch consists of two branches of odd parity solutions. Solid green cross-connecting branches consist of four sets of asymmetric solutions. *Right:* Schematic of the bifurcation diagram for a perturbed system as in (1.2) with  $\varepsilon \neq 0$ . Snaking branches for even symmetric patterns with central maximum and minimum are shown in dark and light blue dashed, respectively. Asymmetric branches are in solid black and green. Dashed vertical lines indicate the saddle node locations from the unperturbed system.

cally, we emphasize that our results are not specific to the Swift–Hohenberg setting.

The effect of perturbative terms added to (1.1) posed on the real line was recently explored numerically by Houghton and Knobloch [26]. In particular, Houghton and Knobloch examined<sup>1</sup> the variational system

$$u_t = -(1 + \partial_x^2)^2 u - \mu u + \nu u^3 - u^5 + \varepsilon u^2 \quad (1.2)$$

as well as the non-variational system

$$u_t = -(1 + \partial_x^2)^2 u - \mu u + \nu u^3 - u^5 + \varepsilon (\partial_x u)^2 \quad (1.3)$$

<sup>1</sup>We remark that Houghton and Knobloch used the bifurcation parameter  $r := -\mu$  instead of  $\mu$ : hence, their bifurcation diagrams are flipped in comparison to ours; in our description of their results, we use  $\mu$  as the parameter.

for  $0 < \varepsilon \ll 1$ . For  $0 < \varepsilon \ll 1$ , the systems no longer respect the symmetry  $u \mapsto -u$ , and Figure 6.1 provides a schematic comparison of the bifurcation diagrams for (1.2) with  $\varepsilon = 0$  and  $\varepsilon \neq 0$ . Houghton and Knobloch observed that the even solutions persist along unbroken snaking branches; however, in contrast to the  $\varepsilon = 0$  case, the two snaking branches for the even symmetric solutions with, respectively, a central maximum and a central minimum no longer lie on top of each other due to the broken  $\mathbb{Z}_2$  symmetry. Alternate saddle nodes on the left and right are now offset to the inside and outside of the original branches, so that the resulting bifurcation diagram possesses four snaking limits. Meanwhile the odd solutions are destroyed, and two types of asymmetric solution branches are formed, termed S and Z branches in accordance with their shapes. The Z branches start and end on the same symmetric branch, whereas the S branches connect the two symmetric solution branches to each other.

As outlined above, our goal is to explain the effects of breaking variational structure and  $\mathbb{Z}_2$  symmetry rigorously and to predict branch rearrangement and drift speeds of patterns using solutions of the unperturbed system only. We refer also to Chapter 2 for a general framework and preview of the results in this chapter. The chapter is organized as follows: in Section 6.2, we detail predictions on the evolution of bifurcation diagrams upon the introduction of perturbative symmetry breaking terms. In Section 6.3, we derive conditions that allow us to predict bifurcation diagrams and drift speeds upon adding perturbative terms to the underlying system; these conditions rely on evaluation of the perturbative terms along solutions of the unperturbed system. Specifically, in Section 6.3.1, we detail the effects of perturbative terms breaking variational structure; in Section 6.3.2, we show how to use our earlier results to make predictions for specific perturbations breaking  $\mathbb{Z}_2$  symmetry; and in Section 6.3.3, we show how our methods may be employed to anticipate which

of two types of bifurcation diagram emerges upon the introduction of nonreversible terms, where the two types have been identified previously in [37, 59]. Finally, in Section 6.4, we provide numerical studies supporting our analytical results using the 1D and 2D Swift–Hohenberg equations.

**Remark 6.1.1.** *A comment on notation: in this chapter we work primarily with the PDE rather than ODE formulation; as such, we chose to employ the variable  $u$  for the PDE and  $U$  for the ODE, in contrast to our convention elsewhere.*

## 6.2 Predicting results of breaking $\mathbb{Z}_2$ symmetry

### 6.2.1 Dynamical reformulation of the problem

Our goal now is to start with a system that respects the  $\mathbb{Z}_2$  symmetry  $\kappa$  for all  $\mu$ , and to describe what happens under forced symmetry breaking. To illustrate our approach, we start with the case where  $z(L)$  possesses one maximum and one minimum for each period  $\pi$ , where the  $\pi$ -periodicity is enforced by the presence of a  $\mathbb{Z}_2$  symmetry  $\kappa$ . We will be interested in perturbative terms breaking the  $\kappa$  symmetry when a second parameter  $\varepsilon$  is switched on, i.e., when  $\varepsilon \neq 0$ .

In Figure 6.2a we provide two equivalent renderings of the solution branches of localized structures in a system possessing  $\kappa$  symmetry and with  $z(L)$  having a single maximum per period. We illustrate the branches of even and odd symmetric structures ( $\mathcal{R}$ - and  $\kappa\mathcal{R}$ -symmetric, respectively) as well as the asymmetric solution branches. The left panel shows the phase  $\varphi$  along the  $x$ -axis, and the half-pulse length  $L$  along the  $y$ -axis, while the center panel shows the solutions in the  $(\mu, L)$

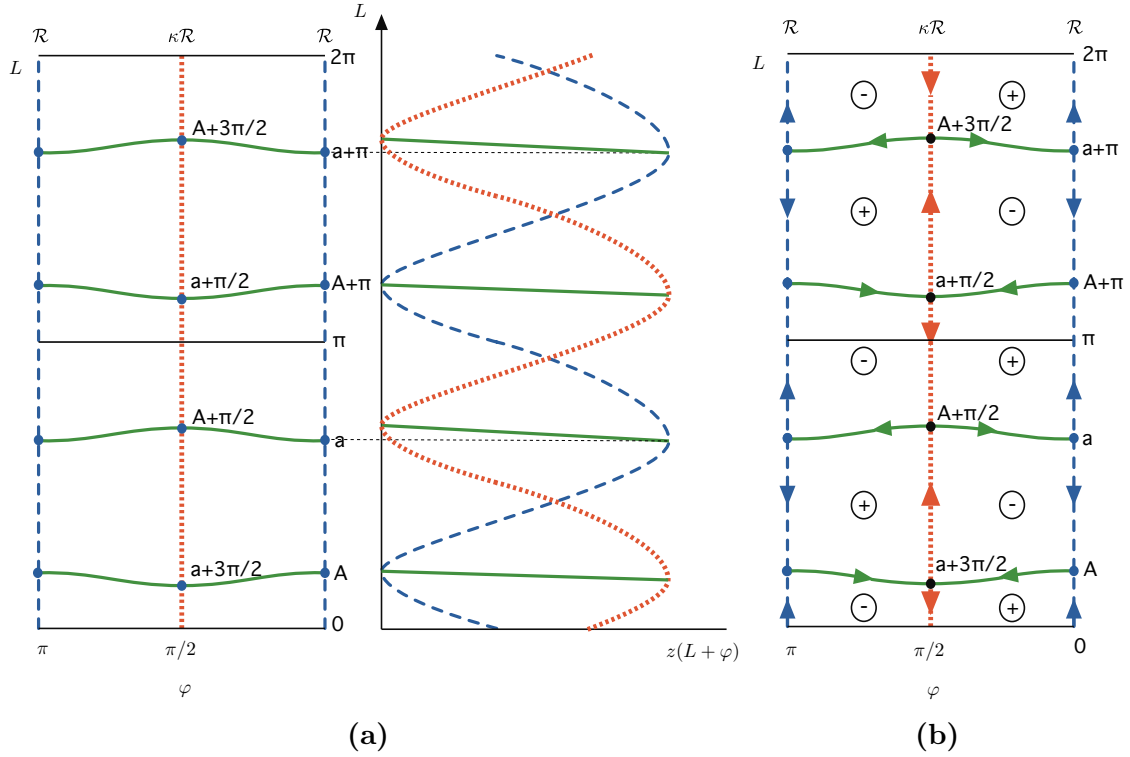


**Figure 6.2:** Different renderings of the bifurcation diagram for a system characterized by  $z$  possessing exactly one maximum and one minimum per period. **(a) Left:** The solution set of the bifurcation equations  $z(L - \varphi) = z(L + \varphi)$  is shown in the  $(\varphi, L)$ -plane. **Center:** The bifurcation diagram in the  $(\mu, L)$ -plane, using the relation  $\mu = z(L + \varphi)$ .  $\mathcal{R}$ -symmetric solution branches with  $\varphi = 0, \pi$  are shown in dashed blue,  $\kappa\mathcal{R}$ -symmetric with  $\varphi = \frac{\pi}{2}, \frac{3\pi}{2}$  in dotted orange, and asymmetric in solid green. Light dotted lines indicate correspondence of  $a$  and  $a + \pi$  with minima. **(b) Right:** Reformulation of the left panel as a Hamiltonian system; see the text for full details.

plane via the function  $\mu = z(L + \varphi)$  for solutions  $(L, \varphi)$  of

$$Z(L, \varphi) := z(L + \varphi) - z(L - \varphi) = 0.$$

This is analogous to our usual bifurcation diagram, with length  $L$  being equivalent to the  $L^2$  norm. The formulation in the left panel will provide a natural way to understand the effects of symmetry breaking perturbations, while the center panel provides the link to familiar bifurcation diagrams. We see that, before perturbation, the  $\mathcal{R}$ -symmetric solutions at  $\varphi = 0$  and  $\varphi = \pi$  coincide in the  $(\mu, L)$  plane, as do the  $\kappa\mathcal{R}$ -symmetric solutions at  $\varphi = \frac{\pi}{2}$  and  $\varphi = \frac{3\pi}{2}$  (latter not shown). We also note that, due to the  $\pi$ -periodicity of  $z$ , all information is actually contained in a single quadrant of the left panel, but we show the larger diagram here for easier comparison with the diagram after symmetry breaking.

We now drop the assumption that  $z$  has only one maximum per period. We argued formally in Section 2.2 that it suffices to solve

$$Z(L, \varphi) := z(L + \varphi) - z(L - \varphi) = 0 \tag{2.1}$$

for  $(L, \varphi)$  in order to find symmetric and asymmetric solution branches. Indeed, it was shown in [4] that the bifurcation equations for symmetric and asymmetric solutions are given by (2.1) with an additional error term of order  $O(e^{-KL})$  for some  $K > 0$ : in particular, regular zeros of (2.1) persist as solutions to the full bifurcation equations for all sufficiently large  $L$ . The analysis in [4] applies to reversible PDEs with or without variational structure on cylinders provided the spatial dynamical system associated with the steady-state equation falls under the class considered in [51].

Our goal here is to study the effect of perturbative terms breaking the  $\kappa$  symmetry. It will be useful to consider the system presented in the left panel of Figure 6.2a as a dynamical system in its own right, a technique employed in [4]. We let  $\bar{S}^1 := [0, \pi] / \sim$ , set  $Q := \bar{S}^1 \times [0, \frac{\pi}{2}]$ , and define

$$\Lambda := \{(L, \varphi) \in Q : Z(L, \varphi) = 0\}, \quad \Lambda_{bif} := \{(L, \varphi) \in \partial Q : z'(L + \varphi) = 0\}.$$

We introduce the planar Hamiltonian vector field

$$\begin{pmatrix} L_s \\ \varphi_s \end{pmatrix} = F(L, \varphi) := \begin{pmatrix} 0 & 1 \\ -1 & 0 \end{pmatrix} \nabla Z(L, \varphi) \quad (2.2)$$

whose zero energy level is precisely equal to the set  $\Lambda$ . We note that

$$\nabla Z(L, \varphi) = \begin{pmatrix} 1 & -1 \\ 1 & 1 \end{pmatrix} \begin{pmatrix} z'(L + \varphi) \\ z'(L - \varphi) \end{pmatrix}.$$

Hence we have  $\nabla Z(L, \varphi) = 0$  if and only if  $z'(L + \varphi) = z'(L - \varphi) = 0$ . Assuming nondegeneracy of the maxima and minima of  $z$ , i.e., assuming  $z(L_1) = z(L_2)$  and  $z'(L_1) = z'(L_2) = 0$  imply  $L_1 = L_2 \bmod \pi$ , we conclude that  $\nabla Z(L, \varphi) = 0$  for  $(L, \varphi) \in \Lambda$  if and only if  $\varphi \in \{0, \frac{\pi}{2}\}$ . Thus all equilibria of (2.2) in  $\Lambda$  lie in  $\Lambda_{bif}$ . Furthermore, assuming  $z'(L) = 0$  implies  $z''(L) \neq 0$ , all equilibria in  $\Lambda$  are hyperbolic saddles, since at these points we have

$$DF(L, \varphi_0) = 2 \begin{pmatrix} z''(L + \varphi_0) & 0 \\ 0 & -z''(L + \varphi_0) \end{pmatrix}, \quad \varphi_0 \in \left\{0, \frac{\pi}{2}\right\}.$$

So by Poincaré–Bendixson,  $\Lambda \setminus \Lambda_{bif}$  must be a 1D manifold consisting of the hetero-

clinic orbits that start and end at  $\Lambda_{bif}$ , and finitely many periodic orbits. Thus each element  $(L_*, 0)$  and  $(L_*, \frac{\pi}{2})$  of  $\Lambda_{bif}$  is a generic pitchfork bifurcation point, which gives rise to a unique global branch of solutions of (2.1) in  $Q$ . These branches do not cross, and they begin and end in  $\Lambda_{bif}$ . In Figure 6.2b we reproduce the left panel of Figure 6.2a with arrows indicating the flow of (2.2) within the zero energy level set  $\Lambda$  of the Hamiltonian system just described, as well as plus and minus signs indicating the sign of the energy  $Z(L, \varphi)$ .

We are now ready to consider a perturbation which breaks the  $\kappa$  symmetry, but preserves the other characteristics of our system, meaning in particular that the reversibility is unaffected so that we retain the  $2\pi$ -periodicity of  $z$ . Such a symmetry breaking perturbation will, however, typically break the  $\pi$ -periodicity of  $z$  and therefore break up the  $\kappa\mathcal{R}$ -symmetric branch. On the level of the vector field interpretation, this manifests itself as the fact that the saddle equilibria persist, but generically move outside the zero-level set of  $Z$ .

**Lemma 6.2.1.** *Suppose  $z(L)$  is  $\pi$ -periodic, satisfying (a)  $z(L_1) = z(L_2)$  and  $z'(L_1) = z'(L_2)$  only if  $L_1 = L_2 \bmod \pi$  and (b)  $z'(L) = 0$  implies  $z''(L) \neq 0$ . Let  $(L_0, \varphi_0)$  be a hyperbolic equilibrium of (2.2) satisfying (2.1). Assume  $\tilde{z}(L, \varepsilon) := z(L) + \varepsilon z_1(L) + O(\varepsilon^2)$ , with  $\tilde{z}(L, \varepsilon)$ , and therefore  $z_1(L)$ ,  $2\pi$ -periodic in  $L$ . Further define  $\tilde{Z}(L, \varphi, \varepsilon) := \tilde{z}(L + \varphi, \varepsilon) - \tilde{z}(L - \varphi, \varepsilon)$ , and consider*

$$\begin{pmatrix} L_s \\ \varphi_s \end{pmatrix} = \tilde{F}(L, \varphi, \varepsilon) := \begin{pmatrix} 0 & 1 \\ -1 & 0 \end{pmatrix} \nabla \tilde{Z}(L, \varphi, \varepsilon). \quad (2.3)$$

Then there exists an  $\varepsilon_0 > 0$  such that the following hold:

- (i) If  $\varphi_0 \in \{0, \pi\}$ , then for all  $|\varepsilon| < \varepsilon_0$  there exists a unique  $\tilde{L}_0(\varepsilon)$  close to  $L_0$  such that  $(\tilde{L}_0(\varepsilon), \varphi_0, \varepsilon)$  is a hyperbolic equilibrium of (2.3), and  $\tilde{Z}(\tilde{L}_0(\varepsilon), \varphi_0, \varepsilon) = 0$ .

Furthermore, the function  $\varepsilon \mapsto \tilde{L}_0(\varepsilon)$  is smooth.

(ii) If  $\varphi_0 \in \{\frac{\pi}{2}, \frac{3\pi}{2}\}$ , then for all  $|\varepsilon| < \varepsilon_0$  there exists a unique  $(\tilde{L}_0, \tilde{\varphi}_0)(\varepsilon)$  close to  $(L_0, \varphi_0)$  such that  $((\tilde{L}_0, \tilde{\varphi}_0)(\varepsilon), \varepsilon)$  is a hyperbolic equilibrium of (2.3). Furthermore, the function  $\varepsilon \mapsto (\tilde{L}_0, \tilde{\varphi}_0)(\varepsilon)$  is smooth, and if  $z_1(L_0 + \varphi_0) \neq z_1(L_0 - \varphi_0)$ , then  $\tilde{Z}((\tilde{L}_0, \tilde{\varphi}_0)(\varepsilon), \varepsilon) \neq 0$ .

**Proof.** Given  $\tilde{F}$  as defined in (2.3), we can write  $\tilde{F}$  explicitly as

$$\begin{aligned} \tilde{F}(L, \varphi, \varepsilon) &= \begin{pmatrix} \tilde{z}(L + \varphi, \varepsilon) + \tilde{z}(L - \varphi, \varepsilon) \\ -\tilde{z}(L + \varphi, \varepsilon) + \tilde{z}(L - \varphi, \varepsilon) \end{pmatrix} \\ &= \begin{pmatrix} z'(L + \varphi) + \varepsilon z'_1(L + \varphi) + z'(L - \varphi) + \varepsilon z'_1(L - \varphi) + O(\varepsilon^2) \\ -z'(L + \varphi) - \varepsilon z'_1(L + \varphi) + z'(L - \varphi) + \varepsilon z'_1(L - \varphi) + O(\varepsilon^2) \end{pmatrix}. \end{aligned}$$

Whether we are in case (i) where  $\varphi_0 \in \{0, \pi\}$ , or case (ii) where  $\varphi_0 \in \{\frac{\pi}{2}, \frac{3\pi}{2}\}$ , the  $\pi$ -periodicity of  $z$  implies  $z''(L_0 + \varphi_0) = z''(L_0 - \varphi_0)$  so that

$$D\tilde{F}(L_0, \varphi_0, 0) = \begin{pmatrix} 2z''(L_0 + \varphi_0) & 0 & z'_1(L_0 + \varphi_0) + z'_1(L_0 - \varphi_0) \\ 0 & -2z''(L_0 + \varphi_0) & -z'_1(L_0 + \varphi_0) + z'_1(L_0 - \varphi_0) \end{pmatrix}. \quad (2.4)$$

Since we have assumed  $z''(L_0 + \varphi_0) \neq 0$ , this implies that there exists a  $\varepsilon_0 > 0$  such that for all  $|\varepsilon| < \varepsilon_0$ , there exists a unique  $(\tilde{L}_0, \tilde{\varphi}_0)(\varepsilon)$  close to  $(L_0, \varphi_0)$  such that  $((\tilde{L}_0, \tilde{\varphi}_0)(\varepsilon), \varepsilon)$  is a hyperbolic equilibrium of (2.3), and the map  $\varepsilon \mapsto (\tilde{L}_0, \tilde{\varphi}_0)(\varepsilon)$  is smooth.

In particular, we can solve for  $(\tilde{L}_0, \tilde{\varphi}_0)(\varepsilon)$  as:

$$\tilde{F}(L, \varphi, \varepsilon) = \tilde{F}(L_0, \varphi_0, 0) + D\tilde{F}(L_0, \varphi_0, 0) \begin{pmatrix} L - L_0 \\ \varphi - \varphi_0 \\ \varepsilon \end{pmatrix} + O(\varepsilon^2) = \begin{pmatrix} 0 \\ 0 \end{pmatrix}$$

so

$$\begin{pmatrix} 2z''(L_0 + \varphi_0)(L - L_0) + (z'_1(L_0 + \varphi_0) + z'_1(L_0 - \varphi_0))\varepsilon \\ -2z''(L_0 + \varphi_0)(\varphi - \varphi_0) + (-z'_1(L_0 + \varphi_0) + z'_1(L_0 - \varphi_0))\varepsilon \end{pmatrix} + O(\varepsilon^2) = \begin{pmatrix} 0 \\ 0 \end{pmatrix}$$

yielding

$$L - L_0 = \varepsilon \left( \frac{-z'_1(L_0 + \varphi_0) - z'_1(L_0 - \varphi_0)}{2z''(L_0 + \varphi_0)} \right) + O(\varepsilon^2)$$

$$\varphi - \varphi_0 = \varepsilon \left( \frac{-z'_1(L_0 + \varphi_0) + z'_1(L_0 - \varphi_0)}{2z''(L_0 + \varphi_0)} \right) + O(\varepsilon^2)$$

or

$$\begin{aligned} (\tilde{L}_0, \tilde{\varphi}_0)(\varepsilon) &= (L_0, \varphi_0) + \frac{\varepsilon}{2z''(L_0 + \varphi_0)} (-z'_1(L_0 + \varphi_0) - z'_1(L_0 - \varphi_0), -z'_1(L_0 + \varphi_0) + z'_1(L_0 - \varphi_0)) \\ &\quad + O(\varepsilon^2). \end{aligned}$$

In case (i) where  $\varphi_0 \in \{0, \pi\}$ , the  $2\pi$ -periodicity of  $z_1(L)$  yields

$$(\tilde{L}_0, \tilde{\varphi}_0)(\varepsilon) = (L_0, \varphi_0) + \frac{\varepsilon}{2z''(L_0 + \varphi_0)} (-2z'_1(L_0 + \varphi_0), 0) + O(\varepsilon^2).$$

In fact, for  $\varphi_0 \in \{0, \pi\}$ , the  $2\pi$ -periodicity of  $\tilde{z}(L, \varepsilon)$  in  $L$  implies that

$$\tilde{F}(L, \varphi_0, \varepsilon) = 2 \begin{pmatrix} \tilde{z}'(L + \varphi_0) \\ 0 \end{pmatrix}.$$

So the unique  $(\tilde{L}_0, \tilde{\varphi}_0)(\varepsilon)$  near  $(L_0, \varphi_0)$  satisfying  $\tilde{F}((\tilde{L}_0, \tilde{\varphi}_0)(\varepsilon), \varepsilon) = 0$  must be of the form  $(\tilde{L}_0(\varepsilon), \varphi_0)$  where  $\tilde{L}_0(\varepsilon)$  satisfies  $z'(\tilde{L}_0(\varepsilon) + \varphi_0) + \varepsilon z'_1(\tilde{L}_0(\varepsilon) + \varphi_0) = 0$ .

This then implies

$$\tilde{Z}(\tilde{L}_0(\varepsilon), \varphi_0, \varepsilon) = z(\tilde{L}_0(\varepsilon) + \varphi_0) + \varepsilon z_1(\tilde{L}_0(\varepsilon) + \varphi_0) - z(\tilde{L}_0(\varepsilon) - \varphi_0) + \varepsilon z_1(\tilde{L}_0(\varepsilon) - \varphi_0) = 0$$

as  $\tilde{z}$  is  $2\pi$ -periodic. Thus we have shown (i).

In case (ii) where  $\varphi_0 \in \{\frac{\pi}{2}, \frac{3\pi}{2}\}$  we have

$$\begin{aligned} \tilde{Z}((\tilde{L}_0, \tilde{\varphi}_0)(\varepsilon), \varepsilon) &= z\left(L_0 + \varphi_0 - \frac{\varepsilon z'_1(L_0 + \varphi_0)}{z''(L_0 + \varphi_0)}\right) + \varepsilon z_1\left(L_0 + \varphi_0 - \frac{\varepsilon z'_1(L_0 + \varphi_0)}{z''(L_0 + \varphi_0)}\right) \\ &\quad - z\left(L_0 - \varphi_0 - \frac{\varepsilon z'_1(L_0 - \varphi_0)}{z''(L_0 + \varphi_0)}\right) - \varepsilon z_1\left(L_0 - \varphi_0 - \frac{\varepsilon z'_1(L_0 - \varphi_0)}{z''(L_0 + \varphi_0)}\right) + O(\varepsilon^2). \end{aligned} \quad (2.5)$$

We expand

$$z\left(L_0 + \varphi_0 - \frac{\varepsilon z'_1(L_0 + \varphi_0)}{z''(L_0 + \varphi_0)}\right) = z(L_0 + \varphi_0) + 2z'(L_0 + \varphi_0) \left(\frac{-\varepsilon z'_1(L_0 + \varphi_0)}{z''(L_0 + \varphi_0)}\right) + O(\varepsilon^2)$$

and similarly for  $z\left(L_0 - \varphi_0 - \frac{\varepsilon z'_1(L_0 - \varphi_0)}{z''(L_0 + \varphi_0)}\right)$ .

We also recall that  $z'(L_0 + \varphi_0) = z'(L_0 - \varphi_0) = 0$ , and  $z(L_0 + \varphi_0) - z(L_0 - \varphi_0) = 0$ .

Thus we rewrite (2.5) as

$$\tilde{Z}((\tilde{L}_0, \tilde{\varphi}_0)(\varepsilon), \varepsilon) = \varepsilon z_1(L_0 + \varphi_0) - \varepsilon z_1(L_0 - \varphi_0) + O(\varepsilon^2)$$

so that  $\tilde{Z}((\tilde{L}_0, \tilde{\varphi}_0)(\varepsilon), \varepsilon) \neq 0$  as long as  $z_1(L_0 + \varphi_0) \neq z_1(L_0 - \varphi_0)$ . This completes

the proof of (ii). ■

The key point of the above is that saddle equilibria corresponding to pitchfork bifurcations from the  $\kappa\mathcal{R}$ -symmetric branches generically do not remain in the zero-level set of  $Z$  once the  $\kappa$  symmetry is broken, so that the  $\kappa\mathcal{R}$ -symmetric branches are themselves broken in a manner consistent with the Hamiltonian vector field formulation described above.

## 6.2.2 Implications for particular forms of $z$

### Systems such that $z$ has a single maximum per period

Returning to the case where  $z$  has only one maximum and minimum per period, in Figure 6.3 we illustrate one possible result of  $\kappa$  symmetry breaking in such a system. In particular, using notation from the figure and Lemma 6.2.1, we have illustrated the case where  $z_1(A) > z_1(A + \pi)$  and  $z_1(a) > z_1(a + \pi)$ . This means that the saddle equilibrium near  $(\frac{\pi}{2}, A + \frac{\pi}{2})$  will now lie in the region where  $\tilde{Z} < 0$ , since

$$z_1\left(\left(A + \frac{\pi}{2}\right) + \frac{\pi}{2}\right) = z_1(A + \pi) < z_1(A) = z_1\left(\left(A + \frac{\pi}{2}\right) - \frac{\pi}{2}\right).$$

Similarly, the equilibrium near  $(a - \frac{\pi}{2}, \frac{\pi}{2})$  will lie in the region where  $\tilde{Z} > 0$ , since

$$z_1\left(\left(a - \frac{\pi}{2}\right) + \frac{\pi}{2}\right) = z_1(a) > z_1(a + \pi) = z_1(a - \pi) = z_1\left(\left(a - \frac{\pi}{2}\right) - \frac{\pi}{2}\right).$$

Note that the  $2\pi$ -periodicity of  $z_1$  implies that the sign of  $\tilde{Z}$  for the saddle equilibria with  $L \in [0, \pi)$  fixes the sign of  $\tilde{Z}$  for the saddle equilibria with  $L \in [\pi, 2\pi)$ ; specifically, the sign will be opposite.

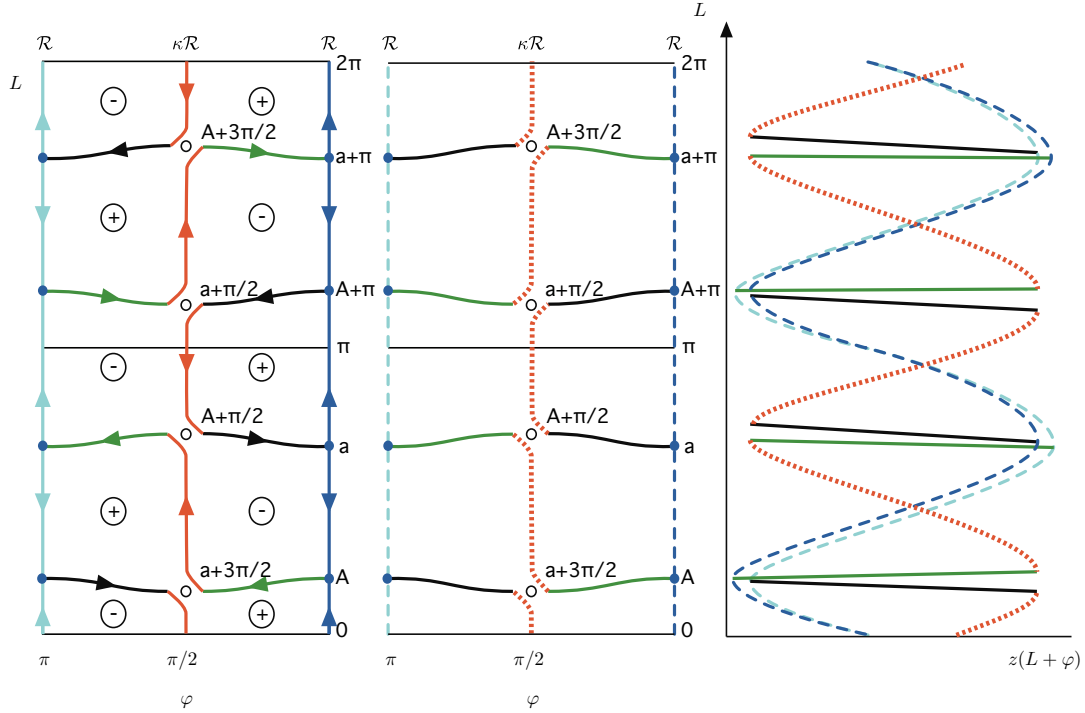


**Figure 6.3:** Bifurcation diagram for a system as in Figure 6.2a after  $\kappa$  symmetry breaking. On the left is the interpretation of the branches as zero energy solutions of a Hamiltonian system, as in Figure 6.2b; in the center is the same diagram without the vector field interpretation; and on the right the branches are shown in the  $(\mu = z(L + \varphi), L)$  plane. The  $\mathcal{R}$ -symmetric branches, now appearing as two branches in the right-hand figure are shown in dashed dark and light blue for  $\varphi = 0$  and  $\pi$ , respectively. The remains of the  $\kappa\mathcal{R}$  symmetric branch, which now form sections of asymmetric branches, are shown in dotted orange. The portions of the asymmetric solution branches that were already asymmetric branches in the unperturbed case are shown in solid green and solid black to facilitate comparison of the diagrams.

Technically there are four possible generic bifurcation diagrams, one for each of the four possible combinations of the sign of  $\tilde{Z}$  at saddle equilibria near  $(\frac{\pi}{2}, A + \frac{\pi}{2})$  and  $(\frac{\pi}{2}, a - \frac{\pi}{2})$ . However, as is clear from the preceding discussion, the sign combinations  $(+, +)$  and  $(-, -)$  are equivalent under translation by  $\pi$  in  $L$ , which amounts to swapping our definition of the  $\varphi = 0$  and  $\varphi = \pi$  branches. This equivalence also holds for the sign combinations  $(+, -)$  and  $(-, +)$ . Furthermore, these two sets of “same sign” and “opposite sign” bifurcation diagrams are in fact qualitatively equivalent as both result in a series of alternating cross-connecting and self-connecting asymmetric branches, each with two saddle nodes. In terms of the familiar bifurcation diagram in the  $(\mu, L)$  plane, self-connecting branches will appear as ‘S’ shaped curves and

cross-connecting as ‘Z’ shaped curves for perturbations such that the sign of  $\tilde{Z}$  is the same  $[(+, +)$  or  $(-, -)]$  for saddle equilibria with  $L \in [0, \pi)$  near  $\varphi = \pi/2$ . The opposite is true for perturbations such that the sign of  $\tilde{Z}$  is  $(+, -)$  or  $(-, +)$ . As we will see below, when  $z$  has two or more maxima, different symmetry breaking perturbations may result in distinct bifurcation diagrams, which are not reducible via reflections or translations.

We note that these results are applicable to localized roll solutions of the one-dimensional Swift–Hohenberg model

$$u_t = -(1 + \partial_x^2)^2 u - \mu u + \nu u^3 - u^5, \quad x \in \mathbb{R} \quad (2.6)$$

with the addition of perturbative terms, regardless of whether these terms preserve the variational structure. Indeed, we observe that these findings are entirely consistent with the numerical results of Houghton and Knobloch, including the breaking up of the odd parity branches, broadening of the snaking region, and appearance of S and Z asymmetric branches.

### **Systems such that $z$ has at least two maxima per period**

We now turn to the somewhat more complicated situation where  $z(L)$  possesses two maxima and minima per period  $\pi$ ; of course the periodicity implies that maxima and minima must occur in pairs.

Figure 6.4 shows a rendering of the resulting bifurcation structure for such a  $z$ . Again the left and center panels show the phase  $\varphi$  along the  $x$ -axis the pulse length  $L$  along the  $y$ -axis, while the right-hand figure shows the analogous plot to

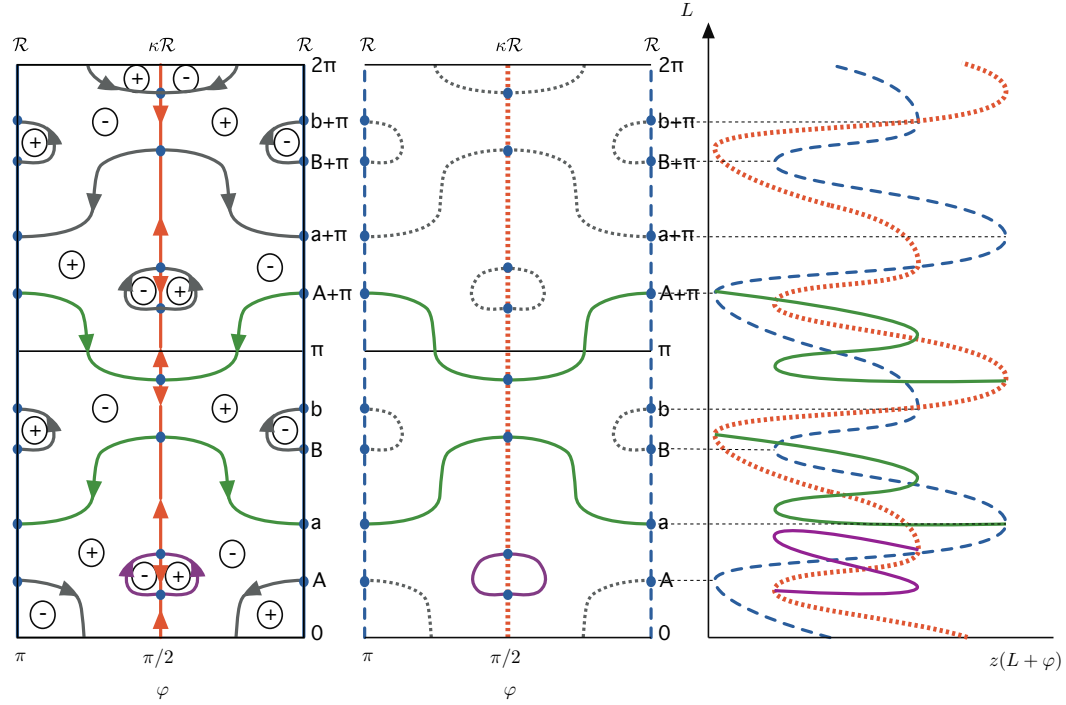


**Figure 6.4:** Bifurcation structure of a system characterized by  $\pi$ -periodic  $z$  possessing two distinct maxima per period. Again, we illustrate the solution branches in the  $(\varphi, L)$  plane, both with and without the vector field interpretation, as well as in the  $(\mu = z(L + \varphi), L)$  plane, where the actual bifurcation branches will be exponentially close in  $L$  to the ones shown. As before,  $\mathcal{R}$ -symmetric solution branches are shown in dashed blue, and  $\kappa\mathcal{R}$ -symmetric in dotted orange. Particular asymmetric solution branches are shown in solid purple and green. For clarity, not all asymmetric solution branches are shown in the right-most rendering; branches not shown on the right are rendered in thin dotted gray in the center illustration. The light dashed horizontal lines show the correspondence between the hyperbolic equilibria at  $A, a, B, b$ , etc. and the maxima and minima on the right.

a typical bifurcation diagram. Once more, prior to perturbation, the  $\mathcal{R}$ -symmetric solutions at  $0$  and  $\pi$  coincide in the  $(\mu = z(L + \varphi), L)$  plane, as do the  $\kappa\mathcal{R}$ -symmetric solutions at  $\frac{\pi}{2}$  and  $\frac{3\pi}{2}$ . Again to enable later comparisons, we show the right and center diagrams for  $(\varphi, L) \in [0, \pi] \times [0, 2\pi]$  even though all information is contained in the  $[0, \frac{\pi}{2}] \times [0, \pi]$  quadrant.

We note that this form of  $z$  is observed for the planar stripe and spot patterns seen in the cubic-quintic Swift–Hohenberg posed on a cylinder, i.e.,

$$u_t = -(1 + \partial_x^2 + \partial_y^2)^2 u - \mu u + \nu u^3 - u^5, \quad (x, y) \in S^1 \times \mathbb{R} \quad (2.7)$$

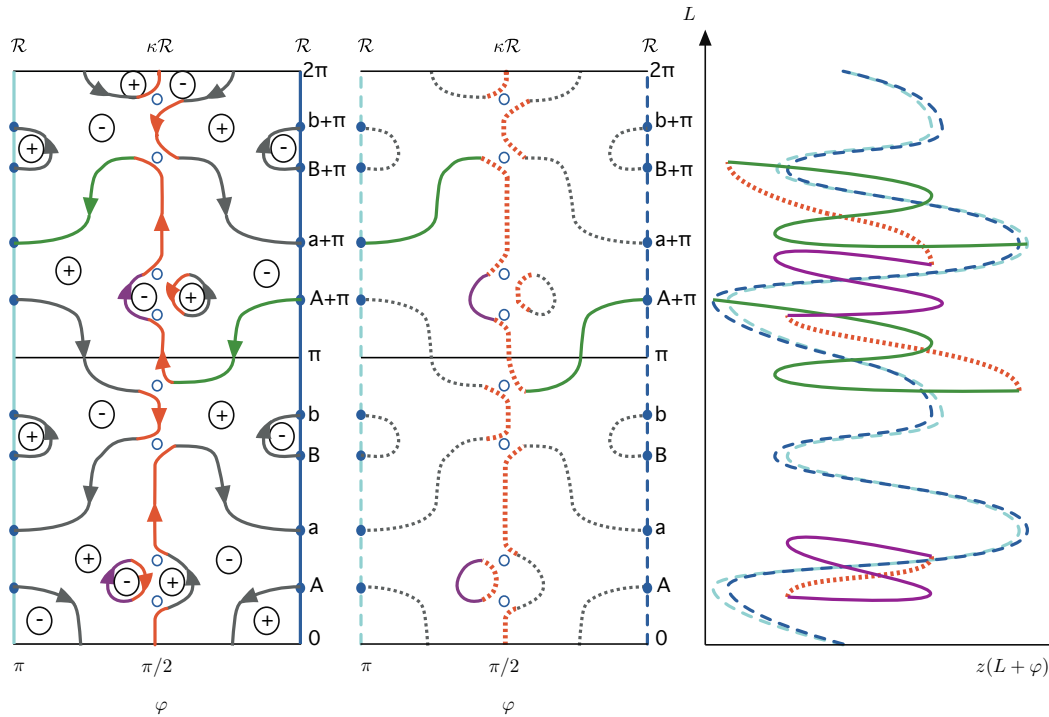


**Figure 6.5:** Bifurcation structure of the system illustrated in Figure 6.4, after the addition of a  $\kappa$  symmetry breaking perturbative term causing the sign of  $Z$  to be the same at adjacent local extrema. Again for clarity, only a selection of asymmetric solution branches are shown in the right-most figure. The coloring and line styles from Figure 6.4 have been preserved to show the portions of each solution branch arising from the original branches in the unperturbed case. Note that although all branch segments bifurcating from the  $\kappa\mathcal{R}$ -symmetric branch remain dotted orange in the center figure, not all segments are shown on the right.

where  $S^1 = \mathbb{R}/2L_x\mathbb{Z}$  for some  $L_x > 0$ , and that the branches in Figure 6.4 are indeed consistent with the full bifurcation structure of the almost-planar stripe and spot patterns in the cubic-quintic Swift–Hohenberg model, as reported in [3] and also verified in Section 6.4 below.

Upon introduction of a perturbative term breaking the  $\kappa$  symmetry, we again expect that the  $\kappa\mathcal{R}$ -symmetric branches will break up, with the saddle equilibria generically moving outside the zero-level set of  $\tilde{Z}$  due to the loss of  $\pi$ -periodicity of  $z$ , i.e., due to the fact that generically  $z_1(L_0 + \varphi_0) \neq z_1(L_0 - \varphi_0)$ . However, in contrast to the single maximum system discussed above, here we find that we obtain qualitatively different bifurcation diagrams depending on whether the new sign of  $\tilde{Z}$

at adjacent saddle equilibria matches or differs.

In particular, there are now sixteen possible generic bifurcation diagrams, one for each of the possible combinations for the sign of  $\tilde{Z}$  at saddle equilibria near  $(\frac{\pi}{2}, B - \frac{\pi}{2})$ ,  $(\frac{\pi}{2}, b - \frac{\pi}{2})$ ,  $(\frac{\pi}{2}, A + \frac{\pi}{2})$  and  $(\frac{\pi}{2}, a + \frac{\pi}{2})$ , where the labels correspond to those used in Figure 6.4. Once again the  $2\pi$ -periodicity of  $z_1$  implies that the saddle equilibria with  $L \in [\pi, 2\pi)$  will have  $\tilde{Z}$  of the opposite sign as the corresponding saddle equilibria with  $L \in [0, \pi)$ .

Noting that  $B$  and  $b$  are local (rather than global) extrema of the function  $z$ , the biggest qualitative difference in possible bifurcation diagrams is between those in which the saddle equilibria near  $(\frac{\pi}{2}, B - \frac{\pi}{2})$  and  $(\frac{\pi}{2}, b - \frac{\pi}{2})$  have  $\tilde{Z}$  with the same sign, versus those in which the sign of  $\tilde{Z}$  is different. In the former case, the bifurcation diagram for the perturbed system will possess isolas formed from the reorganization of asymmetric and  $\kappa\mathcal{R}$ -symmetric branches, whereas in the latter the bifurcation diagram will have self-connecting asymmetric branches with many saddle nodes, but no isolas.

This distinction holds regardless of the sign of  $\tilde{Z}$  at the remaining saddle equilibria, i.e., those corresponding to global maxima and minima. Differences in the sign of  $\tilde{Z}$  for the saddle equilibria near  $(\frac{\pi}{2}, A + \frac{\pi}{2})$  and  $(\frac{\pi}{2}, a + \frac{\pi}{2})$  affect the number of saddle nodes in each asymmetric branch, but do not affect the formation of isolas. We note that, by inspection of the Hamiltonian vector field formulation, the exact number of saddle nodes on any given bifurcation branch can be determined by counting the number of tangencies to one of the vectors  $(\pm 1, \pm 1)$  in the  $(\varphi, L)$  plane.

In Figure 6.5, we illustrate the form the bifurcation diagram should take under a perturbation such that  $z_1$  at adjacent local extrema  $B$  and  $b$  satisfies  $z_1(B) >$

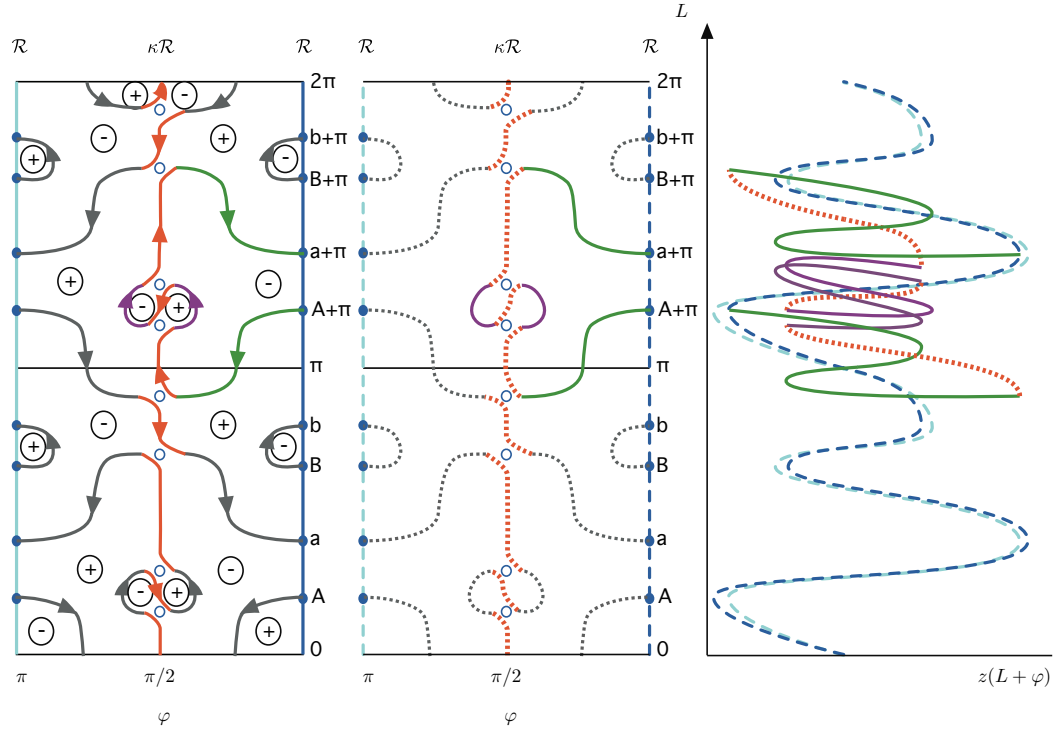


**Figure 6.6:** Symmetry breaking with the opposite relative movement of adjacent local extrema from that displayed in Figure 6.5. Note that for clarity we no longer show a cross-connecting asymmetric solution, but focus instead on one of the self-connecting asymmetric branch with 14 saddle nodes.

$z_1(B + \pi)$  and  $z_1(b) > z_1(b + \pi)$ . This means that the saddle equilibrium near  $(\frac{\pi}{2}, B - \frac{\pi}{2})$  will now lie in the region where  $\tilde{Z} > 0$ , since

$$z_1\left(\left(B - \frac{\pi}{2}\right) + \frac{\pi}{2}\right) = z_1(B) > z_1(B + \pi) = z_1(B - \pi) = z_1\left(\left(B - \frac{\pi}{2}\right) - \frac{\pi}{2}\right).$$

The equilibrium near  $(\frac{\pi}{2}, b - \frac{\pi}{2})$  will also lie in the region where  $\tilde{Z} > 0$ , since

$$z_1\left(\left(b - \frac{\pi}{2}\right) + \frac{\pi}{2}\right) = z_1(b) > z_1(b + \pi) = z_1(b - \pi) = z_1\left(\left(b - \frac{\pi}{2}\right) - \frac{\pi}{2}\right).$$

Again we observe that whether  $z_1(B) > z_1(B + \pi)$  and  $z_1(b) > z_1(b + \pi)$  or the opposite inequalities hold is immaterial as long as they are both in the same direction. Identifying these two cases amounts to reversing our conventions for defining  $\varphi = 0$

and  $\varphi = \pi$ . In Section 6.4, we demonstrate the formation of isolas numerically for the Swift–Hohenberg model, with symmetry-breaking perturbation  $\varepsilon u^2$ .

In contrast, in the case where the perturbation causes one local extremum to move up and the other to move down relative to those at distance  $\pi$ , we do not expect isolas, but rather anticipate a complicated asymmetric branch possessing 14 saddle nodes, as shown in Figure 6.6. In particular, we illustrate the case where  $z_1(B) < z_1(B + \pi)$  and  $z_1(b) > z_1(b + \pi)$ , along with  $z_1(A) > z_1(A + \pi)$  and  $z_1(a) < z_1(a + \pi)$ . As seen in Section 6.4, this type of behavior is observed in the Swift–Hohenberg model with the perturbative term  $\varepsilon u^4$ .

This sort of analysis can be continued for  $z$  possessing more than two maxima per period. We reiterate that in order for symmetry breaking to produce isolas, a minimum of two maxima (and minima) are required prior to the introduction of symmetry breaking terms.

### 6.3 Full *a priori* characterization of perturbed bifurcation diagrams

We now derive conditions that allow us to predict bifurcation diagrams and drift speeds upon adding perturbative terms to the underlying system; these conditions rely on evaluation of the perturbative terms along solutions of the unperturbed system. We begin by examining the effects of breaking variational structure, then revisit perturbations breaking  $\mathbb{Z}_2$  symmetry, and finally look at perturbations breaking reversibility.

### 6.3.1 Breaking variational structure

We begin by considering the drift speed  $c$ , which will generically be nonzero for the asymmetric branches of the perturbed system in the case where the perturbation  $G(u)$  is nonvariational:

**Lemma 6.3.1.** *Assume that  $u(x-ct)$  is a localized solution of  $u_t = -\nabla\mathcal{E}(u) + G(u)$ , where we assume that*

$$\mathcal{E}(u) = \int_{\mathbb{R}} \mathcal{L}(u(x), u_x(x), u_{xx}(x)) dx$$

and

$$[G(u)](x) = g(u, u_x, u_{xx}, u_{xxx}). \quad (3.1)$$

Then  $c = -\frac{1}{\|u_x\|_{L^2}^2} \langle u_x, G(u) \rangle_{L^2}$ .

**Proof.** The function  $u(x)$  satisfies  $-\nabla\mathcal{E}(u) + cu_x + G(u) = 0$ . Taking the scalar product with  $u_x$  we get

$$\begin{aligned} 0 &= - \int_{\mathbb{R}} \left( \mathcal{L}_u + \mathcal{L}_{u_x} \frac{\partial}{\partial x} + \mathcal{L}_{u_{xx}} \frac{\partial^2}{\partial x^2} \right) u_x dx + c \|u_x\|_{L^2}^2 \\ &\quad + \int_{\mathbb{R}} u_x(x) g(u(x), u_x(x), u_{xx}(x), u_{xxx}(x)) dx \\ &= - \int_{\mathbb{R}} \frac{d}{dx} \mathcal{L}(u(x), u_x(x), u_{xx}(x)) dx + c \|u_x\|_{L^2}^2 \\ &\quad + \int_{\mathbb{R}} u_x(x) g(u(x), u_x(x), u_{xx}(x), u_{xxx}(x)) dx \\ &= c \|u_x\|_{L^2}^2 + \int_{\mathbb{R}} u_x(x) g(u(x), u_x(x), u_{xx}(x), u_{xxx}(x)) dx, \end{aligned}$$

where we have used the fact that  $u$  is localized to conclude that  $\int \frac{d}{dx} \mathcal{L}(u(x), u_x(x), u_{xx}(x)) =$

0. Hence,  $c = -\frac{1}{\|u_x\|_{L^2}^2} \langle u_x, G(u) \rangle_{L^2}$ . ■

Thus, given a perturbation  $\varepsilon G(u)$ , the speed  $c^\varepsilon$  along a perturbed branch  $u^\varepsilon$  will be

$$c^\varepsilon = -\frac{1}{\|u_x^\varepsilon\|_{L^2}^2} \langle u_x^\varepsilon, \varepsilon G(u^\varepsilon) \rangle_{L^2}.$$

Evaluating this directly requires knowledge of the perturbed solution profiles. However, for  $\varepsilon$  small, we can predict the speeds of the perturbed solutions using only the original (unperturbed) solution profiles since

$$\left. \frac{dc}{d\varepsilon} \right|_{\varepsilon=0} = -\frac{1}{\|u_x^0\|_{L^2}^2} \langle u_x^0, G(u^0) \rangle_{L^2}, \quad (3.2)$$

where the right-hand side is computed for the unperturbed solutions. We now record a few consequences of this expression.

First, we reiterate that any solution which respects a reverser (either  $\mathcal{R}$  or  $\kappa\mathcal{R}$ ) must necessarily be stationary. However, as we will see explicitly in Section 6.4, once the reverser  $\kappa\mathcal{R}$  is broken, a solution may be very close to respecting this (now nonexistent) reverser, and yet have a relatively large drift.

Second, we observe that drift speeds approach zero for reversible perturbations that break the variational structure as we proceed up the bifurcation diagram: if we decompose the inner products into contributions from the tails and the periodic orbits, we can write

$$\|u_x^0\|_{L^2}^2 \approx 2C_1 + N \int_0^{2\pi} u_x^0(x)^2 dx,$$

where  $N$  is the number of oscillations and  $C_1$  arises from the integral over the tails and is independent of  $N$ ; similarly

$$\langle u_x^0, G(u^0) \rangle_{L^2} \approx 2C_2 + N \int_0^{2\pi} u_x^0(x) g(u^0(x), u_x^0(x), u_{xx}^0(x), u_{xxx}^0(x)) dx,$$

where again  $C_2$  arises from the tails. Thus

$$\frac{dc}{d\varepsilon} \approx \frac{\int_0^{2\pi} u_x^0(x)g(u^0(x), u_x^0(x), u_{xx}^0(x), u_{xxx}^0(x))dx}{\int_0^{2\pi} u_x^0(x)^2 dx} + O\left(\frac{1}{N}\right).$$

However, along the wavetrains,  $\int_0^{2\pi} u_x^0(x)g(u^0(x), u_x^0(x), u_{xx}^0(x), u_{xxx}^0(x))dx$  will in fact be zero, as wave trains and the perturbation  $g$  are reversible, and we conclude that  $dc/d\varepsilon$  indeed decays with rate at least  $1/N$ .

Finally, we remark that additional insight into the drift speed may be gained by approaching the problem via the spatial Hamiltonian, and verifying that we arrive at the same formula for the speed  $c$ . We do this for the one-dimensional Swift–Hohenberg equation, as we have an explicit expression for its Hamiltonian  $H$ . The main point we take away from the computation is that the speed is selected to guarantee spatial energy balance across the pattern. We start by writing

$$u_t = -(1 + \partial_x^2)^2 u - \mu u + cu_x + \nu u^3 - u^5 + \varepsilon G(u).$$

We define  $U = (U_0, U_1, U_2, U_3) = (u, u', u'', u''')$  so that the vector field is given by

$$U_x = F(U) + (c(U_1) + \varepsilon g(U_0, U_1, U_2, U_3)) \cdot (0 \ 0 \ 0 \ 1)^\top$$

with

$$F(U) = \begin{pmatrix} 0 & 1 & 0 & 0 \\ 0 & 0 & 1 & 0 \\ 0 & 0 & 0 & 1 \\ -(1 + \mu) & 0 & -2 & 0 \end{pmatrix} \begin{pmatrix} U_0 \\ U_1 \\ U_2 \\ U_3 \end{pmatrix} + \begin{pmatrix} 0 \\ 0 \\ 0 \\ \nu U_0^3 - U_0^5 \end{pmatrix}.$$

The spatial Hamiltonian is given by

$$H(U) = U_1 U_3 - \frac{U_2^2}{2} + U_1^2 + \frac{(1 + \mu)U_0^2}{2} - \frac{\nu U_0^4}{4} + \frac{U_0^6}{6}.$$

In order to balance the Hamiltonian across a localized pattern  $U(x)$ , we should have

$$\begin{aligned} 0 &= H(U(+\infty)) - H(U(-\infty)) \\ &= \int_{\mathbb{R}} \frac{d}{dx} H(U(x)) dx \\ &= \int_{\mathbb{R}} \nabla H(U(x)) \cdot U_x(x) dx \\ &= \int_{\mathbb{R}} \nabla H(U(x)) \cdot (F(U(x)) + [c(U_1(x)) + \varepsilon g(U_0(x), U_1(x), U_2(x), U_3(x))] \cdot (0 \ 0 \ 0 \ 1)^T) dx \\ &= \int_{\mathbb{R}} \begin{pmatrix} (1 + \mu)U_0(x) - \nu U_0(x)^3 + U_0(x)^5 \\ 2U_1(x) + U_3(x) \\ -U_2(x) \\ U_1(x) \end{pmatrix}^T \times \\ &\quad \times \begin{pmatrix} 0 \\ 0 \\ 0 \\ 1 \end{pmatrix} dx \\ &= \varepsilon \int_{\mathbb{R}} U_1(x) g(U_0(x), U_1(x), U_2(x), U_3(x)) dx + c \int_{\mathbb{R}} U_1(x)^2 dx, \end{aligned}$$

where we use the fact that  $\nabla H(U(x)) \cdot F(U(x)) = 0$ . Our final expression is, of course, the same expression we arrived at originally in Lemma 6.3.1. Thus we have the alternative interpretation that the speed is determined by the need to balance the spatial energy across the pattern.

### 6.3.2 Breaking $\mathbb{Z}_2$ symmetry

The analysis in Section 6.2 rigorously predicts the results of symmetry breaking and allows us to categorize all possible scenarios resulting from different forms of  $\tilde{z}$ . It does not, however, immediately provide a means to predict the particular reorganization resulting from a given perturbative term. In the following, we provide a method for predicting the full bifurcation diagram induced by a particular perturbation without the need for any computations on the perturbed system. For clarity we carry out our analysis for the Swift–Hohenberg model equation in one dimension, but it should be clear how to adapt this to more general settings.

We define

$$F(u, \mu, c, \varepsilon) := -(1 + \partial_x^2)^2 u - \mu u + cu_x + bu^3 - u^5 + \varepsilon G(u) \quad (3.3)$$

where the perturbative term  $G(u)$  is of the form given in (3.1), e.g.,  $u^2$  or  $u_x^2$ , and we have added the  $cu_x$  term to account for the fact that localized solutions may now drift so we may need to view them in a moving frame. We can then parameterize a solution branch for the unperturbed system as  $(u^0(s), \mu^0(s))$ , where  $s$  is, for instance, arc length along the branch, so that

$$F(u^0(s), \mu^0(s), 0, 0) = 0$$

for all  $s$ . We denote the tangent vector to this solution branch by

$$(u_s^0, \mu_s^0) := \frac{d}{ds}(u^0, \mu^0)(s).$$

For  $\varepsilon$  nonzero, the persisting  $\mathcal{R}$ -symmetric branch will be given by  $(u^\varepsilon(s), \mu^\varepsilon(s), c^\varepsilon(s))$ ,

which satisfies

$$F(u^\varepsilon(s), \mu^\varepsilon(s), c^\varepsilon(s), \varepsilon) = 0.$$

Differentiating this with respect to  $\varepsilon$  and evaluating at  $\varepsilon = 0$ , we obtain

$$F_u u_\varepsilon^0 + F_\mu \mu_\varepsilon^0 + F_c c_\varepsilon^0 + F_\varepsilon = 0, \quad (3.4)$$

where the derivatives of  $F$  are evaluated along  $(u^0, \mu^0, c^0)$ . Whether the perturbation  $G(u)$  is variational or not, as shown in Lemma 6.2.1, the only information we need to complete the full bifurcation diagram of the perturbed system is local information on  $z_1$  at  $L_0 + \varphi_0$  and  $L_0 - \varphi_0$ . Thus we are only interested in what we will refer to as the “splitting distances,” i.e., the difference between the values of  $\mu$  at the saddle nodes of the unperturbed and perturbed  $\mathcal{R}$ -symmetric branches, which persist for any perturbation preserving the reverser  $\mathcal{R}$ . Consequently, we only require computations along the  $\mathcal{R}$ -symmetric branch, which continues to have  $c = 0$  for  $\varepsilon \neq 0$  as long as the reverser  $\mathcal{R}$  persists. Defining  $\mathcal{L} = -(1 + \partial_x^2)^2 - \mu + 3bu^2 - 5u^4$  for a particular solution  $(u, \mu) = (u^0, \mu^0)$ , we see that

$$\begin{cases} \mathcal{L}u_\varepsilon^0 - u^0\mu_\varepsilon^0 + G(u^0) = 0 \\ \langle u_\varepsilon^0, u_s^0 \rangle_{L^2} + \mu_\varepsilon^0\mu_s^0 = 0. \end{cases} \quad (3.5)$$

Conversely, the system

$$\begin{cases} \mathcal{L}\tilde{u} - u^0\tilde{\mu} + G(u^0) = 0 \\ \langle \tilde{u}, \mu_s^0 \rangle_{L^2} + \tilde{\mu}\mu_s^0 = 0 \end{cases} \quad (3.6)$$

has generically a unique solution, which is therefore  $(\tilde{u}, \tilde{\mu}) = (u_\varepsilon^0, \mu_\varepsilon^0)$ . Thus the offset along the solution branch will be given by  $\mu_\varepsilon^0\varepsilon + O(\varepsilon^2)$ . We can find  $\mu_\varepsilon^0$  anywhere along the solution branch by solving the linear system (3.6).

Alternatively, we note that, at a saddle node, we have  $\mu_s^0 = 0$  so that  $\mathcal{L}u_s^0 = 0$ ;

since  $\mathcal{L}$  is self-adjoint in  $L^2$ , applying  $\langle u_s^0, \cdot \rangle_{L^2}$  to the first equation in (3.5) yields

$$-\langle u_s^0, u^0 \mu_\varepsilon^0 \rangle_{L^2} + \langle u_s^0, G(u^0) \rangle_{L^2} = 0$$

or

$$\mu_\varepsilon^0 = \frac{\langle u_s^0, G(u^0) \rangle_{L^2}}{\langle u_s^0, u^0 \rangle_{L^2}}, \quad \mathcal{L}u_s^0 = 0. \quad (3.7)$$

Thus we need only to calculate a solution  $(u^0, \mu^0)$  and its associated eigenfunction  $u_s^0$  to compute the offset at a saddle node. While the method of directly solving the linear system (3.6) is somewhat more robust numerically, the latter method given by (3.7) provides helpful insight, particularly in the one-dimensional case, and we refer to Section 6.4 for computations.

We emphasize that, whichever method we use, this calculation allows us to describe the full bifurcation diagram without the need for any computations on the perturbed system. The quantity  $\mu_\varepsilon^0$  corresponds to  $z_1$  as defined in Lemma 6.2.1, which in turn determines which class of bifurcation diagram the perturbed system will exhibit. For example, in the case of a system with two left and two right saddle nodes per period  $\pi$ , we have seen that the formation of isolas depends on the relative signs of the difference in offsets for the inner saddle nodes at distance  $\pi$ . Indicating these nodes by  $B, B + \pi, b, b + \pi$  as in Section 6.2.2, isolas will be formed if the quantity

$$\delta_{\mathbb{Z}_2} = (z_1(B) - z_1(B + \pi))(z_1(b) - z_1(b + \pi))$$

is greater than zero, but not if  $\delta_{\mathbb{Z}_2}$  is less than zero.

Finally, while we know that for any perturbation  $G(u)$  preserving  $\mathbb{Z}_2$  symmetry, the function  $z_1$  must remain  $\pi$ -periodic and therefore  $\delta_{\mathbb{Z}_2}$  will be zero, it is instructive to understand heuristically why this quantity is zero for such a perturbation. Noting

that the eigenfunctions are exponentially localized at the interfaces, and that at the interfaces solutions at distance  $\pi$  are related by  $\kappa$  symmetry, we see that for perturbations such that  $G(\kappa u) = \kappa G(u)$ , we will have  $z_1(L) = z_1(L + \pi)$  for any  $L$  corresponding to a saddle node. Thus we will have  $\delta_{\mathbb{Z}_2} = 0$  for a perturbation respecting  $\kappa$  symmetry so that the bifurcation diagram is topologically preserved.

### 6.3.3 Breaking reversibility

As mentioned in section 2.2, front solutions  $u_f(x)$  and back solutions  $u_b(x)$  in reversible systems are pairwise related via  $u_b(x) = u_f(-x)$ . In other words, the function  $\mu = z(L)$  that connects interface length and parameter is the same for the front  $u_f(x)$  and the back  $u_b(x) = u_f(-x)$ . This is no longer the case when perturbations of amplitude  $\varepsilon$  are added to the system that break the reversibility. Both fronts and backs will persist but they will, in general, no longer be related by reflection symmetry: in particular, the existence region of fronts and backs are described by functions  $z_{f,b}(L, \varepsilon) = z(L) + \varepsilon w_{f,b}(L) + O(\varepsilon^2)$ , respectively, where generally  $w_f \neq w_b$ . We assume that  $z(L)$  has precisely one minimum at  $L = L_m$  and one maximum at  $L = L_M$ , both therefore corresponding to saddle-nodes in the unperturbed bifurcation diagram. As shown in [37, 59], there are two qualitatively different bifurcation diagrams for  $\varepsilon \neq 0$  that depend on whether the quantity

$$\delta_{rev} = (w_f(L_M) - w_b(L_M))(w_f(L_m) - w_b(L_m))$$

is positive or negative. In both references, explicit perturbations, found by trial and error, were presented that yield either inequality. Here, we demonstrate that we can predict the sign of this quality a priori, using numerical computations of the unperturbed system only.

For the sake of clarity, we focus once more on the one-dimensional quadratic-cubic Swift–Hohenberg equation given by

$$u_t = -(1 + \partial_x^2)^2 u - \mu u + bu^2 - u^3 + \varepsilon g(u, u_x, u_{xx}, u_{xxx}),$$

where we added a perturbation  $g$  that breaks the reversibility operation  $x \mapsto -x$ . We can now determine the offset  $\mu' = d\mu/\varepsilon(0) = w_f(L_{M,m})$  as before separately at the left and right saddle-node bifurcations via

$$w_f(L_{M,m}) = \frac{\langle v_f, g(u_f(\cdot), u_f'(\cdot), u_f''(\cdot), u_f'''(\cdot)) \rangle_{L^2}}{\langle v_f, u_f \rangle_{L^2}},$$

where  $u_f$  is the unperturbed front solution at the left or right saddle-node, while  $v_f$  is the associated eigenfunction of the linearization of the unperturbed Swift–Hohenberg equation at  $\varepsilon = 0$ . A similar expression holds for  $w_b(L_{M,m})$ . Noting that the unperturbed front  $u_f$  and back  $u_b$  as well as the eigenfunctions  $v_f$  and  $v_b$  are related by symmetry, it is easy to show that we have

$$w_f(L_{M,m}) - w_b(L_{M,m}) = \frac{\langle v_f, [g(u_f(\cdot), u_f'(\cdot), u_f''(\cdot), u_f'''(\cdot)) - g(u_f(\cdot), -u_f'(\cdot), u_f''(\cdot), -u_f'''(\cdot))] \rangle_{L^2}}{\langle v_f, u_f \rangle_{L^2}}, \quad (3.8)$$

again with the convention that  $u_f$  and  $v_f$  are calculated at the folds corresponding to  $L = L_{M,m}$ .

Equation (3.8) can now be evaluated by computing  $u_f$  and  $v_f$  numerically. Recall that symmetric localized patterns of length  $2L$  arise by gluing a front and a back together. Hence, computing half of a localized pattern on a sufficiently large domain gives an accurate approximation of the front up to terms that are exponentially small in  $L$ .

## 6.4 Numerical confirmation of predictions

We now present several numerical studies supporting our analytical results. We examine perturbations breaking  $\mathbb{Z}_2$  symmetry, variational structure, and reversibility using the Swift–Hohenberg equations posed on both the line and the plane.

### 6.4.1 1D Swift–Hohenberg

In this section we illustrate how our analysis can be used to understand previously published work, and present new results. In Sections 6.4.1 and 6.4.1 we consider the family of equations

$$u_t = -(1 + \partial_x^2)^2 u - \mu u + \nu u^3 - u^5 + \varepsilon G(u) \quad (4.1)$$

posed on the real line, while in Section 6.4.1 we consider

$$u_t = -(1 + \partial_x^2)^2 u - \mu u + \nu u^2 - u^3 + \varepsilon G(u) \quad (4.2)$$

again posed on the real line, with a particular form for  $G(u)$  introduced in [37].

#### Breaking $\mathbb{Z}_2$ symmetry

The bifurcation diagram for (4.1) with  $G(u) = u^2$  was published in [26], and we have already seen how our analysis allows us to understand the form of the diagram. In addition to allowing us to predict the topological form of the bifurcation diagram given any perturbation, our approach has the added benefit of allowing us to under-

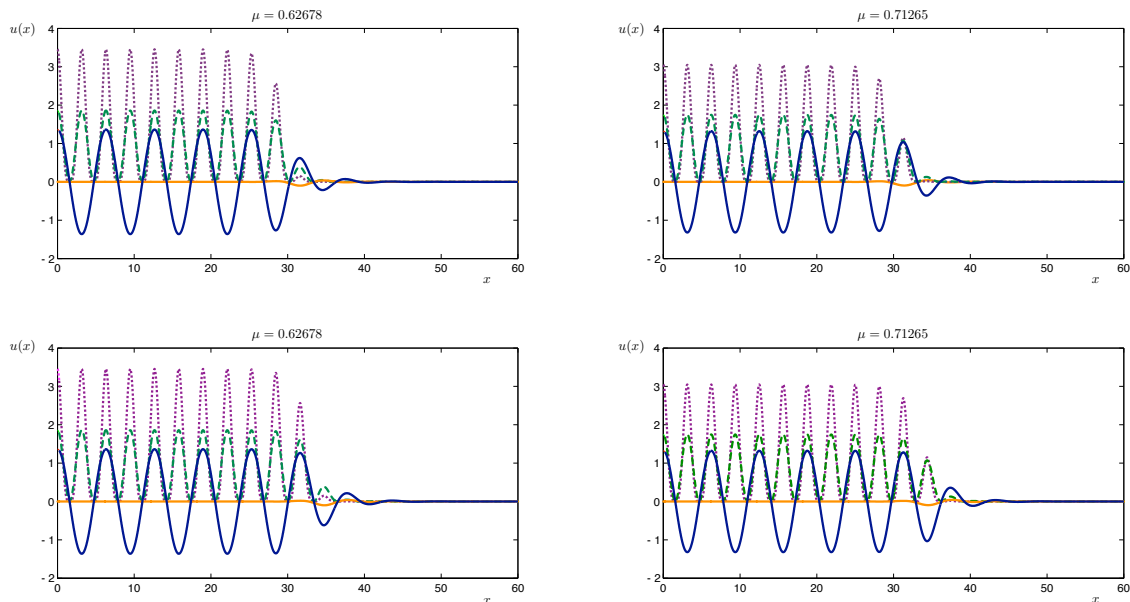


**Figure 6.7:** Four successive saddle nodes, i.e., one full  $2\pi$ -period along the snaking  $\mathcal{R}$ -symmetric branch, for the one-dimensional Swift–Hohenberg equation without perturbation. Solution  $u(x)$  in solid blue, saddle node eigenfunction  $v(x)$  in solid orange,  $G(u) = u^2$  in dashed green and  $G(u) = u^4$  in dotted purple.

stand particular features, such as the numerically observed unequal splitting on the left and right sides of snaking bifurcation diagrams, i.e., the fact that saddle nodes shift more on one side of the snaking diagram than on the other side upon introduction of symmetry breaking perturbative terms. Houghton and Knobloch noted this in their numerical study of symmetry-breaking in the one-dimensional cubic-quintic Swift–Hohenberg model, and we can see this in the numerically computed bifurcation diagrams shown in Figures 6.12a and 6.12b (or in Table 6.1) in Section 6.4.2, which exhibit greater displacement of the outer saddle nodes on the left compared to those on the right.

In Figure 6.7 we show four successive saddle nodes for the one-dimensional cubic-quintic Swift–Hohenberg equation prior to perturbation. We see that the solution  $u(x)$  at successive left-hand saddle nodes is related by  $u \mapsto -u$  symmetry, and similarly on the right. We also graph the saddle node eigenfunction  $v(x)$  and the perturbative terms  $u^2(x)$  and  $u^4(x)$ . Recalling that the offset will be determined

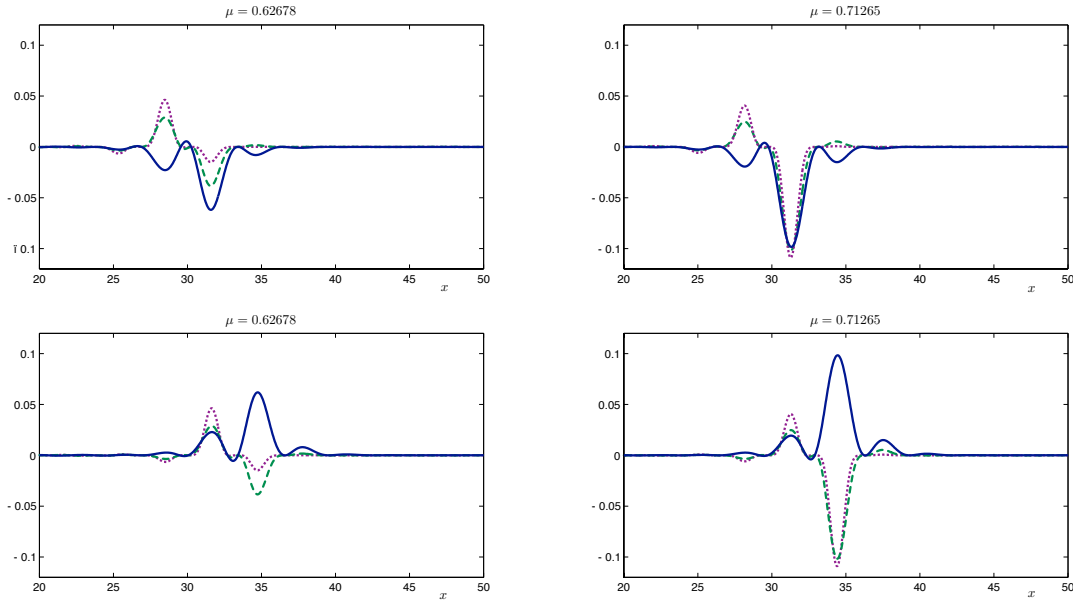


**Figure 6.8:** The same four successive saddle nodes as in Figure 6.7, but now showing the pointwise product of the eigenfunction  $v(x)$  with  $u(x)$ ,  $u^2(x)$ , and  $u^4(x)$ . The function  $(uv)(x)$  is shown in solid blue,  $(u^2v)(x)$  in dashed green and  $(u^4v)(x)$  in dotted purple.

by the ratio of the inner product  $\langle v, G(u) \rangle_{L^2}$  to  $\langle v, u \rangle_{L^2}$ , in Figure 6.8 we show the pointwise products of  $v(x)$  with  $u(x)$ ,  $u^2(x)$ , and  $u^4(x)$ . We observe that at the left saddle node, the peaks of  $(u^2v)(x)$  and  $(u^4v)(x)$  are approximately the same size, leading to a small value for  $\langle v, G(u) \rangle_{L^2}$ , which results in a smaller offset. On the other hand, for the saddle nodes on the right,  $u^2$  and  $u^4$  both exhibit a dominant peak, so that  $\langle v, G(u) \rangle_{L^2}$  is of similar order to  $\langle v, u \rangle_{L^2}$ , resulting in a larger offset. The difference between the signs of the offsets for  $G(u) = u^2$  and  $G(u) = u^4$  is somewhat more subtle, though as we have noted already, in the one-dimensional case all offsets lead to qualitatively similar bifurcation diagrams.

## Breaking variational structure

We next illustrate how our results can be used to understand the effects of the perturbation  $\varepsilon u_x^2$ , which breaks both the  $\mathbb{Z}_2$  symmetry and the variational structure

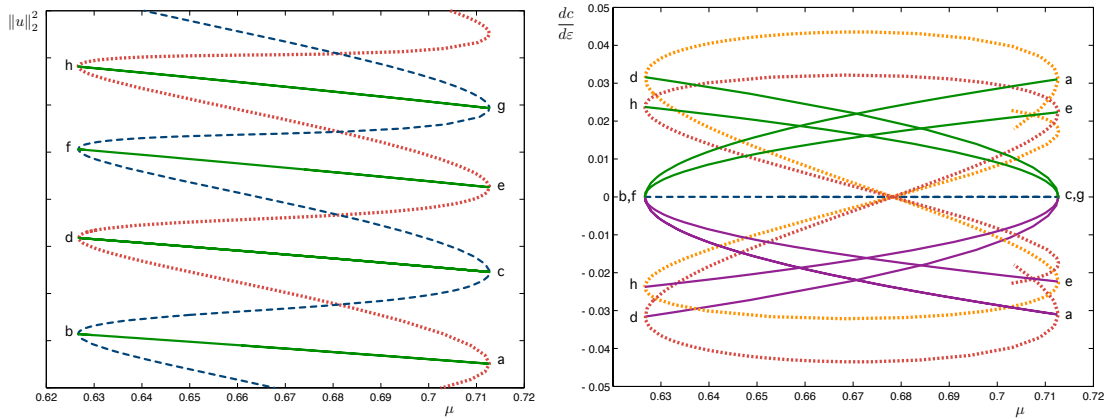


**Figure 6.9:** *Left:* Bifurcation diagram for the one-dimensional cubic-quintic Swift–Hohenberg equation, with  $\varepsilon = 0$ ; the  $\mathcal{R}$ -symmetric branch is shown in dashed blue,  $\kappa\mathcal{R}$ -symmetric branch in dotted orange, and four asymmetric branches in solid green. Saddle nodes are labeled (a) - (h) for comparison with right panel as well as left and right panels in Figure 6.10. *Right:*  $\frac{dc}{d\varepsilon}$  for the perturbation  $G(u) = u_x^2$ , computed along the unperturbed branches shown at left:  $\mathcal{R}$ -symmetric in dashed blue at 0;  $\kappa\mathcal{R}$ -symmetric in dotted light and dark orange for the two profiles that drift in opposite directions; and asymmetric branches in solid green and purple for the two sets of two profiles that drift in opposite directions. Labels (a) - (h) correspond to the saddle nodes indicated at left.

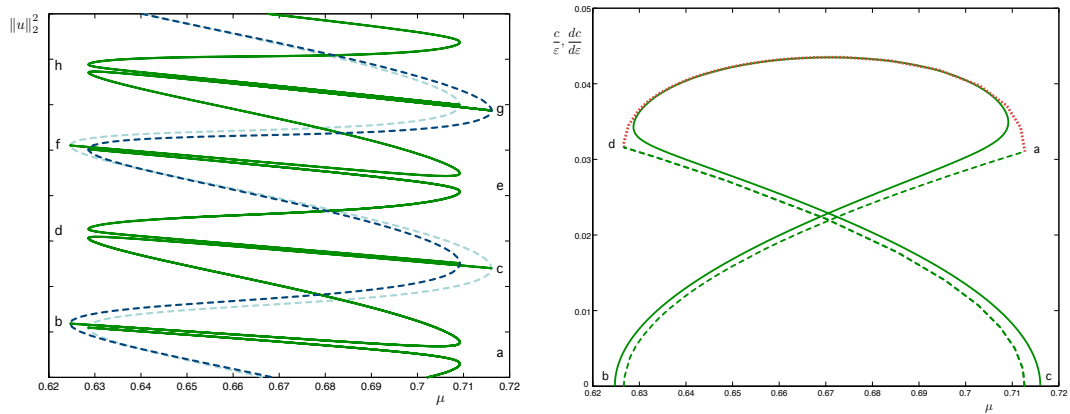


**Figure 6.10:** *Left:* Bifurcation diagram for (4.1) with  $G(u) = u_x^2$ , and  $\varepsilon = 0.01$ . One  $\mathcal{R}$ -symmetric branch is shown in dashed dark blue, and the other  $\mathcal{R}$ -symmetric branch is shown in dashed light blue. Asymmetric branches are shown in solid green. Labels (a) - (h) correspond to the saddle nodes indicated in Figure 6.9. Note that the asymmetric branch originating near (b) and terminating near (c) connects the  $\mathcal{R}$ -symmetric branches, as does that originating near (f) and terminating near (g). On the other hand the asymmetric branch originating near (c) and terminating near (f) begins and ends on the same dark blue  $\mathcal{R}$ -symmetric branch. The partial branches ending near (b) and originating near (g) both begin and end on the light blue  $\mathcal{R}$ -symmetric branch. *Right:* Solid green: the numerically observed drift speed,  $c$ , divided by  $\varepsilon = 0.01$  for an asymmetric branch with the perturbation  $G(u) = u_x^2$ . Dotted orange: computed value of  $\frac{dc}{d\varepsilon}$  along the relevant portion of the unperturbed  $\kappa\mathcal{R}$ -symmetric branch. Dashed green: computed value of  $\frac{dc}{d\varepsilon}$  along two successive unperturbed asymmetric branches. Labels (a) - (d) correspond to the saddle nodes indicated in Figure 6.9.

of (4.1). The bifurcation diagram for this equation was also studied in [26].

In Figure 6.9 on the left we show a partial bifurcation diagram for (4.1), and on the right of Figure 6.9 we show the predicted values of  $\frac{\partial c}{\partial \varepsilon}$  with the perturbative term  $\varepsilon G(u) = \varepsilon u_x^2$  for the same set of branches. The latter are computed from the unperturbed solution profiles using (3.2). The  $\mathcal{R}$ -symmetric branch consisting of two solutions will not move: though the variational structure is broken, the reverser  $\mathcal{R}$  remains upon introduction of  $\varepsilon$ . Conversely, the solutions along the  $\kappa\mathcal{R}$ -symmetric branch will begin to move since this reverser will no longer exist. We note that these observations are automatically encoded in the formula (3.2), and do not require any special enforcement. We also observe that the drift speeds are predicted to be largest low on the bifurcation diagram, and will decrease moving up along the bifurcation diagram, as noted in Section 6.3.1. With the exception of isolated solutions with zero predicted drift speed, we also further observe that at each point along the  $\kappa\mathcal{R}$  symmetric-branch, one solution will begin to drift with positive speed and the other with equal and opposite speed (i.e., one will drift left and the other right.) This is actually particular to the perturbation: the solutions are related by  $\kappa : u \mapsto -u$ , and in this case  $G(\kappa u) = G(u)$ . This also explains the alternating positive and negative signs of the drift speeds along the  $\kappa\mathcal{R}$  solution branch: the fronts at distance  $\pi$  (successive saddle nodes on the same side assuming one maximum per period  $\pi$ ) are related by  $\kappa$  symmetry, and thus must have opposite signs. Turning to the four sets of asymmetric solutions along each of the asymmetric branches, two are predicted to move with positive speed (green branches) and two with negative speed of equal magnitude (purple branches), again due to their relationships via symmetry. These speeds decrease moving up the bifurcation diagram, but we note that branches come in pairs, with the speeds along the first approximately mirroring the speeds along the next one up. Of course, on each asymmetric branch, the solutions near the  $\mathcal{R}$

branch will have drift speed near zero, while the solutions near a  $\kappa\mathcal{R}$  branch will match the speed of the branch to which they connect.

In Figure 6.10, we first show the perturbed bifurcation diagram with  $\varepsilon = .01$ , and then compare the predictions for  $\frac{\partial c}{\partial \varepsilon}$  from the right panel of Figure 6.9 with the drift speeds computed by direct numerical continuation. For clarity, we show the comparison for a single asymmetric branch: the drift speed  $c$  along the branch divided by  $\varepsilon = 0.01$  is shown in solid green, while the predicted values of  $\frac{\partial c}{\partial \varepsilon}$  computed along the relevant  $\kappa\mathcal{R}$ -symmetric and asymmetric branches are shown in dotted orange and dashed green, respectively. We further note that there is no relationship between distance from  $\kappa\mathcal{R}$  symmetry and drift speed: while solutions along the portion of the asymmetric branch derived from the  $\kappa\mathcal{R}$ -symmetric branch will remain close to possessing  $\kappa\mathcal{R}$  symmetry, they will have relatively large drift speeds. See also Figure 6.13 for plots of the distance from  $\kappa\mathcal{R}$  along asymmetric branches in the planar Swift–Hohenberg system.

### Breaking reversibility

Snaking systems without reversibility have been studied both in perturbative [37] and nonperturbative [59] regimes. Here we demonstrate that the methods described in Section 6.3.3 can be used to predict whether snaking or isolas will be observed. As a particular application, the system

$$u_t = -(1 + \partial_x^2)^2 u - \mu u + \nu u^2 - u^3 + \varepsilon(\tau(3u_x u_{xx}^2 + u_x^2 u_{xxx}) + (1 - \tau)(3u_x u_{xx})) \quad (4.3)$$

was considered in [37]<sup>2</sup> with  $\nu = 2$  and  $\varepsilon = 0.3$ . It was noted there that the term  $3u_x u_{xx}^2 + u_x^2 u_{xxx}$  alone leads to isolas, and  $3u_x u_{xx}$  alone to snaking. By repeatedly computing the full bifurcation diagram for many values of  $\tau$  (with  $\nu = 2$  and  $\varepsilon = 0.3$  fixed), it was determined in [37] that a transition between snaking and isolas occurs for  $\tau \approx 0.1$ . Here we use our methods to predict the value of  $\tau$  at which the switch from snaking to isolas occurs based only on the unperturbed bifurcation diagram, assuming that  $\varepsilon$  is small so that we are in a perturbative setting. We take the further step of computing this transition for a range of values of  $\nu$ . Using AUTO07P, we computed the unperturbed bifurcation diagram for  $\nu = 1.6$ , and then continued two successive saddle nodes in  $\mu$  and  $\nu$  to allow computation of the transition point across a range of  $\nu$  values. We then used the two saddle node solutions as described in Section 6.3.3 to predict the value of  $\tau$  at which the transition from snaking to isolas should occur for a range of values of  $\nu$ . This curve is plotted in the center panel of Figure 6.11. We also directly computed the bifurcation diagrams for selected values of  $\nu$  and  $\tau$  to confirm that they match our predictions. We note that the value of  $\tau$  we compute for  $\nu = 2$  is larger than that found in [37]; however, the value of  $\varepsilon$  used there is outside the perturbative regime.

## 6.4.2 Planar Swift–Hohenberg

In this section we will be interested in planar stripe and spot patterns of the cubic–quintic Swift–Hohenberg equation:

$$u_t = -(1 + \partial_x^2 + \partial_y^2)^2 u - \mu u + \nu u^3 - u^5, \quad (x, y) \in S^1 \times \mathbb{R} \quad (4.4)$$

---

<sup>2</sup>We use a minus sign in front of the  $\mu u$  term in contrast to [37] so that the region of interest is  $\mu > 0$  rather than  $\mu < 0$ . We also use  $\varepsilon$  instead of  $\lambda$  for consistency with the rest of our paper.

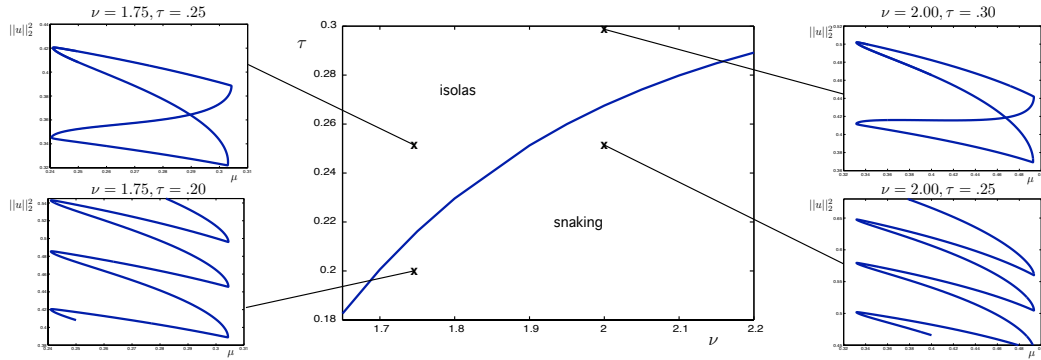


**Figure 6.11:** Center panel: Value of  $\tau$  at which transition from snaking to isolas occurs as a function of  $\nu$ , as predicted from the unperturbed bifurcation diagram. Side panels: Bifurcation diagrams for (4.3) with  $\varepsilon = 0.01$  and values of  $\nu$  and  $\tau$  as indicated above each plot and by  $x$ 's in the center panel, confirming predictions.

where  $S^1 = \mathbb{R}/2L_x\mathbb{Z}$  for some  $L_x > 0$ .

We begin by observing that these patterns have the bifurcation structure diagrammed in Figure 6.4 of Section 6.2 above; see Figure 3.3 in Section 3.4. We are not certain why the stripe and spot patterns possess a function  $z$  with two maxima and minima per period  $\pi$ ; we believe these patterns arise in a transverse pitchfork bifurcation which may be related to secondary snaking, but have left this line of investigation for future work.

### Breaking $\mathbb{Z}_2$ symmetry

As noted in Section 6.3.2, computations made only on an unperturbed snaking system allow us to predict the bifurcation diagram resulting from any particular perturbative term. Furthermore, having performed these calculations once, the marginal cost of analyzing the result of any number of alternative perturbations is minimal.

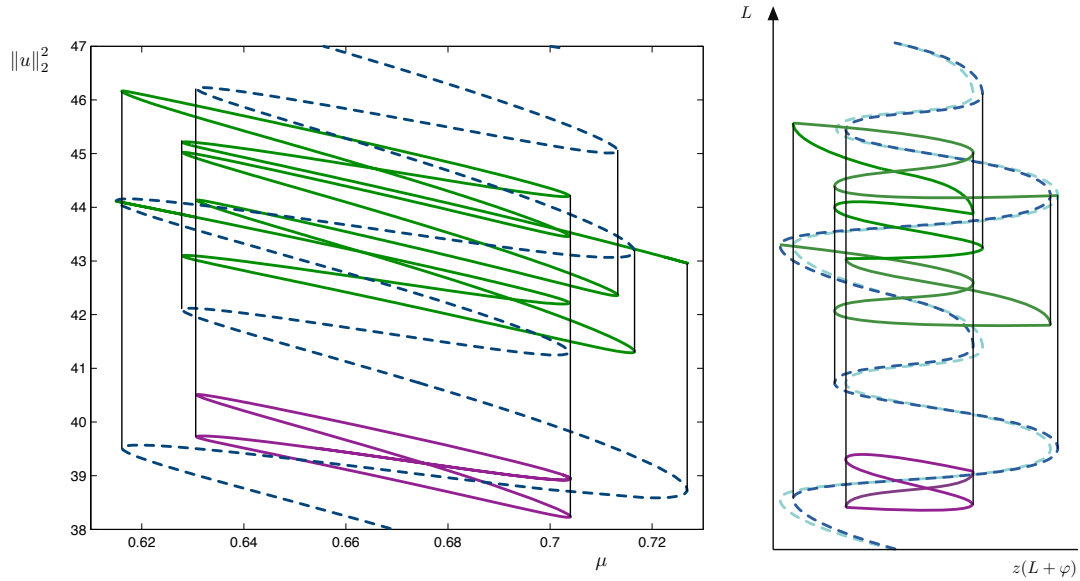
In Table 6.1 we show the results of solving for  $\mu_\varepsilon^0$  using the linear system (3.6):

$\mu$ at saddle node	$G(u) = u^2$		$G(u) = u^4$	
	observed offset	calculated offset	observed offset	calculated offset
0.7084	-0.4472	-0.4322	-0.2996	-0.2833
0.6156	-0.0426	-0.0470	0.1667	0.1612
0.7218	-0.4713	-0.4668	-0.3581	-0.3585
0.6294	0.1231	0.1235	-0.2331	-0.2237
0.7084	0.4361	0.4269	0.2669	0.2883
0.6156	0.0611	0.0514	-0.1508	-0.1590
0.7218	0.4833	0.4669	0.3581	0.3575
0.6294	-0.1352	-0.1228	0.2083	0.2241

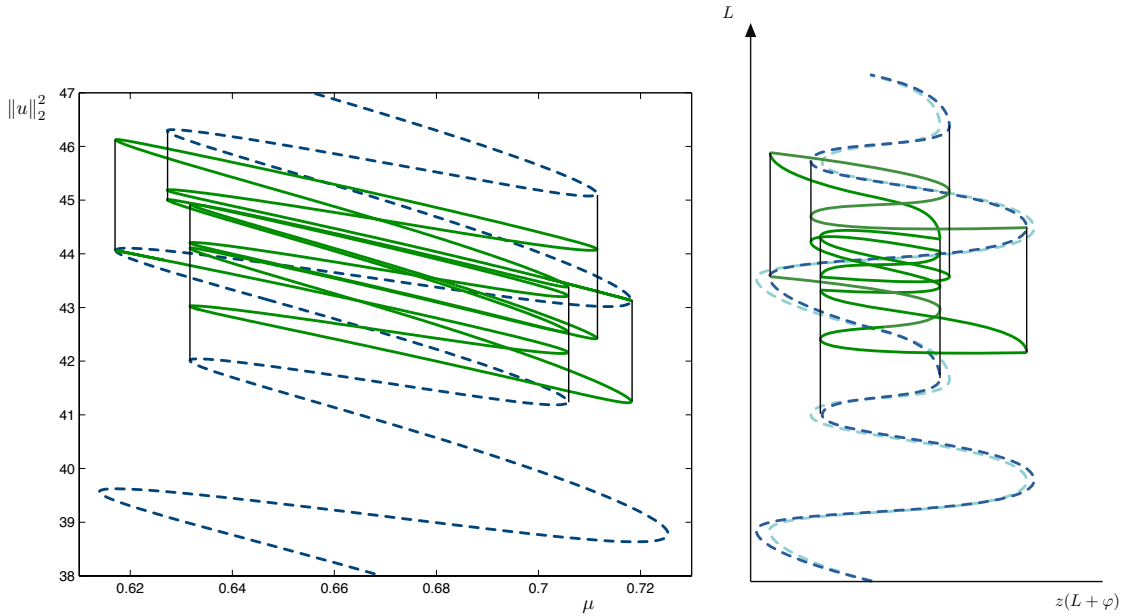
**Table 6.1:** Observed and calculated offsets over 8 saddle nodes, i.e., a full  $2\pi$  period of the function  $z$ , for the planar stripe and spot pattern of (4.4), with additional perturbative term  $\varepsilon G(u)$  as indicated. The values of  $\varepsilon$  used in the continuation were  $\varepsilon = -0.0108$  for  $G(u) = u^2$ , and  $\varepsilon = 0.01008$  for  $G(u) = u^4$ .

the calculated offset is the value of  $\mu_\varepsilon^0$ , computed by solving the linear system (3.6) at a saved solution  $(u, \mu)$  near each saddle node in the original  $\varepsilon = 0$  bifurcation diagram. The observed offset is the difference between the original  $\mu$  at the saddle node and that seen in numerical continuation for the perturbed system, divided by the  $\varepsilon$  used in the continuation. We note that finer meshes (e.g., 16 Fourier modes instead of 8) and more accurate calculation of the saddle node locations lead to somewhat higher accuracy, but since there is already some difference in the absolute value of the offsets at successive saddle nodes at distance  $\pi$ , e.g., between the second and sixth saddle nodes in Table 1, there are nonlinear effects which would necessitate the inclusion of higher order derivatives in  $\varepsilon$  for a complete match. Nonetheless, we see that the agreement is quite good.

For the purposes of predicting the form of the bifurcation structure, we only need the sign of the offset at the saddle nodes. In particular, to decide whether our perturbed bifurcation diagram will feature isolas, the question is simply whether adjacent inner saddle nodes are offset in the same direction. Thus we see that with



(a) *Left*: Partial bifurcation diagram for (4.5) with  $\varepsilon = -0.01$ , showing one of two  $\mathcal{R}$ -symmetric branches in dashed blue, an isola in solid purple, and a cross-connecting asymmetric branch in solid green. The cross-connecting asymmetric branch extends beyond the  $\mathcal{R}$ -symmetric branch as it terminates at the other  $\mathcal{R}$ -symmetric branch with phase  $\varphi = \pi$  (not shown.) *Right*: Reproduction of the predicted bifurcation diagram from Figure 6.5.



(b) *Left*: Partial bifurcation diagram for (4.6) with  $\varepsilon = -0.01$ , showing one of two  $\mathcal{R}$ -symmetric branches in dashed blue, and a self-connecting asymmetric branch in solid green. *Right*: Reproduction of the predicted bifurcation diagram from Figure 6.6.

**Figure 6.12:** Comparison of numerically computed bifurcation diagrams for (4.5) and (4.6) with predicted bifurcation diagrams according to the analysis in Section 6.2. Vertical lines indicate the correspondence between the extrema (saddle nodes) of the  $\mathcal{R}$ -symmetric branch and the saddle nodes of the asymmetric branches, including the isola.

the perturbative term  $\varepsilon u^2$ , i.e.,

$$u_t = -(1 + \Delta)^2 u - \mu u + \nu u^3 - u^5 + \varepsilon u^2, \quad (4.5)$$

adjacent inner saddle nodes at  $\mu = 0.7084$  and  $\mu = 0.6156$  are offset in the same direction, and thus the perturbed bifurcation diagram will be of the form depicted in Figure 6.5 of Section 6.2. By direct numerical continuation, we find that we do indeed observe the predicted isolas bifurcating where we expect them, as shown in Figure 6.12a, as well as Figure 6.13, left panel. We can also calculate the distance from  $\kappa\mathcal{R}$  symmetry for each solution lying along the branch; doing this for the isola, we note that the middle portion is indeed almost perfectly  $\kappa\mathcal{R}$  symmetric, as expected; see Figure 6.13, center and right panels.

On the other hand, our calculated offsets from Table 6.1 show that the perturbative term  $\varepsilon u^4$  causes adjacent saddle equilibria to move in opposite directions, or equivalently that one local extremum moves up while the other to moves down relative to the local extrema at distance  $\pi$ . Consequently this bifurcation diagram corresponds to the schematic displayed in Figure 6.6. In Figure 6.12b we show the results of numerical continuation on the planar stripe and spot patterns with perturbative term  $\varepsilon u^4$ , i.e.,

$$u_t = -(1 + \Delta)^2 u - \mu u + \nu u^3 - u^5 + \varepsilon u^4 \quad (4.6)$$

and see that bifurcation diagram has the anticipated form.

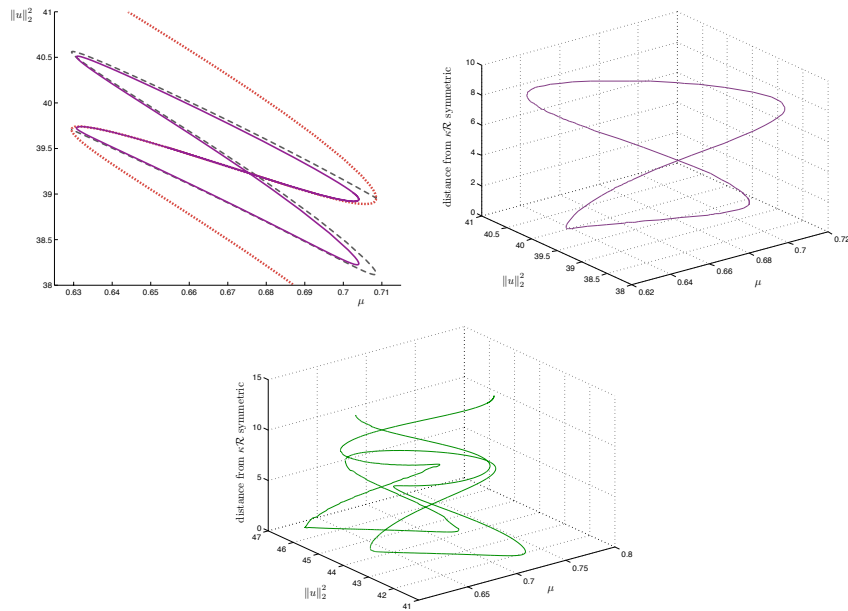


**Figure 6.13:** *Left:* For comparison purposes, the isola for (4.5) with  $\varepsilon = -0.01$  is shown in solid purple, along with the original ( $\varepsilon = 0$ )  $\kappa\mathcal{R}$ -symmetric branch in dotted orange, and the original ( $\varepsilon = 0$ ) self-connecting asymmetric branch in dashed gray. *Center:* Another view of the isola, demonstrating that the symmetries are consistent with construction by combining a portion of the  $\kappa\mathcal{R}$  symmetric solution branch with an asymmetric solution branch. The distance from  $\kappa\mathcal{R}$ -symmetry is computed as the  $L^2$  norm of the difference between a given solution profile and the profile obtained by flipping across the  $y$ -axis, shifting by  $\pi$  in the  $x$ -direction, and multiplying by  $-1$ . Due to the approximate translation invariance of the solutions, this difference is minimized over translations in  $y$ . *Right:* A view of the cross-connecting branch found above, also consistent with construction via combination of  $\kappa\mathcal{R}$ -symmetric and asymmetric branches.

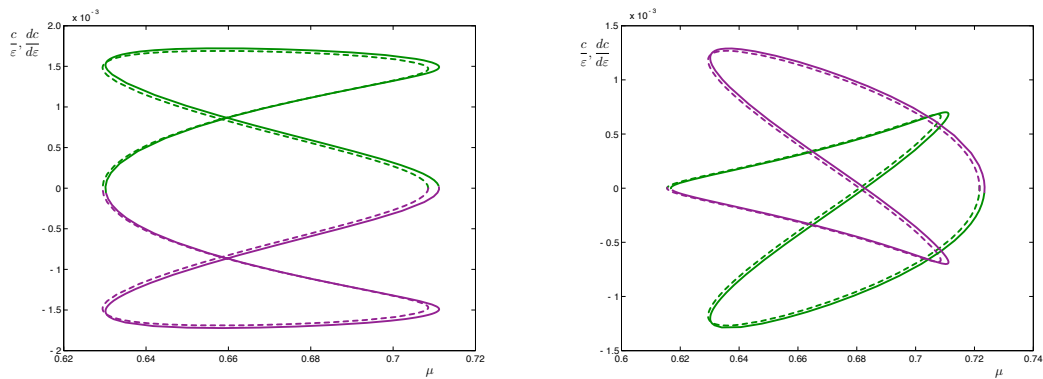


**Figure 6.14:** Comparison of predicted and observed speeds for stripe and spot solutions to (4.7). The left panel corresponds to a self-connecting asymmetric branch, while the right panel corresponds to a cross-connecting asymmetric branch. Dashed lines indicate predicted speeds calculated from the unperturbed solution branches via (3.2), and solid lines indicate speeds observed via numerical continuation with  $\varepsilon = 0.01$ . Purple and green correspond to solutions on either side of the pitchfork bifurcations.

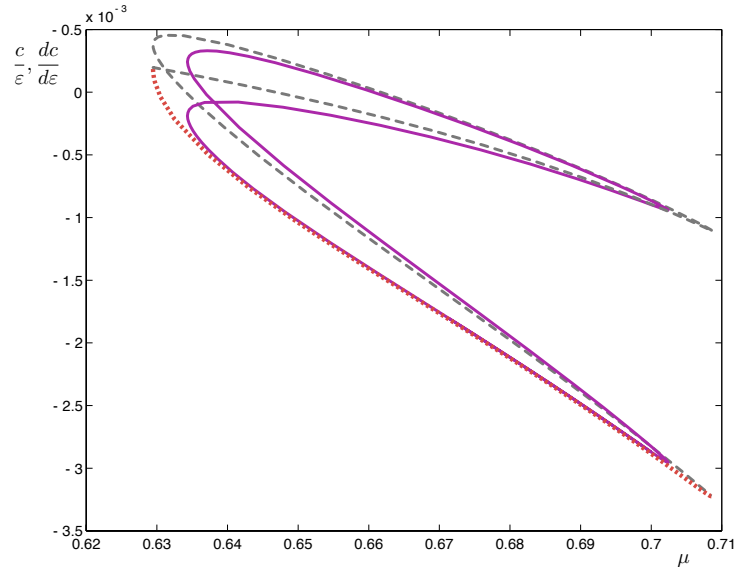


**Figure 6.15:** Computed speed (solid purple) via numerical continuation along a newly formed isola, and predicted speeds from the appropriate original asymmetric branch (dashed grey) and relevant portion of the  $\kappa\mathcal{R}$ -symmetric branch (dotted orange), for the system (4.8) with  $\varepsilon = 0.01$ .

### Breaking variational structure

Turning to perturbations which break the variational structure, we first consider the perturbed system

$$u_t = -(1 + \Delta)^2 u - \mu u + \nu u^3 - u^5 + \varepsilon u u_x^2, \quad (4.7)$$

which breaks the variational structure of (4.4) without breaking the additional  $\kappa$  symmetry. We therefore expect no changes to the topological structure of the bifurcation diagram of localized stripe and spot solutions as a result of the perturbative term, and indeed see none (not shown.) However, we expect that the asymmetric solutions will begin to drift. In Figure 6.14 we plot the predicted and observed drift speeds for solutions along self-connecting and cross-connecting asymmetric branches; in each case we see excellent agreement.

We next consider the perturbed system

$$u_t = -(1 + \Delta)^2 u - \mu u + \nu u^3 - u^5 + \varepsilon u_x^2, \quad (4.8)$$

which breaks both the variational structure of (4.4) as well as the additional  $\kappa$  symmetry. Using (3.7) computed along the  $\mathcal{R}$ -symmetric branch of stripe and spot solutions, we find that the perturbation  $u_x^2$  will lead to the formation of isolas, and in Figure 6.15 we compare the drift speed observed via numerical continuation along such an isola with the speeds predicted by evaluating (3.2) along the appropriate sections of the unperturbed  $\kappa\mathcal{R}$ -symmetric and asymmetric branches. There is of course some difference in the speeds due to the (anticipated) branch reorganization at the outer limits of the isola, but we again see that the agreement is quite good.

# CHAPTER SEVEN

---

## Conclusion

In the preceding, we have rigorously shown that both symmetric and asymmetric solutions may be constructed by combining front and back solutions, and that the resulting localized solutions are exponentially close in the length  $L$  of the patterned region to the underlying fronts and backs. We have also illustrated this construction numerically.

We then used this formulation to demonstrate that in the right half plane, eigenvalues of the localized solution are exponentially close in  $L$  to those of the front and back, and are added with multiplicity. Consequently, if the underlying front and back have no eigenvalues in the open right half plane, the only possible scenario leading to eigenvalues of the localized solution in the open right half plane would be the creation of a pair eigenvalues near the origin, assuming that the front and back each have simple translation eigenvalues. This is the situation for monotone pulses, but we show it does not occur here.

To address this last point, we constructed an extended Evans function of the front, necessitated by the fact that the essential spectrum of the periodic solution extends up to the imaginary axis. We then demonstrated that there is a single eigenvalue of the localized solution in the closed right half plane near  $\lambda = 0$ , which consequently sits at  $\lambda = 0$  due to translation invariance, and no additional eigenvalues are created for the localized solution near 0. In summary, we have shown that if the front and back have no eigenvalues in the open right half plane, then neither do the localized solutions.

Finally, we have predicted on analytical grounds the evolution of localized snaking solutions and bifurcation branches in the presence of perturbative terms, and provided a new approach to the *a priori* prediction of the effects of perturbative terms, including predicting the drift speeds of one and two-dimensional patterns in the pres-

ence of perturbations breaking variational structure. We have used this method, or collection of related methods, in a number of numerical demonstrations.

One interesting line of inquiry raised in the preceding concerns the appearance of numerically computed spectra, in which eigenvalues persist upon entering the essential spectrum of the wave trains, as was seen in [3, 8], and here in Figures 4.3, for example. As noted previously, this behavior is unexpected in the context of [31, 32]. We have provided an initial explanation of this phenomenon, which is consistent both qualitatively and quantitatively with the observed numerical behavior, and we believe that the framework provided in Chapter 5 is the appropriate one in which to address this phenomenon. However, our current understanding does yet not seem sufficient to predict how systems will behave upon perturbation, for example, or to categorize which systems generically do or do not support this type of behavior.

Moving beyond the present work, localized hexagon patches (see, for example, [41] and Figure 1.9) and other fully localized structures in two or higher dimensions remain challenging phenomena where even the bifurcation structures remain poorly understood. There is numerical and theoretical support for the role of Bravais-Miller indices of interfaces between patterned and homogeneous states in determining the snaking limits of the bifurcation diagrams; see again [41], as well as [39], the latter of which employs an asymptotics beyond all orders approach. Nonetheless, rigorous analysis of fully localized structures in multiple dimensions seems to require a wholly new mathematical approach, and it is not yet clear what such an approach would be, though very recent advances replacing spatial dynamics techniques with Fredholm operator operator analysis, e.g., [22], may enable progress in this direction. At the same time, advances in computing power should make the numerical computation of bifurcation diagrams for fully localized structures less onerous, which may lead to new insights.

# APPENDIX A

---

## Foundational Theorems, Definitions and Formulae

## A.1 Exponential dichotomies

**Definition 1.1.1.** *Consider the system*

$$u_x = A(x, \lambda)u, \quad (1.1)$$

with  $(u, \lambda) \in \mathbb{C}^n \times \mathbb{C}$ ,  $x \in \mathbb{R}$  and  $A(\cdot, \lambda) \in C^0(\mathbb{R}, \mathbb{C}^{n \times n})$ . We denote the evolution operator associated with (1.1) by  $\Phi(x, y; \lambda)$ . For a fixed  $\lambda = \lambda_*$ , and  $I = \mathbb{R}^+, \mathbb{R}^-$ , or  $\mathbb{R}$  we say that (1.1) has an exponential dichotomy on  $I$  if the following holds: there exist constants  $C > 0$  and  $\alpha^s < 0 < \alpha^u$  and projections  $P(x)$  defined and continuous for  $x \in I$  such that

- With  $\Phi^s(x, y; \lambda_*) := P(x)\Phi(x, y; \lambda_*)$ ,

$$|\Phi^s(x, y; \lambda_*)| \leq Ce^{\alpha^s|x-y|}, \quad x \geq y, \quad x, y \in I. \quad (1.2)$$

- With  $\Phi^u(x, y; \lambda_*) := (id - P(x))\Phi(x, y; \lambda_*)$ ,

$$|\Phi^u(x, y; \lambda_*)| \leq Ce^{-\alpha^u|x-y|}, \quad x \leq y, \quad x, y \in I. \quad (1.3)$$

- The projections commute with the evolution operators, i.e.,  $\Phi(x, y)P(y) = P(x)\Phi(x, y)$ , so that

$$\Phi^s(x, y)u_0 \in \text{Rg}(P(x)), \quad x \geq y, \quad x, y \in I \quad (1.4)$$

$$\Phi^u(x, y)u_0 \in \text{N}(P(x)), \quad x \leq y, \quad x, y \in I. \quad (1.5)$$

The existence of exponential dichotomies are a useful tool in both existence and stability results. As such, we consider exponential dichotomies with dependence

either: (1) on a general system parameter, e.g.,  $\mu$  rather than  $\lambda$ , in which case we assume some smoothness of  $A$  in the parameter(s) but generally not analyticity; or (2) on a parameter  $\lambda$  arising from a stability problem, in which case we enforce analyticity of  $A$  in  $\lambda$ .

**Remark 1.1.2.** *If (1.1) has an exponential dichotomy on  $I$  with  $\lambda = \lambda_*$ , and  $A$  is analytic in  $\lambda$ , the projections and evolution operators in Definition 1.1.1 may be chosen to depend analytically on  $\lambda \in U_\delta(\lambda_*)$  for some  $\delta > 0$ .*

**Remark 1.1.3.** *We may in fact weaken the condition  $\alpha^s < 0 < \alpha^u$  in Definition 1.1.1 to  $\alpha^s < \alpha^u$ , corresponding to the existence of a spectral gap not necessarily at 0. Depending on the context, we may write the associated dichotomies as  $\Phi^{cs}(x, y)$  and  $\Phi^u(x, y)$  when considering a gap at  $\eta > 0$ , or as  $\Phi^s(x, y)$  and  $\Phi^{cu}(x, y)$  for a gap at  $\eta < 0$ .*

We will also make use of the roughness theorem for exponential dichotomies:

**Theorem 1.1.** *([11]) Let  $I = \mathbb{R}^+$  or  $\mathbb{R}^-$ . Suppose that for  $\lambda = \lambda_*$ , (1.1) has an exponential dichotomy on  $I$  with constants  $C, \alpha^s, \alpha^u$ . There are positive constants  $\delta_*$  and  $K$  such that the following is true. If  $B(\cdot) \in C^0(I, \mathbb{C}^{n \times n})$  such that  $\sup_{x \in I, |x| \geq L} |B(x)| < \delta/K$  for some  $\delta < \delta_*$  and  $L \geq 0$ , then there exists a  $\tilde{C} > 0$  such that*

$$u_x = (A(x, \lambda_*) + B(x))u, \quad (1.6)$$

*has an exponential dichotomy on  $I$  with constants  $\tilde{C}, \alpha^s + \delta, \alpha^u - \delta$ . Moreover, the projections  $P(x)$  and evolution operators  $\Phi^s(x, y)$  and  $\Phi^u(x, y)$  associated with (1.6) are  $\delta$ -close to those associated with (1.1) for all  $x, y \in I$  with  $|x|, |y| \geq L$ . If  $I = \mathbb{R}$ , the above holds with  $L = 0$ .*

## A.2 Variation of constants with exponential dichotomies

In working with systems for which we have exponential dichotomies, we will frequently use the following strategy, or variations thereof.

First suppose we have a system

$$u_x = A(x)u \tag{2.1}$$

with associated evolution operator  $\Phi(x, y)$ . Then the solution of the initial value problem

$$u_x = A(x)u + g(x, u), \quad u(x_0) = u_0 \tag{2.2}$$

is given by:

$$u(x) = \Phi(x, x_0)u_0 + \int_{x_0}^x \Phi(x, s)g(s, u(s))ds. \tag{2.3}$$

We refer to this result as the variation of constants formula.

Now suppose the system (2.1) has exponential dichotomies  $\Phi^s(x, y)$  and  $\Phi^u(x, y)$  on  $I$ , and we are interested in finding a general solution to

$$u_x = A(x)u + g(x, u) \tag{2.4}$$

for  $x \in [x_1, x_2] \subset I$ . Then by the variation of constants formula we have

$$u(x) = \Phi(x, x_1)u(x_1) + \int_{x_1}^x \Phi(x, s)g(s, u(s))ds. \tag{2.5}$$

Applying  $P^s(x)$  to this yields

$$P^s(x)u(x) = \Phi^s(x, x_1)u(x_1) + \int_{x_1}^x \Phi^s(x, s)g(s, u(s))ds. \quad (2.6)$$

Similarly, we have

$$u(x) = \Phi(x, x_2)u(x_2) + \int_{x_2}^x \Phi(x, s)g(s, u(s))ds \quad (2.7)$$

so that

$$P^s(x)u(x) = \Phi^s(x, x_1)u(x_2) + \int_{x_1}^x \Phi^s(x, s)g(s, u(s))ds. \quad (2.8)$$

Since  $P^s(x) + P^u(x) = id$ , we can combine these expressions to get

$$u(x) = \Phi^s(x, x_1)u(x_1) + \int_{x_1}^x \Phi^s(x, s)g(s, u(s))ds + \Phi^u(x, x_2)u(x_2) + \int_{x_2}^x \Phi^u(x, s)g(s, u(s))ds \quad (2.9)$$

or, letting  $a, b$  be arbitrary elements with  $a \in \text{Rg } P^s(x_1)$  and  $b \in \text{Rg } P^u(x_2)$ ,

$$u(x) = \Phi^s(x, x_1)a + \int_{x_1}^x \Phi^s(x, s)g(s, u(s))ds + \Phi^u(x, x_2)b + \int_{x_2}^x \Phi^u(x, s)g(s, u(s))ds \quad (2.10)$$

We note that we can and will apply this in a parameter dependent fashion, as well as in situations where we have a spectral gap rather than hyperbolic matrices, as in Remark 1.1.3 above.

# APPENDIX B

---

## Elements of Spectral Stability Analysis

In the following we relate spectral properties of the operator  $\mathcal{L}$ , arising from the linearization of a PDE about a traveling wave, to exponential dichotomies of the corresponding ODE, and to Fredholm properties of the corresponding operator  $\mathcal{T}(\lambda)$ . We note that this material—and much more—is covered in [56] along with examples and extensive references. The recent book [29] also provides an excellent reference.

## B.1 Setting the stage: PDE and ODE formulations

We consider PDEs of the form

$$U_t = \mathcal{A}(\partial_x)U + \mathcal{N}(U, \mu), \quad x \in \mathbb{R}, \quad U \in \mathcal{X}, \quad \mu \in \mathbb{R} \quad (1.1)$$

where  $\mathcal{A}(\cdot)$  is a vector-valued polynomial,  $\mathcal{X}$  is a Banach space of functions  $U(x)$  so that  $\mathcal{A}(\partial_x) : \mathcal{X} \rightarrow \mathcal{X}$  is closed and densely defined, and  $\mathcal{N} : \mathcal{X} \times \mathbb{R} \rightarrow \mathcal{X}$  is some nonlinearity defined for each  $\mu$  via pointwise evaluation of  $U$  and possibly derivatives of  $U$ .

We note that temporally stationary solutions  $U(x, t) = U(x)$  of (1.1) correspond to solutions of the first-order ODE

$$u_x = f(u, \mu), \quad (1.2)$$

where  $u = (U, U_x, \dots)^T \in \mathbb{R}^n$  and  $n$  is the order of the polynomial  $\mathcal{A}$ , for an appropriately defined  $f$ . See Section 2.1 for an example. We can of course generalize this to treat traveling wave solutions, i.e., solutions  $U(x, t) = Q(x - ct)$  by introducing

the variable  $\xi = x - ct$ , but we will focus on stationary solutions in the following.

Now given a particular (possibly parameter-dependent) stationary solution  $Q(x, \mu)$  of the PDE (1.1), we have the associated linear operator

$$\mathcal{L}U := \mathcal{A}(\partial_x)U + \partial_U \mathcal{N}(Q(x, \mu), \mu)U \quad (1.3)$$

and associated eigenvalue problem

$$\lambda U = \mathcal{L}U. \quad (1.4)$$

We then have the associated first order system

$$u_x = [f_u(q(x, \mu), \mu) + \lambda B(x)]u =: [\hat{A}(x) + \lambda B(x)]u =: A(x, \lambda)u \quad (1.5)$$

where  $u(x) = (U, U_x, \dots)^T \in \mathbb{C}^n$  and  $q(x, \mu) = (Q, Q_x, \dots)^T \in \mathbb{R}^n$ . We assume  $\hat{A}(\cdot)$  and  $B(\cdot)$  are in  $C^\infty(\mathbb{R}, \mathbb{R}^{n \times n})$

The relationship between the spectrum of  $\mathcal{L}$  defined in (1.3) and the system (1.5) is the focus of the following.

## B.2 The operator family $\mathcal{T}(\lambda)$ , Fredholm properties and exponential dichotomies

We now define the family of linear operators

$$\begin{aligned} \mathcal{T}(\lambda) : \mathcal{D} &\rightarrow \mathcal{H} \\ u &\mapsto \frac{du}{dx} - A(\cdot; \lambda)u \end{aligned} \quad (2.1)$$

with  $\lambda \in \mathbb{C}$  and either  $\mathcal{D} = C_{unif}^1(\mathbb{R}, \mathbb{C}^n)$ ,  $\mathcal{H} = C_{unif}^0(\mathbb{R}, \mathbb{C}^n)$  or  $\mathcal{D} = H^1(\mathbb{R}, \mathbb{C}^n)$ ,  $\mathcal{H} = L^2(\mathbb{R}, \mathbb{C}^n)$ .

**Definition 2.2.1.** *The spectrum  $\Sigma$  of  $\mathcal{T}$  consists of all  $\lambda$  such that  $\mathcal{T}(\lambda)$  is not invertible. The resolvent set of  $\mathcal{T}$  is the complement of  $\Sigma$  in  $\mathbb{C}$ . We will sometimes denote the resolvent set by  $\rho(\mathcal{T})$ .*

Before defining the point spectrum and essential spectrum of  $\mathcal{T}$ , we recall the definition of Fredholm operators:

**Definition 2.2.2.** *An operator  $\mathcal{L} : \mathcal{X} \rightarrow \mathcal{Y}$  is a Fredholm operator if  $\text{Rg}(\mathcal{L})$  is closed in  $\mathcal{Y}$  and both  $\dim \text{N}(\mathcal{L})$  and  $\text{codim } \text{Rg}(\mathcal{L})$  are finite. The Fredholm index of a Fredholm operator is a measure of the solvability of  $\mathcal{L}x = y$ , and is defined as  $\dim \text{N}(\mathcal{L}) - \text{codim } \text{Rg}(\mathcal{L})$ .*

We then define the point spectrum and essential spectrum of  $\mathcal{T}$ :

**Definition 2.2.3.** *The point spectrum  $\Sigma_{pt}$  of  $\mathcal{T}$  consists of all  $\lambda \in \Sigma$  such that  $\mathcal{T}(\lambda)$  is Fredholm with index zero. Elements of  $\Sigma_{pt}$  are also referred to as eigenvalues. The essential spectrum of  $\mathcal{T}$  is the complement of the point spectrum:  $\Sigma_{ess} = \Sigma \setminus \Sigma_{pt}$ .*

We note that the above definition differs slightly from the definition of the point spectrum as all isolated eigenvalues with finite multiplicity. The latter is equivalent to the set of  $\lambda$  such that  $\mathcal{T}(\lambda)$  is Fredholm with index 0, has nontrivial null space, and is invertible for all  $\tilde{\lambda}$  in a small neighborhood of  $\lambda$ , whereas this last requirement is not part of our definition. The set of  $\lambda$  such that  $\mathcal{T}(\lambda)$  has Fredholm index 0 is open, and taking any connected component  $\mathcal{C}$  of this set, we have that either all  $\mathcal{T}(\lambda)$  is invertible for all but a discrete set of elements of  $\mathcal{C}$ , or that  $\mathcal{T}(\lambda)$  has nontrivial null space and so is not invertible for all  $\lambda$  in  $\mathcal{C}$ . Generically, and in all cases we will study, we expect that the first of these possibilities occurs.

We now define the multiplicity of  $\lambda \in \Sigma_{pt}$  for  $\mathcal{T}$ . We first suppose  $\lambda$  is such that  $N(\mathcal{T}(\lambda)) = \text{span}\{u_1\}$ . In this case  $\lambda$  has multiplicity  $\ell$  if there exist  $u_j \in \mathcal{D}$  with  $j = 2, \dots, \ell$  such that

$$\frac{d}{dx}u_j = (\hat{A}(x) + \lambda B(x))u_j(x) + B(x)u_{j-1}(x)$$

but there does not exist a solution  $u \in \mathcal{D}$  of the equation

$$\frac{d}{dx}u = (\hat{A}(x) + \lambda B(x))u(x) + B(x)u_\ell(x).$$

The multiplicity of a general  $\lambda \in \Sigma_{pt}$  is then defined as the sum of the multiplicities of the elements spanning  $N(\mathcal{T}(\lambda))$ .

In the case of a reaction diffusion system, it can be shown that the Fredholm properties and Fredholm indices of  $\mathcal{T}$  and  $\mathcal{L} - \lambda$  as defined in (1.3) are the same. Moreover for any  $\lambda$  in the spectrum of  $\mathcal{L}$  and  $\mathcal{T}$ , the Jordan-block structures of  $\mathcal{L} - \lambda$  and  $\mathcal{T}(\lambda)$  are the same, which justifies the above definition of multiplicity.

We now have the following theorem due to Palmer [48, 49]:

**Theorem 2.1.** *For any fixed  $\lambda$  in  $\mathbb{C}$ , the following hold:*

- (i)  $\lambda \in \rho(\mathcal{T})$ , the resolvent set of  $\mathcal{T}$ , if and only if (1.5) has an exponential dichotomy on  $\mathbb{R}$ .
- (ii)  $\lambda \in \Sigma_{pt}$ , the point spectrum of  $\mathcal{T}$ , if and only if (1.5) has an exponential dichotomies on  $\mathbb{R}^+$  and  $\mathbb{R}^-$  with the same Morse index  $i_+(\lambda) = i_-(\lambda)$ .
- (iii)  $\lambda \in \Sigma_{ess}$ , the essential spectrum of  $\mathcal{T}$ , if and only if either (1.5) does not have an exponential dichotomy on  $\mathbb{R}^+$  and  $\mathbb{R}^-$ , or it does but the Morse indices  $i_+(\lambda)$  and  $i_-(\lambda)$  differ.

We note in particular that  $\mathcal{T}$  is Fredholm if and only if (1.5) has exponential dichotomies on  $\mathbb{R}^+$  and  $\mathbb{R}^-$ . We also have from [48, 49] that the Fredholm index of the operator  $\mathcal{T}$  is given by the difference in the Morse indices of the exponential dichotomies on  $\mathbb{R}^+$  and  $\mathbb{R}^-$ .

### B.3 Locating the essential spectrum

The essential spectrum is usually easier to locate than the point spectrum; for stationary solutions which are asymptotically constant or periodic, locating the essential spectrum involves solving linear dispersion relations. Note that when we refer to the essential spectrum of a particular solution type in the following, we mean of the operator  $\mathcal{T}(\lambda)$  corresponding to the eigenvalue problem involving linearization about such a solution, as in (1.5).

Starting with the constant coefficient system corresponding to a homogenous rest state,

$$u_x = A(\lambda)u$$

we have that  $\lambda \in \Sigma_{ess}$  if and only if  $A(\lambda)$  is not hyperbolic, i.e.  $\Sigma_{ess} = \{\lambda \in \mathbb{C} : \text{spec}(A(\lambda)) \cap i\mathbb{R} \neq \emptyset\}$  This is of course equivalent to the condition

$$d(\lambda, k) := \det[A(\lambda) - ik] = 0$$

for  $k \in \mathbb{R}$ , and  $d(\lambda, k)$  is called the linear dispersion relation.

Turning to periodic solutions, where

$$u_x = A_{per}(x, \lambda)u$$

we have that  $\Sigma_{ess} = \{\lambda \in \mathbb{C} : \text{spec}(R(\lambda)) \cap i\mathbb{R} \neq \emptyset\}$ , where  $R(\lambda)$  is the Floquet matrix associated to  $A_{per}(x, \lambda)$ . Thus the dispersion relation for periodic systems is defined in a similar manner to homogeneous rest states, with the constant coefficient matrix replaced by the Floquet matrix associated to the periodic system.

Other solutions types for which the essential spectrum is easily computable are those for which the corresponding operator  $\mathcal{T}(\lambda)$  is a relatively compact perturbation of the operators for one of the above two cases. In particular, for a front connecting two, possibly distinct, homogeneous rest states, we have

$$u_x = A(x, \lambda)u$$

where

$$\lim_{x \rightarrow -\infty} A(x, \lambda) = A_-(\lambda), \quad \lim_{x \rightarrow \infty} A(x, \lambda) = A_+(\lambda).$$

In this case we will have  $\lambda \in \Sigma_{ess}$  if and only if either at least one of  $A_{\pm}(\lambda)$  is not hyperbolic, or if both  $A_{\pm}(\lambda)$  are hyperbolic but their Morse indices differ.

The essential spectrum for fonts connecting periodic solutions to each other or periodic solutions to homogeneous rest states is located analogously. We again refer to [56] for additional details.

## B.4 Locating the point spectrum: the Evans function

The Evans function was first introduced in [18, 19], and developed in a fully rigorous way in the context of reaction-diffusion systems in [1]. Essentially, it is a tool to locate point spectrum: its roots correspond to values of  $\lambda$  for which there are nontrivial intersections of the spaces of solutions which decay in backward and forward time, respectively. In other words, a zero of the Evans function indicates a bounded solution of the associated eigenvalue problem.

In particular, from Theorem 2.1 we have that  $\lambda \in \Sigma_{pt}$  (again for  $\mathcal{T}$  as in (2.1)) if and only if

$$N(T(\lambda)) = \text{Rg } P_-^u(0; \lambda) \cap \text{Rg } P_+^s(0; \lambda) \neq \{0\}$$

where  $P_-^u(x; \lambda)$  and  $P_+^s(x; \lambda)$  are projections associated with the exponential dichotomies of (1.5) on  $\mathbb{R}^+$  and  $\mathbb{R}^-$ , respectively.

We now fix  $\Omega$  to be a connected component of  $\mathbb{C} \setminus \Sigma_{ess}$  and note that the Morse index  $\dim \text{Rg } P_-^u(\lambda) = \dim \mathbb{N}P_+^s(\lambda)$  is constant for  $\lambda \in \Omega$ . Supposing this constant to be  $k$ , we have  $\dim \text{Rg } P_-^u(\lambda) + \dim \text{Rg } P_+^s(\lambda) = k + (n - k) = n$  for any  $\lambda \in \Omega$ .

**Definition 2.4.1.** Let  $[u_1(\lambda), \dots, u_k(\lambda)]$  and  $[u_{k+1}(\lambda), \dots, u_n(\lambda)]$  be analytic bases of  $\text{Rg } P_-^u(0; \lambda)$  and  $\text{Rg } P_+^s(0; \lambda)$  respectively. Then the Evans function is defined as

$$D(\lambda) = \det(u_1(\lambda), \dots, u_n(\lambda)). \quad (4.1)$$

It is possible to choose analytic bases by the results in [33]. The Evans function is only unique up to the choice of basis vectors, but any two Evans function differ only by a nonzero factor. The Evans function then has the following properties [1, 18, 20, 50]:

**Theorem 2.2.**  $D(\lambda)$  has the following properties:

- (i)  $D(\lambda)$  is analytic in  $\lambda \in \Omega$ .
- (ii)  $D(\lambda) = 0$  if and only if  $\lambda \in \Sigma_{pt}$  of  $\mathcal{T}$ .
- (iii) The order of  $\lambda_*$  as a zero of  $D(\lambda)$  is equal to the algebraic multiplicity of  $\lambda_*$  as an eigenvalue of  $\mathcal{T}$ .

## APPENDIX C

---

### **Further Analysis: Simple Eigenvalue of a Front**

Here we give the full set-up and proof for Theorem 4.2 given in Section 4.5.

## C.1 Problem and system set-up

We will use the same set-up and hypotheses as in Section 4.3, but will make the additional assumptions that at a particular  $\lambda = \lambda_*$ , we have a simple eigenvalue of the front, and no eigenvalue for the back; we will make this precise momentarily. We also distinguish the rates associated to the exponential dichotomy of the trivial solution and that of the periodic solution, denoting the former by  $\alpha > 0$  (with  $\alpha = \min\{-\alpha^s, \alpha^u\}$  in the absence of reversibility), and the latter by  $\eta > 0$ . We assume that  $\eta < \alpha$ , so that terms of the form  $O(e^{-\eta L} + e^{-\alpha L})$  will reduce to  $O(e^{-\eta L})$ .

First recall that we are interested in

$$u_x = f(u, \mu) \tag{1.1}$$

with  $u \in \mathbb{R}^{2n}$  and  $\mu \in \mathbb{R}$ , and the associated eigenvalue problem

$$\dot{v} = [f_u(u_{\ell,L}(x)) + \lambda B(u_{\ell,L}(x))] v, \tag{1.2}$$

where the family  $u_{\ell,L}(x)$  is as defined in Hypothesis 4.3.1. We further recall from

this hypothesis that

$$u_{\ell,L}(x) = \begin{cases} u_f(x+L) + w_f^-(x+L;L), & x \leq -L \\ u_f(x+L) + w_f^+(x+L;L), & x \in [-L, 0] \\ u_b(x-L) + w_b^-(x-L;L), & x \in [0, L] \\ u_b(x-L) + w_b^+(x-L;L), & x \geq L \end{cases} \quad (1.3)$$

and

$$|w_f^-(x;L)| \leq Ce^{-\eta(L-x)}, \quad x \leq 0 \quad (1.4)$$

$$|w_f^+(x;L)| \leq Ce^{-\eta L}, \quad x \in [0, L] \quad (1.5)$$

$$|w_b^-(x;L)| \leq Ce^{-\eta L}, \quad x \in [-L, 0] \quad (1.6)$$

$$|w_b^+(x;L)| \leq Ce^{-\eta(L+x)}, \quad x \geq 0. \quad (1.7)$$

We now make the further assumption that  $\lambda_*$  is a simple eigenvalue of

$$\dot{v} = [f_u(u_f(x, \mu), \mu) + \lambda B(u_f(x, \mu), \mu)] v \quad (1.8)$$

with eigenfunction  $v_{f^*}(x)$ . That is, we suppose

$$T_{v_{f^*}(0)} W_f^u(0, \mu, \lambda_*) \cap T_{v_{f^*}(0)} W_f^s(0, \mu, \lambda_*) = \mathbb{C} \dot{v}_{f^*}(0) \quad (1.9)$$

where  $W_f^u(0, \mu, \lambda)$  and  $W_f^s(0, \mu, \lambda)$  denote the stable and unstable manifolds of (1.8).

Then

$$\dot{w} = -[f_u(u_f(x, \mu), \mu) + \lambda_* B(u_f(x, \mu), \mu)]^* w \quad (1.10)$$

also has a unique bounded solution  $\psi_*(x)$  that satisfies

$$\psi_*(x) \perp T_{v_{f^*}(0)}W_f^u(0, \mu, \lambda_*) + T_{v_{f^*}(0)}W_f^s(0, \mu, \lambda_*). \quad (1.11)$$

We decompose the space at  $v_{f^*}(0)$  as

$$\mathbb{C}^{2n} = \mathbb{C}\psi_*(0) \oplus \mathbb{C}\dot{v}_f(0) \oplus Y^+ \oplus Y^-,$$

where

$$\begin{aligned} \mathbb{C}\dot{v}_f(0) \oplus Y^- &= T_{v_{f^*}(0)}W_f^u(0, \mu, \lambda_*) \\ \mathbb{C}\dot{v}_f(0) \oplus Y^+ &= T_{v_{f^*}(0)}W_f^s(0, \mu, \lambda_*). \end{aligned}$$

Note that we have both  $|v_{f^*}(x)| \leq Ce^{-\alpha|x|}$  and  $|\psi_*(x)| \leq Ce^{-\alpha|x|}$ .

Now returning to (1.2), and suppressing the  $\mu$  dependence, we rewrite the eigenvalue problem as

$$\begin{aligned} \dot{v}_f^-(x) &= [f_u(u_f(x+L) + w_f^-(x+L)) + \lambda B(u_f(x+L) + w_f^-(x+L))] v_f^-(x), \quad x \leq -L \\ \dot{v}_f^+(x) &= [f_u(u_f(x+L) + w_f^+(x+L)) + \lambda B(u_f(x+L) + w_f^+(x+L))] v_f^+(x), \quad -L \leq x \leq 0 \\ \dot{v}_b^-(x) &= [f_u(u_b(x-L) + w_b^-(x-L)) + \lambda B(u_b(x-L) + w_b^-(x-L))] v_b^-(x), \quad 0 \leq x \leq L \\ \dot{v}_b^+(x) &= [f_u(u_b(x-L) + w_b^+(x-L)) + \lambda B(u_b(x-L) + w_b^+(x-L))] v_b^+(x), \quad L \leq x \\ \dot{v}_f^-(-L) &= \dot{v}_f^+(-L) \\ \dot{v}_f^+(0) &= \dot{v}_b^-(0) \\ \dot{v}_b^-(L) &= \dot{v}_b^+(L). \end{aligned} \quad (1.12)$$

We decompose  $v_f^\pm$  as

$$v_f^\pm(x) = dv_{f^*}(x+L) + \tilde{w}_f^\pm(x+L) \quad (1.13)$$

on  $x \in (-\infty, -L]$  and  $[-L, 0]$ , respectively, for some  $d \in \mathbb{C}$ .

Now we further assume  $\lambda^*$  is not an eigenvalue of

$$\dot{v} = [f_u(u_b(x, \mu), \mu) + \lambda B(u_b(x, \mu), \mu)] v \quad (1.14)$$

so that the only solution  $v_{b^*}(x)$  of (1.14) with  $\lambda = \lambda_*$  satisfying  $|v_{b^*}(x)| \rightarrow 0$  as  $x \rightarrow 0$  is  $v_{b^*} \equiv 0$ . In other words, we have  $W_b^s(0, \mu, \lambda_*) \cap W_b^u(0, \mu, \lambda_*) = \emptyset$  for the stable and unstable manifolds of (1.14). We will then seek  $v_b^\pm(x) = \tilde{w}_b^\pm(x-L)$  on  $x \in [0, L]$  and  $[L, \infty)$ , respectively.

Defining  $y = x + L$ , we see that in order for the decomposition (1.13) to satisfy the first two equations in (1.12), we have

$$d\dot{v}_f(y) + \dot{\tilde{w}}_f^\pm(y) = [f_u(u_f(y) + w_f^\pm(y)) + \lambda B(u_f(y) + w_f^\pm(y))] (dv_{f^*}(y) + \tilde{w}_f^\pm(y)) \quad (1.15)$$

on  $y \leq 0$  and  $0 \leq y \leq L$  respectively. Thus  $\tilde{w}_f^\pm(y)$  satisfy

$$\begin{aligned} \dot{\tilde{w}}_f^\pm &= [f_u(u_f(y)) + \lambda_* B(u_f(y))] \tilde{w}_f^\pm \\ &+ [(f_u(u_f(y) + w^-(y)) - f_u(u_f(y))) + (\lambda - \lambda_*) B(u_f(y) + w^-(y))] \\ &+ \lambda_* (B(u_f(y) + w^-(y)) - B(u_f(y))) (dv_{f^*} + \tilde{w}_f^\pm) \end{aligned} \quad (1.16)$$

We rewrite this as

$$\dot{w}_f^\pm = [f_u(u_f(y)) + \lambda_* B(u_f(y))] \tilde{w}_f^\pm + [G_f^\pm(y) + (\lambda - \lambda_*) B_{f,1}^\pm(y) + \lambda_* B_{f,2}^\pm(y)] (dv_{f_*} + \tilde{w}_f^\pm). \quad (1.17)$$

where we have defined

$$\begin{aligned} G_f^\pm(y) &= f_u(u_f(y) + w_f^\pm(y)) - f_u(u_f(y)) \\ B_{f,1}^\pm(y) &= B(u_f(y) + w_f^\pm(y)) \\ B_{f,2}^\pm(y) &= B(u_f(y) + w_f^\pm(y)) - B(u_f(y)). \end{aligned}$$

We also have

$$\dot{w}_b^\pm = [f_u(u_b(y)) + \lambda_* B(u_b(y))] \tilde{w}_b^\pm + [G_b^\pm(y) + (\lambda - \lambda_*) B_{b,1}^\pm(y) + \lambda_* B_{b,2}^\pm(y)] \tilde{w}_b^\pm, \quad (1.18)$$

with the analogous definitions for  $G_b^\pm(y), B_{b,1}^\pm(y), B_{b,2}^\pm(y)$ .

In the following we investigate the system

$$\begin{aligned} (i) \quad & \dot{w}_f^\pm = [f_u(u_f(y)) + \lambda_* B(u_f(y))] \tilde{w}_f^\pm + [G_f^\pm(y) + (\lambda - \lambda_*) B_{f,1}^\pm(y) + \lambda_* B_{f,2}^\pm(y)] (dv_{f_*} + \tilde{w}_f^\pm) \\ (ii) \quad & \dot{w}_b^\pm = [f_u(u_b(y)) + \lambda_* B(u_b(y))] \tilde{w}_b^\pm + [G_b^\pm(y) + (\lambda - \lambda_*) B_{b,1}^\pm(y) + \lambda_* B_{b,2}^\pm(y)] \tilde{w}_b^\pm \\ (iii) \quad & \tilde{w}_f^\pm(0) \in \mathbb{C}\psi_*(0) \oplus Y^+ \oplus Y^- \\ (iv) \quad & \tilde{w}_f^+(0) - \tilde{w}_f^-(0) \in \mathbb{C}\psi_*(0) \\ (v) \quad & \tilde{w}_b^+(0) \in E_b^s(0; \lambda_*) \\ (vi) \quad & \tilde{w}_b^+(0) - \tilde{w}_b^-(0) = 0 \\ (vii) \quad & \tilde{w}_f^+(L) - \tilde{w}_b(-L) = -dv_{f_*}(L) \end{aligned} \quad (1.19)$$

where a solution  $(w_f^-, w_f^+, w_b^-, w_b^+, d)$  of (1.19) solves (1.12) if and only if

$$\xi_f := \langle \psi_*(0), w_f^+(0) - w_f^-(0) \rangle = 0. \quad (1.20)$$

The first part of (1.19)(i) (i.e., (1.8)) has exponential dichotomies on  $\mathbb{R}^+$  and  $\mathbb{R}^-$ , which we denote by  $\Phi_{f,\pm}^{s,u}(x, y; \lambda)$ , while the first part of (1.19)(ii) (i.e., (1.14)) has an exponential dichotomy on  $\mathbb{R}$ , which we denote by  $\Phi_b^{s,u}(x, y; \lambda)$ .

We also note that by Hypothesis 4.3.2 and Hypothesis 4.3.6, we have that for  $\lambda$  near  $\lambda_*$ ,

$$\begin{aligned} |\Phi_{f,+}^u(L, L; \lambda) - \Phi_\gamma^u(0, 0; \lambda)| &\leq C e^{-\eta L} \\ |\Phi_b^s(-L, -L; \lambda) - \Phi_\gamma^s(0, 0; \lambda)| &\leq C e^{-\eta L} \end{aligned} \quad (1.21)$$

with  $C, \eta > 0$ , where we recall  $\Phi_\gamma^{s,u}(x, y; \lambda)$  is the exponential dichotomy associated to the eigenvalue problem for the periodic solution  $\gamma(x)$ . We also recall that projections will be denoted as:

$$\begin{aligned} P_\gamma^{s,u}(x; \lambda) &:= \Phi_\gamma^{s,u}(x, x; \lambda) \\ P_{f,\pm}^{s,u}(x; \lambda) &:= \Phi_{f,\pm}^{s,u}(x, x; \lambda) \\ P_b^{s,u}(x; \lambda) &:= \Phi_b^{s,u}(x, x; \lambda). \end{aligned} \quad (1.22)$$

Now by the variation of constants formula we have the following fixed point

equation:

$$\begin{aligned}
\tilde{w}_f^-(y) &= \Phi_{f,-}^u(y, 0; \lambda_*) b_f^- \\
&\quad + \int_0^y \Phi_{f,-}^u(y, s; \lambda_*) [G_f^-(s) + (\lambda - \lambda_*) B_{f,1}^-(s) + \lambda_* B_{f,2}^-(s)] (dv_{f^*}(s) + \tilde{w}_f^-(s)) ds \\
&\quad + \int_{-\infty}^y \Phi_{f,-}^s(y, s; \lambda_*) [G_f^-(s) + (\lambda - \lambda_*) B_{f,1}^-(s) + \lambda_* B_{f,2}^-(s)] (dv_{f^*}(s) + \tilde{w}_f^-(s)) ds \\
\tilde{w}_f^+(y) &= \Phi_{f,+}^u(y, L; \lambda_*) a_f^+ \\
&\quad + \int_L^y \Phi_{f,+}^u(y, s; \lambda_*) [G_f^+(s) + (\lambda - \lambda_*) B_{f,1}^+(s) + \lambda_* B_{f,2}^+(s)] (dv_{f^*}(s) + \tilde{w}_f^+(s)) ds \\
&\quad + \Phi_{f,+}^s(y, 0; \lambda_*) b_f^+ \\
&\quad + \int_0^y \Phi_{f,+}^s(y, s; \lambda_*) [G_f^+(s) + (\lambda - \lambda_*) B_{f,1}^+(s) + \lambda_* B_{f,2}^+(s)] (dv_{f^*}(s) + \tilde{w}_f^+(s)) ds \\
\tilde{w}_b^-(y) &= \Phi_b^u(y, 0; \lambda_*) b_b^- + \int_0^y \Phi_b^u(y, s; \lambda_*) [G_b^-(s) + (\lambda - \lambda_*) B_{b,1}^-(s) + \lambda_* B_{b,2}^-(s)] \tilde{w}_b^-(s) ds \\
&\quad + \Phi_b^s(y, -L; \lambda_*) a_b^- + \int_{-L}^y \Phi_b^s(y, s; \lambda_*) [G_b^-(s) + (\lambda - \lambda_*) B_{b,1}^-(s) + \lambda_* B_{b,2}^-(s)] \tilde{w}_b^-(s) ds \\
\tilde{w}_b^+(y) &= \Phi_b^s(y, 0; \lambda_*) b_b^+ + \int_{\infty}^y \Phi_b^u(y, s; \lambda_*) [G_b^+(s) + (\lambda - \lambda_*) B_{b,1}^+(s) + \lambda_* B_{b,2}^+(s)] \tilde{w}_b^+(s) ds \\
&\quad + \int_0^y \Phi_b^s(y, s; \lambda_*) [G_b^+(s) + (\lambda - \lambda_*) B_{b,1}^+(s) + \lambda_* B_{b,2}^+(s)] \tilde{w}_b^+(s) ds \quad (1.23)
\end{aligned}$$

where we have

$$b_f^- \in \text{Rg } \Phi_{f,-}^u(0, 0; \lambda_*) = \mathbb{C} \dot{v}_{f^*}(0) \oplus Y^-$$

$$b_f^+ \in \text{Rg } \Phi_{f,+}^s(0, 0; \lambda_*) = \mathbb{C} \dot{v}_{f^*}(0) \oplus Y^+$$

and we will return to  $a_f^+, a_b^-, b_b^-, b_b^+$  momentarily. Since we have an exponential

dichotomy on all of  $\mathbb{R}$ , we define

$$\begin{aligned}
 G_b(y) &= \begin{cases} G_b^-(y) & -L \leq y \leq 0 \\ G_b^+(y) & 0 \leq y \end{cases} \\
 B_{b,1} &= \begin{cases} B_{b,1}^-(y) & -L \leq y \leq 0 \\ B_{b,1}^+(y) & 0 \leq y \end{cases} \\
 B_{b,2} &= \begin{cases} B_{b,2}^-(y) & -L \leq y \leq 0 \\ B_{b,2}^+(y) & 0 \leq y \end{cases}
 \end{aligned}$$

We write the fixed point equation in (1.23) as

$$\tilde{w}(y) = [\mathcal{F}(a, b, d, \lambda, \tilde{w})](y) \quad (1.24)$$

with  $a = (a_f^+, a_b^-) \in V_a$ ,  $b = ((b_f^-, b_f^+), (b_b^-, b_b^+)) \in V_b$ ,  $d \in \mathbb{C}$ ,  $\lambda \in V_\lambda$ ,  $\tilde{w} = (\tilde{w}_f^-, \tilde{w}_f^+, \tilde{w}_b^-, \tilde{w}_b^+) \in V_{\tilde{w}}$ , where

$$V_a := E_\gamma^u(0; \lambda_*) \oplus E_\gamma^s(0; \lambda_*)$$

$$V_b := ((\mathbb{C}\dot{v}_{f^*}(0) \oplus Y^-) \oplus (\mathbb{C}\dot{v}_{f^*}(0) \oplus Y^+)) \times (E_b^u(0; \lambda_*) \oplus E_b^s(0; \lambda_*))$$

$$V_\lambda := U_\delta(\lambda_*) \subset \mathbb{C}$$

$$V_{\tilde{w}} := C^0((-\infty, 0], \mathbb{C}^{2n}) \times C^0([0, L], \mathbb{C}^{2n}) \times C^0([-L, 0], \mathbb{C}^{2n}) \times C^0([0, \infty), \mathbb{C}^{2n})$$

where  $E_b^{s,u}(0; \lambda_*) := \text{Rg } P_b^{s,u}(0; \lambda_*)$  respectively, and we use the maximum norm over the components in  $V_b$ .

We proceed in steps; the basic outline is as follows:

- (i) First, we show that we have a solution operator that solves (1.24) (which corresponds to (1.19)(i), (ii)) for  $\tilde{w}$  as a function of  $(\lambda, a, b, d)$ . [Lemma 3.2.1]
- (ii) Using this, we solve (1.19)(i), (ii), (vii) for  $(a, \tilde{w})$  as a function of  $(\lambda, b, d)$ . [Lemma 3.3.1]
- (iii) We then add the conditions (1.19)(iii) – (vi) to solve for  $(a, b, \tilde{w})$  as a function of  $(\lambda, d)$ . [Lemma 3.4.1]
- (iv) Finally we use  $\lambda$  and  $d$  to satisfy the jump condition

$$\xi_f := \langle \psi_*(0), w_f^+(0) - w_f^-(0) \rangle = 0. \quad (1.25)$$

For convenience we define  $\tilde{\lambda} := \lambda - \lambda_*$ , and by a small abuse of notation, drop the tilde.

## C.2 Solving the fixed point equation for $\tilde{w}$

**Lemma 3.2.1.** *There exists an  $L_*$  such that for all  $L \geq L_*$ , the following holds uniformly in  $L$ . There exists an operator  $\tilde{W}_1 : V_\lambda \times V_a \times V_b \times \mathbb{C} \rightarrow V_{\tilde{w}}$  such that*

$$\tilde{w} := \tilde{W}_1(\lambda)(a, b, d) \quad (2.1)$$

*solves (1.24) for any  $(a, b, d)$  and  $\lambda$ . Moreover, any bounded solution of (1.24) is given by (2.1). The operator  $\tilde{W}_1$  is analytic in  $\lambda$ , linear in  $(a, b, d)$ , and satisfies the estimate*

$$\|\tilde{W}_1(\lambda)(a, b, d)\| \leq C(|a| + |b| + (e^{-\eta L_*} + |\lambda|)|d|) \quad (2.2)$$

**Proof.** We rewrite (1.24) as

$$(id - L_1(\lambda))\tilde{w} = L_2(\lambda)(a, b, d) \quad (2.3)$$

with

$$\begin{aligned} (L_1(\lambda)\tilde{w})_f^-(y) &= \int_0^y \Phi_{f,-}^u(y, s; \lambda_*) [G_f^-(s) + \lambda B_{f,1}^-(s) + \lambda_* B_{f,2}^-(s)] \tilde{w}_f^-(s) ds \\ &\quad + \int_{-\infty}^y \Phi_{f,-}^s(y, s; \lambda_*) [G_f^-(s) + \lambda B_{f,1}^-(s) + \lambda_* B_{f,2}^-(s)] \tilde{w}_f^-(s) ds \\ (L_1(\lambda)\tilde{w})_f^+(y) &= \int_L^y \Phi_{f,+}^u(y, s; \lambda_*) [G_f^+(s) + \lambda B_{f,1}^+(s) + \lambda_* B_{f,2}^+(s)] \tilde{w}_f^+(s) ds \\ &\quad + \int_0^y \Phi_{f,+}^s(y, s; \lambda_*) [G_f^+(s) + \lambda B_{f,1}^+(s) + \lambda_* B_{f,2}^+(s)] \tilde{w}_f^+(s) ds \\ (L_1(\lambda)\tilde{w})_b^-(y) &= \int_0^y \Phi_b^u(y, s; \lambda_*) [G_b^-(s) + \lambda B_{b,1}^-(s) + \lambda_* B_{b,2}^-(s)] \tilde{w}_b^-(s) ds \\ &\quad + \int_{-L}^y \Phi_b^s(y, s; \lambda_*) [G_b^-(s) + \lambda B_{b,1}^-(s) + \lambda_* B_{b,2}^-(s)] \tilde{w}_b^-(s) ds \\ (L_1(\lambda)\tilde{w})_b^+(y) &= \int_{\infty}^y \Phi_b^u(y, s; \lambda_*) [G_b^+(s) + \lambda B_{b,1}^+(s) + \lambda_* B_{b,2}^+(s)] \tilde{w}_b^+(s) ds \\ &\quad + \int_0^y \Phi_b^s(y, s; \lambda_*) [G_b^+(s) + \lambda B_{b,1}^+(s) + \lambda_* B_{b,2}^+(s)] \tilde{w}_b^+(s) ds \end{aligned} \quad (2.4)$$

and

$$\begin{aligned}
(L_2(\lambda)(a, b, d))_f^-(y) &= \Phi_{f,-}^u(y, 0; \lambda_*) b_f^- \\
&\quad + \int_0^y \Phi_{f,-}^u(y, s; \lambda_*) [G_f^-(s) + \lambda B_{f,1}^-(s) + \lambda_* B_{f,2}^-(s)] dv_{f^*}(s) ds \\
&\quad + \int_{-\infty}^y \Phi_{f,-}^s(y, s; \lambda_*) [G_f^-(s) + \lambda B_{f,1}^-(s) + \lambda_* B_{f,2}^-(s)] dv_{f^*}(s) ds \\
(L_2(\lambda)(a, b, d))_f^+(y) &= \Phi_{f,+}^u(y, L; \lambda_*) a_f^+ \\
&\quad + \int_L^y \Phi_{f,+}^u(y, s; \lambda_*) [G_f^+(s) + \lambda B_{f,1}^+(s) + \lambda_* B_{f,2}^+(s)] dv_{f^*}(s) ds \\
&\quad + \Phi_{f,+}^s(y, 0; \lambda_*) b_f^+ \\
&\quad + \int_0^y \Phi_{f,+}^s(y, s; \lambda_*) [G_f^+(s) + \lambda B_{f,1}^+(s) + \lambda_* B_{f,2}^+(s)] dv_{f^*}(s) ds \\
(L_2(\lambda)(a, b, d))_b^-(y) &= \Phi_b^u(y, 0; \lambda_*) b_b^- + \Phi_b^s(y, -L; \lambda_*) a_b^- \\
(L_2(\lambda)(a, b, d))_b^+(y) &= \Phi_b^s(y, 0; \lambda_*) b_b^+ \tag{2.5}
\end{aligned}$$

We then arrive at the estimates

$$\|L_1(\lambda)\tilde{w}\| \leq C(e^{-\eta L^*} + |\lambda|)\|w\| \leq C\delta\|\tilde{w}\| \tag{2.6}$$

$$\|L_2(\lambda)(a, b, d)\| \leq C(|a| + |b| + (e^{-\eta L^*} + |\lambda|)|d|) \tag{2.7}$$

so that  $id - L_1(\lambda)$  is invertible on  $V_{\tilde{w}}$ . The inverse is analytic in  $\lambda$  and we have the solution

$$w = (id - L_1(\lambda))^{-1} L_2(\lambda)(a, b, d) =: \tilde{W}_1(\lambda)(a, b, d) \tag{2.8}$$

which depends linearly on  $(a, b, d) \in V_a \times V_b \times V_d$  and analytically on  $\lambda \in V_\lambda$ . ■

### C.3 Solving for $(a, \tilde{w})$

We next consider (1.19)(vii):

$$\tilde{w}_f^+(L) - \tilde{w}_b(-L) = -dv_{f^*}(L). \quad (3.1)$$

**Lemma 3.3.1.** *There exists an  $L_*$  such that for all  $L \geq L_*$ , the following holds uniformly in  $L$ . There exist operators*

$$A_1 : V_\lambda \times V_b \times \mathbb{C} \rightarrow V_a$$

$$\tilde{W}_2 : V_\lambda \times V_b \times \mathbb{C} \rightarrow V_{\tilde{w}}$$

such that

$$(a, \tilde{w}) := (A_1(\lambda)(b, d), \tilde{W}_2(\lambda)(b, d)) \quad (3.2)$$

solves (1.24) and (3.1) for any  $(b, d)$  and  $\lambda$ . In addition, any bounded solution of these equations is given by (3.2). The operators  $A_1$  and  $\tilde{W}_2$  are analytic in  $\lambda$  and linear in  $(b, d)$  and satisfy

$$|A_1(\lambda)(b, d)| \leq C((e^{-\eta L_*} + e^{-\alpha L_*} + |\lambda|)|b| + (|v_{f^*}(L_*)| + e^{-\eta L_*} + |\lambda|)|d|)$$

$$\|\tilde{W}_2(\lambda)(b, d)\| \leq C((1 + e^{-\eta L_*} + e^{-\alpha L_*} + |\lambda|)|b| + (|v_{f^*}(L_*)| + e^{-\eta L_*} + |\lambda|)|d|)$$

uniformly in  $L \geq L_*$ . Moreover, writing  $A_1(\lambda)(b, d) = ((A_1(\lambda)(b, d))_f^+, A_1(\lambda)(b, d)_b^-)$ , we have

$$(A_1(\lambda)(b, d))_f^+ = -P_\gamma^u(0; \lambda_*)v_{f^*}(L)d - (A_2(\lambda)(b, d))_f^+$$

$$(A_1(\lambda)(b, d))_b^- = P_\gamma^s(0; \lambda_*)v_{f^*}(L)d + (A_2(\lambda)(b, d))_b^-$$

where

$$|A_2(\lambda)(b, d)| \leq C((e^{-\eta L_*} + e^{-\alpha L_*} + |\lambda|)|b| + (|v_{f_*}(L_*)| + e^{-\eta L_*} + |\lambda|)d).$$

**Proof.** Substituting from the fixed point equation into the left hand side, we have

$$\begin{aligned} -dv_{f_*}(L) &= \Phi_{f,+}^u(L, L; \lambda_*)a_f^+ - \Phi_b^s(-L, -L; \lambda_*)a_b^- + \Phi_{f,+}^s(L, 0; \lambda_*)b_f^+ - \Phi_b^u(-L, 0; \lambda_*)b_b^- \\ &\quad + \int_0^L \Phi_{f,+}^s(L, s; \lambda_*) [G_f^+(s) + \lambda B_{f,1}^+(s) + \lambda_* B_{f,2}^+(s)] (dv_{f_*}(s) + \tilde{w}_f^+(s))ds \\ &\quad + \int_{-L}^0 \Phi_b^u(-L, s; \lambda_*) [G_b(s) + \lambda B_{b,1}(s) + \lambda_* B_{b,2}(s)] \tilde{w}_b(s)ds. \end{aligned}$$

Recalling that  $(a_f^+, a_b^-) \in V_a := E_\gamma^u(0; \lambda_*) \oplus E_\gamma^s(0; \lambda_*)$ , so that using the notation introduced in (1.22),  $P_\gamma^u(0, \lambda_*)a_f^+ = a_f^+$  and  $P_\gamma^s(0, \lambda_*)a_b^- = a_b^-$ , we then have:

$$\begin{aligned} &\Phi_{f,+}^u(L, L; \lambda_*)a_f^+ - \Phi_b^s(-L, -L; \lambda_*)a_b^- \\ &= P_{f,+}^u(L, \lambda_*)a_f^+ + P_b^s(-L, \lambda_*)a_b^- - P_\gamma^u(0, \lambda_*)a_f^+ + a_f^+ + P_\gamma^s(0; \lambda_*)a_b^- - a_b^- \\ &= a_f^+ - a_b^- + (P_{f,+}^u(L, \lambda_*) - P_\gamma^u(0, \lambda_*))a_f^+ + (P_\gamma^s(0; \lambda_*) - P_b^s(-L, \lambda_*))a_b^-. \end{aligned}$$

Thus we have

$$-dv_{f_*}(L) = a_f^+ - a_b^- + L_3(\lambda)(a, b, d) \tag{3.3}$$

or, explicitly,

$$\begin{aligned} L_3(\lambda)(a, b, d) &= (P_{f,+}^u(L, \lambda_*) - P_\gamma^u(0, \lambda_*))a_f^+ + (P_\gamma^s(0; \lambda_*) - P_b^s(-L, \lambda_*))a_b^- \\ &\quad + \Phi_{f,+}^s(L, 0; \lambda_*)b_f^+ - \Phi_b^u(-L, 0; \lambda_*)b_b^- \\ &\quad + \int_0^L \Phi_{f,+}^s(L, s; \lambda_*) [G_f^+(s) + \lambda B_{f,1}^+(s) + \lambda_* B_{f,2}^+(s)] (dv_{f_*}(s) + \tilde{w}_f^+(s))ds \\ &\quad + \int_{-L}^0 \Phi_b^u(-L, s; \lambda_*) [G_b(s) + \lambda B_{b,1}(s) + \lambda_* B_{b,2}(s)] \tilde{w}_b(s)ds. \end{aligned}$$

Sustituting  $\tilde{W}_1(\lambda)(a, b, d)$  from Lemma 3.2.1 and (1.21), we have

$$|L_3(\lambda)(a, b, d)| \leq C(e^{-\eta L}|a| + e^{-\alpha L}|b| + (e^{-\eta L} + |\lambda|)(|d| + \|W_1(\lambda)(a, b, d)\|)).$$

Moreover, by Lemma 3.2.1,

$$\begin{aligned} |L_3(\lambda)(a, b, d)| &\leq C(e^{-\eta L_*}|a| + e^{-\alpha L_*}|b| + (e^{-\eta L_*} + |\lambda|)(|d| + |a| + |b| + (e^{-\eta L_*} + |\lambda|)|d|)) \\ &\leq C((e^{-\eta L_*} + |\lambda|)(|a| + |d|) + (e^{-\eta L_*} + e^{-\alpha L_*} + |\lambda|)|b|) \\ &\leq C\delta(|a| + |b| + |d|) \end{aligned}$$

for  $L_*$  sufficiently large, uniformly in  $L$ . Since  $E_\gamma^s(0; \lambda_*) \oplus E_\gamma^u(0; \lambda_*) = \mathbb{C}^{2n}$ , the map  $J_1$ , defined as

$$\begin{aligned} J_1 : V_a &\rightarrow \mathbb{C}^{2n} \\ (a_f^+, a_b^-) &\mapsto (a_f^+ - a_b^-), \end{aligned}$$

is a linear isomorphism. So for  $\delta > 0$  sufficiently small, we can invert the operator

$$a \mapsto J_1 a + L_3(\lambda)(a, 0, 0). \quad (3.4)$$

Thus, defining  $I_1 a := (a, 0, 0)$ , we have

$$a = (J_1 + L_3(\lambda)I_1)^{-1}(-dv_{f^*}(L) - L_3(\lambda)(0, b, d)) =: A_1(\lambda)(b, d). \quad (3.5)$$

Moreover, defining

$$\tilde{W}_2(\lambda)(b, d) := \tilde{W}_1(\lambda)(A_1(\lambda)(b, d), b, d), \quad (3.6)$$

then

$$(\lambda, a, b, d, \tilde{w}) = (\lambda, A_1(\lambda)(b, d), b, d, \tilde{W}_2(\lambda)(b, d))$$

solves (1.24) and (3.1). We also have

$$|A_1(\lambda)(b, d)| \leq C((e^{-\eta L_*} + e^{-\alpha L_*} + |\lambda|)|b| + (|v_{f_*}(L_*)| + e^{-\eta L_*} + |\lambda|)|d|)$$

and so

$$\begin{aligned} \|\tilde{W}_2(\lambda)(b, d)\| &\leq C(|A_1(\lambda)(b, d)| + |b| + (e^{-\eta L_*} + |\lambda|)|d|) \\ &\leq C((1 + e^{-\eta L_*} + e^{-\alpha L_*} + |\lambda|)|b| + (|v_{f_*}(L_*)| + e^{-\eta L_*} + |\lambda|)|d|). \end{aligned}$$

Finally, applying the complementary projections  $P_\gamma^s(0; \lambda_*)$  and  $P_\gamma^u(0; \lambda_*)$  to (3.3), we have

$$\begin{aligned} a_f^+ &= -P_\gamma^u(0; \lambda_*)v_{f_*}(L)d - P_\gamma^u(0; \lambda_*)(L_3(\lambda)(a, b, d)) \\ a_b^- &= P_\gamma^s(0; \lambda_*)v_{f_*}(L)d + P_\gamma^s(0; \lambda_*)(L_3(\lambda)(a, b, d)) \end{aligned}$$

and then substituting  $a = A_1(\lambda)(b, d)$  yields

$$\begin{aligned} A_1(\lambda)(b, d)_f^+ &= -P_\gamma^u(0; \lambda_*)v_{f_*}(L)d - P_\gamma^u(0; \lambda_*)(L_3(\lambda)(A_1(\lambda)(b, d), b, d)) \\ &=: -P_\gamma^u(0; \lambda_*)v_{f_*}(L)d - (A_2(\lambda)(b, d))_f^+ \\ A_1(\lambda)(b, d)_b^- &= P_\gamma^s(0; \lambda_*)v_{f_*}(L)d + P_\gamma^s(0; \lambda_*)(L_3(\lambda)(A_1(\lambda)(b, d), b, d)) \\ &=: P_\gamma^s(0; \lambda_*)v_{f_*}(L)d + (A_2(\lambda)(b, d))_b^-. \end{aligned}$$

So we have the estimate

$$\begin{aligned} |A_2(\lambda)(b, d)| &\leq C(|v_{f^*}(L_*)|d + |L_3(\lambda)(A_1(\lambda)(b, d), b, d)|) \\ &\leq C((e^{-\eta L_*} + e^{-\alpha L_*} + |\lambda|)|b| + (|v_{f^*}(L_*)| + e^{-\eta L_*} + |\lambda|)|d|) \end{aligned}$$

as claimed. ■

## C.4 Solving for $(a, b, \tilde{w})$

We now look to satisfy the conditions involving  $\tilde{w}_{f,b}^\pm(0)$  given in (1.19)(iii) – (vi):

$$\begin{aligned} \tilde{w}_f^-(0) &\in \mathbb{C}\psi_*(0) \oplus Y^+ \oplus Y^- \\ \tilde{w}_f^+(0) &\in \mathbb{C}\psi_*(0) \oplus Y^+ \oplus Y^- \\ \tilde{w}_f^+(0) - \tilde{w}_f^-(0) &\in \mathbb{C}\psi_*(0) \\ \tilde{w}_b^+(0) &\in E_b^s(0; \lambda_*) \\ \tilde{w}_b^+(0) - \tilde{w}_b^-(0) &= 0. \end{aligned} \tag{4.1}$$

**Lemma 3.4.1.** *There exists an  $L_*$  such that for all  $L \geq L_*$ , the following holds uniformly in  $L$ . There exist operators*

$$\begin{aligned} A_3 : V_\lambda \times \mathbb{C} &\rightarrow V_a \\ B_1 : V_\lambda \times \mathbb{C} &\rightarrow V_b \\ \tilde{W}_3 : V_\lambda \times \mathbb{C} &\rightarrow V_{\tilde{w}} \end{aligned}$$

such that

$$(a, b, \tilde{w}) := (A_3(\lambda)d, B_3(\lambda)d, \tilde{W}_3(\lambda)d) \tag{4.2}$$

solves (1.24), (3.1) and (4.1) for any  $d$  and  $\lambda$ . Moreover, any bounded solution of these equations is given by (4.2). The operators are analytic in  $\lambda$  and linear in  $d$  and satisfy the estimates

$$\begin{aligned} |A_3(\lambda)d| &\leq C(|v_{f^*}(L_*)| + e^{-\eta L_*} + |\lambda|)|d| \\ |B_1(\lambda)d| &\leq C(|v_{f^*}(L_*)| + e^{-\eta L_*} + |\lambda|)|d| \\ \|W_3(\lambda)d\| &\leq C(|v_{f^*}(L_*)| + e^{-\eta L_*} + |\lambda|)|d| \end{aligned} \quad (4.3)$$

uniformly in  $L > L_*$ . We also have that  $A_3(\lambda)d = ((A_3(\lambda)d)_f^+, (A_3(\lambda)d)_b^-)$  can be written as

$$\begin{aligned} (A_3(\lambda)d)_f^+ &= -P_\gamma^u(0; \lambda_*)v_{f^*}(L)d - (A_4(\lambda)d)_f^+ \\ (A_3(\lambda)d)_b^- &= P_\gamma^s(0; \lambda_*)v_{f^*}(L)d + (A_4(\lambda)d)_b^- \end{aligned} \quad (4.4)$$

for  $A_4$  linear in  $d$  and analytic in  $\lambda$  satisfying

$$|A_4(\lambda)d| \leq C(|v_{f^*}(L_*)| + e^{-\eta L_*} + |\lambda|)|d| \quad (4.5)$$

**Proof.** From (1.24) we have

$$\begin{aligned} \tilde{w}_f^-(0) &= b_f^- + \int_{-\infty}^0 \Phi_{f,-}^s(0, s; \lambda_*) [G_f^-(s) + \lambda B_{f,1}^-(s) + \lambda_* B_{f,2}^-(s)] (dv_{f^*}(s) + \tilde{w}_f^-(s))ds \\ \tilde{w}_f^+(0) &= b_f^+ + \Phi_{f,+}^u(0, L; \lambda_*)a_f^+ \\ &\quad + \int_L^0 \Phi_{f,+}^u(0, s; \lambda_*) [G_f^+(s) + \lambda B_{f,1}^+(s) + \lambda_* B_{f,2}^+(s)] (dv_{f^*}(s) + \tilde{w}_f^+(s))ds \\ \tilde{w}_b^-(0) &= b_b^- + \Phi_b^s(0, -L; \lambda_*)a_b^- + \int_{-L}^0 \Phi_b^s(0, s; \lambda_*) [G_b^-(s) + \lambda B_{b,1}^-(s) + \lambda_* B_{b,2}^-(s)] \tilde{w}_b^-(s)ds \\ \tilde{w}_b^+(0) &= b_b^+ + \int_{\infty}^0 \Phi_b^u(0, s; \lambda_*) [G_b^+(s) + \lambda B_{b,1}^+(s) + \lambda_* B_{b,2}^+(s)] \tilde{w}_b^+(s)ds \end{aligned} \quad (4.6)$$

with  $\tilde{w}$  and  $a$  given by Lemma 3.3.1. By the definition of  $V_b$ , we can decompose

$b_f = (b_f^-, b_f^+)$  uniquely according to

$$b_f^- = x_f^- + y_f^-$$

$$b_f^+ = x_f^+ + y_f^+$$

where  $x_f^\pm \in \mathbb{C}\dot{v}_{f*}(0)$  and  $y_f^\pm \in Y^\pm$  respectively. In other words we have  $b_f = x_f + y_f$  where  $x_f \in \mathbb{C}\dot{v}_{f*}(0) \times \mathbb{C}\dot{v}_{f*}(0)$  and  $y_f \in Y^- \times Y^+$ . Recalling that

$$\mathbb{C}^{2n} = \mathbb{C}\psi_*(0) \oplus \mathbb{C}\dot{v}_{f*}(0) \oplus Y^+ \oplus Y^-, \quad (4.7)$$

we have that the first three equations in (4.1) are equivalent to the system

$$P(\mathbb{C}\dot{v}_{f*}(0), \mathbb{C}\psi_*(0) \oplus Y^+ \oplus Y^-)\tilde{w}_f^-(0) = 0$$

$$P(\mathbb{C}\dot{v}_{f*}(0), \mathbb{C}\psi_*(0) \oplus Y^+ \oplus Y^-)\tilde{w}_f^+(0) = 0$$

$$P(Y^+ \oplus Y^-, \mathbb{C}\dot{v}_{f*}(0) \oplus \mathbb{C}\psi_*(0))(\tilde{w}_f^+(0) - \tilde{w}_f^-(0)) = 0 \quad (4.8)$$

where  $P(X, Y)$  denotes the projection onto  $X$  with kernel  $Y$ . Substituting from (4.6)

into the above and using  $b_f = x + y$  gives

$$\begin{aligned}
0 &= x_f^- + P(\mathbb{C}\dot{v}_{f*}(0), \mathbb{C}\psi_*(0) \oplus Y^+ \oplus Y^-) \left( \int_{-\infty}^0 \Phi_{f,-}^s(0, s; \lambda_*) \right. \\
&\quad \left. [G_f^-(s) + \lambda B_{f,1}^-(s) + \lambda_* B_{f,2}^-(s)] (dv_{f*}(s) + \tilde{w}_f^-(s)) ds \right) \\
0 &= x_f^+ + P(\mathbb{C}\dot{v}_{f*}(0), \mathbb{C}\psi_*(0) \oplus Y^+ \oplus Y^-) \left( \Phi_{f,+}^u(0, L; \lambda_*) a_f^+ \right. \\
&\quad \left. + \int_L^0 \Phi_{f,+}^u(0, s; \lambda_*) [G_f^+(s) + \lambda B_{f,1}^+(s) + \lambda_* B_{f,2}^+(s)] (dv_{f*}(s) + \tilde{w}_f^+(s)) ds \right) \\
0 &= y_f^+ - y_f^- + P(Y^+ \oplus Y^-, \mathbb{C}\dot{v}_{f*}(0) \oplus \mathbb{C}\psi_*(0)) \left( \Phi_{f,+}^u(0, L; \lambda_*) a_f^+ \right. \\
&\quad \left. + \int_L^0 \Phi_{f,+}^u(0, s; \lambda_*) [G_f^+(s) + \lambda B_{f,1}^+(s) + \lambda_* B_{f,2}^+(s)] (dv_{f*}(s) + \tilde{w}_f^+(s)) ds \right. \\
&\quad \left. - \int_{-\infty}^0 \Phi_{f,-}^s(0, s; \lambda_*) [G_f^-(s) + \lambda B_{f,1}^-(s) + \lambda_* B_{f,2}^-(s)] (dv_{f*}(s) + \tilde{w}_f^-(s)) ds \right)
\end{aligned} \tag{4.9}$$

where again we have  $(a_f, \tilde{w}_f)$  from Lemma 3.3.1. We can then write this as

$$\begin{pmatrix} x_f^- \\ x_f^+ \\ y_f^+ - y_f^- \end{pmatrix} + (L_4(\lambda)(b, d))_f = 0. \tag{4.10}$$

where  $(L_4)_f : (\lambda, b, d) \rightarrow \mathbb{C}\dot{v}_{f*}(0) \times \mathbb{C}\dot{v}_{f*}(0) \times (Y^+ \oplus Y^-)$ . From (1.21) and (3.3) we have the estimate

$$\begin{aligned}
|(L_4(\lambda)(b, d))_f| &\leq C(|A_1(\lambda)(b, d)| + (e^{-\eta L_*} + |\lambda|)(|d| + \|W_2(b, d)\|)) \\
&\leq C((e^{-\eta L_*} + e^{-\alpha L_*} + |\lambda|)|b| + (|v_{f*}(L_*)| + e^{-\eta L_*} + |\lambda|)|d| + \\
&\quad + (e^{-\eta L_*} + |\lambda|)(|d| + (1 + e^{-\eta L_*} + e^{-\alpha L_*} + |\lambda|)|b| + (|v_{f*}(L_*)| + e^{-\eta L_*} + |\lambda|)|d|)) \\
&\leq C((e^{-\eta L_*} + e^{-\alpha L_*} + |\lambda|)|b| + (|v_{f*}(L_*)| + e^{-\eta L_*} + |\lambda|)|d|) \\
&\leq C\delta(|b| + |d|)
\end{aligned} \tag{4.11}$$

for  $L_*$  sufficiently large, uniformly in  $L$ . The map  $J_{2,f}$  given by

$$\begin{aligned} J_{2,f} : (\mathbb{C}\dot{v}_{f^*}(0) \times \mathbb{C}\dot{v}_{f^*}(0)) \times (Y^- \times Y^+) &\rightarrow \mathbb{C}\dot{v}_{f^*}(0) \times \mathbb{C}\dot{v}_{f^*}(0) \times (Y^+ \oplus Y^-) \\ ((x_f^-, x_f^+), (y_f^-, y_f^+)) &\mapsto (x_f^-, x_f^+, y_f^- - y_f^+) \end{aligned}$$

is a linear isomorphism by (4.7).

Turning now to  $b_b$ , we have  $(b_b^-, b_b^+) \in E_b^u(0; \lambda_*) \oplus E_b^s(0; \lambda_*)$ . Using the same notation as above, we require

$$\begin{aligned} P(E_b^s(0, \lambda_*), E_b^u(0, \lambda_*))\tilde{w}_b^+(0) &= 0 \\ \tilde{w}_b^+(0) - \tilde{w}_b^-(0) &= 0, \end{aligned} \tag{4.12}$$

so substituting from (4.6) we have

$$\begin{aligned} 0 &= b_b^+ + P(E_b^s(0, \lambda_*), E_b^u(0, \lambda_*)) \left( \int_{-\infty}^0 \Phi_b^u(0, s; \lambda_*) [G_b^+(s) + \lambda B_{b,1}^+(s) + \lambda_* B_{b,2}^+(s)] \tilde{w}_b^+(s) ds \right) \\ 0 &= b_b^+ - b_b^- + \int_{-\infty}^0 \Phi_b^u(0, s; \lambda_*) [G_b^+(s) + \lambda B_{b,1}^+(s) + \lambda_* B_{b,2}^+(s)] \tilde{w}_b^+(s) ds \\ &\quad - \Phi_b^s(0, -L; \lambda_*) a_b^- - \int_{-L}^0 \Phi_b^s(0, s; \lambda_*) [G_b^-(s) + \lambda B_{b,1}^-(s) + \lambda_* B_{b,2}^-(s)] \tilde{w}_b^-(s) ds. \end{aligned} \tag{4.13}$$

We write this as

$$\begin{pmatrix} b_b^+ \\ b_b^+ - b_b^- \end{pmatrix} + (L_4(\lambda)(b, d))_b = 0. \tag{4.14}$$

Then

$$\begin{aligned}
|(L_4(\lambda)(b, d))_b| &\leq C(|A_1(\lambda)(b, d)| + (e^{-\eta L_*} + |\lambda|)\|\tilde{W}_2(\lambda)(b, d)\|) \\
&\leq C((e^{-\eta L_*} + e^{-\alpha L_*} + |\lambda|)|b| + (|v_{f_*}(L_*)| + e^{-\eta L_*} + |\lambda|)|d| + \\
&\quad + (e^{-\eta L_*} + |\lambda|)((1 + e^{-\eta L_*} + e^{-\alpha L_*} + |\lambda|)|b| + (|v_{f_*}(L_*)| + e^{-\eta L_*} + |\lambda|)|d|)) \\
&\leq C((e^{-\eta L_*} + e^{-\alpha L_*} + |\lambda|)|b| + (|v_{f_*}(L_*)| + e^{-\eta L_*} + |\lambda|)|d|) \\
&\leq C\delta(|b| + |d|)
\end{aligned} \tag{4.15}$$

for  $L_*$  sufficiently large, uniformly in  $L$ . So trivially combining the estimates we have

$$\begin{aligned}
|(L_4(\lambda)(b, d))| &\leq C((e^{-\eta L_*} + e^{-\alpha L_*} + |\lambda|)|b| + (|v_{f_*}(L_*)| + e^{-\eta L_*} + |\lambda|)|d|) \\
&\leq C\delta(|b| + |d|).
\end{aligned} \tag{4.16}$$

The map  $J_{2,b}$  given by

$$\begin{aligned}
J_{2,b} : E_b^u(0; \lambda_*) \times E_b^s(0; \lambda_*) &\rightarrow E_b^s(0; \lambda_*) \times \mathbb{C}^{2n} \\
(b_b^-, b_b^+) &\mapsto (b_b^+, b_b^+ - b_b^-)
\end{aligned}$$

is a linear isomorphism since  $E_b^u(0; \lambda_*) \oplus E_b^s(0; \lambda_*) = \mathbb{C}^{2n}$ . Thus the map  $J_2 : (b_f, b_b) \mapsto (J_{2,f}(x_f + y_f), J_{2,b}(b_b))$  is also a linear isomorphism, and the operator

$$b \mapsto J_2(b) + L_4(\lambda)(b, 0)$$

is invertible due to (4.16). Then defining  $I_2 b = (b, 0)$ , we have the solution operator

$$b = -(J_2 + L_4(\lambda)I_2)^{-1}(L_4(\lambda)(0, d)) =: B_1(\lambda)d \tag{4.17}$$

Then from (4.16) we have

$$|B_1(\lambda)d| \leq C(|v_{f^*}(L_*)| + e^{-\eta L^*} + |\lambda|)|d|.$$

We now substitute  $b = B_1(\lambda)d$  into  $A_1$  and  $\tilde{W}_2$  so that

$$A_3(\lambda)d := A_1(\lambda)(B_1(\lambda)d, d)$$

$$\tilde{W}_3(\lambda)d := \tilde{W}_2(\lambda)(B_1(\lambda)d, d)$$

and the estimates

$$\begin{aligned} |A_3(\lambda)d| &\leq C((e^{-\eta L^*} + e^{-\alpha L^*} + |\lambda|)(|v_{f^*}(L_*)| + e^{-\eta L^*} + |\lambda|)|d|) + (|v_{f^*}(L_*)| + e^{-\eta L^*} + |\lambda|)|d|) \\ &\leq C(|v_{f^*}(L_*)| + e^{-\eta L^*} + |\lambda|)|d| \end{aligned}$$

$$\begin{aligned} \|\tilde{W}_3(\lambda)d\| &\leq C((1 + e^{-\eta L^*} + e^{-\alpha L^*} + |\lambda|)(|v_{f^*}(L_*)| + e^{-\eta L^*} + |\lambda|)|d|) \\ &\quad + (|v_{f^*}(L_*)| + e^{-\eta L^*} + |\lambda|)|d|) \\ &\leq C(|v_{f^*}(L_*)| + e^{-\eta L^*} + |\lambda|)|d| \end{aligned}$$

follow. Finally, we set

$$(A_4(\lambda)d)_f^+ = (A_2(\lambda)(B_1(\lambda)d, d))_f^+$$

$$(A_4(\lambda)d)_b^- = (A_2(\lambda)(B_1(\lambda)d, d))_b^-$$

so that (4.4) and (4.5) follow. ■

## C.5 Satisfying the jump condition

Having completed the first three steps in our outline, we have that  $(\lambda, a, b, d, \tilde{w})$  is a bounded solution of eq:reform if and only if it has the form

$$(\lambda, a, b, d, \tilde{w}) = (\lambda, A_3(\lambda)d, B_1(\lambda)d, d, \tilde{W}_3(\lambda)d),$$

where each of the operators is analytic in  $\lambda$  and linear in  $d$ . We conclude by examining the jump condition  $\xi_f = \langle \psi_*(0), \tilde{w}_f^+(0) - \tilde{w}_f^-(0) \rangle = 0$ .

**Lemma 3.5.1.** *Let  $(\lambda, a, b, d, \tilde{w})$  be given by*

$$(\lambda, a, b, d, \tilde{w}) = (\lambda, A_3(\lambda)d, B_1(\lambda)d, d, \tilde{W}_3(\lambda)d). \quad (5.1)$$

*Then  $w_f^+(0) - \tilde{w}_f^-(0)$  holds if and only if*

$$\xi_f = \langle \psi_*(0), \tilde{w}_f^+(0) - \tilde{w}_f^-(0) \rangle = 0.$$

*Moreover,  $\xi_f$  can be written as*

$$\xi_f = -\left\langle \psi_*(L), P_\gamma^u(0; \lambda_*)v_{f_*}(L)d \right\rangle - \lambda d \int_{-\infty}^{\infty} \left\langle \psi_*(s), B(u_f(s))v_{f_*}(s) \right\rangle ds + R(\lambda)d \quad (5.2)$$

*for some function  $R : V_\lambda \times \mathbb{C} \rightarrow \mathbb{C}$  analytic in  $\lambda$  and linear in  $d$  admitting the estimate*

$$|R(\lambda)d| \leq C \left( e^{-\alpha L_*} \left( \sup_{s \geq L_*} |B(u_f)(s)v_{f_*}(s)| + |v_{f_*}(L_*)| + e^{-\eta L_*} + |\lambda| \right) + e^{-\eta L_*} (1 + |v_{f_*}(0)|) \right) |d| \quad (5.3)$$

**Proof.** We have already shown the first statement. Throughout we choose  $(\lambda, a, b, d, \tilde{w})$

according to (5.1) so that  $\xi_f$  is analytic in  $\lambda$  and linear in  $d$ . Since  $\langle \psi_*(0), b_f^\pm \rangle = 0$ , we have

$$\begin{aligned}
& \langle \psi_*(0), \tilde{w}_f^+(0) - \tilde{w}_f^-(0) \rangle = \\
& \left\langle \psi_*(0), \Phi_{f,+}^u(0, L; \lambda_*) a_f^+ \right. \\
& + \int_L^0 \Phi_{f,+}^u(0, s; \lambda_*) [G_f^+(s) + \lambda B_{f,1}^+(s) + \lambda_* B_{f,2}^+(s)] (dv_{f^*}(s) + \tilde{w}_f^+(s)) ds \\
& \left. - \int_{-\infty}^0 \Phi_{f,-}^s(0, s; \lambda_*) [G_f^-(s) + \lambda B_{f,1}^-(s) + \lambda_* B_{f,2}^-(s)] (dv_{f^*}(s) + \tilde{w}_f^-(s)) ds \right\rangle \\
& = \langle \psi_*(L), a_f^+ \rangle \\
& - \int_0^L \langle \psi_*(s), [G_f^+(s) + \lambda B_{f,1}^+(s) + \lambda_* B_{f,2}^+(s)] (dv_{f^*}(s) + \tilde{w}_f^+(s)) \rangle ds \\
& - \int_{-\infty}^0 \langle \psi_*(s), [G_f^-(s) + \lambda B_{f,1}^-(s) + \lambda_* B_{f,2}^-(s)] (dv_{f^*}(s) + \tilde{w}_f^-(s)) \rangle ds
\end{aligned} \tag{5.4}$$

Then using Lemma 3.4.1 and

$$|\psi_*(x)| \leq C e^{-\alpha|x|} \tag{5.5}$$

we have

$$\begin{aligned}
\langle \psi_*(L), a_f^+ \rangle &= \langle \psi_*(L), (A_3(\lambda) d)_f^+ \rangle \\
&= - \left\langle \psi_*(L), P_\gamma^u(0; \lambda_*) v_{f^*}(L) d \right\rangle - \left\langle \psi_*(L), (A_4(\lambda) d)_f^+ \right\rangle \\
&= - \left\langle \psi_*(L), P_\gamma^u(0; \lambda_*) v_{f^*}(L) d \right\rangle + O(e^{-\alpha L_*} (|v_{f^*}(L_*)| + e^{-\eta L_*} + |\lambda|) |d|)
\end{aligned} \tag{5.6}$$

Again using (5.5) and the definition of  $B_{f,1}^\pm$ , we have

$$\begin{aligned} & \int_0^L \langle \psi_*(s), \lambda B_{f,1}^+(s) dv_{f^*}(s) \rangle ds + \int_{-\infty}^0 \langle \psi_*(s), \lambda B_{f,1}^-(s) dv_{f^*}(s) \rangle ds \\ &= \lambda d \int_{-\infty}^{\infty} \langle \psi_*(s), B(u_f(s)) v_{f^*}(s) \rangle ds + O\left(|d|(e^{-\alpha L_*} \sup_{s \geq L_*} |B(u_f)(s) v_{f^*}(s)| + e^{-\eta L_*})\right). \end{aligned} \quad (5.7)$$

We also have

$$\begin{aligned} & \left| \int_0^L \langle \psi_*(s), (G_f^+(s) + \lambda_* B_{f,2}^+(s)) dv_{f^*}(s) \rangle ds + \int_{-\infty}^0 \langle \psi_*(s), (G_f^-(s) + \lambda_* B_{f,2}^-(s)) dv_{f^*}(s) \rangle ds \right| \\ & \leq C|d| \left( \left| \int_0^L e^{-\alpha s} |G_f^+(s) + \lambda_* B_{f,2}^+(s)| |dv_{f^*}(s)| ds \right| + \left| \int_{-\infty}^0 e^{\alpha s} |G_f^-(s) + \lambda_* B_{f,2}^-(s)| |dv_{f^*}(s)| ds \right| \right) \\ & \leq C|d| (e^{-(\alpha+2\eta)L_*} |v_{f^*}(L_*)| + e^{-\eta L_*} |v_{f^*}(0)|). \end{aligned} \quad (5.8)$$

Now turning to the terms involving  $\tilde{w}_f^\pm$ , we have

$$\begin{aligned} & \left| \int_0^L \langle \psi_*(s), [G_f^+(s) + \lambda B_{f,1}^+(s) + \lambda_* B_{f,2}^+(s)] \tilde{w}_f^+(s) \rangle ds \right. \\ & \quad \left. + \int_{-\infty}^0 \langle \psi_*(s), [G_f^-(s) + \lambda B_{f,1}^-(s) + \lambda_* B_{f,2}^-(s)] \tilde{w}_f^-(s) \rangle ds \right| \\ & \leq \|\tilde{W}_3(\lambda)d\| \left| \int_0^L e^{-\alpha s} |G_f^+(s) + \lambda B_{f,1}^+(s) + \lambda_* B_{f,2}^+(s)| ds \right. \\ & \quad \left. + \int_{-\infty}^0 e^{\alpha s} |G_f^-(s) + \lambda B_{f,1}^-(s) + \lambda_* B_{f,2}^-(s)| ds \right| \\ & \leq C|d| (|v_{f^*}(L_*)| + e^{-\eta L_*} + |\lambda|) (e^{-(\alpha+2\eta)L_*} + e^{-\eta L_*} + |\lambda|). \end{aligned} \quad (5.9)$$

Thus combining (5.6)—(5.9) we arrive at (5.2) with remainder estimate given in (5.3). ■

# Bibliography

- [1] Alexander, J.C., Gardner, R.A., Jones, C.K.R.T.. A topological invariant arising in the stability analysis of travelling waves. *J Reine Angew Math* 1990;410(167–212).
- [2] Astrov, Y., Logvin, Y.. Formation of clusters of localized states in a gas discharge system via a self-completion scenario. *Phys Rev Lett* 1997;79(16):2983–2986.
- [3] Avitabile, D., Lloyd, D.J.B., Burke, J., Knobloch, E., Sandstede, B.. To snake or not to snake in the planar Swift-Hohenberg equation. *SIAM J Appl Dyn Syst* 2010;9(3):704–733.
- [4] Beck, M., Knobloch, J., Lloyd, D.J.B., Sandstede, B., Wagenknecht, T.. Snakes, ladders, and isolas of localized patterns. *SIAM J Math Anal* 2009;41(3):936–972.
- [5] Blanchflower, S.. Magneto hydrodynamic convectons. *Phys A* 1999;261(1-2):74–81.
- [6] Bortolozzo, U., Clerc, M.G., Residori, S.. Solitary localized structures in a liquid crystal light-valve experiment. *New J Phys* 2009;11:093037.
- [7] Burke, J., Houghton, S., Knobloch, E.. Swift–Hohenberg equation with broken reflection symmetry. *Phys Rev E* 2009;80:036202.
- [8] Burke, J., Knobloch, E.. Localized states in the generalized Swift-Hohenberg equation. *Phys Rev E* 2006;73(5):056211.
- [9] Chapman, S.J., Kozyreff, G.. Exponential asymptotics of localised patterns and snaking bifurcation diagrams. *Phys D* 2009;238(3):319–354.
- [10] Chicone, C.. *Ordinary Differential Equations with Applications*. 2nd ed. Springer, 2006.
- [11] Coppel, W.A.. *Dichotomies in Stability Theory*. volume 629 of *Lecture Notes in Mathematics*. Berlin: Springer, 1978.

- [12] Couillet, P., Riera, C., Tresser, C.. Stable static localized structures in one dimension. *Phys Rev Lett* 2000;84(14):3069–3072.
- [13] Cross, M., Hohenberg, P.. Pattern formation outside of equilibrium. *Rev Mod Phys* 1993;65(3):851–1112.
- [14] Dankowicz, H., Schilder, F.. An extended continuation problem for bifurcation analysis in the presence of constraints. *ASME J Comp Nonlin Dyn* 2011;6(3):031003.
- [15] Dawes, J.H.P.. The emergence of a coherent structure for coherent structures: localized states in nonlinear systems. *Philos Trans R Soc Lond Ser A Math Phys Eng Sci* 2010;368(1924):3519–3534.
- [16] Devaney, R.. Blue sky catastrophes in reversible and Hamiltonian systems. *Indiana Univ Math J* 1977;26:247–263.
- [17] Dias, F., Iooss, G.. Capillary-gravity interfacial water waves in infinite depth. *Eur J Mech B/Fluids* 1996;15(3):367–393.
- [18] Evans, J.W.. Nerve axon equations. iii. stability of the nerve impulse. *Indiana Univ Math J* 1972;22:577–593.
- [19] Evans, J.W.. Nerve axon equations. iv. the stable and unstable impulse. *Indiana Univ Math J* 1975;24:1169–1190.
- [20] Gardner, R.A., Jones, C.K.R.T.. Traveling waves of a perturbed diffusion equation arising in a phase field model. *Indiana Univ Math J* 1990;39:1197–1222.
- [21] Gardner, R.A., Zumbrun, K.. The gap lemma and geometric criteria for instability of viscous shock profiles. *Comm Pure Appl Math* 1998;51(7):797–855.
- [22] Goh, R., Scheel, A.. Hopf bifurcation from fronts in the Cahn–Hilliard equation. *Arch Rational Mech Anal* 2015;217:1219–1263.
- [23] Hartman, P.. *Ordinary Differential Equations*. 2nd ed. Society for Industrial and Applied Mathematics, 2002.
- [24] Henry, D.. *Geometric Theory of Semilinear Parabolic Equations*. volume 840 of *Lecture Notes in Mathematics*. Springer-Verlag, 1981.
- [25] Hilali, M.F., Metens, S., Borckmans, P., Dewel, G.. Pattern selection in the generalised Swift-Hohenberg model. *Phys Rev E* 1995;51(3):2046–2052.
- [26] Houghton, S.M., Knobloch, E.. Swift–Hohenberg equation with broken cubic–quintic nonlinearity. *Phys Rev E* 2011;84:016204.
- [27] Hunt, G.W., Peletier, M.A., Champneys, A.R., Woods, P.D., Wadee, M.A., Budd, C.J., Lord, G.J.. Cellular buckling in long structures. *Nonlin Dynam* 2000;21(1):3–29.

- [28] Iooss, G.. Existence d'orbites homoclines á unéquilibre elliptique pour un systéme réversible. *C R Acad Sci Paris* 1997;324(1):993–997.
- [29] Kapitula, T., Promislow, K.. Spectral and Dynamical Stability of Nonlinear Waves. volume 185 of *Applied Mathematical Sciences*. Springer, 2013.
- [30] Kapitula, T., Sandstede, B.. Stability of bright solitary-wave solutions to perturbed nonlinear Schrödinger equations. *Phys D* 1998;124(1-3):58–103.
- [31] Kapitula, T., Sandstede, B.. Edge bifurcations for near integrable systems via Evans function techniques. *SIAM J Math Anal* 2002;33(5):1117–1143.
- [32] Kapitula, T., Sandstede, B.. Eigenvalues and resonances using the Evans function. *Discr Cont Dyn Syst* 2004;10(4):857–869.
- [33] Kato, T.. Perturbation theory for linear operators. Springer, 1966.
- [34] Kirchgässner, K.. Wave-solutions of reversible systems and applications. *J Diff Eqns* 1982;45:113–127.
- [35] Knobloch, E.. Spatially localized structures in dissipative systems: open problems. *Nonlinearity* 2008;21:45–60.
- [36] Knobloch, E.. Spatial localization in dissipative systems. *Ann Rev Condens Matter Phys* 2015;6:325–359.
- [37] Knobloch, J., Vielitz, M., Wagenknecht, T.. Non-reversible perturbations of homoclinic snaking. *Nonlinearity* 2012;25:3469–3485.
- [38] Kozyreff, G., Chapman, S.J.. Asymptotics of large bound states of localized structures. *Phys Rev Lett* 2006;97(4):044502.
- [39] Kozyreff, G., Chapman, S.J.. Analytical results for front pinning between an hexagonal pattern and a uniform state in pattern-formation systems. *Phys Rev Lett* 2013;111.
- [40] Lloyd, D.J.B., O'Farrell, H.. On localised hotspots of an urban crime model. *Physica D* 2013;253:23–39.
- [41] Lloyd, D.J.B., Sandstede, B., Avitabile, D., Champneys, A.R.. Localized hexagon patterns of the planar Swift–Hohenberg equation. *SIAM J Appl Dyn Syst* 2008;7:1049–1100.
- [42] Makrides, E., Sandstede, B.. Predicting the bifurcation structure of localized snaking patterns. *Phys D* 2014;268:59–78.
- [43] McCalla, S., Sandstede, B.. Spots in the swift–hohenberg equation. *SIAM J Appl Dyn Syst* 2013;12(2):831–877.
- [44] McSloy, J.M., Firth, W.J., Harkness, G.K., Oppo, G.L.. Computationally determined existence and stability of transverse structures II. Multi-peaked cavity solitons. *Phys Rev E* 2002;66:046606.

- [45] Meron, E.. Pattern-formation approach to modelling spatially extended ecosystems. *Ecological Modelling* 2012;234:70–82.
- [46] Métivier, G., Zumbrun, K.. Large viscous boundary layers for noncharacteristic nonlinear hyperbolic problems. *Mem Amer Math Soc* 2005;175(826):vi+107.
- [47] Nii, S.. An extension of the stability index for traveling-wave solutions and its application to bifurcations. *SIAM J Math Anal* 1997;28(2):402–433.
- [48] Palmer, K.J.. Exponential dichotomies and transversal homoclinic points. *J Diff Eqns* 1984;55:225–256.
- [49] Palmer, K.J.. Exponential dichotomies and Fredholm operators. *Proc Amer Math Soc* 1988;104:149–156.
- [50] Pego, R.L., Weinstein, M.I.. Eigenvalues, and instabilities of solitary waves. *Phil Trans R Soc Lond A* 1992;340:47–94.
- [51] Peterhof, D., Sandstede, B., Scheel, A.. Exponential dichotomies for solitary-wave solutions of semilinear elliptic equations on infinite cylinders. *J Diff Eqns* 1997;140(2):266–308.
- [52] Pirkl, S., Ribière, P., Oswald, P.. Forming process and stability of bubble domains in dielectrically positive cholesteric liquid crystals. *Liquid Crystals* 1993;13:413–415.
- [53] Pomeau, Y.. Front motion, metastability, and subcritical bifurcations in hydrodynamics. *Phys D* 1986;23(1-3):3–11.
- [54] Sakaguchi, H., Brand, H.R.. Stable localized squares in pattern-forming nonequilibrium systems. *Europhys Lett* 1997;38(5):341–346.
- [55] Sandstede, B.. Stability of multiple-pulse solutions. *Trans Amer Math Soc* 1998;350(2):429–472.
- [56] Sandstede, B.. Stability of traveling waves. In: Fiedler, B., editor. *Handbook of Dynamical Systems II*. Elsevier; 2004. p. 983–1055.
- [57] Sandstede, B., Scheel, A.. Absolute and convective instabilities of waves on unbounded and large bounded domains. *Physica D* 2000;145:233–277.
- [58] Sandstede, B., Scheel, A.. Defects in oscillatory media: toward a classification. *SIAM J Appl Dyn Syst* 2004;3(1):1–68.
- [59] Sandstede, B., Xu, Y.. Snakes and isolas in non-reversible conservative systems. *Dyn Syst* 2012;27(3):317–329.
- [60] Schneider, T.M., Gibson, J.F., Burke, J.. Snakes and ladders: localized solutions of plane Couette flow. *Phys Rev Lett* 2010;104:104501.
- [61] Short, M.B., D’Orsogna, M.R., Pasour, V.B., Tita, G.E., Brantingham, P.J., Bertozzi, A.L., Chayes, L.B.. A statistical model of criminal behavior. *Mathematical Models and Methods in Applied Sciences* 2008;18:1249–1267.

- [62] Vanderbauwhede, A., Fiedler, B.. Homoclinic period blow-up in reversible and conservative systems. *Z Angew Math Phys* 1992;43(2):292–318.
- [63] Woods, P.D., Champneys, A.R.. Heteroclinic tangles and homoclinic snaking in the unfolding of a degenerate reversible Hamiltonian-Hopf bifurcation. *Phys D* 1999;129(3-4):147–170.